

António Gaspar Lopes da Cunha

**Modelling and Optimisation of  
Single Screw Extrusion**

Tese submetida à Universidade do Minho para a  
obtenção do grau de Doutor em Ciência e  
Engenharia de Polímeros

Universidade do Minho

1999

## SUMÁRIO

A produção de produtos em plástico por extrusão ou injeção é precedida pela plasticização dos polímeros em unidades monofuso. Os mecanismos envolvidos neste processo são complexos e dependem do material, da geometria e das condições de operação utilizados. Usualmente, a definição das condições de operação ou da geometria do parafuso é baseada num processo de tentativa e erro. Um método mais eficiente seria a determinação das condições de operação ou da geometria do parafuso de forma a obter-se o desempenho desejado, ou seja, resolver o problema inverso. Isto não é uma tarefa fácil, dado que a formulação inversa da plasticização não pode ser obtida explicitamente. Além disso, a solução pode não ser única, dado que diferentes combinações da geometria do parafuso e/ou das condições de operação podem produzir o mesmo desempenho. Uma estratégia alternativa é desenvolver um algoritmo de optimização onde, as equações disponíveis para resolver o problema directo são usadas iterativamente até que a solução convirja para um óptimo.

Neste trabalho implementa-se este esquema automático de optimização. Para isso seleccionaram-se os Algoritmos Genéticos como algoritmo de optimização, devido à sua capacidade para lidar com problemas combinatórios e ao facto de não necessitarem do cálculo de derivadas nem de outro tipo de informação adicional. O desempenho de um esquema de optimização deste tipo depende, primariamente, da validade das predições, e também, da sensibilidade da rotina de modelação a variações nos dados de entrada. Desta forma, foi implementada e validada uma rotina de modelação capaz de ter estes aspectos em consideração e, simultaneamente, produzir resultados em pouco tempo de computação.

A ligação do algoritmo de optimização com a rotina de modelação é feita através de uma função objectivo que quantifica os critérios relevantes bem como a sua relativa importância para o processo. Tendo em conta a complexidade do espaço de procura e a existência de conflitos entre os critérios foi desenvolvido um novo algoritmo de optimização multiobjectivo usando Algoritmos Genéticos – *Reduced Pareto Set Genetic Algorithm* (RPSGA). Este método incorpora uma técnica de redução do conjunto de Pareto. O algoritmo foi validado usando problemas de teste (*benchmark problems*) conhecidos. Ao mesmo tempo, a metodologia foi usada para a resolução de um problema real de extrusão e o seu desempenho foi comparado com o de outro algoritmo *Nondominated Sorting Genetic Algorithm* (NSGA). Os resultados obtidos parecem indicar que este algoritmo pode ser muito útil, especialmente

quando são necessárias populações de grandes dimensões. Verificou-se, também, que a metodologia é capaz de produzir resultados com significado físico.

A metodologia de otimização aqui desenvolvida foi aplicada na otimização das condições operatórias e no desenho de parafusos para casos de estudo específicos. Com o objectivo de validar a metodologia de otimização computacional comparam-se os resultados de uma análise factorial *completa*, usando experiências de extrusão, com os resultados obtidos quer por uma rotina analítica (previamente implementada) quer pela rotina numérica implementada neste trabalho. É possível verificar que o modelo numérico produz melhores resultados. No caso do desenho de parafusos, verifica-se que os resultados obtidos são sensíveis à importância relativa dos diferentes critérios e a mudanças nas condições operatórias e nas propriedades dos polímeros.

## SUMMARY

Upon manufacturing plastics parts by extrusion or injection, polymers are plasticised in single screw units. The mechanisms involved in this process are complex and material, geometry and operation dependent. Usually, the setting of the extruder operating conditions or the establishment of the adequate screw geometry is based on trial-and-error. A more efficient method consists in determining the operating conditions or screw geometry that produce the desired performance, i.e. to solve the inverse problem. This is not an easy task, since the inverse formulation of plasticating extrusion cannot be explicitly obtained. Also, the solution is probably not unique, since different combinations of screw geometry and/or operating conditions might produce the same performance. An alternative strategy is to develop an optimisation algorithm, where the equations available to solve the direct problem are used iteratively, until the solution converges to an optimum.

In this work such an automatic optimisation scheme is implemented. Genetic Algorithms (GAs) are chosen as the optimisation algorithm, given their capacity for dealing with combinatorial-type problems and the fact that they do not require neither derivative information nor other additional knowledge. The performance of such an optimisation scheme depends, mainly, on the validity of the predictions and also, on the sensitivity of the modelling package to changes in the input variables. Therefore, a numerical modelling package able to take these aspects into consideration and, simultaneously, produce results with lower computation time, is also implemented and validated.

The linkage between the optimisation algorithm and the modelling package is made through an objective function that quantifies the relevant criteria and their relative importance to the process. Given the complexity of the search space and the existence of some conflicting criteria a new multiobjective optimisation method using GAs – Reduced Pareto Set Genetic Algorithm (RPSGA) – was developed. This method incorporates a technique for reducing the Pareto set. Well known benchmark problems were used to validate the algorithm. Also, a “real world” extrusion problem is solved. Comparisons are made with Nondominated Sorting Genetic Algorithm (NSGA). The results obtained seem to indicate that this approach can be very useful, especially where there is the need to use large populations. This optimisation methodology is able to produce results with physical meaning.

The methodology developed in this work is applied to the optimisation of the operating conditions and screw design for specific case studies. A full factorial analysis, using extrusion experiments, was carried out in order to assess the computational results, obtained by both analytical (implemented previously) and numerical modelling packages. The results allow one to conclude that the approaches where the numerical model is used yield better results. The results obtained for screw design show that the optimisation algorithm is sensitive to the importance of the different criteria, to changes in the operating conditions and to changes in the polymer properties.

## ACKNOWLEDGEMENTS

I take this opportunity to express my deep gratitude to my research and scientific advisor, Prof. José António Covas, for his support, encouragement and availability. I am indebted to him for the opportunity to work in the area of polymer extrusion. I hope to continue this profitable collaboration in the future.

I am also indebted to Prof. Pedro Oliveira for his important support and contribution on the field of optimisation.

I would like to thank the *Departamento de Engenharia de Polímeros*, the *Instituto de Materiais* and the *Centro de Engenharia de Polímeros* of the University of Minho for the facilities, equipment and financial support provided.

I would also like to thank the *Centre de Mise en Forme des Materiaux*, specially Professors Jean François Agassant and Bruno Vergnes, for the facilities and equipment provided as well their friendly hospitality.

The financial support provided by the co-operation programme of the *Junta Nacional de Investigação Científica e Tecnológica* and the French Embassy in Portugal was also very useful.

The contribution of all the people of DEP, in particular João Manuel Maia, is also gratefully acknowledged.

At last, but not least, my gratitude goes to my family without whom this work would not have materialised.

---

## INDEX

Sumário	iii
Summary	v
Acknowledgements	vii
Index	ix
Nomenclature	xi
1- Introduction	1
2- Extrusion optimisation	3
2.1- Introduction	3
2.2- Optimisation techniques	5
2.3- Genetic Algorithms	14
2.3.1- Genetic operators	19
2.3.2- Sizing the population	26
2.3.3- Niching and speciation on GAs	27
2.4- Objective function	33
2.5- Multiobjective optimisation	35
2.5.1- Reduced Pareto set	38
3- Modelling of single screw extrusion	45
3.1- Introduction	45
3.2- Extruder geometry	46
3.3- Solids conveying	49
3.4- Delay	59
3.5- Melting	68
3.6- Melt conveying	75
3.7- Computer implementation	81
4- Experimental work	91
4.1- Polymer properties	91
4.2- Extruder	93
4.3- Statistical design of experiments	95
4.4- Optimisation related to the assessment of GAs	96
5- Results and discussion	99
5.1- Introduction	99
5.2- Case studies	99
5.3- Modelling results	102
5.3.1- Setting the numerical modelling parameters	102
5.3.2- Parameters definition	108
5.3.3- Assessing the modelling results	111
5.4- Optimisation results	123
5.4.1- Setting the GA parameters	123
5.4.2- Optimisation of the processing conditions	141
5.4.3- Screw design	150

---

6- Conclusions	165
7- Suggestions for further work	169
8- References	171
9- Appendices	179
A- Grooved feed sections	179
B- Polymer properties	189
C- Setting the numerical parameters	197
D- Results of the numerical modelling routine	205



## NOMENCLATURE

### Greek characters

$\alpha$	inclination angle of the screw channel
$\alpha$	constant (equation 2.11, genetic algorithms)
$\alpha_s$	thermal diffusivity of the solid plug
$\delta(H)$	length of scheme $H$
$\delta_C$	thickness of the melt film C (delay and melting zones)
$\delta_{DE}$	thickness of the melt film D/E (delay zone II and melting zone)
$\delta_f$	flight clearance
$\phi$	solids conveying angle
$\gamma$	shear strain
$\bar{\gamma}$	weighted average total strain (WATS)
$\dot{\gamma}$	shear rate
$\bar{\dot{\gamma}}$	mean shear rate
$\eta$	melt viscosity
$\eta_{i,j}$	viscosity on the point of coordinates $i,j$ of the finite differences grid
$\lambda$	heat of fusion of the polymer
$\bar{\theta}$	average helix angle
$\theta$	helix angle
$\theta_b$	helix angle at the barrel surface
$\theta_s$	helix angle at the root of screw
$\rho_m$	melt density
$\rho_s$	solid bed density
$\sigma_{\text{share}}$	radius of a circumference that is the maximum distance between chromosomes
$\tau$	shear stress
$\tau_{y x C}$	shear stress acting on the interface A-C in the direction $x$
$\tau_{y x DE}$	shear stress acting on the interface A-DE in the direction $x$
$\tau_{yz}$	shear stress acting in the direction $z$

### Roman characters

$A$	slope of the taper
$A_1, A_2$	constants of the pressure profile equation for solids conveying zone
$A'_1$	constant of the pressure profile equation for delay zone I
$a$	constant of the power law viscosity equation
$a_{ij}$	regression constants (equation 2.6)
$B_1, B_2$	constants of the pressure profile equation for solids conveying zone
$B'_1$	constant of the pressure profile equation for delay zone I

---

$b$	distance of the temperature controller to the interface
$b_N$	groove width
$c$	constant
$c_p$	specific heat of the melt
$D_b$	internal barrel diameter
$D_i$	internal screw diameter
$D_s$	external screw diameter
$\bar{D}$	average screw diameter
$d$	is the distance in the $y$ direction such that $T_{s1}(y = d) = T_{s2}(y = d)$
$D_{pointer}$	distance between pointers (equation 2.10)
$d_{ij}$	distance between individuals $i$ and $j$
$e$	flight width
$e_m$	total mechanical power consumption for melting zone
$e_{mbp}$	mechanical power required to build up pressure (melting zone)
$e_{mcl}$	mechanical power dissipated on the clearance (melting zone)
$e_{mfC}$	mechanical power dissipated on the melt film C (melting zone)
$e_{mfDE}$	mechanical power dissipated on the melt film DE (melting zone)
$e_{mp}$	mechanical power dissipated on the melt pool (melting zone)
$e_p$	total mechanical power consumption for melt conveying zone
$e_{pcl}$	mechanical power dissipated on the clearance (melt conveying zone)
$e_{pp}$	mechanical power required to build up pressure (melt conveying zone)
$e_{psc}$	mechanical power dissipated on the screw channel (melt conveying zone)
$e_w$	total mechanical power consumption for solids conveying zone
$e'_w$	mechanical power consumption (delay zone I)
$e_{wb}$	mechanical power dissipated on the barrel surface (solids zone)
$e'_{wb}$	mechanical power dissipated on the barrel surface (delay zone I)
$e_{wf}$	mechanical power dissipated on the flights
$e_{wp}$	mechanical power consumption for compression
$e_{ws}$	mechanical power dissipated on the screw root
$F$	performance measure
$\nabla F$	gradient of $F$
$F_1$	friction force between the barrel and the solid bed
$F_2, F_6$	forces due to the pressure gradient
$F_3, F_4$	friction forces due to the contact of solid bed with screw walls
$F_5$	friction force due to the contact of solid bed with screw root
$F_8, F_8$	normal reactions
$FO_I$	objective function of individual $I$
$\bar{f}$	mean value of the objective function of all population
$f$	objective function
$f_b$	polymer friction coefficients at barrel surfaces
$f_s$	polymer friction coefficient at screw surface
$f(H)$	mean value of the objective function of all individuals of generation $t$

---

$f(t)dt$	residence time distribution function (RTD)
$G$	function
$g_j$	$j$ inequality constraints
$H$	scheme (genetic algorithms)
$H$	channel height
$H_1$	channel height in the feed zone
$H_2$	channel height in the metering zone
$H_s$	height of the solid bed
$h_k$	$k$ equality constraints
$h_N$	groove height
$h_{N0}$	maximum groove height
$K$	constant of the pressure profile equation for solids conveying zone
$k_0$	constant of the power law viscosity equation
$k_b$	thermal conductivity of the barrel (metal)
$k_m$	thermal conductivity of the melt
$k_p$	thermal conductivity of the screw (metal).
$k_s$	thermal conductivity of the solid polymer
$l$	number of alleles or genes
<i>limit</i>	indifference limit above which the performance of the solutions is considered as similar
$\dot{m}_{A z}$	down-channel mass flow rate in the solid bed, at localisation $z$
$\dot{m}_{A z+\Delta z}$	down-channel mass flow rate in the solid bed, at localisation $z+\Delta z$
$\dot{m}_{B z}$	rate of melt circulation thorough the pool in $x$ - $y$ plane
$\dot{m}_{C z}$	down-channel mass flow rate, for zone C at localisation $z$
$\dot{m}_{Cx z}$	net flow rate out of the film, to melt pool, in the $x$ direction
$\dot{m}_{C z+\Delta z}$	down-channel mass flow rate of the melt film C, at localisation $z+\Delta z$
$\dot{m}_{DE z}$	down-channel mass flow rate of the melt film DE, at localisation $z$
$\dot{m}_{DEx z}$	net flow rate out of the film D/E, to melt film C, in the $x$ direction
$\dot{m}_{DE z+\Delta z}$	down-channel mass flow rate of the melt film DE, at localisation $z+\Delta z$
$m(H,t)$	number of copies of the scheme $H$ on generation $t$
$m'_I$	niche count of individual $i$
$\dot{m}_T$	total down-channel mass flow rate
$N$	number of individuals on the population (genetic algorithms)
$N$	screw speed
$N_1, N_2$	range of variation of screw speed
$N\_ranks$	pre-defined number of ranks
$N_{max}$	maximum number of possible values for screw speed
$NS$	number of individuals to be selected
$n$	constant of the power law viscosity equation
$o(H)$	scheme order
$P$	pressure
$P_{i,j}$	pressure on the point of coordinates $i,j$ of the finite differences grid
$P_1, P_2$	pressures at the at down-channel distance $z_1$ and $z_2$ , respectively
$p$	number of screw flights in parallel
$p_c$	crossover rate

---

$p_m$	mutation rate
q	number of peaks
Q	global quality function (equation 2.28)
$Q$	volumetric output
$Q^*$	volumetric flow rate associated with the neighbourhoods of plane y
$Q_c^*$	volumetric flow rate associated with the neighbourhoods of plane $y_c$
$q_b$	heat flux on the barrel
$q_f$	heat flux on the flights
$q_s$	heat flux on the root of the screw
$R_C$	melting rate over interface A-C
$R_D$	melting rate over interface A-D
$R_E$	melting rate over interface A-E
r	sphere radius that contains the total space (equation 2.17)
S	screw pitch
Sh()	sharing function
SP	selection pressure
T	temperature
$T_0$	constant of the power law viscosity equation
$T(y)$	cross temperature profile (direction y)
$T_b$	barrel temperature
$T_{b1}, T_{b2}$	range of variation of barrel temperature
$T_{bmax}$	maximum number of possible values for barrel temperature
$T_{i,j}$	temperature on the point of coordinates $i,j$ of the finite differences grid
$T_m$	melting temperature
$T_s$	temperature at screw surface
$T_{s0}$	temperature of the polymer at extruder entrance
$T_{s1}$	temperature profile for region 1
$T_{s2}$	temperature profile for region 2
t	generation number (genetic algorithms)
t	polymer residence time inside the extruder
$t(y)$	residence time associated with each path-pair ( $y-y_c$ )
$t_f$	time fraction that a fluid element spends on the upper portion of the channel
$t_{dom}$	size of the comparison set
$t_{max}$	maximum number of generations
V	volume that contains the total space (equation 2.18)
$V_b$	barrel velocity
$V_{bx}$	barrel velocity in transversal direction
$V_{bz}$	barrel velocity in down-channel direction
$V_L$	melt velocity in the direction of screw axis
$V_{sy}$	velocity of the solid towards solid-melt film interface (delay zone I)
$V_{sy1}$	velocity of the solid towards the solid-melt film C interface
$V_{sy2}$	velocity of the solid towards the solid-melt film E interface
$V_{sz}$	solid bed velocity
$V_x$	velocity profile in x-direction
$V_z$	velocity profile in z-direction
$\overline{V}_z$	average of the $V_z$ velocity in x direction
W	channel width
$W_b$	channel width at the barrel surface

---

$W_s$	channel width at the root of screw
$W_B$	melt pool width
$\bar{W}$	average channel width
$w_j$	weight attributed to criterion $j$
$X$	coordinate $x$ of finite differences grid points
$x$	Cartesian coordinate
$\Delta x$	differential element in the $x$ direction
$Y$	coordinate $y$ of finite differences grid points
$y$	Cartesian coordinate
$y_c$	lower position a polymer particle on the channel (direction $y$ )
$\Delta y$	differential element in the $y$ direction
$z_1, z_2$	down-channel distances
$z_m$	helical distance from the hopper to the location where the lower and lateral melt films form
$\Delta z$	differential element in the $z$ direction



## 1- INTRODUCTION

Single screw extrusion is one of most important polymer processing techniques and is also the basis of a number of other important processing technologies. This explains the amount of both experimental [MAD 59, STR 61] and theoretical work [TAD 70]. The pioneering work of Maddock and Street [MAD 59, STR 61], on the understanding of the physical mechanisms taking place inside the extruder, induced a number of new developments, such as barrier screws, mixing sections, grooved barrels, etc. Moreover, the mathematical modelling of the phenomena developing inside the extruder [AGA 96, O'BR 92], enabled the use of software to study the performance of existing systems and, eventually, to define the processing conditions (and/or the equipment characteristics) for new materials/applications, with a minimum of experimental effort.

The available software is able to predict some important process performance parameters, such as mass throughput, power consumption, melt temperature and melt temperature homogeneity, degree of mixing, length of screw required for melting and pressure generation, for a given set of screw geometry, material properties and operating conditions. Nevertheless, the definition of the operating conditions or the design of a new screw is a trial and error process, where the operating conditions or the screw geometry are changed until they meet the desirable performance measures. Presently, the challenge is to solve this optimisation problem automatically, i.e., to obtain the optimal operating conditions or screw geometry for a given polymer and screw geometry or processing conditions, respectively. This is not an easy task, since the inverse formulation of plasticating extrusion cannot be explicitly obtained. Also, the solution is probably not unique, since different combinations of screw geometry and/or operating conditions might produce the same performance [COV 95]. Therefore, the development of an optimisation algorithm, where the equations available to solve the direct problem are used iteratively, until the convergence of the solution to an optimum, is necessary [COV 99].

This work discusses the implementation of such automatic optimisation scheme for plasticating single screw extrusion. Genetic algorithms were selected for this purpose, given their capacity for dealing with combinatorial-type problems and the fact that they do not require derivative information neither another additional knowledge [GOL 89a].

The results produced by any optimisation algorithm depend, principally, of the modelling package, i.e., of their sensitivity to changes in the input variables and their correspondence

with the real problem under study. Given their complexity and the number of variables involved, this is a challenging problem. This probably also explains the scarcity of literature on the subject [POT 94, FAS 94].

In chapter 2 the optimisation algorithm (Genetic Algorithms) used in this work is described and compared with other techniques. Simultaneously, the methods used to quantify the system performance, a conventional objective function and a new multiobjective optimisation scheme, are presented.

Since it is important that process modelling produces adequate results, a compromise between complexity and computing time vs. relaxation of simplifications frequently assumed, must be discussed. Chapter 3 presents the global modelling package implemented. The functional zones in the screw are considered sequentially, and the results, such as cross temperature profiles, pressure, output, residence time distribution, power consumption and solid bed profile, are computed.

Extrusion experiments were carried out, using a full factorial analysis, in order to verify the validity of the computational results. The results, either using an analytical or numerical model, are compared with experimental data in chapter 5. In the same chapter, the optimisation methodology developed in this work is applied in the optimisation of the operating conditions and to the design of a screw for specific case studies.

## 2- EXTRUSION OPTIMISATION

### 2.1- Introduction

A plasticating extruder receives the polymer from the hopper, melts and homogenises it and pumps it to the die. The physical phenomena developed inside the machine are complex, and were only fully understood after intense experimental and theoretical work [TAD 70, RAU 86, AME 89, AGA 96]. They correspond to a set of sequential functional zones that are usually identified as (Figure 2.1):

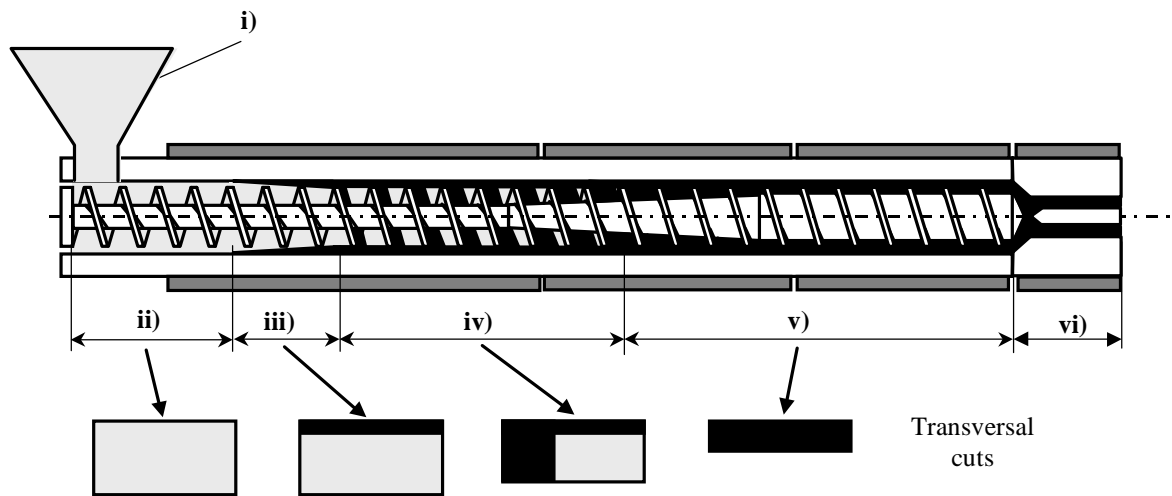


Figure 2.1- Physical phenomena inside the extruder.

- i) **Solids conveying in the hopper** - gravity conveying of granular materials;
- ii) **Solids conveying in the screw** - friction drag solids conveying;
- iii) **Delay zone** - conveying of solids (partially) surrounded by a melt film;
- iv) **Melting zone** - with a specific melting mechanism;
- v) **Melt conveying**;
- vi) **Melt flow** through the die.

For modelling purposes these functional zones are sequentially connected using the appropriate boundary conditions, i.e., the results obtained within one zone are the input conditions for the subsequent one. The system geometry, the polymer properties and the operating conditions are taken into account, in order to obtain some performance measure of the process, such as output, melt temperature, power consumption or degree of mixing.

However, in the most situations, it is necessary to define the operating conditions and/or the system geometry in order to obtain the best system performance. This corresponds to the inverse formulation of the problem that can be understood as an optimisation problem.

At present, the most common method used for optimisation and design of the extrusion process is that of trial-and-error. The operating conditions (screw speed and barrel temperatures) are varied and the corresponding performance is analysed until they meet the necessary specifications. This process can be carried out either using software or by experimentation.

In this approach optimisation corresponds to the resolution of the inverse problem (by opposition to the direct problem, where for a specific geometry, operating conditions and material properties, equations are solved in order to the process performance parameters), i.e., obtaining the operating conditions or the screw geometry that satisfy the performance parameters, such as output maximisation, melt temperature minimisation, degree of mixing maximisation, etc.

The most efficient and intuitive way of solving extrusion optimisation problems is through their inverse formulation, where the equations that govern the process are solved in order to the operating conditions or to the screw geometry and taking into account the boundary conditions. This is not an easy task, especially for such a complex process as plasticating extrusion where the inverse formulation cannot be explicitly obtained. Also, the problem is ill posed, i.e., the solution is not unique, since different operating conditions or screw geometry can produce identical performance measures [COV 95].

Therefore, the use of an optimisation methodology coupled to the available software to solve the direct problem through an objective function that quantifies the performance is necessary. Figure 2.2 illustrates such a methodology. The optimisation algorithm uses the modelling package, iteratively, to obtain information about the process through this objective function. For that, the modelling package receives, from the optimisation algorithm, the values of the variables to optimise and evaluates the corresponding system performance, using the database. A measure of the system performance is passed to the optimisation algorithm through an objective function that takes into account the several performance parameters and their relative importance.

There are several optimisation algorithms able to satisfy these requirements and several ways to quantify the process performance. This chapter discusses the implementation of the above methodology to polymer extrusion process.

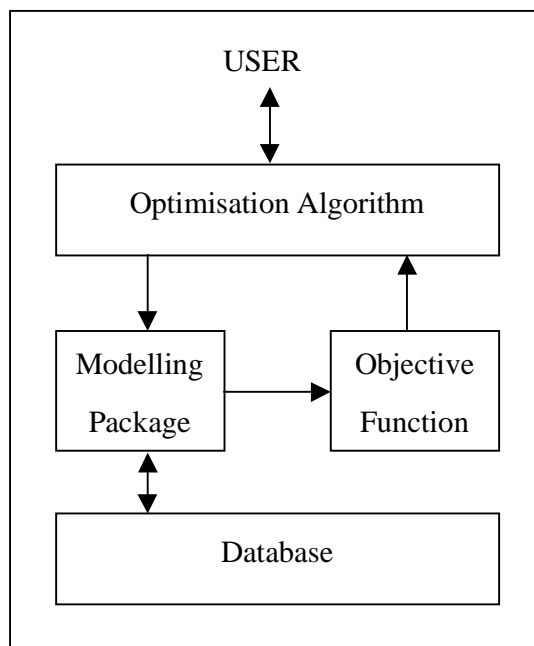


Figure 2.2- Optimisation methodology.

## 2.2- Optimisation techniques

The role of optimisation is to find the best set of parameters that optimise an objective function, particularly by improving the performance in the direction of some optimal point or points [GOL 89a]. In general, the aim is approach to the **global** optimum, on a given search space, by maximising or minimising the objective function, which can be subjected to equality or/and inequality constraints. In the case of a maximisation problem, the mathematical formulation is the following:

$$\begin{aligned}
 &\text{maximise} && f(x_i) && i = 1, \dots, N \\
 &\text{subject to} && g_j(x_i) \geq 0 && j = 1, \dots, J \\
 &&& h_k(x_i) = 0 && k = 1, \dots, K
 \end{aligned} \tag{2.1}$$

where  $f$  is the objective function of the  $N$  parameters  $x_i$ ,  $g_j$  are the  $J$  ( $J \geq 0$ ) inequality constraints, and  $h_k$  are the  $K$  ( $K \geq 0$ ) equality constraints.

Real world optimisation problems (like polymer processing) might involve linear or non-linear objective functions, linear or non-linear constraints, integer and/or continuous variables, stochastic or deterministic inputs, and single or multiple criteria. Therefore, some algorithms may be better adapted to the characteristics of specific problems, while others can work satisfactory across a large spectrum of problems [GOL 89a].

---

The aim of this section is to point out the characteristics of some general purpose optimisation techniques, in order to select the more adequate for the problem under study.

### Random search

This technique consists simply in selecting randomly points from the search space and evaluating them. This technique has the limitation of working with one point each time, which does not provide an amplifying overview of the search space; moreover, search is very slow since the technique does not use any available information on the problem. Random search is seldom used [BEA 93a].

### Gradient Methods

These methods use information about the objective function gradient in order to establish the search direction. For instance if the objective is to optimise the function  $y = f(x_1, x_2)$ , from a given starting point  $P(x_1^{(0)}, x_2^{(0)})$  the gradient vector used is:

$$\text{grad } f = \left\{ \frac{\partial f}{\partial x_1}, \frac{\partial f}{\partial x_2} \right\} \quad (2.2)$$

It can be proved that this vector has the direction of the largest increase of  $f$  [TOL 75]. These methods perform well with unimodal functions, but they have the tendency to converge to the first peak found with multimodal functions (Figure 2.3). Also, when the derivative (or an approximation to the derivative) cannot be determined these methods cannot be used. The search is local, since the search stops when one optimum is found [BEA 93a]. Gradient methods can be combined with random search in order to overcome this problem. After locating one peak using the gradient method, a new starting point is randomly chosen in order to find a new peak. The process is repeated until a number of prescribed peaks are detected. However, each of *hillclimbings* is carried out in isolation, i.e., the method evaluates the same number of points on the various regions of the search space regardless of their objective function values [BEA 93a].

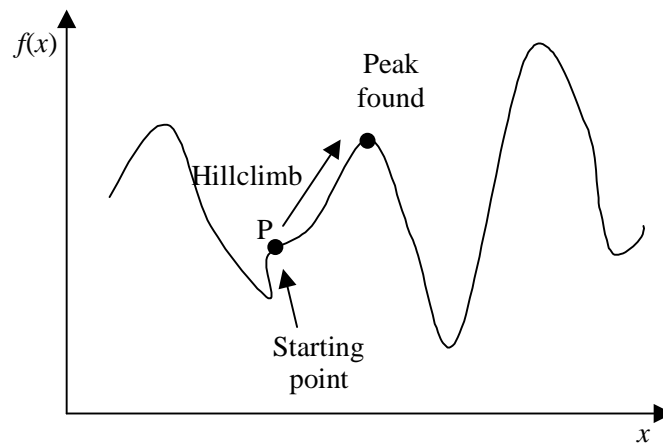


Figure 2.3- The search by gradient methods.

### Simulated Annealing

Simulated annealing makes a parallelism with the way liquids freeze or metals recrystallise during the annealing process. When a melt, initially at high temperature and disordered, is slowly cooled down, the system at any time is approximately under thermodynamic equilibrium. The system becomes progressively ordered and approaches a frozen ground state. When the initial temperature is too low, or the cooling is insufficiently slow, the system may become quenched, i.e., trapped in a local minimum energy state [RUT 89].

By analogy, simulated annealing optimisation starts from one point randomly selected from the search space (an initial thermodynamic state with a given energy -  $E$  - and temperature -  $T$ ), and makes a random movement (keeping the temperature constant, the initial configuration is perturbed and this energy change -  $\Delta E$  - is computed). This movement will be accepted if improvement is obtained (i.e. if the change in energy is negative), and accepted with a determined probability in the opposite case (positive change in energy). As the search proceeds, this probability decreases from a value close to 1 to near zero (in the physical analogy the probability is given by the Boltzman distribution -  $\exp[\Delta E/T]$ ). For the current temperature, the process is repeated a number of times sufficient to produce a good sampling of the search space. Then, the temperature is decreased and the entire process repeated until a frozen state is attained ( $T=0$ ). The application of this algorithm requires the choice of the initial temperature, the number of iterations to be performed at each temperature, and how much the temperature is decremented at each step [RUT 89]. As in the case of the random search, the method works only with one point each time [BEA 93a].

### Neural networks

Neural networks are search algorithms based on the structure and the working of the human neuron. Optimisation is carried out after identifying and learning the patterns that relate the input to the output data. Figure 2.4 illustrates a simple neural network structure the Feedforward Artificial Neural Network (FANN) or back-propagation network [RUM 86], used commonly for modelling and control purposes. It is constituted by an input layer (given by the parameters to optimise), an output layer (representing the objective function) and a hidden layer that makes the connection between the two. A network of nodes (named neurones) constitutes each of these layers. The output of a neurone is affected by a weight (the parameters of the network) and passed to all neurones in the subsequent. Such weights modify the value of the signals that cross a given connection, thus making possible to produce a desired output value for a given set of inputs. They are defined after an adaptation and learning state using training data.

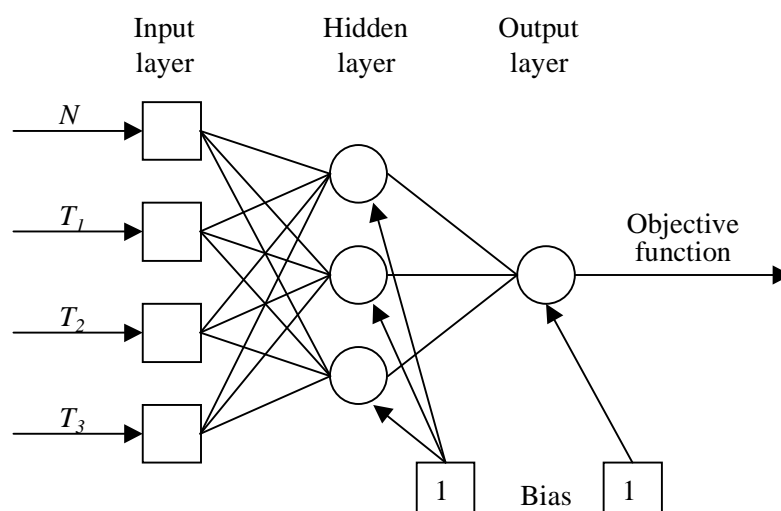


Figure 2.4- Structure of a simple neural network.

The network is evaluated by furnishing input data to the neurones in the input layer. The data is passed to the hidden layer without calculations, where it is processed by the neurones and propagated to subsequent layers. The output of the network is a function representing the sum of the contributions of the inputs to that network. If the biological analogies are ignored, this methodology fits the neural network parameters to data, i.e., is a form of non-linear regression.

Although this technique is well suited to a wide range of problems, the learning stage can be very long and new training is required when considerable modifications to the problem conditions are made [WAS 89, DIR 93, DIR 95].

### Expert systems

An expert system simulates the interaction of the user with a specialist to solve a problem. It comprises (Figure 2.5) a knowledge base, a knowledge acquisition component, an interactive component, an explanation component, and an inference component [WOR 94]. All the facts, rules and know-how are collected in the knowledge base, where the knowledge acquisition component provides communication between the specialists of the process and the knowledge base. New information is incorporated in the base, for example, by monitoring how human specialists solve various typical problems. A lot of interaction with the specialists is thus necessary, in order to create a data base with the adequate dimension, able to work with variations on the operating conditions, materials properties and system geometry. The interactive component is the link between the final users and the knowledge base, either by solving the problem (inference component) or by explaining the solutions (explanation component) and the decision-making process to the user. This methodology has been used to solve several design problems [BRO 86, THO 89, POW 89, WOR 94].

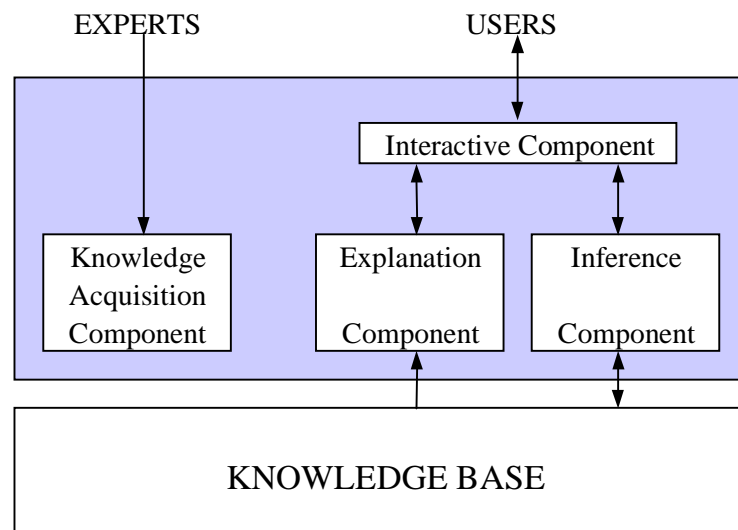


Figure 2.5- Expert system [WOR 94].

### Sensitivity analysis

A sensitivity analysis is generally used to quantify the relationship between variations of the parameters to optimise (independent variables) and variations of the objective function (dependent variables). It considers the change in a performance measure  $F$  as a function of the parameter  $x$ , through a function  $G$  [SMI 94]:

$$F(x) = G(f(x), x) \quad (2.3)$$

where  $f$  is the objective function or the criterion to satisfy. The gradient (the design sensitivity) is given by:

$$\nabla F(x) = \frac{DF(x)}{Dx} = \frac{DG(f(x),x)}{\partial f} \frac{Df(x)}{Dx} + \frac{DG(f(x),x)}{\partial x} \quad (2.4)$$

Once this sensitivity is known, the effects of a variation of the parameter  $\delta x$  on the objective function can be estimated using e.g. finite differences (forward differences):

$$\frac{DF(x)}{Dx} = \frac{F(x + \delta x) - F(x)}{\delta x} \quad (2.5)$$

Despite its simplicity, the finite difference method is often inaccurate and inefficient, making it necessary to use other techniques, such as direct differentiation or adjoint methods, which complicate the optimisation scheme [SMI 94].

## Statistical methods

The aim here is to evaluate data, obtained either by computer modelling or by experimental means, through the use of an objective function [TAD 70]. Several experimental designs are available, such as full factorial, central composite, latin square, Plackett-Burman, Box-Behnken, Taguchi and simplex design [MON 91]. The choice of a method depends on the characteristics of the problem under study, namely the number of factors and levels for each factor, the factors type (continuous or discrete), the type of response variable to study, the sample size (number of replicates) and the restrictions involved [MON 91].

In polymer extrusion, assuming uniform temperature along the barrel, the full factorial method produces an equation, for each one of the dependent variables, of the type:

$$f_j(N, T_b) = a_0 + a_1 N + a_2 T_b + a_{11} N^2 + a_{22} T_b^2 + a_{12} N T_b \quad (2.6)$$

where  $f_j$  is one of the  $j$  dependent variables,  $N$  is the screw speed,  $T_b$  is the barrel temperature, and  $a_k$  and  $a_{kl}$  are constants determined by regression analysis from experimental or modelling data. The optimum of this function can be determined either by calculating the gradient vector (equation 2.2) or by using graphical means. In real problems the temperature along the barrel is not constant, which might increase the number of independent variables beyond reasonable limits.

When the relations between the criteria and the independent variables are established from the results of a mathematical model, it is not possible to detect eventual interactions between the variables, since the experimental variation is not present [MEN 92].

## **Evolutionary Algorithms**

Evolutionary Algorithms (EAs) are a class of stochastic search techniques. They include the following methods [SPE 93a, CHI 95a]:

- Genetic Algorithms (GAs), proposed by John Holland [HOL 75];
- Evolutionary Strategies (ESs), proposed by Rechenberg [REC 73];
- Evolutionary Programming (EP), proposed by Fogel *et al.* [FOG 66];
- Genetic Programming (GP), proposed by Koza [KOZ 91].

Starting from a pool of points they confine progressively the region where the optimum is located through the application of genetic operators (Figure 2.6).

The differences between the various techniques are related to the coding representation of the search space, to the types of selection mechanisms used, to the structure of the operators, and to the measures of accomplishment. Evolutionary programming (EP) is mainly used in artificial intelligence, whereas genetic programming is used to develop more complex structures such as Lisp expressions or neural networks to solve specific problems. Genetic Algorithms (GAs) and Evolutionary Strategies (ESs) are mainly used in optimisation problems and have similar performance [SPE 93a]. GAs have probably received more attention in the literature, particularly to tackle multiobjective optimisation problems [FON 93, HOR 94, SRI 95].

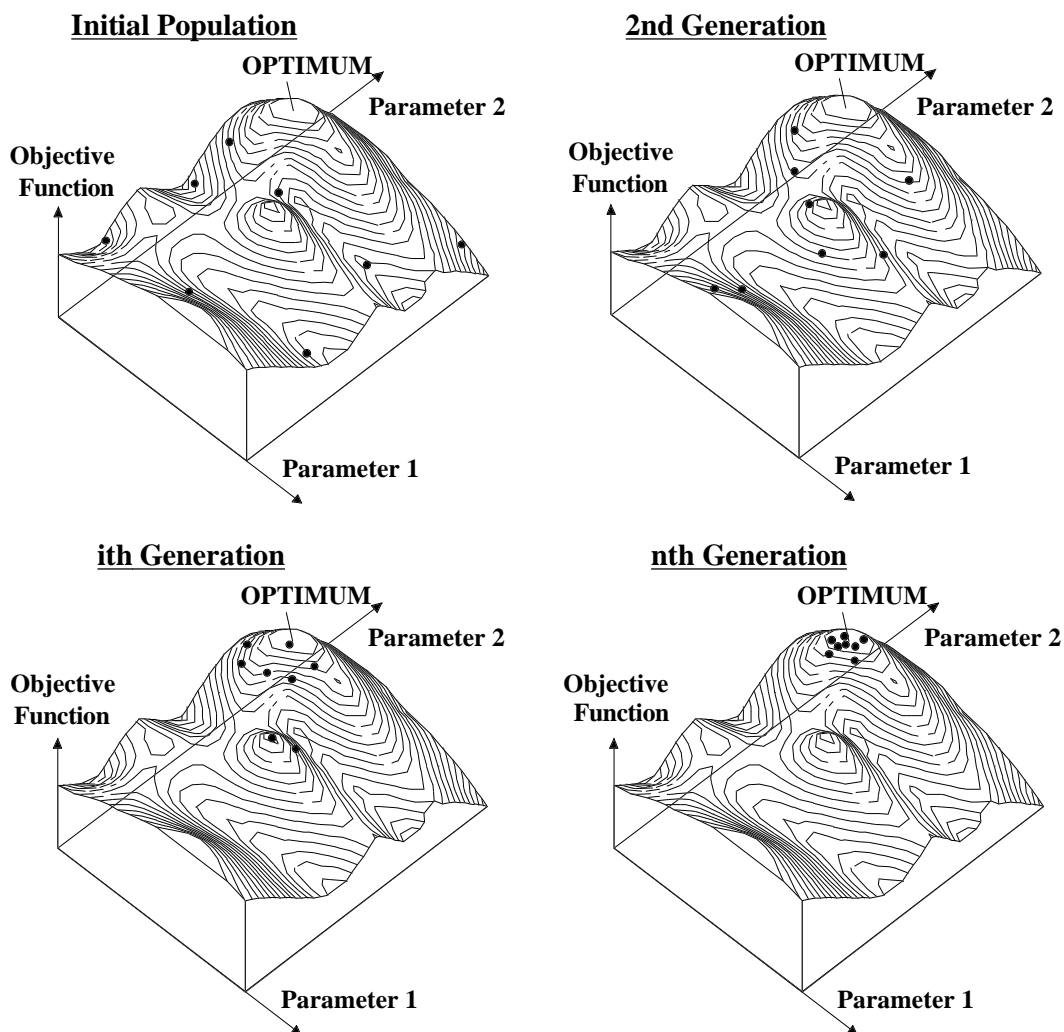


Figure 2.6- How EAs work.

## General comments

Most optimisation methods start from one point of the search space and move to another using a transition rule. However, in multimodal problems when a local peak is found it is difficult to ensure that the algorithm will continue its search. Since Genetic Algorithms work with a population of points that climb many peaks in parallel, the probability of converging to a false peak is reduced, in comparison with other methods. Therefore, it is clear that GAs are substantially different from the other search methods [GOL 89a]:

- They require the codification of the set of parameters;
- They carry out the search on a population, not in a single point;
- They do not require information concerning derivatives nor another auxiliary knowledge, but only the value of the objective function; other methods, such as gradient techniques

also require derivatives of the objective function; neural networks and expert systems need some form of previous knowledge on the process;

- They use probabilistic transition rules, not deterministic rules;
- They obtain more than a single solution, leaving the final choice up to the user.

The robustness of an optimisation method, i.e., the balance between efficiency (when the algorithm is able to attain the optimum in a specific problem) and efficacy (when the algorithm performs well in several types of problems) is another significant characteristic. Figure 2.7 illustrates this point plotting efficiency against the problem type. The most advantageous method has a curve defined as robust scheme (good efficiency and efficacy), where the attainment of an optimum on a specific problem is passed to a second level, in order to achieve good performance in several types of problems [GOL 89a]. Combinatorial problems have a linear or non-linear objective function defined over a set of finite but very large solutions. Unimodal problems have one global optimum, whereas multimodal problems have two or more local optima. Enumeration or random walk methods have little efficiency and the efficacy remains practically constant for all types of problems. The gradient (specialised) scheme performs well in a narrow class of problems (unimodal), but is of little utility in other types of problems. Other specialised algorithms such as simulated annealing for combinatorial problems can be efficient for another type of problems.

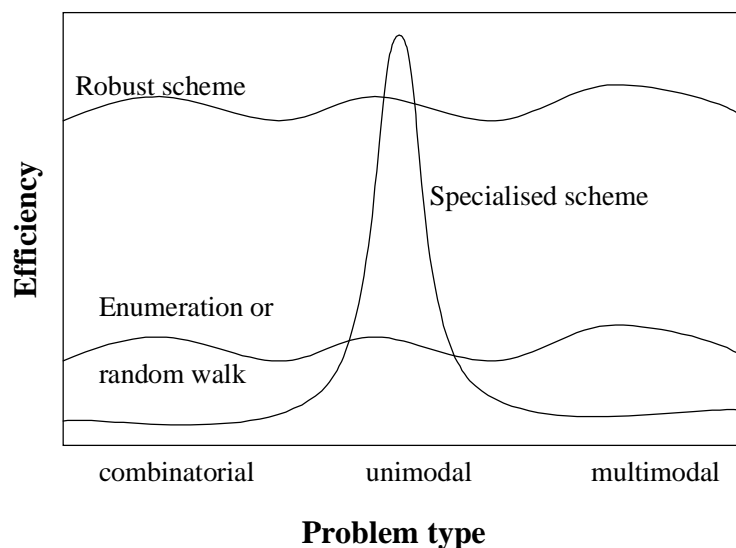


Figure 2.7- Efficiency vs. problem type for several methods [GOL 89a].

Genetic Algorithms are a robust method that can be applied with success in several types of problems. Since they work with a population of points it is possible to obtain more than one solution on the search space, as it will be reported later, when niching and speciation are

discussed. The use of probabilistic transition rules does not mean that the method is a simple random search, but is used to conduct the search to regions not previously explored. GAs are of easy and direct application because they only need to know what the parameters to optimise are (in order to code them) and what the objective function value is [GOL 89a]. This characteristic is useful for complex problems such as polymer extrusion optimisation, where it is not possible to obtain an explicit equation for the objective function.

### 2.3- Genetic Algorithms

Genetic Algorithms (GAs) are search and optimisation methods that mimic natural evolution through genetic operators like crossover and mutation. They work with a population of points, each one representing a possible solution in the search space. Each individual has a value associated to it (fitness or objective function), which is a measure of its performance on the system. Individuals with greater performance have a bigger opportunity for reproduction, i.e. to pass their characteristics to future generations [GOL 89a].

The link between the algorithm and the real problem under study is made: i) through coding the solution space (generally a binary codification) where each solution is transformed into a string defined as chromosome; ii) via an objective function that quantifies the performance of each individual (solution or chromosome).

The flowchart depicted in Figure 2.8 shows the various steps of the algorithm [HOL 75, GOL 89a]. The initial population individuals are obtained randomly in the Initialisation module. Next, these elements are evaluated as a function of their performance on the problem under study, i.e., evaluation consists in modelling the extrusion process using as input data each *chromosome* representing the parameters to optimise (e.g. screw speed, barrel temperature profile, etc). As a result, the values of the parameters to be considered in the objective function are obtained. In the following step a new population is produced from the previous one. In order to do that, the genetic operators (crossover, mutation and/or inversion) are applied to elements of the initial population that were selected on the basis of their fitness values. Consequently, a new population is obtained. If the number of prescribed generations has not been reached ( $t > t_{max}$ ), this new population follows the same route (evaluation, selection, crossover, etc) [HOL 75, GOL 89a].

The methodology will be illustrated with an example, where the aim is to define the screw speed and the barrel temperature that maximise the output of a given extruder and polymer. First, is necessary to define the range of variation of the parameters to optimise (screw speed -  $N \in [N_1, N_2]$ , and barrel temperature -  $T_b \in [T_{b1}, T_{b2}]$ ) and their variation intervals  $\Delta N$  and  $\Delta T_b$ , respectively (i.e., the maximum number of possible values for screw speed is  $N_{\max} = \frac{N_2 - N_1}{\Delta N} + 1$  and similarly for the barrel temperature). Then, the population is initialised, i.e., values of  $N$  and  $T_b$  are obtained randomly in their range of variation  $[0, N_{\max} - 1]$ . Table 2.1 illustrates this procedure, considering a population of 10 individuals, the screw speed varying between 30 and 50 rpm, the barrel temperature lying between 160 and 180°C,  $\Delta N = \Delta T_b = 1$  and  $N_{\max} = T_{b\max} = 21$ . Each chromosome comprises 10 positions, 5 corresponding to screw speed and 5 to barrel temperature. Each of these positions is named a gene or an allele.

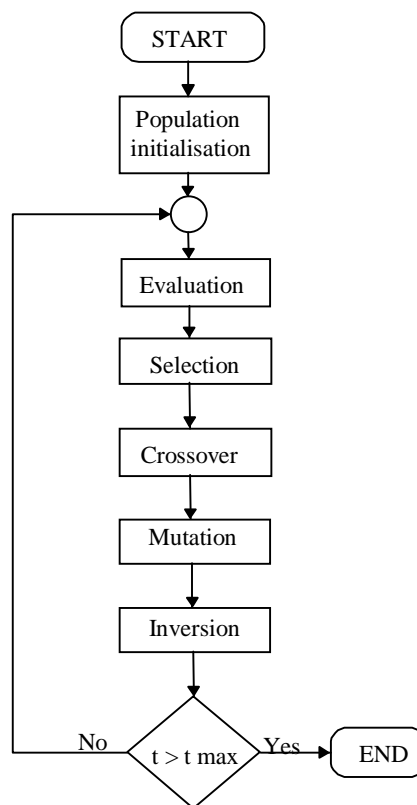


Figure 2.8- GA flowchart.

The first iteration starts with the evaluation of all the individuals. An extrusion modelling package calculates the output for the system geometry, polymer properties and the specific operating conditions. The individuals are sorted by descending order of the output. A pre-

defined number of individuals is selected for crossover, mutation and inversion (in this example only crossover will be used). Individuals with greater performance (output) will be given a greater opportunity to be selected. Table 2.2 presents the results obtained for the 10 individuals of the initial population.

**Table 2.1- Generation of the initial population for the example under study.**

Individual	Transformed variables		Real variables		Chromosome	
	$N$	$T_b$	$N$	$T_b$	$N$	$T_b$
1	10	1	40	161	01010	00001
2	0	12	30	172	00000	01100
3	5	20	35	180	00101	10100
4	14	15	44	175	01110	01111
5	6	4	36	164	00110	00100
6	20	18	50	178	10100	10010
7	5	2	35	162	00101	00010
8	18	4	48	164	10010	00100
9	6	14	36	174	00110	01110
10	18	11	48	171	10010	01011

**Table 2.2- Initial population for the example under study.**

Individual	Chromosome		Transformed variables		Output (kg/hr)	Crossover Position	Parents
	$N$	$T_b$	$N$	$T_b$			
1	10100	10010	20	18	8.5	2	1,3
2	10010	00100	18	4	8.1	6	2,4
3	10010	01011	18	11	8.0	8	1,10
4	01110	01111	14	15	7.7		
5	01010	00001	10	1	7.0		
6	00110	00100	6	4	6.2		
7	00110	01110	6	14	6.0		
8	00101	00010	5	2	6.0		
9	00101	10100	5	20	5.8		
10	00000	01100	0	12	5.2		
					$\bar{Q} = 6.85$		

The next generation includes the best individuals from the previous one (in this case 40%) and new individuals obtained by crossover between the parents selected previously (carried out on a random selected position). Crossover consists in the interchange of genes between the parents. Figure 2.9 illustrates this procedure for the crossover between individuals 1 and 3 on position 2. The other individuals are obtained by crossover between individuals 2 and 4 and between individuals 1 and 10, on positions 6 and 8, respectively. Table 2.3 presents this second generation and the corresponding mass outputs. As can be observed the output average

was increased from 6.85 to 7.8 kg/hr. This process is repeated until the maximum number of iterations is reached or some convergence criterion is satisfied (such as, a percentage of the population converges for the same value).

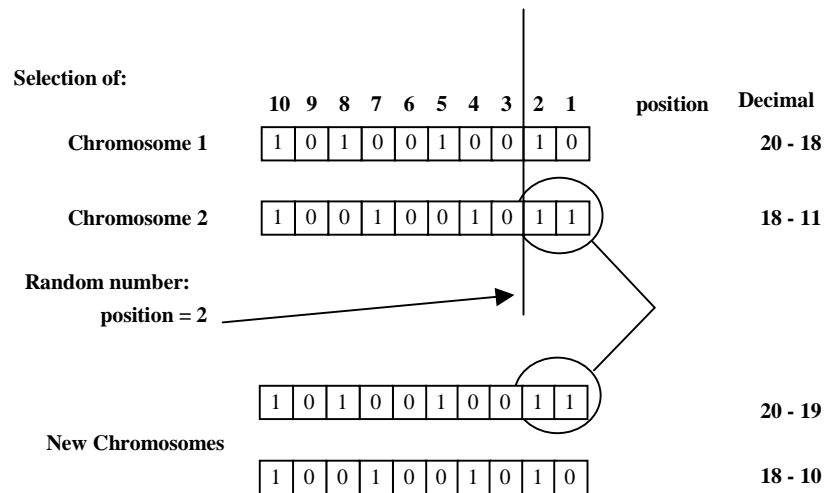


Figure 2.9- Example of crossover.

Table 2.3- Second generation for the example under study.

Individual	Chromosome		Transformed variables		Output (kg/hr)
	$N$	$T_b$	$N$	$T_b$	
1	10100	10010	20	18	8.5
2	10010	00100	18	4	8.1
3	10010	01011	18	11	8.0
4	01110	01111	14	15	7.7
5	10100	10011	20	19	8.5
6	10010	01010	18	10	8.0
7	10010	00100	18	4	8.1
8	01110	01111	14	15	7.7
9	10000	10010	16	18	7.8
10	00100	01100	4	12	5.6
					$\bar{Q} = 7.8$

The improvement in performance throughout the various generations can be explained with the aid of the Schemata Theory [GOL 89a], together with the properties of the genetic operators. A schema describes a set of chromosomes with fixed genes (alleles) in certain positions. For example, in binary representation, the chromosomes (010), (011) and (000) can be represented by the scheme  $H = 0**$ , where the asterisk is a meta symbol, representing a position of indifference (i.e., either 0 or 1). This means that three characters constitute a

scheme,  $V^+ = \{0, 1, *\}$ . A population of  $N$  individuals can be represented by  $2^l$  to  $N \cdot 2^l$  schemes, where  $l$  is the number of alleles in each scheme.

The differences between the several schemes are quantified using the concept of scheme order,  $o(H)$ , and scheme length,  $\delta(H)$ . Scheme order represents the number of fixed positions that the scheme contains (in a binary representation this corresponds to the number of 0s and 1s), e.g.,  $o(1*01*) = 3$  and  $o(*1**0) = 2$ . The scheme length is the distance between the first and the last fixed positions, e.g.,  $\delta(1*01*) = 4 - 1 = 3$  and  $\delta(*1**0) = 5 - 2 = 3$ .

For example, when proportional selection, simple crossover and mutation are used, the lower limit of the expected number of copies of the scheme  $H$ , included in the generation  $(t+1)$ , is given by [GOL 89a]:

$$m(H, t+1) \geq m(H, t) \frac{f(H)}{\bar{f}} \left[ 1 - p_c \frac{\delta(H)}{l-1} - p_m o(H) \right] \quad (2.7)$$

where  $m(H, t+1)$  and  $m(H, t)$  are the number of copies of the scheme  $H$  on the generations  $t+1$  and  $t$ , respectively;  $f(H)$  is the mean value of the objective function of all individuals of generation  $t$  which are represented by the scheme  $H$ ;  $\bar{f}$  is the mean value of the objective function of the entire population;  $p_c$  and  $p_m$  are the probabilities of crossover and mutation, respectively. The number of copies of the schemes having a mean value of the objective function greater than  $[f(H)]$  increases as the search progresses. This search is a geometric progression that promotes the exponential increase of the best individuals on future generations.

The schemata theory will be illustrated with an example where the aim is to maximise the  $\sin(x)$  function ( $0 \leq x \leq \pi$ ). Table 2.4 represents the initial population of 5 individuals.

The best individual of the initial population (individual 2) will be the first individual of the second generation, while the others will be obtained by crossover between parents 1 and 2 on string point 2 and between parents 2 and 5 on string point 3. For crossover purposes the parents are picked up using a selection technique (roulette-wheel, introduced in the next section) based on their performance, while the crossover points are obtained randomly. The improvement obtained with this new generation is evident, since the average of the objective function increased from 0.559 to 0.76. The optimal string in this problem is (10000), which

represents  $x = \pi/2$ . This string is contained in the scheme  $H_1=(1****)$  that represents two individuals of the initial population and four of the second generation, whereas scheme  $H_2=(0****)$  is represented by three individuals of the initial population and by one on the new population. Since the objective is to maximise  $\sin(x)$  function, it is desirable to have more copies of scheme  $H_1$  than  $H_2$ . This improvement in performance by simple manipulation of the strings and ignoring the complete search space illustrates the potential of GAs. These short and above-average schemata are known as *building blocks*. As the search proceeds, the combination of these blocks produces better building blocks, until convergence to the optimum [GOL 89a].

**Table 2.4- Example of the GA working for the  $\sin(x)$  function.**

Initial population						New population		
Individual	String	$x$	$f(x)$	Crossover Point	Parents	String	$x$	$f(x)$
1	01001	0.90	0.783	2	1,2	10100	2.00	0.909
2	10100	2.00	0.909	3	2,5	01000	0.80	0.717
3	00010	0.20	0.199			10101	2.10	0.863
4	00100	0.40	0.389			10010	1.80	0.974
5	11010	2.60	0.516			11100	2.80	0.335
			$\bar{f}(x) =$ 0.559					$\bar{f}(x) =$ 0.760

### 2.3.1- Genetic operators

#### A- Selection

The selection operator determines which individuals of the current population will act as parents of the next generation. The process has two steps. First, a value is attributed to the objective function of each individual. This can be done either by attributing a value proportional to the performance of each individual (objective function value), or by ranking the population according to the corresponding value of the objective function and subsequently attributing a value to the objective function of each individual that depends solely on its position on that ranking.

This scheme introduces a uniform scaling of the entire population and a simple and effective way of controlling the selection pressure -  $SP$  (representing the probability of selection of the best individual in comparison with the average probability of all individuals). Ranking can be linear or exponential [BAK 85]:

$$FO_i = 2 - SP + \frac{2(SP - 1)(N + 1 - i)}{N} \quad (2.8)$$

$$FO_i = \frac{c - 1}{c^N - 1} c^{N-i} \quad (2.9)$$

respectively, where  $N$  is the number of population individuals,  $FO_i$  is the objective function value for individual  $i$ ,  $SP$  is the selection pressure ( $1.0 < SP \leq 2.0$ ) and  $c$  is a constant that controls the selection pressure on the exponential ranking ( $0 < c < 1$ ).

The second step of this operator consists in the selection of the parents according to the value previously attributed. Several techniques are available:

- Roulette-wheel selection,
- Tournament selection,
- Stochastic universal selection,
- Local selection,
- Truncation selection.

i) *Roulette wheel selection*

This is the simplest selection technique, and consists on [BAK 87]:

1. ordering the population individuals by descending order of their objective function value;
2. calculating their cumulative sum;
3. generating a random number between 0 and the total of the above sum;
4. selecting an individual whose cumulative sum will be closer but greater than the number generated previously;
5. repeating steps 3 and 4 until the total number of individuals is selected.

Tables 2.5 and 2.6 describe this procedure, considering a population of 10 individuals ( $N=10$ ) and that the objective function value was determined according to the linear ranking scheme (equation 2.8), with a selection pressure of 2 ( $SP=2$ ). The probability of each individual being selected was calculated. Table 2.6 illustrates the selection of 6 individuals: First, a random number is obtained and compared with the cumulative sum; the first individual that has a cumulative sum equal or greater than this number will be selected.

**Table 2.5- Roulette wheel selection.**

Individual order	1	2	3	4	5	6	7	8	9	10
Objective function	2.0	1.8	1.6	1.4	1.2	1.0	0.8	0.6	0.4	0.2
Cumulative sum	2.0	3.8	5.4	6.8	8	9.0	9.8	10.4	10.8	11.0
Selection probability	0.18	0.16	0.15	0.13	0.11	0.09	0.07	0.06	0.03	0.02

**Table 2.6- Selection of 6 individuals using the roulette wheel method.**

Random number (between 0 and 11.0)	3.1	0.5	7.1	10.6	6.1	5.2
<u>Individual selected</u>	2	1	5	8	4	3

ii) *Tournament selection*

This technique consists on the random selection of a fixed number of individuals ( $N_{tour}$ ) from the entire population. The best is picked up from this sub-group and used as parent. The process is repeated whenever necessary to produce a new individual. The value of  $N_{tour}$  can be defined as a percentage of the total population ( $N$ ) and can vary between 2 and  $N$ .

iii) *Stochastic universal selection*

This procedure is similar to the roulette-wheel selection, but now pointers equally separated replace the random numbers. The first pointer is obtained from a number generated randomly ranging between 0 and the prescribed distance,  $D_{pointer}$ , where:

$$D_{pointer} = \frac{\sum_{i=1}^N FO_i}{NS} \quad (2.10)$$

and  $NS$  is the number of individuals to be selected [BAK 87].

Tables 2.7 and 2.8 show the results obtained using the previous example. The distance between pointers is 1.833 (11/6) and the number randomly generated is 0.516.

**Table 2.7- Stochastic selection.**

<u>Individual order</u>	1	2	3	4	5	6	7	8	9	10
Objective function	2.0	1.8	1.6	1.4	1.2	1.0	0.8	0.6	0.4	0.2
Cumulative sum	2.0	3.8	5.4	6.8	8	9.0	9.8	10.4	10.8	11.0

**Table 2.8- Selection of 6 individuals using the stochastic selection method.**

Pointer	0.516	2.349	4.182	6.015	7.848	9.681
Individual selected	1	2	3	4	5	7

#### iv) *Local selection*

In this case, the individual to be selected is conditioned to a zone called local neighbourhood. Neighbourhood is defined by the structure through which the population is distributed and can be interpreted as a group of potential associated individuals. Initially, half of the population is selected, either randomly or by one of the methods described above. Next, a neighbourhood is defined for each of these individuals, their parents being selected from within. The structure of the neighbourhood can be linear (full and half ring), two-dimensional (full cross, half cross, full star and half star) or three-dimensional [GOR 91].

The structure defines the neighbourhood size (i.e., number of individuals). Information interchange between all the population is guaranteed by the overlapping of the neighbourhood [GOR 91].

#### v) *Truncation selection*

In this technique only part of the population can be selected. The population is grouped by decreasing order of the individual objective function values and only the first  $N_{trunc}$  (a percentage of the total population, which generally stands between 10% and 50%) individuals are selected [BLI 95].

Although there have been efforts for developing strategies to compare the efficiency of the various selection techniques proposed, is not possible to define in advance the best selection technique to be used in a particular optimisation problem. Empirical studies on the real problem should therefore, be carried out [BLI 95].

### **B- Crossover**

This operator enables the production of two new chromosomes (offspring) of a new generation from two existing chromosomes in the current population (parents), by genes interchange between them. This interchange is carried out from one or more positions in the chromosome, thus defining the type of crossover to be applied:

- Crossover in one position;
- Crossover in multiple positions;
- Uniform crossover;

This is the most powerful process of information modification that GAs use for searching, since it allows a rapid exploration of the search space. As the information that passes to future

generations is obtained from individuals with greater performance, this is not a random search but explores the best regions of the search space [GOL 89a, BEA 93b].

i) *Crossover in one position*

As shown in Figure 2.10, a random position is selected in the parents chromosomes, the genes are exchanged between them and two individuals are created. In this example, crossover is carried out between two chromosomes of length 6 (0 to 5), between positions 3 and 4. Crossover only involves the exchange of genes in the chromosomes [GOL 89a].

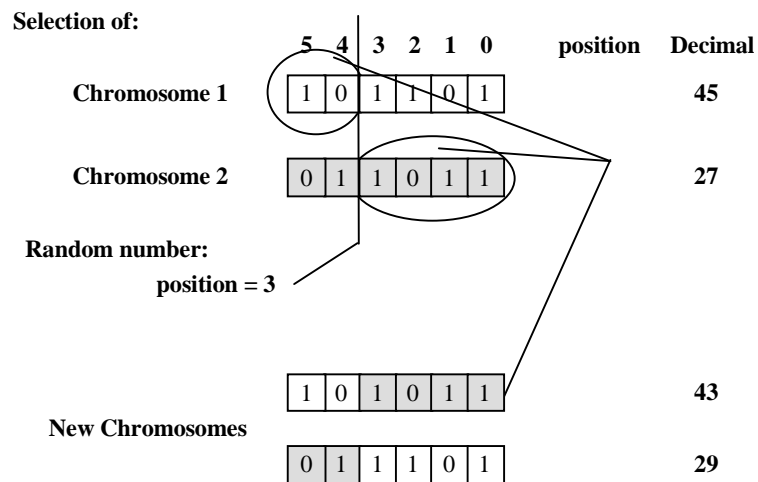


Figure 2.10- Example of crossover in one position.

ii) *Crossover in multiple positions*

In this case,  $m$  positions are picked randomly, from 1 until the maximum number of genes, without repetition. These positions are then ordered and the genes between the successive positions are interchanged [SPE 91]. Figure 2.11 exemplifies this process for the case of two positions ( $m = 2$ ). Crossover occurs between two chromosomes of length 6 (0 to 5), between positions 1 and 2 and between positions 4 and 5.

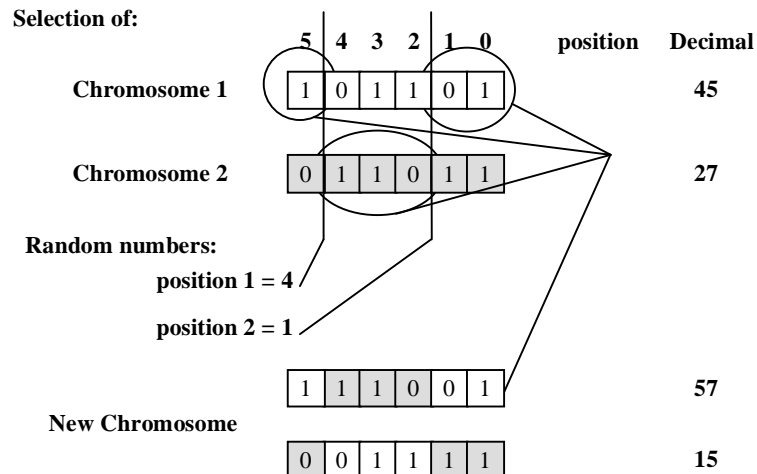


Figure 2.11- Example of crossover in two points.

### iii) *Uniform crossover*

Uniform crossover generalises the previous scheme, since each gene is a point for potential crossover. The concept is based on the random definition of two masks with the same number of genes as the chromosomes. Each mask gene identifies the parents that provide the gene for the offspring. Generally, the second mask is the inverse of the first one. Each gene of the new individual is equal to the corresponding gene of parent 1 if the gene of the mask is 1, and equal to the corresponding gene of parent 2 if the gene is 0 [BEA 93b, SYS 89]. Figure 2.12 illustrates this type of crossover. Offspring 1 remains with the genes of parent 1 when the corresponding position on the mask is 1, otherwise it will have the genes of parent 2.

Other crossover techniques have been proposed, but they have little application [GOL 85, SYS 91, DAV 91]. Despite several comparative studies [BEA 93b, SYS 89], it is difficult to define the best crossover technique for a particular problem, hence the choice of one method, as well as of the best crossover ratio, should be based upon experimental evaluation.

### C- *Mutation*

In this process, one chromosome position is randomly selected and the value of the gene is changed, thus causing the destruction of the existing information. The need for this operator comes from the fact that, along the various iterations relevant information may be lost when the worst chromosomes are eliminated. Through this occasional random change, GAs guarantee that new areas of the search space are explored [BEA 93b]. Due to their characteristic (destruction of information), the probability of occurrence of mutation must be lower, in the order of  $1/N$  [BÄC 91].

Selection of:	5	4	3	2	1	0	position	Decimal	
Chromosome 1	1	0	1	1	0	1		45	
Chromosome 2	0	1	1	0	1	1		27	
Random numbers:									
mask 1 =	0	1	1	0	0	0			
mask 2 =	1	0	0	1	1	1			
New Chromosomes	0	0	1	0	1	1		11	
	1	1	1	1	0	1		61	

Figure 2.12- Example of uniform crossover.

Figure 2.13 shows an example of mutation. First, a random number that defines the mutation position is selected. Then, another random number between 0.00 and 1.00 is obtained and compared with the **mutation ratio** (in this case **0.08**). If the number is smaller, then the gene in this position is subjected to mutation, i.e., a random integer number (**0** or **1**) is placed in the position previously selected (this means 50% of probability). Mutation only occurs if this last number is different from the gene in the selected position, and will only be carried out for a given number of chromosomes, defined for the **mutation rate** (considering a rate of **0.1**, the probability of mutation will be  $(0.1 \times 0.08 \times 0.5) \times 100 = 0.4\%$ ).

Selection of:	5	4	3	2	1	0	position	Decimal	
Chromosome	1	0	1	1	0	1		45	
Random numbers:									
position = 3									
n. between 0 and 1 = 0.05								Smaller than the mutation ratio = 0.08	
integer n. between 0 e 1 =									
New Chromosome	0	1	0	0	1	0	1	37	
or	1	1	0	1	1	0	1	45	

Figure 2.13- Example of mutation.

The theoretical demonstration of the efficiency of any of these techniques is yet to be done. In fact, the importance of crossover and mutation is still a matter of debate [SPE 93b].

## D- *Inversion*

Inversion produces the interchange of information inside one chromosome. It is used with the objective of reordering the genes inside the chromosomes, in order to increase the potential for evolution [GOL 89a, BEA 93b]. Two points of the chromosome are randomly selected and their genes are inverted, as illustrated in Figure 2.14. This operator is particularly useful when the objective function varies with time, which is not the case of polymer extrusion.

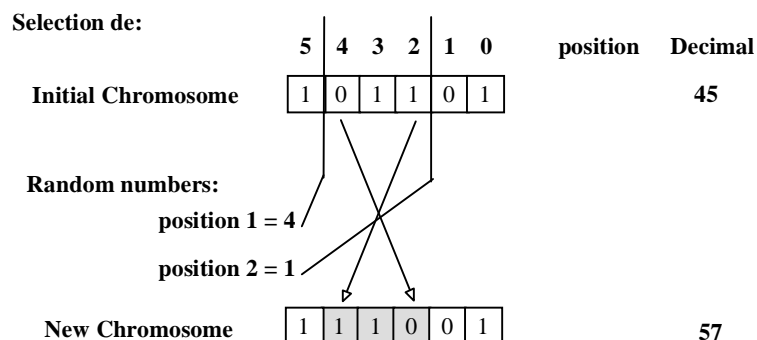


Figure 2.14- Example of inversion.

### 2.3.2- Sizing the population

Defining the population size (or length) to be used on a specific problem is of primal importance. A too small population does not process sufficient schemes to attain the optimum and may converge quickly to another point. On the other hand, the choice of excessive length results in a useless increase of the computation times [GOL 89b].

The population size depends essentially on the number of genes in the chromosomes (schemes) to be processed ( $l$ ) and on the degree of computer parallelism (algorithm) [GOL 89b, GOL 92].

Goldberg *et al.* [GOL 92] showed that the optimum population size depends also on the selection method used and on the characteristics of the specific problem under study (Table 2.9). De Jong and Spears [DeJ 90] confirmed these results and concluded that the choice of the population size has a strong interacting effect on the results. The number of individuals required for convergence is lower when the stochastic universal selection method is used, but this supremacy is offset by greater computational costs [GOL 92].

Most of these studies are empirical and limited to a particular type of problems. Thus, a practical assessment of the population size is required for each new particular problem.

**Table 2.9- Influence of the selection method on the population size (RW- roulette-wheel selection, TS- tournament selection, R- ranking e SUS- stochastic universal selection).**

$l$	$N$			
	RW	TS	R	SUS
20	109	54	109	21
50	271	135	271	82
200	1084	1084	1084	144

### 2.3.3- Niching and speciation

#### Multimodal functions

In most optimisation problems it is necessary not only to find the overall optimum, but also to identify the various local optima. Conventional GAs are not able to do this, since they converge necessarily to one point of the overall search space [GOL 89a].

As demonstrated in Figures 2.15 and 2.16 (representing the functions  $f_1(x) = \sin^6(5\pi x)$  and

$f_2(x) = e^{-2\ln 2 \left(\frac{x-0.1}{0.8}\right)^2} \sin^6(5\pi x)$ , in the interval  $0 \leq x \leq 1$ , respectively) the individual optima of

a multimodal function can have identical or different values. If GAs are applied repeatedly to determine of the maximum of the first function, they converge indifferently to any single peak. This happens because the population cannot have an infinite dimension, as assumed by the schemata theory. The problem is designated by “genetic drift” and can cause the accumulation of errors as the search proceeds [GOL 87]. However, convergence to a single peak is not desirable in functions with various similar maxima. Generally, when the search space has local maxima with different values, it will be interesting that convergence occurs to the peak with the greatest value, but also that a determined number of individuals converge for each individual peak. This is particularly important in the case of complex functions, as it provides the characterisation of their topography.

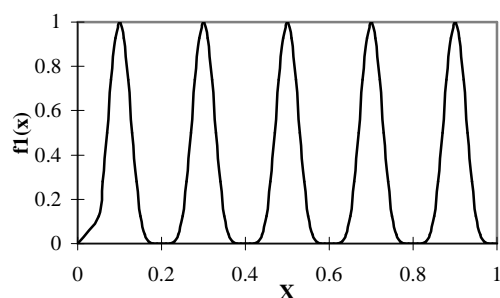


Figure 2.15- Multimodal function with maximum of equal values.

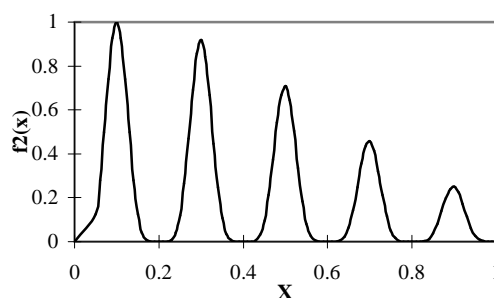


Figure 2.16- Multimodal function with maximum of different values.

In order to deal with the above, the concepts of **niching** and **speciation** of natural evolution should be introduced in a population of chromosomes. This is based on the idea of forming stable populations of organisms by creating separated niches where they are forced to **share** the available resources [GOL 87, DEB 89].

There are several niching methods that can extend the concept of GAs to domains that require the identification of multiple solutions. Mahfoud [MAH 95] compared four niching methods (sharing, crowding, sequential niching and parallel hillclimbing) and concluded that parallel hillclimbing fails on problems of high complexity, that sequential niching [BEA 93c] is weak on easy problems and unable to solve harder problems, that sharing [GOL 87] works well on problems with varying levels of complexity and that its performance can be improved through the application of fitness scaling, and finally, that deterministic crowding [MAH 92, MAH 94] is able to deal with problems of all levels of complexity, but it may lose the lower optima as the search proceeds. Therefore, sharing seems to be the most promising method.

Sharing analogue forms can be created through modifications to the theory of natural niche and specie formation. Goldberg and Richardson [GOL 87] proposed that they should be implemented in the chromosomes based on the distance between them  $d_{ij}$ , i.e., a sharing function,  $Sh(d_{ij})$ , should be defined as:

$$Sh(d_{ij}) = \begin{cases} 1 - \left( \frac{d_{ij}}{\sigma_{share}} \right)^\alpha, & \text{if } d_{ij} < \sigma_{share} \\ 0, & \text{otherwise} \end{cases} \quad (2.11)$$

where  $\alpha$  is a constant and  $\sigma_{share}$  is the radius of a circumference defining the maximum distance between chromosomes, in order to form as many niches as the number of peaks on the search space. The sharing function has three properties:

1.  $0 \leq Sh(d_{ij}) \leq 1, \forall d_{ij}$
2.  $Sh(0) = 1$
3.  $\lim_{d_{ij} \rightarrow \infty} Sh(d_{ij}) = 0$

Figure 2.17 illustrates this concept. The function  $f_i(x)$  considered in Figure 2.15 has 5 maxima in the search space ( $0 \leq x \leq 1$ ). The niche size is given by the ratio between the size of the search space and the number of peaks, i.e.,  $1/5=0.2$ ; consequently,  $\sigma_{share}$  is 0.1.

Since the basic idea of sharing is that the objective function of an individual diminishes in the presence of its neighbours, the final objective function value ( $FO'_i$ ) will result from the ratio between the initial evaluation ( $FO_i$ ) and its niche count ( $m'_i$ ).

$$FO'_i = \frac{FO_i}{m'_i} \quad (2.13)$$

where  $m'_i$  is the sum of all the sharing functions related to this individual.

$$m'_i = \sum_{j=1}^N sh(d_{ij}) \quad (2.14)$$

The sharing function with himself [ $sh(d_{ii})=1$ ] will be also included.

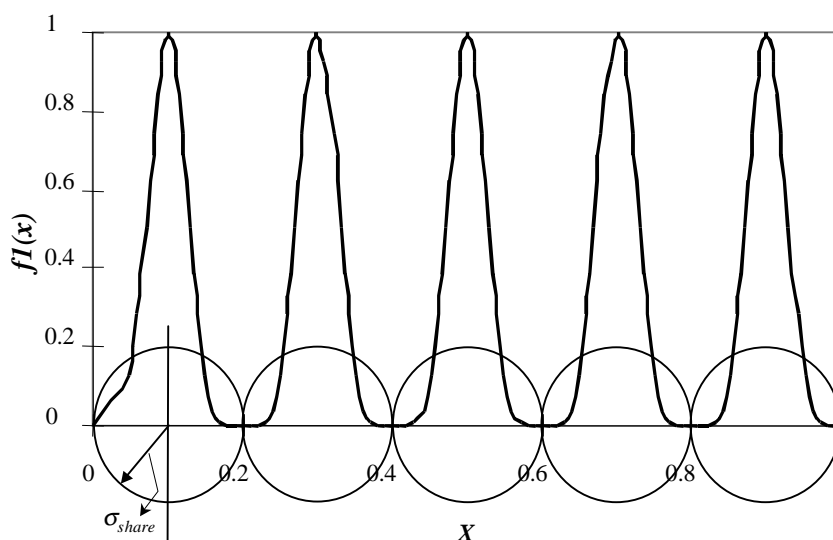


Figure 2.17- Definition of  $\sigma_{share}$  for implementing sharing.

The distance between individuals can be determined in the real parameter space, (**phenotypic sharing**) or in the codified space (**genotype sharing**). The former will be adopted, since it has physical meaning and greater performance (according to Deb [DEB 89]). Two individuals ( $X_i$  e  $X_j$ ) on a  $p$  dimensional space can be defined as:

$$X_i = [x_{1,i}; x_{2,i}; \dots; x_{p,i}] \quad (2.15)$$

$$X_j = [x_{1,j}; x_{2,j}; \dots; x_{p,j}]$$

The distance between them ( $d_{ij}$ ) can be defined using the norm on a  $p$  dimensional space, using the Euclidean distance.

$$d_{ij} = \sqrt{\sum_{k=1}^p (x_{k,i} - x_{k,j})^2} \quad (2.16)$$

In most practical optimisation problems,  $\sigma_{share}$  cannot be determined as easily as in the previous example (Figure 2.17). If each niche is contained in one  $p$ -dimensional space with radius equal to  $\sigma_{share}$ , this means that each sphere contains  $1/q$  of the total volume of the search space, where  $q$  is the number of peaks in that space. The sphere radius ( $r$ ) that contains the total space is therefore given by [DEB 89]:

$$r = \frac{1}{2} \sqrt{\sum_{k=1}^p (x_{k,max} - x_{k,min})^2} \quad (2.17)$$

and the volume ( $V$ ) is:

$$V = c r^p \quad (2.18)$$

where  $c$  is a constant and  $x_{k,min}$  and  $x_{k,max}$  are the minimum and maximum values for the parameter  $k$  in all the population, respectively.

The parameter  $\sigma_{share}$  may be calculated from [DEB 89]:

$$\sigma_{share} = \frac{r}{\sqrt[p]{q}} \quad (2.19)$$

where  $q$  is the number of peaks that are expected to exist.

If this analysis is applied to the function  $f_I(x)$  represented in Figure 2.17, with  $p=1$ ,  $x_{k,min}=0$ ,  $x_{k,max}=1$  and  $q=5$  one obtains  $r=0.5$  and  $\sigma_{share}=0.1$ .

Since in most optimisation problems the number of peaks is unknown, the use of the above methodology to define the value of  $\sigma_{share}$ , implies the use of a trial and error procedure.

Sharing can be indistinctly applied in the space of the variables to optimise, or in the criteria space, depending on which niching is necessary. Generally it is applied in the criteria space, where the choice of the solution is carried out and where diversity along the Pareto frontier is required.

During sharing process, scaling of all space parameters in the same interval (for example between 0 and 1) is indispensable in order to avoid the comparison between values that can be very different. For example, if in a polymer extrusion problem only the output and the power consumption are considered as relevant criteria, with their value ranging between 2 and 10kg/hr and between 1000 and 3000W, respectively, and if 4 peaks exist, the value of  $\sigma_{share}$ , becomes 500.004. As shown in Figure 2.18-A one unique niche comprises the entire range of the output parameter. Conversely, if both parameters are scaled between 0 and 1, the value of  $\sigma_{share}$  is  $\sqrt{2}/4$ , which corresponds to the radius of the circumferences shown in Figure 2.18-B.

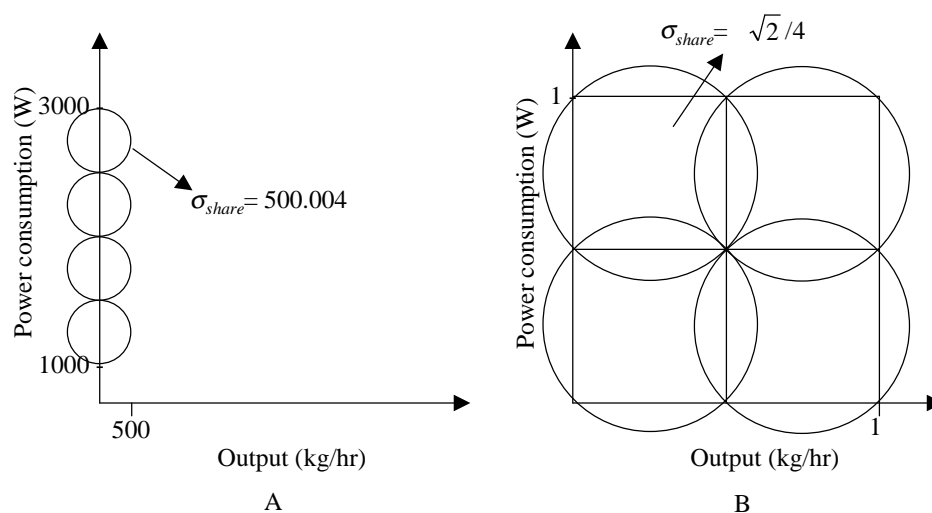


Figure 2.18- The importance of scaling the variables.

As  $\sigma_{share}$ , the  $\alpha$  parameter (equation 2.11) controls the radial size of the niche “radius” (see Figure 2.19) [GOL 87, HOR 93].

The variation of the degree of the Holder metric used in the equation 2.16 changes the shape of the niche [HOR 94]:

$$d_{ij} = \left( \sum_{k=1}^p |x_{k,i} - x_{k,j}|^s \right)^{1/s} \quad (2.20)$$

where  $s$  is the metric degree. Figure 2.20 shows the variation of the niche shape in two-dimensional space with the value of  $s$ .

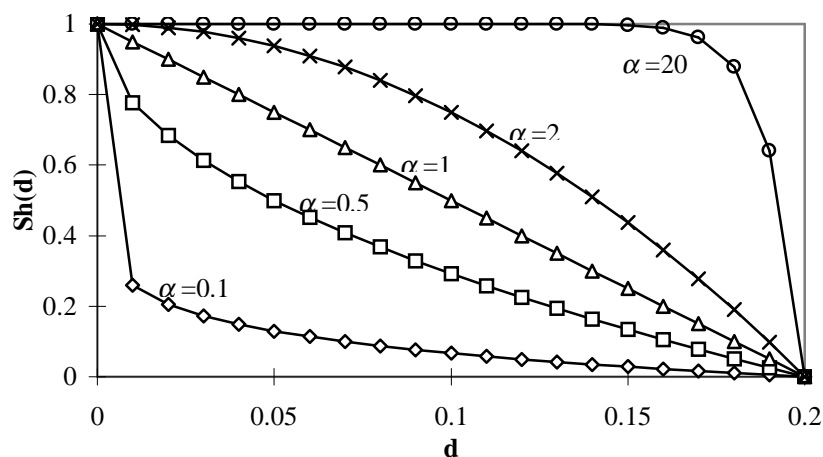


Figure 2.19- Influence of  $\alpha$  on the sharing function.

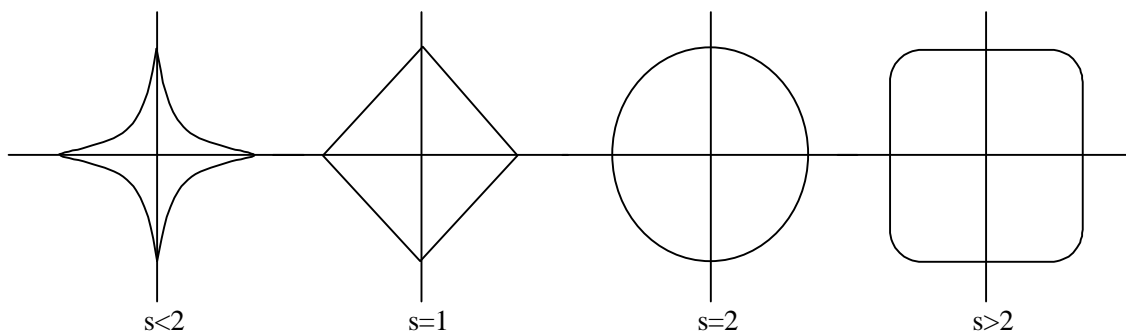


Figure 2.20- Niche shapes as a function of Holder metric, in two dimensions.

When optimising multimodal functions, the performance of the genetic algorithm could be affected when crossover is applied between individuals from different peaks, as the new individuals generally do not belong to any of them. This can be avoided by reducing the frequency of crossover between the individuals of different peaks. A new parameter  $\sigma_{mating}$ , similar to  $\sigma_{share}$ , does not allow crossover between individuals whenever the distance between themselves is greater than  $\sigma_{mating}$ ; since  $\sigma_{mating}$  belongs to the same space that  $\sigma_{share}$  (and is also a measure of the distance between two individuals), these parameters can be identical [GOL 89a, FON 93, DEB 89, MAH 94].

#### 2.4- Objective function

**The optimisation of polymer plasticating extrusion is a multiobjective problem, where it is necessary to satisfy simultaneously several system performance measures (criteria, attributes or objectives), such as output, length of screw required for melting, melt temperature, power consumption, degree of mixture. Some of these are conflicting, e.g., maximise the output and minimise the power consumption simultaneously.**

**Moreover, their relative importance to the global process performance is subjective and can be considered differently. The mathematical formulation of a multiobjective optimisation problem (by modification of equation 2.1)**

$$\begin{aligned} & \text{is:} \\ \text{maximise} \quad & f_m(x_i) \quad i = 1, \dots, N; \quad m = 1, \dots, M \quad (2.21) \\ \text{subject to} \quad & g_j(x_i) = 0 \quad j = 1, \dots, J \\ & h_k(x_i) \geq 0 \quad k = 1, \dots, K \end{aligned}$$

where  $M$  is the number of criteria to satisfy.

The various objectives can be taken into account in two ways. Usually, a global objective function, that includes all the criteria, is considered. However, the decision-maker may be interested in obtaining if possible several alternative solutions. Other methods have been developed for this purpose, taking advantage from the fact that GAs work with a population of individuals [GOL 89a, FON 93, HOR 94, SRI 95].

### **i) Global objective function methods**

In this case the individual criteria are combined in order to form a global objective function with one unique value. The global objective function can be calculated using various possibilities, such as the weighted sum of the criteria, the distance between the criteria, the Min-Max formulation [SRI 95] and the product of the criteria [POT 93, POT 94, POT 96, POT 97].

The weighted sum of the criteria is obtained from [SRI 95]:

$$FO_i = \sum_{j=1}^q w_j F_j \quad (2.22)$$

where  $q$  is the number of criteria,  $w_j$  is the weight attributed to each criterion (which can vary between 0 and 1, with  $\sum w_j = 1$ ) and  $F_j$  is the objective function of criterion  $j$ , which can take two forms, depending whether one wishes to maximise or to minimise the criterion  $X_j$ :

$$F_j = \frac{X_j - X_{j_{\min}}}{X_{j_{\max}} - X_{j_{\min}}} \quad (2.23)$$

$$F_j = 1 - \frac{X_j - X_{j_{\min}}}{X_{j_{\max}} - X_{j_{\min}}} \quad (2.24)$$

$X_j$  is the value that results from the evaluation of the criterion  $j$ , while  $X_{jmin}$  and  $X_{jmax}$  are the minimum and maximum values that this criterion can take, respectively. By definition, each individual objective function value ranges between 0 and 1 and, consequently, so does the value of the global objective function. The reduction of all values to the same non-dimensional scale is, therefore, assured.

The global objective function can also be a measure of the distance between the values of the individual objective functions and a demand-level vector ( $y_j$ ), which has to be defined by the decision-maker:

$$FO_i = \left[ \sum_{j=1}^q |F_j - y_j|^r \right]^{1/r} \quad (2.25)$$

where  $r$  is the metric constant ( $1 \leq r < \infty$ ). Usually a Euclidean metric ( $r = 2$ ) is used.

The Min-Max formulation can be presented by modifying equation 2.21 [SRI 95]:

$$\text{maximise } \Gamma = \min |Z_j| \quad j = 1, \dots, q \quad (2.26)$$

where  $Z_j$  is determined by:

$$Z_j = \frac{F_j - y_j}{y_j} \quad (2.27)$$

Potente *et al.* [POT 93, POT 94, POT 96, POT 97] considered the product of individual performance criteria to quantify the global performance of polymer extrusion, in order to avoid the possibility of solutions where any of the single criteria might take a zero value:

$$FO_i = \sum_j^{a_j} \sqrt{\prod_j q_j^{a_j}} \quad (2.28)$$

where  $a_j$  are the weight factors and  $q_j$  are the individual quality criteria.

In this work the weighted sum of the criteria will be used. Since this formulation is probably the simplest, easily takes into account the relative importance of all criteria and scales all space parameters in the same interval (as will be necessary when sharing is applied).

## ii) Pareto Optimum

In a typical multiobjective optimisation, there is a set of solutions that is better than the others when all the objectives are considered simultaneously, but can be worse than some if only specific criteria are considered. Therefore, a solution corresponding to the optimum of all the criteria does not exist in a problem of this type. The concept of **Pareto optimal** or **non-dominated** solutions [GOL 89a, FON 93, HOR 94, SRI 95] is illustrated in Figure 2.21 considering, as an example, two individual criteria relevant to extrusion. If both objectives are to be minimised, point 5 is dominated by point 2, since it represents a condition where both criteria are greater. Therefore, points 5 and 6 are dominated, whereas points 1, 2, 3 and 4 are non-dominated, and make-up the Pareto frontier.

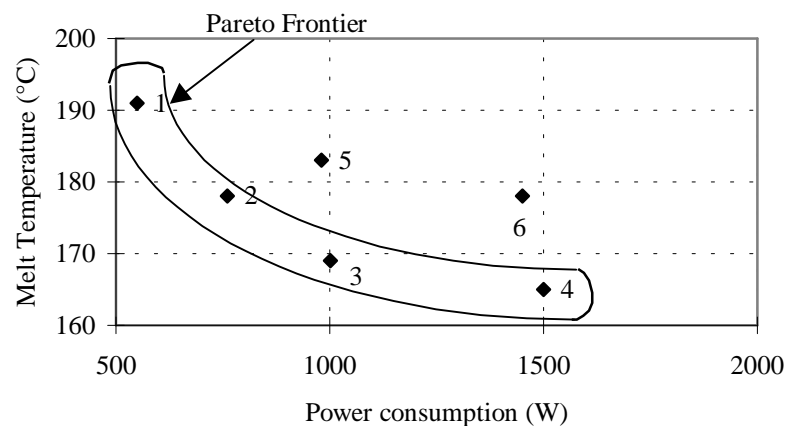


Figure 2.21- Pareto frontier.

## 2.5- Multiobjective optimisation

The concept of non-dominated solutions can be used together with GAs to obtain, simultaneously, several solutions along the Pareto frontier. Selecting one solution along the Pareto frontier requires that the user has some knowledge about the factors that influence the problem. The choice made by one user is not necessarily coincident with the choice of another. Based on the initial idea proposed by Goldberg [GOL 89a], several multiobjective optimisation methods have been developed [FON 93, HOR 94, SRI 95]. They require that the conventional GA be modified in such a way that:

- i) Each individual is evaluated independently in each criterion.

- ii) The selection is made independently in each criterion; several methods, such as **tournament selection** or **ranking schemes** [FON 93, HOR 94, SRI 95] can be adopted. It is necessary to consider the concepts of niching and speciation in order to distribute the population evenly throughout the entire frontier [GOL 87].

Crossover and mutation between individuals are made according to previous selection schemes.

#### i) Method based on ranking schemes

The method proposed by Fonseca and Fleming [FON 93] is based on the attribution of a value to the objective function of each individual through a ranking scheme. Accordingly in each generation position 1 on the scale is attributed to the non-dominated individuals, while the remaining are classified in terms of the number of individuals that dominate them. This is equivalent to writing:

$$rank_i = 1 + n_i \quad (2.29)$$

where  $rank_i$  represents the position of the individual  $i$  on the ranking and  $n_i$  is the number of individuals that dominate  $i$ .

This attribution follows various stages:

- a) The population is ordered following the ranking described above;
- b) The value of the objective function is attributed by interpolating between the “best” ( $rank=1$ ) and the “worst” ( $rank=n*\leq N$ ) individuals, using a ranking function (equation 2.8 or 2.9);
- c) The average value of the objective function is computed from the individuals with the same rank;
- d) Niche count (equation 2.13) is incorporated on the above objective function value, in order to place the individuals inside each rank; consequently, convergence to a unique point is avoided;
- e) Finally, a selection method is applied (e.g. roulette-wheel selection) in order to obtain an individual for reproduction and/or recombination;
- f) The procedure follows the conventional GA route.

#### ii) Method based on tournament selection

Horn, Nafpliotis and Goldberg [HOR 94] modified the tournament selection technique in order to avoid convergence to a single solution, and to maintain multiple non-dominated solutions. This modification was carried out adding tournament by domination followed by sharing whenever it was not possible to choose a parent (solution of the actual population) for reproduction and/or recombination. This selection process follows five steps:

- a) Two individuals are randomly chosen;
- b) A set of individuals ( $t_{dom}$ ) is also chosen randomly for comparison purposes;
- c) Each of the two candidates is compared with the set;
- d) If one of the candidates is dominated by the set and the other is not, the latter is chosen;
- e) If none of them is dominated, sharing is used to choose the winner (the individual with smaller niche count -  $m_i'$ ).

The size of the comparison set ( $t_{dom}$ ) controls the selection pressure. The efficiency of this algorithm depends on the relation between the sharing pressure and the selection applied. Sharing is applied on the attribute space where diversity is desirable.

### iii) Method based on non-dominated sorting

Similarly to the method based on ranking schemes, the basic idea is to use the ranking selection scheme to emphasise the influence of better points, while sharing is used to maintain a stable distribution along the Pareto frontier [SRI 95].

As in the previous algorithms, this method differs from a traditional GA on the selection operator working mechanism. The steps for the selection phase are:

- a) To identify the non-dominated population individuals (that will constitute the first individuals front,  $front = 1$ );
- b) To attribute an objective function value according to the front number (the first will have the highest value) and identically to all the individuals of the same front;
- c) To maintain the diversity, the individuals of this front will be subjected to sharing, i.e., the objective function value will be divided by the niche count;
- d) To proceed to the next front:  $front = front + 1$ ;

- e) To identify the non-dominated individuals of the current population, ignoring for the time being those that have been already classified;
- f) Repeat steps b) to e) while individuals to be classified still exist;
- g) To proceed according to the usual methods of selection, crossover and mutation.

### 2.5.1- Reduced Pareto set

The result of a multiobjective optimisation method using GAs is the Pareto frontier, which usually contain a large number of points (e.g. 500 points). The practical use of this optimal Pareto frontier is reduced if it becomes too problematic to identify the preferred solution from this set of points. Figure 2.22-A illustrates one result with a multiobjective optimisation method applied to the optimisation of the extrusion process where the aim was to minimise melt temperature at die outlet and mechanical power consumption. After reducing the number of points in the frontier (Figure 2.22-B), while maintaining all its characteristics intact, the choice of the optimal point can be easily made, considering the relative importance of the two criteria (the points 1 to 5 are the non-dominated ones).

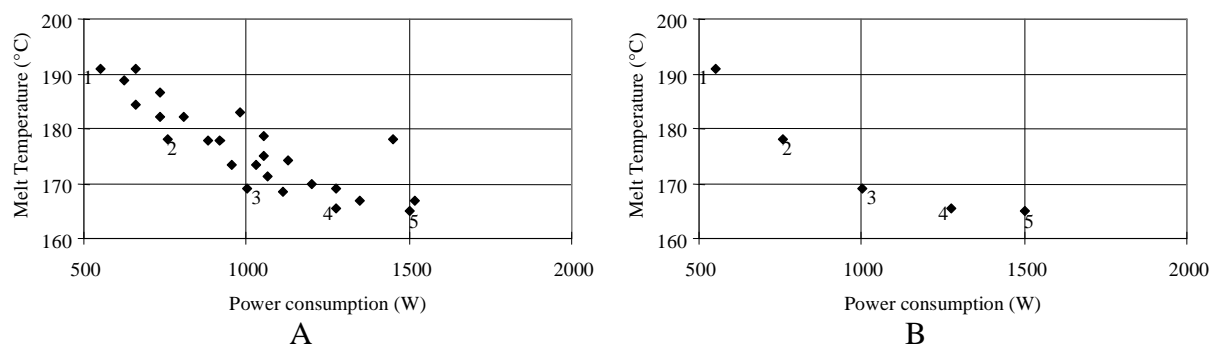


Figure 2.22- Example of reducing the Pareto frontier.

The multiobjective optimisation methods described previously, based on the attribution of an objective function value to the individuals from the set of non-dominated points, have limited application to problems with many criteria, where most points that define the population in each generation are non-dominated. For example, in Figure 2.22-A some of the points presented are dominated, since only two criteria are defined; however, if other criteria were to be considered, these dominated points could be non-dominated in the corresponding Pareto frontiers. Therefore, when a multiobjective optimisation method with GAs is applied the probability that all the individuals of the population will be selected for reproduction is similar, since the selection phase of the above methods is based on the whether the individuals

are non-dominated or not. Pareto frontier reduction together with a multiobjective optimisation algorithm will be very useful, since it provides a clearer separation of the individuals.

Pareto set reduction [ROS 85], based on the clustering of solutions, can be incorporated in two steps of a GA multiobjective optimisation: during the selection of individuals for reproduction and recombination and at the end, for the choice of the preferential solution from the Pareto set obtained.

The method proposed by Roseman and Gero [ROS 85] produces the clustering of solutions that can be considered similar between themselves, in all or in some criteria. Then, inside the groups, the solutions that show to have preferential characteristics are selected. The technique consists in comparing the proximity of solutions on the hyper-space, i.e., the similitude or proximity of two solutions is evaluated through some kind of measure of the distance between them by the aggregation of the various distances in each criteria. The technique used for clustering the solutions was the Complete-linkage method [ROS 85]. It is essential to define an indifference limit, above which the performance of the solutions is considered as similar. This limit, that can be distinct for each criterion, is defined as the percentage of the distance between adjacent groups relative to the total distance (between extreme groups). The algorithm involves the sequence illustrated in Figure 2.23.

Table 2.10 presents an example where the Pareto set contain 5 different polymer extrusion operating conditions (A, B, C, D and E) with performance measures in two criteria (melt temperature and power consumption to be minimised).

Assuming that 10% is an acceptable percentage difference limit for each objective, the groups are sorted in ascending performance order and the initial differences are computed – steps a) to e) of Figure 2.23 (see Table 2.11).

- a) For each objective sort the solutions by ascending order.
- b) For each objective, every solution is treated as one group (one solution per group, except in the case of equal solutions).
- c) In the case of equal solutions, maintain one solution by group, referencing the solution that is kept.
- d) For each objective ( $C_j$ ), calculate the maximum amplitude [ $Range(C_j)$ ]:
- $$Range(C_j) = Max(C_j) - Min(C_j) \quad (2.30)$$
- e) For each objective calculate the differences ( $d_{ij}$ ) between each adjacent group ( $k$  and  $k+1$ ). The differences between adjacent groups are calculated as a percentage of the interval of existent values for each objective. The minimum difference is the ratio of the difference between adjacent groups over the pre-defined difference limits for each objective.
- $$Dif(C_j, k) = \frac{Max(C_j, k+1) - Min(C_j, k)}{Range(C_j)} \quad (2.31)$$
- f) Select the absolute minimal difference.
- g) If this difference exceeds the limit for each objective, select the next minimum difference. If all the limits have been exceeded, the algorithm ends.
- h) Merge the groups whose difference is below the limits for the respective objective.
- i) Recalculate the differences for this objective.
- j) If any solution of the assembled groups is dominated, eliminate this solution. If not, return to step f).
- k) If the number of solutions/groups that remain non-merged is greater than the number of required solutions/groups, return to step f).

Figure 2.23- Algorithm for the reduction of the Pareto set.

**Table 2.10- Pareto optimal set for extrusion example.**

<u>Operating Condition</u>	Melt Temperature (°C)	Power Consumption (W)
A	192	560
B	178	770
C	169	1000
D	165	1450
E	166	1500

**Table 2.11- Example of Pareto set reduction:  
Values sorted and grouped in each objective – 1<sup>st</sup> iteration.**

Group	C1 – Melt temperature (°C)			C2 - Power consumption (W)		
	Operating Conditions	Values	Difference (%)	Operating Conditions	Values	Difference (%)
1	A	192	51.9	E	1500	5.3
2	B	178	33.(3)	D	1450	47.9
3	C	169	11.(1)	C	1000	24.5
4	E	166	3.7	B	770	22.3
5	D	165		A	560	

After the first iteration the minimum difference found in criterion C1 is 3.7% – i.e., step f), between groups 4 and 5, and since it is lower than 10% - step g). The next stage is to merge these groups – step h), and check for domination between them (Table 2.12) – step j). Operating condition D is non-dominated by E, since it has a higher performance in criterion C2, i.e., a higher group, then this solution is not eliminated – step j).

**Table 2.12- Example of Pareto set reduction:  
Check for domination – 1<sup>st</sup> iteration.**

Operating Condition	Groups	
	C1	C2
E	-	1
D	-	2

After the 2<sup>nd</sup> iteration the differences for criterion C1, where the groups 4 and 5 are linked, needs to be recalculated (Table 2.13) – step i).

**Table 2.13- Example of Pareto set reduction:  
Values sorted and grouped in each objective – 2<sup>nd</sup> iteration.**

Group	C1 – Melt temperature (°C)			Group	C2 - Power consumption (W)		
	Operating Conditions	Values	Diff. (%)		Operating Conditions	Values	Diff. (%)
1	A	192	51.9	1	E	1500	5.3
2	B	178	33.(3)	2	D	1450	47.9
3	C	169	14.8	3	C	1000	24.5
4	E	166		4	B	770	22.3
4	D	165		5	A	560	

The minimum difference in criterion C2 is now 5.3% between groups 1 and 2, i.e., operating conditions E and D. Merging groups 1 and 2 and checking for domination is carried out (Table 2.14). In this case operating condition E dominates operating condition D, since they belong to the same group in criterion C1, i.e., operating condition D will be eliminated in all criteria.

**Table 2.14- Example of Pareto set reduction:  
Check for domination – 2<sup>nd</sup> iteration.**

<u>Operating Condition</u>	Groups	
	C1	C2
E	4	-
D	4	-

After recalculating the differences, the results are presented in Table 2.15. The minimum difference found is now 14.8%, which is greater than the pre-defined acceptable limits (10%) – step k), hence the process stops. The operating conditions A, B, C and E define the new reduced Pareto frontier.

**Table 2.15- Example of Pareto set reduction:  
Values sorted and grouped in each objective – 3<sup>rd</sup> iteration.**

Group	C1 – Melt temperature (°C)			Group	C2 - Power consumption (W)		
	Operating Conditions	Values	Diff. (%)		Operating Conditions	Values	Diff. (%)
1	A	192	51.9	1	E	1500	53.2
2	B	178	33.(3)		D	1450	
3	C	169	14.8	2	C	1000	24.5
4	E	166		3	B	770	22.3
	D	165		4	A	560	

### Using the reduction of Pareto set with the GAs

The fundamental objective of multiobjective optimisation with GAs is to distribute the population uniformly along the Pareto frontier and simultaneously to promote the progressive displacement of this frontier towards the improvement of the individual objectives [GOL 89a, FON 93, HOR 94, SRI 95].

Starting with a set of solutions on the Pareto frontier, in any given generation, the method reduces the number of solutions on the efficient frontier, while maintaining the characteristics of the original set. This feature can be incorporated in multiobjective optimization with GAs, by modifying the traditional algorithm in order to include the Pareto set reduction in each generation and to define a ranking scheme of the solutions that considers this reduction. The number of individuals that belong to the Pareto frontier ( $N$ ) is reduced according to a pre-defined number of ranks ( $k = 1, 2, \dots, N\_Ranks$ ). The objective function value is calculated according to the sequence described in Figure 2.24.

- a) Pre-define the number of required ranks,  $N\_Ranks$ ;
- b) First iteration,  $k=1$ ;
- c) While  $k < N\_Ranks$  do:
  1. Reduce the population down to  $k \left( \frac{N}{N\_Ranks} \right)$  individuals
  2. For all the remaining individuals that do not have yet a rank from previous iterations, do  $Rank_k = k$ ;
  3. Go to the next generation,  $k = k + 1$ ;
- d) Assign the individuals to be classified as:  $Rank_i = N\_Ranks$ ;
- e) Calculate the objective function value from this ranking, using equation 2.8 or 2.9, where  $N$  is replaced by  $N\_Ranks$  and  $i$  by  $Rank_i$ ;
- f) Select the individuals for reproduction by one of the available methods (e.g. roulette-wheel selection).

Figure 2.24- Reduced Pareto set with GAs.

This algorithm can also include sharing for a more uniform distribution of the population along the Pareto frontier. In this case, an additional step is inserted between steps e) and f) of Figure 2.24, using equation 2.13 to calculate a new value for the objective function. The selection pressure can be controlled by the value of  $N\_Ranks$  (the smaller this value, the greater the selection pressure), which ranges between 2 and  $N$ . The determination of a precise value requires an empirical study; acceptable values, that do not alter significantly the performance of the algorithm, are usually situated between 10% and 50% of  $N$ .

This algorithm does not require scaling objective values during the Pareto set reduction. Another advantage is the use of a unique parameter,  $N\_Ranks$  (if sharing is not considered) which is easy to determine.



### 3- MODELLING OF SINGLE SCREW EXTRUSION

#### 3.1- Introduction

In a typical single screw extruder an Archimedes type screw rotates inside a heated barrel. The screw has (at least) three distinct geometrical sections (figure 3.1): the feed zone, where the channel depth is constant ( $H_1$ ); the compression zone, where the channel depth changes along the axis; and the metering zone, where the channel depth is again constant but smaller ( $H_2$ ).

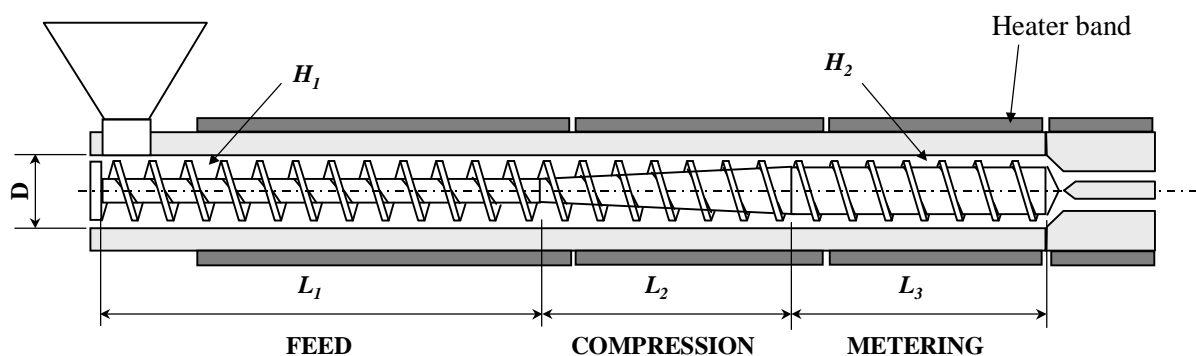


Figure 3.1- Typical single screw extruder.

As stated previously, the objective of this work is to optimise automatically this process through the use of an optimisation algorithm (GAs), i.e., to define the processing conditions (screw speed and barrel temperature profile), or the screw geometry that produce the best system performance. Since, the inverse formulation of this process cannot be explicitly obtained and the solution is probably not unique, the use of an optimisation scheme, like the illustrated by figure 2.1, is adopted. The process modelling package has as input data the polymer properties, screw geometry and processing conditions, and its results (output, melt temperature, length of the screw required for melting, power consumption and degree of mixing) are used to quantify the process performance. The theoretical model must be sensitive to changes on the input data, able to predict the required performance parameters and, simultaneously, must produce results with low computation times (given the intense use required by the optimisation algorithm).

The ability to produce reliable performance parameters and the sensitivity to the input data are usually accomplished via elaborate theoretical mathematical models, which make use of sophisticated, but time consuming, numerical schemes such as finite elements [VIR 84, ZHU 91, PAL 72a, PAL 72b, KIM 95, CHA 95, GHO 96, BRO 97]. Conversely, analytical models [AGA 96, DAR 56, TAD 70, BRO 72, TAD 67, GRI 62], produce results more

quickly but with less accuracy, since the resolution of the constitutive equations is made with some important simplifications. Thus, a compromise between these two approaches must be found. Results such as output, melt temperature, melt temperature distribution, power consumption, solid profile, length of screw required for melting, degree of mixing, residence time distribution, pressure profile, are required for a relevant optimisation. For that, numerical models based on finite differences [TAD 72, ELB 84, LIN 85a, FEN 77] will be used whenever possible. Since their computation time is incomparably lower than the obtained with finite elements. The objective of this chapter is to present and discuss the computer implementing of the mathematical models adopted for each functional zone (see figure 2.1). These individual zones will be considered sequentially and their boundary conditions will be discussed. A global model of the extrusion process, where the aim is the determination of the operational point for a given extruder/die combination will be adopted.

### 3.2- Extruder geometry

Figure 3.2 illustrates a portion of the screw and barrel that is used to define the geometry of a single screw extruder. The internal barrel diameter is  $D_b$ , the internal and external screw diameters are  $D_i$  and  $D_s$ , respectively, and the screw pitch is  $S$ . The channel depth  $H$ , is given by:

$$H = \frac{D_b - D_i}{2} \quad (3.1)$$

The flight clearance is  $\delta_f$ . The helix angle,  $\theta$ , and the channel width,  $W$  vary in the radial direction (at the root of the screw,  $\theta_s$  and  $W_s$ , at the barrel surface,  $\theta_b$  and  $W_b$ ) respectively:

$$\theta_s = \arctg\left(\frac{S}{\pi D_i}\right) \quad (3.2)$$

$$\theta_b = \arctg\left(\frac{S}{\pi D_s}\right) \quad (3.3)$$

$$W_s = S \cos \theta_s - e \quad (3.4)$$

$$W_b = S \cos \theta_b - e \quad (3.5)$$

The flight width,  $e$ , is measured in a direction normal to the flights (as the channel width). Generally, the number of screw flights in parallel,  $p$ , is 1. The channel depth varies in the compression zone of the screw, between  $H_1$  and  $H_2$ :

$$H_2 = H_1 - A L_2 \quad (3.6)$$

$A$  is the slope of the taper.

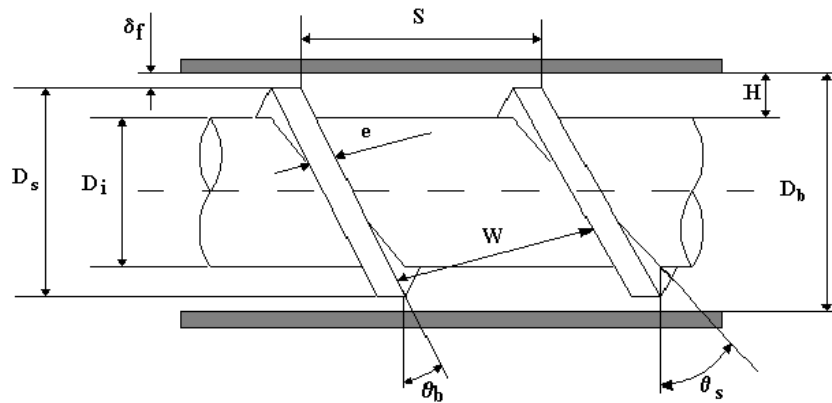


Figure 3.2- Geometry of an extruder screw.

Modern extruders have a number of additional features such as grooved barrel sections, distributive and dispersive mixing sections and barrier screws [RAU 86]. Only the grooved barrel will be considered in this work. The grooves can be longitudinal or helicoidal (figure 3.3). The groove width is  $b_n$ ; the height ( $h_n$ ) is not constant, but decreases linearly from a maximum value at the beginning ( $h_{n0}$ ) to zero.

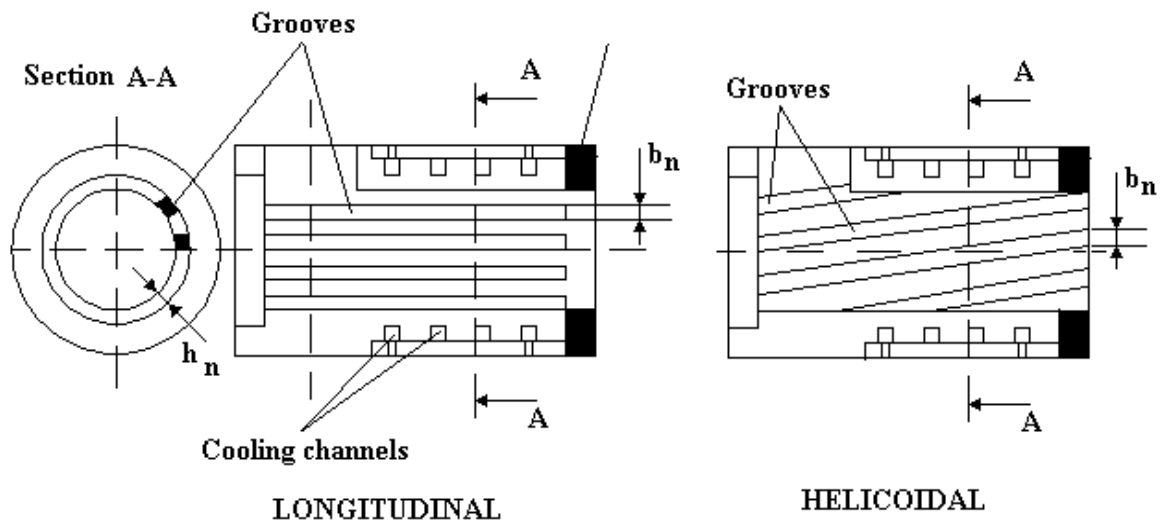


Figure 3.3- Barrel section with longitudinal and helicoidal grooves.

Modelling plasticating single screw extrusion implies necessarily that a number of simplifications need to be made. Some of these are associated with the geometry of the screw channel and to the cinematic conditions [TAD 70]:

- a) The channel can be unrolled and treated as a rectangular cross section, so that Cartesian coordinates are used.

The error introduced by this approximation is negligible, since the channel depth is much smaller than the screw diameter [TAD 70, FEN 79, STE 95]. Therefore, the channel width and the helix angle become constants given by their average values,  $\bar{W}$  and  $\bar{\theta}$ , respectively (equations 3.7 and 3.8).

$$\bar{W} = \frac{W_b + W_s}{2} \quad (3.7)$$

$$\bar{\theta} = \frac{\theta_b + \theta_s}{2} \quad (3.8)$$

- b) The screw is stationary and the barrel rotates.

This simplification is usually adopted since it is easier to visualise and study the extrusion physical phenomena. Tadmor and Klein [TAD 70] discussed this assumption for melt flow in the melt conveying zone. They proved that the tangential velocity profile of an isothermal Newtonian fluid flowing between two infinitely long concentric cylinders, is identical, regardless whether it is the inner or the outer cylinder that rotates, i.e., they concluded about the legitimacy of this assumption. More recently, Rauwendall *et al.* [RAU 98] proved experimentally that this assumption is justified. They derived analytical equations for the flow of a Newtonian fluid in a single screw extruder using two geometrical systems (flat plate and cylindrical) and two cinematic conditions (rotating barrel and rotating screw). They concluded that the velocities and the pressure gradients are exactly the same for the cylindrical system and that for the flat plate system the differences are insignificant if the channel depth is small relatively to the barrel diameter ( $H < 0.2D$ ).

Hence, one can define a barrel velocity ( $V_b$ ) and its components ( $V_{bx}$  and  $V_{bz}$ ) on a Cartesian system (figure 3.4).

$$V_b = \pi N D_b \quad (3.9)$$

$$V_{bz} = V_b \cos \theta_b \quad (3.10)$$

$$V_{bx} = V_b \sin \theta_b \quad (3.11)$$

where  $N$  is the screw speed.

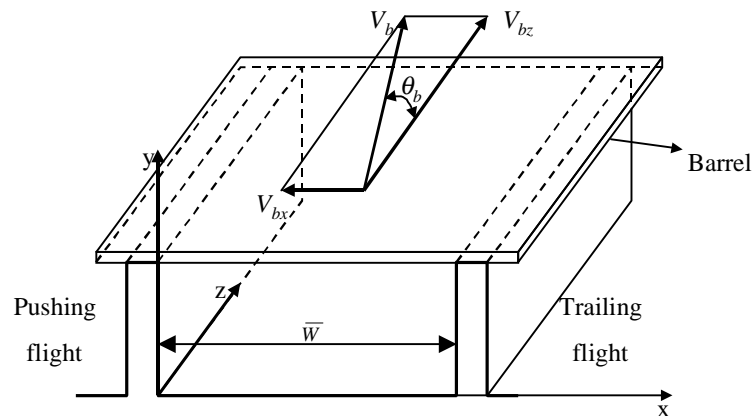


Figure 3.4- Barrel velocity components.

### 3.3- Solids conveying

The solids conveying zone extends from the hopper until the location, on the screw, where the first polymer pellets melt.

## HOPPER

The hopper of an extruder is generally constituted by a sequence of vertical and/or convergent columns. The pellets are transported to the screw by the action of gravity. During this process a stress field is developed in the pellets, which depends on the working conditions, static (hopper closed, during the initial loading) or dynamic stress fields (hopper open, during the discharge), figure 3.5 [WAL 66, WAL 73, THO 95]. In dynamic conditions two types of flow can occur (figure 3.6), funnel flow or mass flow [THO 95], which depends on the converging wall slop. The funnel flow occurs when the slop is shallow, this type of flow is undesirable, and on the contrary the mass flow will occur when the hopper walls are sufficiently smooth. Generally, the hopper on the extrusion process works open but in quasi-static conditions [WAL 66, WAL 73].

The pressure at bottom of the hopper is often considered as an initial condition for the calculations on the solids conveying zone on the screw. It may be estimated by performing a force balance on an elemental horizontal slice of bulk solids material [WAL 66].

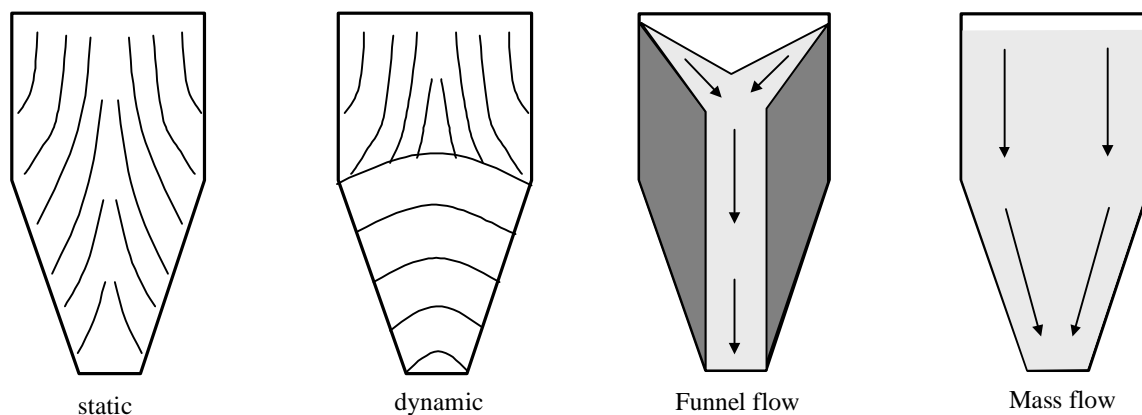


Figure 3.5- Stress fields for static and dynamic conditions.

Figure 3.6- Flow types for dynamic conditions.

## SCREW

The solids conveying zone has received less attention in comparison with the melting and melt conveying zones [AME 89]. This is probably due to the difficulties associated namely in considering that the solid bed does not behave as consistent block, as well as in determining some important polymer physical proprieties (such as bulk density and coefficients of friction) which depend on process variables like temperature, velocity and local pressure.

One of the first attempts to model this zone was carried out by Darnell and Mol [DAR 56], who assumed that the flow of solids (i.e., the movement of a non-deformable elastic solid bed) results from the difference between the friction forces acting on the screw surface and barrel surfaces. Subsequent studies have been proposed, extended this analysis and considered motion due to shear rates in polymer melt films surrounding the solid, non-isothermal conditions, two-dimensional solid bed and fluid containing solid particles [CHU 71, BRO 72, TAD 72, LOV 73, ATT 80]. The model developed by Tadmor and Broyer [TAD 72] deserves a special note, since the original Darnell and Mol's analysis was extended to include the thermal effects that take place on the solid bed, particularly closer to the screw and barrel surfaces.

This decade witnessed new theoretical and experimental studies. After verifying experimentally that the pellets do not behave generally as a coherent bed, some authors [ZHU 91, FAN 91] developed a theoretical model based on finite elements, which takes this fact into consideration, but that introduces also four new material parameters that are difficult to determine in practice. The Spalding and Hyun group developed a non-isothermal model for starve-fed and for flood-fed extruders [STR 92, HYU 97]. A device for measuring solids

conveying rates as a function of barrel and screw temperatures, screw speed, and discharge pressure was developed [HYU 96]. The results obtained with this model are compared with experimental and theoretical data. The results seem to be reasonable, but they need some additional work in order to be validated. Recently Campbell *et al.* [CAM 95, YAM 98] proposed a model assuming that the solid bed behaves as an elastic fluid. The model remains to be completed and validated. Finally, Spalding *et al.* developed methods that allow the quantification of the bulk density and the friction coefficients as a function of temperature, velocity and pressure, which are tested with several polymers [HYU 90, SPA 93, SPA 95a, SPA 95b].

Given the current limitations of the most recent models for solids conveying, the pressure gradient and power consumption will be computed adopting the Broyer and Tadmor analysis [BRO 72, TAD 72]. The temperature profile requires obviously a non-isothermal model, hence the model of Tadmor and Broyer [TAD 72] will be modified and implicit finite differences will be adopted. The method avoids the need of a numeric relation between the value of the differences on the transversal and longitudinal directions.

### Pressure generation

Broyer and Tadmor [BRO 72, TAD 72] considered the following simplifications:

- The pellets behave as a continuous elastic plug;
- The solid plug contacts perfectly all sides of the screw channel and barrel;
- The flight clearance is neglected;
- The various friction coefficients are constant;
- The polymer density is assumed to be constant;
- Gravitational and inertial forces are neglected.

The density and friction coefficients can vary with temperature, pressure, velocity and other variables if the calculations are performed on small down-channel increments.

From simple geometric considerations, the volumetric output is given by [DAR 56, TAD 70, BRO 72]:

$$Q = \pi^2 N H D_b (D_b - H) \frac{tg\phi tg\theta_b}{tg\phi + tg\theta_b} \left[ 1 - \frac{pe}{\pi(D_b - H) \sin\theta} \right] \quad (3.12)$$

where  $\phi$  is the solids conveying angle.

The pressure profile is obtained from force and torque balances made on a differential down-channel element, as shown in figure 3.7 [TAD 70, BRO 72]. The forces include friction ( $F_1$ ) between the barrel and the solid bed (acting in a direction making an angle  $\theta+\phi$  with the down-channel direction), friction due to the contact of the solids with the screw root ( $F_5$ ) and screw walls ( $F_3$  and  $F_4$ ), respectively, normal reactions ( $F_7$  and  $F_8$ ), and forces due to the pressure gradient ( $F_6$  and  $F_2$ ).

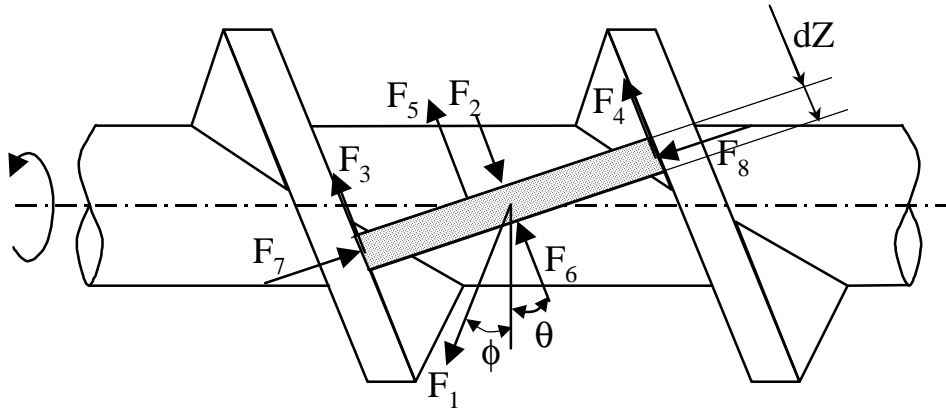


Figure 3.7- Forces acting on a solid bed element.

The pressure rise is given by:

$$P_2 = P_1 \cdot \exp \left[ \int_{z_1}^{z_2} \left( \frac{B_1 - A_1 K}{B_2 + A_2 K} \right) dz \right] \quad (3.13)$$

where  $P_1$  and  $P_2$  are the pressures at down-channel distance  $z_1$  and  $z_2$ , respectively.  $A_1$ ,  $A_2$ ,  $B_1$ ,  $B_2$  and  $K$  are constants given by:

$$A_1 = f_b W_b \sin \phi + 2.H f_s \sin \theta_b + W_s f_s \sin \theta_b \quad (3.14)$$

$$A_2 = H \bar{W} \sin \bar{\theta} \quad (3.15)$$

$$B_1 = f_b W_b \cos \phi - 2.H f_s \sin \theta_b \cdot \cot g \bar{\theta} \cdot \frac{\bar{D}}{D_b} - W_s f_s \sin \theta_b \cot g \theta_s \frac{D_s}{D_b} \quad (3.16)$$

$$B_2 = H \bar{W} \cos \bar{\theta} \frac{\bar{D}}{D_b} \quad (3.17)$$

$$K = \frac{\bar{D} \sin \bar{\theta} + f_s \cos \bar{\theta}}{D_b \cos \bar{\theta} - f_s \sin \bar{\theta}} \quad (3.18)$$

**In these equations,  $f_s$ , and  $f_b$  are the polymer-metal friction coefficients at the screw and barrel surfaces, respectively.**

### Power consumption

The mechanical power consumption in the solids conveying zone ( $e_w$ ) is the product of the friction force at the barrel surface by the barrel velocity in the  $\phi$  direction. In turn, the latter is the product of the local pressure by the interfacial area between the solid bed and the barrel ( $P_2 f_b W_b dz$ ) [BRO 72]:

$$de_w = \pi N D_b f_b W_b P_2 \cos \phi dz \quad (3.19)$$

Upon integration along the down-channel direction:

$$e_w = \pi N D_b f_b W_b P_m \Delta z \cos \phi \quad (3.20)$$

where  $P_m$  is:

$$P_m = \frac{P_2 - P_1}{\ln \frac{P_2}{P_1}} \quad (3.21)$$

The mechanical power consumption results from:

$$e_w = e_{wb} + e_{ws} + e_{wf} + e_{wp} \quad (3.22)$$

where  $e_{wb}$ ,  $e_{ws}$ ,  $e_{wf}$  and  $e_{wp}$  are the mechanical power dissipated on the barrel surface, on the screw root, on the flights and for compression, respectively. The corresponding expressions are:

$$e_{wb} = \pi N D_b f_b W_b P_m \Delta z \frac{\sin \theta_b}{\sin(\theta_b + \phi)} \quad (3.23)$$

$$e_{ws} = \pi N D_s f_s W_b P_m \Delta z \frac{\sin \theta_b}{\sin(\theta_b + \phi)} \frac{\sin \theta_b}{\sin \theta_s} \frac{tg \theta_b}{tg \theta_s} r_1 \quad (3.24)$$

$$e_{wf} = \pi N D_b f_s P_m \Delta z \frac{\sin \phi}{\sin(\theta_b + \phi)} \frac{\sin \theta_b}{\sin \bar{\theta}} \left[ 2H \frac{\sin \theta_b}{\sin \bar{\theta}} + \right. \quad (3.25)$$

$$\left. f_b W_b \left( \sin \phi \cos \bar{\theta} + \frac{D_b}{D} \cos \phi \sin \bar{\theta} \right) + W_s f_s \sin \theta_b \cos \bar{\theta} \left( 1 - \cot g \theta_s tg \bar{\theta} \frac{D_s}{D} \right) \right]$$

$$e_{wp} = \pi N D_b H \bar{W} \frac{\sin \phi}{\sin(\theta_b + \phi)} \frac{\sin \theta_b}{\sin \bar{\theta}} P_m \ln \left( \frac{P_2}{P_1} \right) \quad (3.26)$$

with:

$$r_1 = \frac{1 - \frac{e}{S \cos \theta_s}}{1 - \frac{e}{S \cos \theta_b}} \quad (3.27)$$

### Transversal temperature profile

The temperature profile in the solid plug can be predicted by solving the energy equation, which depends on:

- heat convection along the channel due to the polymer motion;
- heat conduction (in the radial direction) due to the temperature gradients;
- heat conduction in the down-channel direction.

The latter can be neglected when compared with the other two. Thus the temperature profile along the screw channel can be described by equation 3.28, where the left term represents heat convection and right term represents the heat conduction:

$$V_{sz} \frac{\partial T(y)}{\partial z} = \alpha_s \frac{\partial^2 T(y)}{\partial y^2} \quad (3.28)$$

$V_{sz}$  is the solid bed velocity,  $T(y)$  is the cross temperature profile (direction  $y$ ) and  $\alpha_s$  is the thermal diffusivity of the solid plug.

Friction at the polymer-barrel and polymer-screw walls and heat conduction from the barrel increase the temperature of the solid plug (particularly near the surfaces). Pressure, temperature and relative velocity affect the friction coefficients, therefore, the temperature.

Figure 3.8 shows the heat fluxes due to friction on the various surfaces on a differential cross-channel slice of the solid plug. The heat fluxes on the flights ( $q_f$ ) and on the screw root ( $q_s$ ) are generally neglected [TAD 72]. Heat generation on the root of the screw will be considered in this work, in order to define the location where the polymer reaches the melting point and the second part of the delay zone starts (as will be presented in the following section).

Equation 3.28 is solved considering that the heat fluxes (per unit surface) are defined by equations 3.23 and 3.24 divided by the surface where they act ( $W_b \Delta z$  and  $W_s \Delta z$ , respectively). The heat generated at the barrel surface is dissipated in two fluxes, one in the direction of the solids, the other in the direction of the barrel [TAD 72]:

$$q_b = -k_s \left. \frac{\partial T(y)}{\partial y} \right|_{y=H} + k_b \left. \frac{\partial T(y)}{\partial y} \right|_{barrel} \quad (3.29)$$

where  $k_s$  and  $k_b$  are the thermal conductivity of the solid polymer and of the barrel (metal), respectively.

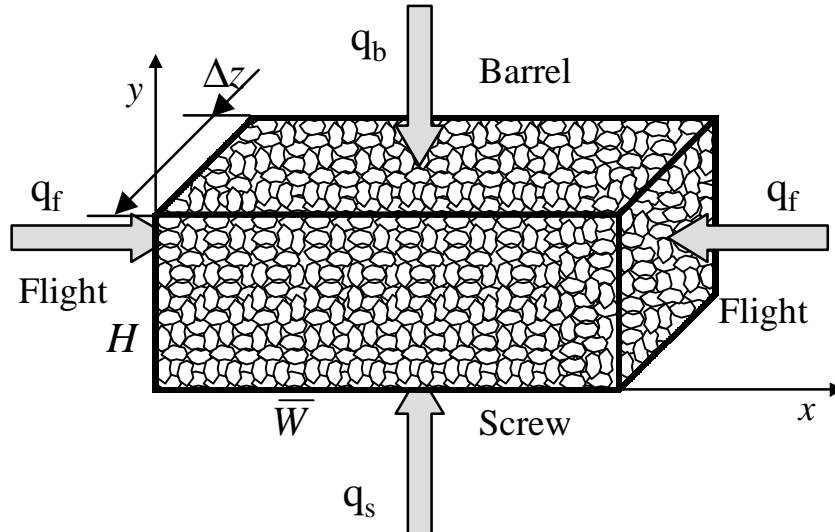


Figure 3.8- Heat fluxes due to friction on solid plug cross-channel slice.

The evaluation of the conductive heat flux on the barrel is made using the barrel temperature value ( $T_b$ ), measured at distance  $b$  from the interface, and considering a linear temperature profile along the barrel thickness:

$$\left. \frac{\partial T(y)}{\partial y} \right|_{\text{barrel}} \approx \frac{T_b - T}{b} \quad (3.30)$$

where  $T$  is the interface temperature.

It is more difficult to compute the heat flux on the screw, because the screw temperature is not known. One can either consider that the temperature at the screw surface ( $T_s$ ) is constant (e.g. equal to the inlet polymer temperature -  $T_{s0}$ ) or assumes an adiabatic screw. In this case, the heat flux is:

$$q_s = k_p \left. \frac{\partial T(y)}{\partial y} \right|_{y=0} \quad (3.31)$$

where  $k_p$  is the thermal conductivity of the screw (metal).

Equation 3.28 can be solved using an implicit finite difference method, such as a Crank-Nicolson scheme, together with the boundary conditions in the barrel (equation 3.29) and in the screw root (equation 3.31). The differential element in the  $y$  direction ( $\Delta y$ ) will be independent of that in the  $z$  direction ( $\Delta z$ ) [TAD 72, MIT 97]. The screw channel is filled with

a rectangular grid with sides parallel to the  $y$  and  $z$  axes (figure 3.9);  $\Delta y$  and  $\Delta z$  are the grid spacing (or differential elements) in the  $y$  and  $z$  directions, respectively. The co-ordinates of the grid points ( $Y,Z$ ) are given by:

$$\begin{cases} Y = j \Delta y \\ Z = i \Delta z \end{cases} \quad (3.32)$$

with  $i = 0, 1, \dots, M$  and  $j = 0, 1, \dots, N$ .

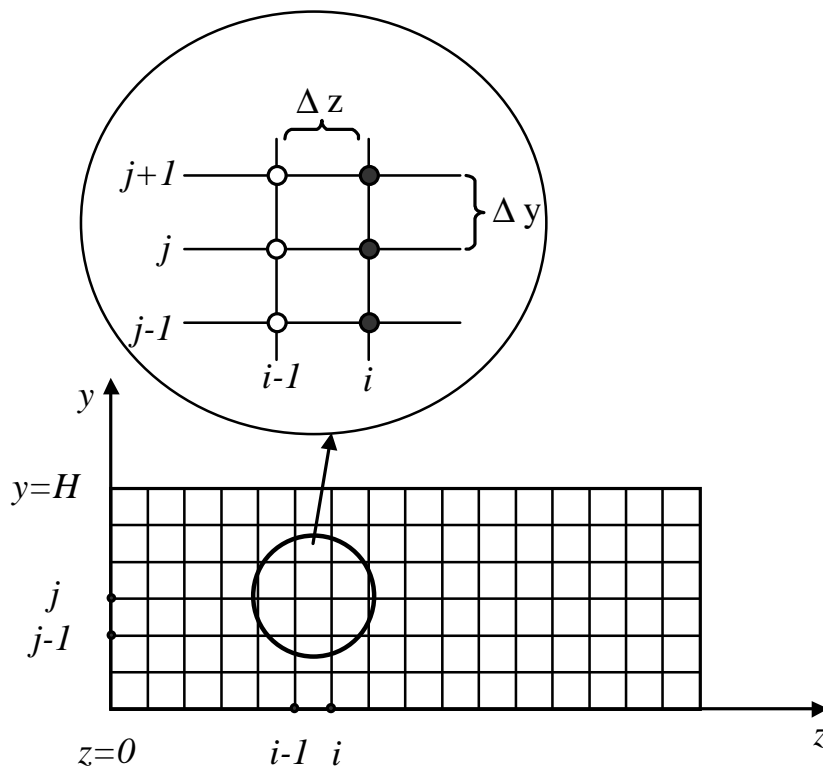


Figure 3.9- Finite differences grid.

The discretisation of equation 3.28 is made using central difference approximations for the first order derivative in the  $z$  and in  $y$  directions, respectively:

$$\left. \frac{\partial T}{\partial z} \right|_{i,j} = \frac{T_{i,j} - T_{i-1,j}}{\Delta z} \quad (3.33)$$

$$\left. \frac{\partial T}{\partial y} \right|_{i,j} = \frac{T_{i,j+1} - T_{i,j-1}}{2 \Delta y} \quad (3.34)$$

Using the Crank-Nicolson scheme for the second order derivatives in the  $y$  direction yields:

$$\left. \frac{\partial^2 T}{\partial y^2} \right|_{i,j} = \frac{1}{2} \left[ \frac{T_{i,j+1} - 2T_{i,j} + T_{i,j-1}}{\Delta y^2} + \frac{T_{i-1,j+1} - 2T_{i-1,j} + T_{i-1,j-1}}{\Delta y^2} \right] \quad (3.35)$$

Figure 3.9 shows the 6 points involved in these approximations for calculating the temperature in the point  $T(i,j)$ . Replacing in equation 3.28 and rearranging:

$$-\frac{\alpha_s}{2 \Delta y^2} T_{i,j-1} + \left( \frac{V_{sz}}{\Delta z} + \frac{\alpha_s}{\Delta y^2} \right) T_{i,j} - \frac{\alpha_s}{2 \Delta y^2} T_{i,j+1} = \frac{\alpha_s}{2 \Delta y^2} (T_{i-1,j-1} - 2 T_{i-1,j} + T_{i-1,j+2}) + \frac{V_{sz}}{\Delta z} T_{i-1,j} \quad (3.36)$$

where the temperatures on the left hand side are unknown and the temperatures on right hand side were computed in the previous step, or correspond to the initial temperatures for  $z=0$  ( $i=0$ ). Replacing  $j$  by 1, 2, ...,  $N-1$  produces a system of equations, that can be put in matrix form:

$$A T = B \quad (3.37)$$

$$A = \begin{bmatrix} -\frac{\alpha_s}{2 \Delta y^2} & \frac{V_{sz}}{\Delta z} + \frac{\alpha_s}{\Delta y^2} & -\frac{\alpha_s}{2 \Delta y^2} & 0 & 0 \\ 0 & -\frac{\alpha_s}{2 \Delta y^2} & \frac{V_{sz}}{\Delta z} + \frac{\alpha_s}{\Delta y^2} & -\frac{\alpha_s}{2 \Delta y^2} & 0 \\ \dots & \dots & \dots & \dots & \dots \\ \dots & \dots & \dots & \dots & \dots \\ 0 & 0 & -\frac{\alpha_s}{2 \Delta y^2} & \frac{V_{sz}}{\Delta z} + \frac{\alpha_s}{\Delta y^2} & -\frac{\alpha_s}{2 \Delta y^2} \end{bmatrix} \quad (3.38)$$

$$T^T = [T_{i,0} \quad T_{i,1} \quad \dots \quad T_{i,N-1} \quad T_{i,N}] \quad (3.39)$$

$$B = \begin{bmatrix} \frac{\alpha_s}{2 \Delta y^2} (T_{i-1,0} - 2 T_{i-1,1} + T_{i-1,2}) + \frac{V_{sz}}{\Delta z} T_{i-1,1} \\ \frac{\alpha_s}{2 \Delta y^2} (T_{i-1,1} - 2 T_{i-1,2} + T_{i-1,3}) + \frac{V_{sz}}{\Delta z} T_{i-1,2} \\ \dots \\ \frac{\alpha_s}{2 \Delta y^2} (T_{i-1,N-3} - 2 T_{i-1,N-2} + T_{i-1,N-1}) + \frac{V_{sz}}{\Delta z} T_{i-1,N-2} \\ \frac{\alpha_s}{2 \Delta y^2} (T_{i-1,N-2} - 2 T_{i-1,N-1} + T_{i-1,N}) + \frac{V_{sz}}{\Delta z} T_{i-1,N-1} \end{bmatrix} \quad (3.40)$$

Since this system has  $N-2$  equations and  $N$  unknowns, the two boundary conditions (equations 3.29 and 3.31) produce two extra equations:

$$\frac{k_s}{2 \Delta y} T_{i,0} - \frac{k_s}{2 \Delta y} T_{i,2} = -q_s \quad (3.41)$$

$$-\frac{k_s}{2 \Delta y} T_{i,N-2} + \left( \frac{k_s}{2 \Delta y} + \frac{k_b}{b} \right) T_{i,N} = -\frac{k_b}{b} T_b - q_b \quad (3.42)$$

Then, the matrix  $A$  (3.38) and the vector  $B$  (3.40) are changed into:

$$A = \begin{bmatrix} \frac{k_s}{2 \Delta y} & 0 & -\frac{k_s}{2 \Delta y} & 0 & 0 & 0 & 0 \\ -\frac{\alpha_s}{2 \Delta y^2} & \frac{V_{sz}}{\Delta z} + \frac{\alpha_s}{\Delta y^2} & -\frac{\alpha_s}{2 \Delta y^2} & 0 & 0 & 0 & 0 \\ 0 & -\frac{\alpha_s}{2 \Delta y^2} & \frac{V_{sz}}{\Delta z} + \frac{\alpha_s}{\Delta y^2} & -\frac{\alpha_s}{2 \Delta y^2} & 0 & 0 & 0 \\ \dots & \dots & \dots & \dots & \dots & \dots & \dots \\ \dots & \dots & \dots & \dots & \dots & \dots & \dots \\ 0 & 0 & 0 & 0 & -\frac{\alpha_s}{2 \Delta y^2} & \frac{V_{sz}}{\Delta z} + \frac{\alpha_s}{\Delta y^2} & -\frac{\alpha_s}{2 \Delta y^2} \\ 0 & 0 & 0 & 0 & -\frac{k_s}{2 \Delta y} & 0 & \frac{k_s}{2 \Delta y} + \frac{k_b}{b} \end{bmatrix} \quad 3.43$$

$$B = \begin{bmatrix} -q_s \\ \frac{\alpha_s}{2 \Delta y^2} (T_{i-1,0} - 2 T_{i-1,1} + T_{i-1,2}) + \frac{V_{sz}}{\Delta z} T_{i-1,1} \\ \frac{\alpha_s}{2 \Delta y^2} (T_{i-1,1} - 2 T_{i-1,2} + T_{i-1,3}) + \frac{V_{sz}}{\Delta z} T_{i-1,2} \\ \dots \\ \frac{\alpha_s}{2 \Delta y^2} (T_{i-1,N-3} - 2 T_{i-1,N-2} + T_{i-1,N-1}) + \frac{V_{sz}}{\Delta z} T_{i-1,N-2} \\ \frac{\alpha_s}{2 \Delta y^2} (T_{i-1,N-2} - 2 T_{i-1,N-1} + T_{i-1,N}) + \frac{V_{sz}}{\Delta z} T_{i-1,N-1} \\ -\frac{k_b}{b} T_b - q_b \end{bmatrix} \quad (3.44)$$

The solution to this system can be obtained using, e.g., the method of Gauss elimination with partial pivoting.

## Barrel grooves

The output capacity of the solids conveying zone, as well its insensitivity to pressure fluctuations can be increased by augmenting the friction coefficient on the internal barrel surface, via machining longitudinal or helicoidal grooves on the barrel (figure 3.3).

Several theoretical and experimental analyse on the grooved section of extruders have been carried out [BOE 90, POT 85, RAU 82a, RAU 82b, GRÜ 84, RAU 86, POT 88, POT 89]. In this work the influence of the grooves will be considered through the use of an equivalent friction coefficient (that depends on the grooves geometry) in the conventional solids conveying analysis. This equivalent (or efficient) friction coefficient will be determined by the contact of the solid bed in screw channel with the barrel flight tip surface and with the solid bed contained by the barrel grooves. The influence of the grooves geometry (groove depth,  $h_N$ , and total groove width - number of grooves multiplied by the groove width,  $b_N$ ) on the performance of four methods to compute the equivalent friction coefficient is presented in Appendix A. As expected, total groove width is the relevant parameter, since the occurrence of a transversal polymer flow on the grooves is determinant for their efficiency. For that reason, the effective friction coefficient only decreases when the groove depth is sufficiently small (towards the end of the grooved section).

### 3.4- Delay

The melting mechanism does not start immediately at the end of solids conveying zone (i.e., when the solid polymer closer to barrel surface reaches the melting temperature). Maddock [MAD 59] and Tadmor *et al.* [TAD 67] reported a two-stage process (figure 3.10):

- The polymer in contact with the barrel surface melts first and forms a film at the barrel-solid polymer interface. This film increases gradually its thickness.
- Subsequently, a melt pool appears near to the active screw flight of the channel and its width increases until the entire polymer melts (this is the melting zone).

There are, at least, two causes for this delay [AGA 96, TAD 67, KAC 72]. The initial melt rather than accumulating near to the active flight will penetrate and fill the voids between pellets, delaying the film formation. After the formation of the melt film, the melting mechanism will only start when the thickness of the melt film exceeds the flight clearance. It is common that the film thickness grows far beyond the value of the clearance, until that a

sufficient cross channel pressure, is able to push and deform the solid bed against the trailing flight [KAC 72, AGA 96].

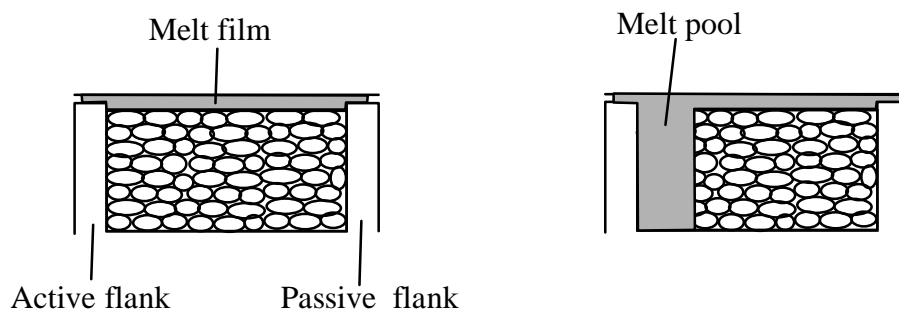


Figure 3.10- Maddock/Tadmor melting mechanism.

In principle, depending on the operating conditions, particularly the screw temperature, it is possible that the polymer closer to the screw surfaces (walls and root) reaches its melting point during the delay zone. As seen in the previous section, at the screw flanks and root there is, also, dissipation by friction, with a consequent gradual increase of the temperature of the solid polymer. Therefore, the delay zone can have two stages (figure 3.11), i.e., from a specified screw location onwards a melt film near all screw surfaces can be formed, and can be maintained through the melting length.

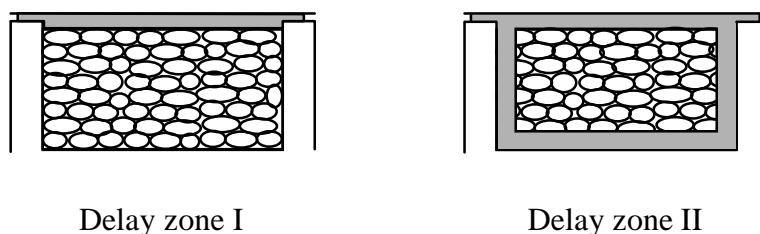


Figure 3.11- Proposed two-stage delay zone.

## DELAY ZONE I

As shown in figure 3.12, the solid bed contacts the screw walls and root, where the local temperature increases due to heat dissipation from friction. This mechanism is completed when the solid polymer reaches its melting point. Simultaneously, the solid polymer continues to melt at the melt film-solid bed interface (the heated barrel and the intense shearing occurring in the film contribute significantly to this process, as will be seen later).

Kacir and Tadmor [KAC 72] developed a theoretical model for this zone that allows the calculation of the film thickness profile, the temperature profiles in the film and in the solid

bed, the pressure generation, the power consumption and the zone length. Additionally, the model developed here considers:

- heat convection in the down-channel direction,
- heat conduction in the radial direction,
- heat convection in the radial direction.

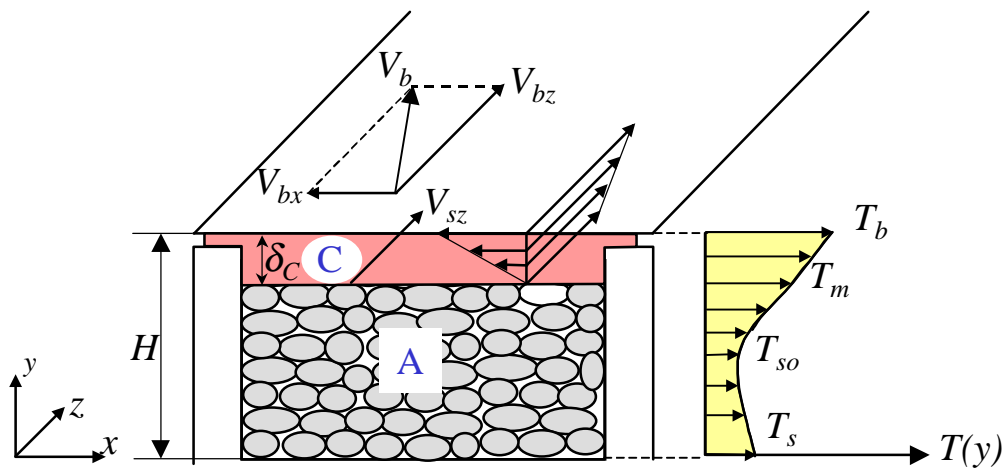


Figure 3.12- Cross-section for delay zone I.

The following assumptions are established:

- The solid bed is an isotropic and homogeneous continuum;
- Melt leakage over the flight tips is neglected;
- The molten polymer is an inelastic viscous fluid;
- The flow is steady;
- The solid-melt interface is smooth;
- The melt film flow is fully developed in the down and cross channel directions (i.e.,  $\partial V_x / \partial x = 0$  and  $\partial V_z / \partial z = 0$ );
- Gravitational and inertial forces are neglected.

### Melt film

The momentum and energy equations are the following [ELB 84, LEE 90, HUA 93, HAN 96]:

$$\frac{\partial P}{\partial x} = \frac{\partial}{\partial y} \left( \eta \frac{\partial V_x}{\partial y} \right) \quad (3.45)$$

$$\frac{\partial P}{\partial y} = 0 \quad (3.46)$$

$$\frac{\partial P}{\partial z} = \frac{\partial}{\partial y} \left( \eta \frac{\partial V_z}{\partial y} \right) \quad (3.47)$$

$$\rho_m c_p V_z(y) \frac{\partial T}{\partial z} = k_m \frac{\partial^2 T}{\partial y^2} + \eta \dot{\gamma}^2 \quad (3.48)$$

where  $\rho_m$  is the melt density,  $c_p$  is the melt specific heat,  $k_m$  is the melt thermal conductivity and  $\eta$  is the melt viscosity, which will be calculated using a temperature dependent power law:

$$\eta = k_0 \exp[-a(T - T_0)] \dot{\gamma}^{n-1} \quad (3.49)$$

$k_0$ ,  $a$ ,  $T_0$  and  $n$  are constants and  $\dot{\gamma}$  is the shear rate, given by:

$$\dot{\gamma} = \left[ \left( \frac{\partial V_z}{\partial y} \right)^2 + \left( \frac{\partial V_x}{\partial y} \right)^2 \right]^{1/2} \quad (3.50)$$

Since the leakage flow is neglected, the melt must recirculate in the  $x$ -direction:

$$\int_0^{\delta_c} V_x(y) dy = 0 \quad (3.51)$$

where  $\delta_c$  is the melt film thickness.

The relevant boundary conditions are:

$$\begin{cases} V_x(y=0) = 0 \\ V_x(y=\delta) = -V_{bx} \end{cases} \quad \begin{cases} V_z(y=0) = V_{sz} \\ V_z(y=\delta) = V_{bz} \end{cases} \quad \begin{cases} T(y=0) = T_m \\ T(y=\delta) = T_b \end{cases} \quad (3.52)$$

where  $T_m$  is the melting temperature.

The resolution of equations 3.45, 3.47, 3.48 and 3.51, coupled to the boundary conditions 3.52, provides the melt film velocity and temperature fields. The mesh is similar to that shown in figure 3.9, where the  $y$  coordinates vary between  $y=0$  (solid-melt interface) and  $y=\delta_c$  (the film thickness). The equations are non-linear, since the viscosity depends on the temperature and on the velocity field, thus involving the use of a specific finite difference discretisation [MIT 80, ZIE 83]. The solution of equations 3.45 and 3.47 can be obtained using the implicit Crank-Nicholson scheme.

$$\frac{\partial P}{\partial x} = \frac{1}{2} \left[ \frac{\eta_{i-1,j+\frac{1}{2}} Vx_{i-1,j+1} - \left( \eta_{i-1,j+\frac{1}{2}} + \eta_{i-1,j-\frac{1}{2}} \right) Vx_{i-1,j} + \eta_{i-1,j-\frac{1}{2}} Vx_{i-1,j-1}}{\Delta y^2} + \right. \quad (3.53)$$

$$\left. \frac{\eta_{i,j+\frac{1}{2}} Vx_{i,j+1} - \left( \eta_{i,j+\frac{1}{2}} + \eta_{i,j-\frac{1}{2}} \right) Vx_{i,j} + \eta_{i,j-\frac{1}{2}} Vx_{i,j-1}}{\Delta y^2} \right]$$

$$\frac{P_{i,j} - P_{i-1,j}}{\Delta z} = \frac{1}{2} \left[ \frac{\eta_{i-1,j+\frac{1}{2}} Vz_{i-1,j+1} - \left( \eta_{i-1,j+\frac{1}{2}} + \eta_{i-1,j-\frac{1}{2}} \right) Vz_{i-1,j} + \eta_{i-1,j-\frac{1}{2}} Vz_{i-1,j-1}}{\Delta y^2} + \right. \quad (3.54)$$

$$\left. \frac{\eta_{i,j+\frac{1}{2}} Vz_{i,j+1} - \left( \eta_{i,j+\frac{1}{2}} + \eta_{i,j-\frac{1}{2}} \right) Vz_{i,j} + \eta_{i,j-\frac{1}{2}} Vz_{i,j-1}}{\Delta y^2} \right]$$

where  $\eta_{i-1,j+\frac{1}{2}}$  is the viscosity calculated using equation 3.49 with an average temperature and

shear rate:

$$\dot{\gamma} = \left[ \left( \frac{Vx_{i-1,j+1} - Vx_{i-1,j}}{\Delta y} \right)^2 + \left( \frac{Vz_{i-1,j+1} - Vz_{i-1,j}}{\Delta y} \right)^2 \right]^{\frac{1}{2}} \quad (3.55)$$

$$T = \frac{T_{i-1,j+1} + T_{i-1,j}}{2} \quad (3.56)$$

$\eta_{i-1,j-\frac{1}{2}}$ ,  $\eta_{i,j+\frac{1}{2}}$  and  $\eta_{i,j-\frac{1}{2}}$  are computed using a similar rule

The differential terms of the energy equation (3.48) need to be replaced by equations 3.33 and 3.35, respectively.

$$\rho_m c_p Vz_{i,j} \frac{T_{i,j} - T_{i-1,j}}{\Delta z} = \quad (3.57)$$

$$k_m \frac{1}{2} \left[ \frac{T_{i,j+1} - 2T_{i,j} + T_{i,j-1}}{\Delta y^2} + \frac{T_{i-1,j+1} - 2T_{i-1,j} + T_{i-1,j-1}}{\Delta y^2} \right] + (\eta \dot{\gamma}^2)_{i,j}$$

Substituting  $j$  by 1, 2, ...,  $N-1$ , produces a system of equations that can be put in matrix form as in equation 3.37. The system is completed with equation 3.51 and with an equation for the mass flow rate in the melt film, obtained by a mass balance.

Figure 3.13 shows the iterative procedure for the simultaneous resolution of equations 3.53, 3.54 and 3.57, where  $V_x(y)$ ,  $V_z(y)$ ,  $\frac{\partial P}{\partial x}$ ,  $P$  and  $T(y)$ , need to be determined for section  $i$ . The numerical resolution is similar to that of the solids conveying zone, when equation 3.28 is put in matrix form (equation 3.37).

Initial values for:

$V_{x_{0,j}}(y)$  (e.g., a linear profile between 0 and  $V_{bx}$ )

$V_{z_{0,j}}(y)$  (e.g., linear variation between  $V_{sz}$  and  $V_{bz}$ )

$T_{0,j}(y)$  (e.g., linear variation between  $T_m$  and  $T_b$ )

do {

do {

        solve equation 3.53 (to obtain  $V_{x_{i,j}}$  and  $\partial P/\partial x$ )

        solve equation 3.54 (to obtain  $V_{z_{i,j}}$  and  $P_i$ )

    } while ( $V_{x_{i,j}}$ ,  $\partial P/\partial x$ ,  $V_{z_{i,j}}$  and  $P_i$  have not converged)

    solve equation 3.57 (to obtain  $T_{i,j}$ )

  } while ( $T_{i,j}$  has not converged)

Figure 3.13- Method for solving a system of non-linear differential equations.

### Solid bed

Here, a displacement of the solids towards the melt film must occur, due to melting [TAD 70, ELB 84]. An additional term in the energy equation (the heat convection in the radial direction) must be included.

$$V_{sy} \frac{\partial T(y)}{\partial y} + V_{sz} \frac{\partial T(y)}{\partial z} = \alpha_s \frac{\partial^2 T(y)}{\partial y^2} \quad (3.58)$$

where  $V_{sy}$  is the velocity towards the solid-melt interface.

At the screw root the heat generated by friction dissipation has two components, one in the solids direction, the other in the screw direction.

$$q_s = k_s \left. \frac{\partial T(y)}{\partial y} \right|_{y=0} - k_p \left. \frac{\partial T(y)}{\partial y} \right|_{y=0} \quad (3.59)$$

The screw temperature must be known. As referred previously this is not an easy task. An empirical equation suggested by Cox and Fenner [COX 80] will be adopted:

$$T_s(z) = T_b [1 - \exp(\beta z)] + T_{so} \exp(\beta z) \quad (3.60)$$

where:

$$\beta = \frac{\ln\left(\frac{T_m - T_b}{T_{so} - T_b}\right)}{z_m} \quad (3.61)$$

and  $z_m$  is the helical distance between the hopper and the location where the lower and lateral melt films first appears.

The discretisation of equation 3.58 is identical to that of equation 3.28.

### Mass and heat balances over the solid-melt interface

The behaviour of the melt film and of the solid bed can be coupled through mass and heat balances in the interface. The mass flow rate in the melt film ( $\dot{m}_{C|z+\Delta z}$ ) is determined by the rate of melting over the interface ( $R_C$ ): see figure 3.14, which represents an elemental portion of the interface between the melt film, C, and the solid bed A (see also figure 3.12).

$$\dot{m}_{C|z+\Delta z} = \dot{m}_{C|z} + R_C \quad (3.62)$$

where:

$$\dot{m}_{C|z} = W_c \rho_m \int_0^{\delta_\epsilon} V_z(y) dy \quad (3.63)$$

$$R_C = \rho_s V_{sy} \Delta z W_c \quad (3.64)$$

where  $\rho_s$  is the solid bed density and the indices  $C|z$  and  $C|z+\Delta z$  refer to the down-channel increment  $z$  and  $z+\Delta z$ , respectively, in zone C.

The mass flow rate in the solid bed ( $\dot{m}_{A|z+\Delta z}$ ) is:

$$\dot{m}_{A|z+\Delta z} = \dot{m}_{A|z} - R_C \quad (3.65)$$

where:

$$\dot{m}_{A|z} = \rho_s V_{sz} (H_{s|z} W_s) \quad (3.66)$$

and  $H_{s|z}$  is the solid bed height. Then, the total mass flow rate ( $\dot{m}_T$ ) is:

$$\dot{m}_T = \dot{m}_{A|z+\Delta z} + \dot{m}_{C|z+\Delta z} \quad (3.67)$$

Finally, a heat balance over the melting interface yields:

$$k_m \left( \frac{\partial T}{\partial y} \right)_{y=H-\delta_c} - k_s \left( \frac{\partial T}{\partial y} \right)_{y=H-\delta_c} = \rho_s \lambda V_{sy} \quad (3.68)$$

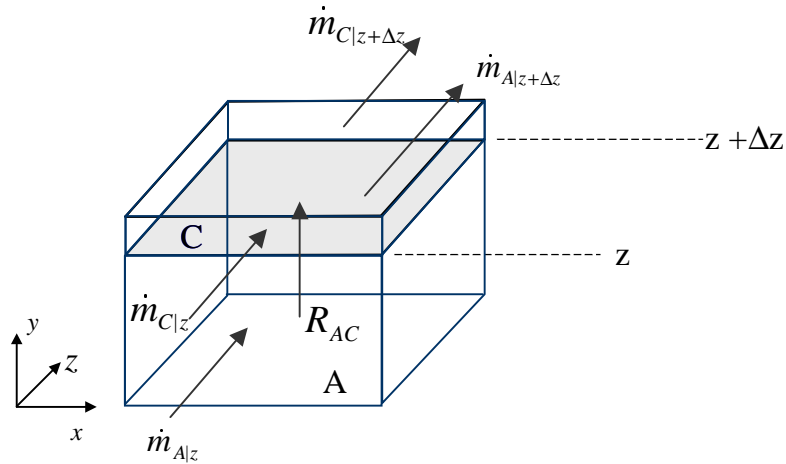


Figure 3.14- Mass balances over the solid-melt interface.

### Pressure gradient

Force and torque balances, identical to those carried out for the solids conveying zone allows the computation of the pressure profile. Here, a viscous force replaces the friction force at the barrel wall [KAC 72]:

$$F_1 = \tau W_b dz \quad (3.69)$$

where  $\tau$  is the shear stress. For isotropic pressure distribution and constant channel depth:

$$P = P_o \exp \left[ \frac{B'_1 + A'_1 K}{B_2 + A_2 K} \Delta z \right] + \frac{\tau W_b (\cos \bar{\theta} - K \sin \bar{\theta})}{B'_1 + A'_1 K} \left\{ \exp \left[ \frac{B'_1 + A'_1 K}{B_2 + A_2 K} \Delta z \right] - 1 \right\} \quad (3.70)$$

where:

$$A'_1 = \bar{W} \operatorname{tg} \alpha \sin \bar{\theta} + 2.H f_s \sin \theta_b + W_s f_s \sin \theta_b \left( \cos \alpha + \frac{\sin \alpha}{f_s} \right) \quad (3.71)$$

$$B'_1 = \bar{W} \operatorname{tg} \alpha \cos \bar{\theta} \frac{\bar{D}}{D_b} - 2.H f_s \sin \theta_b \cdot \cot g \bar{\theta} \cdot \frac{\bar{D}}{D_b} - W_s f_s \left( \cos \alpha + \frac{\sin \alpha}{f_s} \right) \sin \theta_b \cot g \theta_s \frac{D_s}{D_b} \quad (3.72)$$

$A_2$ ,  $B_2$  and  $K$  are defined by equations 3.15, 3.16 and 3.17, respectively, and the mean shear rate,  $\bar{\dot{\gamma}}$ , used to compute  $\tau$  is:

$$\bar{\dot{\gamma}} = \frac{V_b \sin \theta_b}{\delta_c \sin(\theta_b + \phi)} \quad (3.73)$$

### Power consumption

The mechanical power consumption can be calculated following the procedure presented for the solids conveying zone, but replacing the contact with the barrel by a melt film. Then, equation 3.22 becomes [KAC 72]:

$$e'_w = e'_{wb} + e_{ws} + e_{wf} + e_{wp} \quad (3.74)$$

where  $e'_{wb}$  is the power dissipated on the barrel surface, given by:

$$e'_{wb} = \pi N D_b \tau W_b Z_b \frac{\sin \theta_b}{\sin(\theta_b + \phi)} \quad (3.75)$$

### DELAY ZONE II

This zone corresponds to the classic delay zone studied by Chung [CHU 71, CHU 75] who developed a model predicting the pressure profile assuming isothermal conditions.

Instead, in this work this zone will be considered as a particular case of melting where the five distinct sections represented in figure 3.15 can be identified [ELB 84, LIN 85a]. In this way, physical compatibility between adjacent functional zones is ensured.

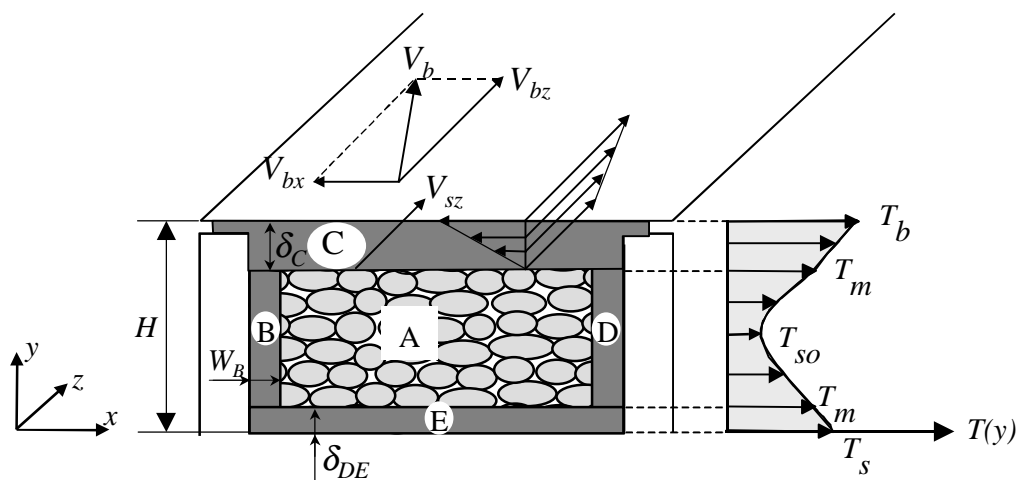


Figure 3.15- Cross-section for delay zone II.

The solid bed (A) is surrounded by melt films adjacent to the barrel wall (C), the screw root (E) and the active (B) and trailing screw flights (D). The delay zone II differs from the melting zone only in terms of melt pool B. The transition of the former to the latter is prescribed by the thickness of B reaching the channel depth [ELB 84]. Whereas in the delay zone II section B is a melt film and calculations will be carried out in the  $x$ -direction, in the melting zone, section B is a melt pool where the melt recirculates, hence a two-dimensional approach will be followed. The model will be presented in the next section.

### 3.5- Melting

A schematic representation of the melting mechanism in a rectangular channel cross-section is shown in Figure 3.16.

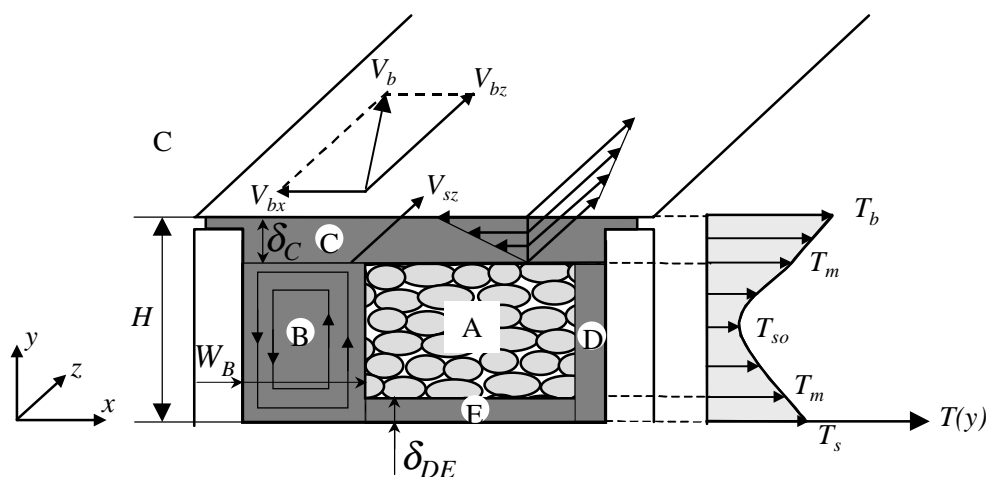


Figure 3.16- Cross-section for melting.

Different forms of the momentum and energy equations describe each of the five individual regions. Boundary conditions and force, heat and mass balances will complete the equations available.

The main assumptions include [ELB 84, LIN 85a]:

- The solid bed is an isotropic and homogeneous continuum;
- Melt leakage over the flight tips is neglected;
- The molten polymer is a purely viscous fluid;
- The flow is steady,
- The solid-melt interfaces are smooth;

- The flow of the melt films is fully developed in the down and cross channel directions (i.e.,  $\partial V_x/\partial x = 0$  and  $\partial V_z/\partial z = 0$ );
- The temperature field, of the melt films is fully developed in the cross channel direction (i.e.,  $\partial T/\partial x = 0$ ), but not in the down channel direction (i.e.,  $\partial T/\partial z \neq 0$ );
- Heat conduction in the down channel direction is neglected (i.e.,  $\partial^2 T/\partial z^2 \ll \partial^2 T/\partial y^2$ );
- Gravitational and inertial forces are neglected;
- The solid bed velocity is constant (this has been reported as producing the best results, especially in association with cross-channel flow [LIN 85a, LIN 85b]).

### Momentum and energy equations

a) Melt films (C, D and E)

Given the above assumptions and the development of cross-channel melt circulation around the solid bed, the momentum and energy equations for films C, D and E are identical. Region D can be considered as an extension of region E, as suggested by previous experimental work [ELB 84]. The flow and the thermal behaviour of regions C and DE can be described by equations 3.45 to 3.50 with the following boundary conditions:

$$\begin{cases} V_x(y=0) = 0 \\ V_x(y=\delta_C) = -V_{bx} \end{cases} \quad \begin{cases} V_z(y=0) = V_{sz} \\ V_z(y=\delta_C) = V_{bz} \end{cases} \quad \begin{cases} T(y=0) = T_m \\ T(y=\delta_C) = T_b \end{cases} \quad (3.76)$$

for region C and

$$\begin{cases} V_x(y=0) = 0 \\ V_x(y=\delta_{DE}) = 0 \end{cases} \quad \begin{cases} V_z(y=0) = 0 \\ V_z(y=\delta_{DE}) = V_{sz} \end{cases} \quad \begin{cases} T(y=0) = T_s \\ T(y=\delta_{DE}) = T_m \end{cases} \quad (3.77)$$

for region DE.

b) Melt pool (zone B)

When the melt pool width ( $W_B$ ) is equal or greater than the screw channel depth recirculation takes place, i.e.,  $\partial V_z/\partial y \neq 0$ . Otherwise, B will behave as C (i.e., delay zone prevails). During melting, the momentum in the  $z$  direction and energy equations (3.47 and 3.48) take the form:

$$\frac{\partial P}{\partial z} = \frac{\partial}{\partial y} \left( \eta \frac{\partial V_z}{\partial x} \right) + \frac{\partial}{\partial y} \left( \eta \frac{\partial V_z}{\partial y} \right) \quad (3.78)$$

$$\rho_m c_p V_z(y) \frac{\partial T}{\partial z} = k_m \left( \frac{\partial^2 T}{\partial x^2} + \frac{\partial^2 T}{\partial y^2} \right) + \eta \dot{\gamma}^2 \quad (3.79)$$

where the shear rate is given by:

$$\dot{\gamma} = \left[ \left( \frac{\partial V_x}{\partial y} \right)^2 + \left( \frac{\partial V_z}{\partial x} \right)^2 + \left( \frac{\partial V_z}{\partial y} \right)^2 \right]^{1/2} \quad (3.80)$$

The boundary conditions are:

$$\begin{cases} V_x(y=0) = 0 \\ V_x(y=H) = -V_{bx} \end{cases} \quad \begin{cases} V_z(x=0) = 0 \\ V_z(x=W_B) = V_{sz} \\ V_z(y=0) = 0 \\ V_z(y=H) = V_{bz} \end{cases} \quad \begin{cases} T(x=0) = T_s \\ T(x=W_B) = T_m \\ T(y=0) = T_s \\ T(y=H) = T_b \end{cases} \quad (3.81)$$

c) Solid bed (zone A)

The solid bed is considered to move in the down channel direction at constant velocity:

$$V_{sz} = \frac{\dot{m}_T H W}{\rho_s} \quad (3.82)$$

Different heat conduction and dissipation rates occur in the two opposite sides of the solid bed and cause an asymmetrical temperature distribution. Consequently, region A can be subdivided in two (see figure 3.17):

$$-\frac{V_{sy1}}{\alpha_s} \frac{\partial T_{s1}}{\partial y} + \frac{V_{sz}}{\alpha_s} \frac{\partial T_{s1}}{\partial z} = \frac{\partial^2 T_{s1}}{\partial y^2} \quad (d \leq y \leq H_{s/z}) \quad (3.83)$$

$$\frac{V_{sy2}}{\alpha_s} \frac{\partial T_{s2}}{\partial y} + \frac{V_{sz}}{\alpha_s} \frac{\partial T_{s2}}{\partial z} = \frac{\partial^2 T_{s2}}{\partial y^2} \quad (0 \leq y \leq d) \quad (3.84)$$

where  $V_{sy1}$  and  $V_{sy2}$  are the solid polymer velocities in the direction of the melt films C and E, respectively,  $T_{s1}$  and  $T_{s2}$  are the temperature profiles for sub-regions 1 and 2, respectively, and  $d$  is the distance in the  $y$  direction such that  $T_{s1}(y=d) = T_{s2}(y=d)$ .

The boundary conditions for these regions are:

$$\begin{array}{cc} \text{Sub-region I} & \text{Sub-region II} \\ \left\{ \begin{array}{l} T_{s1}(y=H_s, z) = T_m \\ \frac{\partial T_{s1}(y=d, z)}{\partial y} = 0 \end{array} \right. & \left\{ \begin{array}{l} T_{s2}(y=0, z) = T_m \\ \frac{\partial T_{s2}(y=d, z)}{\partial y} = 0 \end{array} \right. \end{array} \quad (3.85)$$

Distance  $d$  is calculated through an iterative process, starting with an initial value (for example,  $H_{s/z}/2$ ) until the temperature at  $d$  for the two regions is equal.

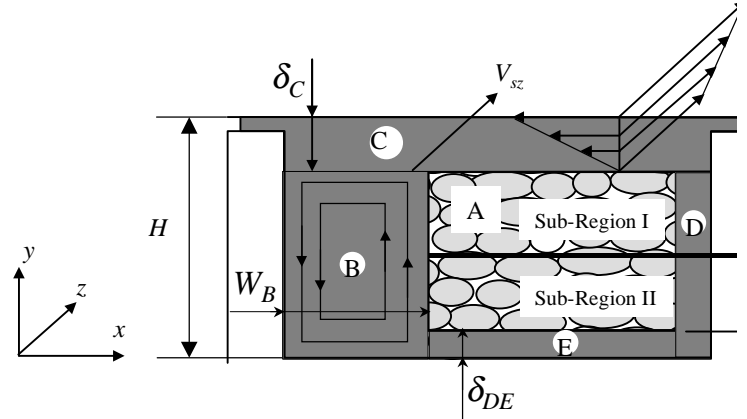


Figure 3.17- Solid bed sub-regions.

### Mass and heat balances

Taking into account melt recirculation around the solid bed, the mass balance for region C is (see figure 3.18, which represents an elemental portion of the interface of the melt film, C, and the solid bed, A; see also figure 3.16):

$$\dot{m}_{C|z+\Delta z} = \dot{m}_{C|z} - \dot{m}_{Cx|z} + \dot{m}_{DEx|z} + R_C \quad (3.86)$$

$$\dot{m}_{C|z} = W_{s|z} \rho_m \int_0^{\delta_{C|z}} V_z^{(C)}(y) dy \quad (3.87)$$

$$\dot{m}_{Cx|z} = \Delta z \rho_m \int_0^{\delta_{C|z}} V_x^{(C)}(y) dy \quad (3.88)$$

$$\dot{m}_{DEx|z} = \Delta z \rho_m \int_0^{\delta_{DE|z}} V_x^{(DE)}(y) dy \quad (3.89)$$

$$R_C = \rho_s V_{sy|z} \Delta z W_{s|z} \quad (3.90)$$

where:

$\dot{m}_{C|z}$  down-channel mass flow rate,

$\dot{m}_{Cx|z}$  net flow rate to the melt pool, in the  $x$  direction,

$\dot{m}_{DEx|z}$  cross-channel flow rate into the film from DE.

In the above equations  $\delta_{DE|z}$  is the thickness of melt film DE.

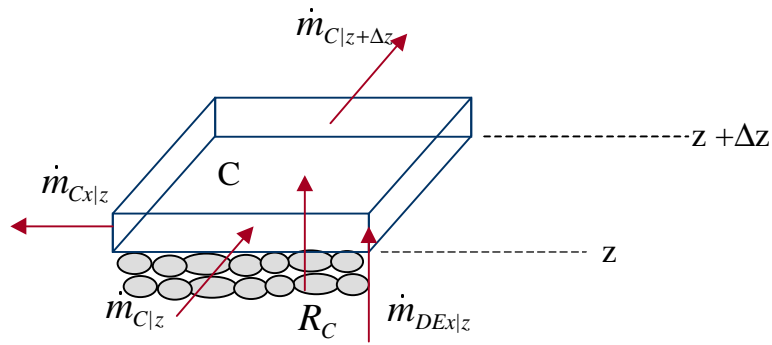


Figure 3.18- Mass balance for region C.

The mass balance for zone DE yields (see figure 3.19, where an elemental portion of the interface between the melt films, DE, and the solid bed, A, is represented, see also figure 3.16):

$$\dot{m}_{DE|z+\Delta z} = \dot{m}_{DE|z} - \dot{m}_{DEx|z} + \dot{m}_{By|z} + R_D + R_E \quad (3.91)$$

where:

$\dot{m}_{DE|z}$  down-channel mass flow rate:

$$\dot{m}_{DE|z} = (W_s + H_s)_{|z} \rho_m \int_0^{\delta_{DE|z}} V_z^{(DE)}(y) dy \quad (3.92)$$

$\dot{m}_{By|z}$  rate of melt circulation through the melt pool in the  $x$ - $y$  plane,

$R_D$  melting rate over the interface A-D for an increment  $\Delta z$ ,

$R_E$  melting rate over the interface A-E for an increment  $\Delta z$ :

$$R_D + R_E = \rho_s V_{sy2|z} \Delta z (W_s + H_s) \quad (3.93)$$

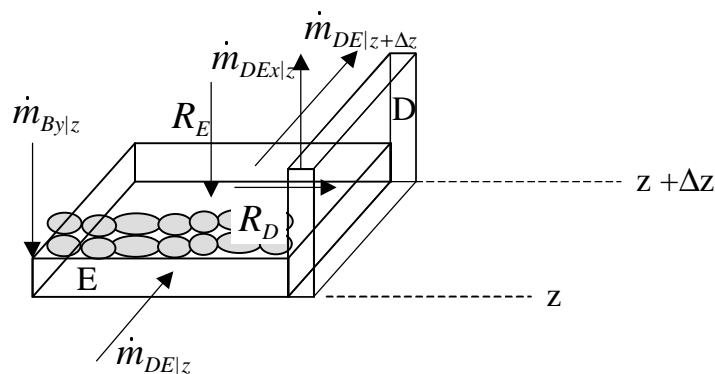


Figure 3.19- Mass balance for region DE.

The mass balance for the solid bed A is (see figure 3.20, where a portion of the interface between the melt pool, B, and the solid bed, A, is represented):

$$\dot{m}_{A/z+\Delta z} = \dot{m}_{A/z} - (R_C + R_B + R_D + R_E) \quad (3.94)$$

with:

$$\dot{m}_{A/z} = \rho_s V_{sz} (H_s W_s)_{/z} \quad (3.95)$$

Finally, the mass balance in the melt pool B (figure 3.20) produces the two following equations, which allow the calculation of  $\dot{m}_{B/y/z}$ .

$$\dot{m}_{B/z+\Delta z} = \dot{m}_{B/z} - \dot{m}_{B/y/z} + \dot{m}_{C/x/z} + R_B \quad (3.96)$$

$$\dot{m}_{B/z+\Delta z} = \dot{m}_T - (\dot{m}_{A/z+\Delta z} + \dot{m}_{C/z+\Delta z} + \dot{m}_{DE/z+\Delta z}) \quad (3.97)$$

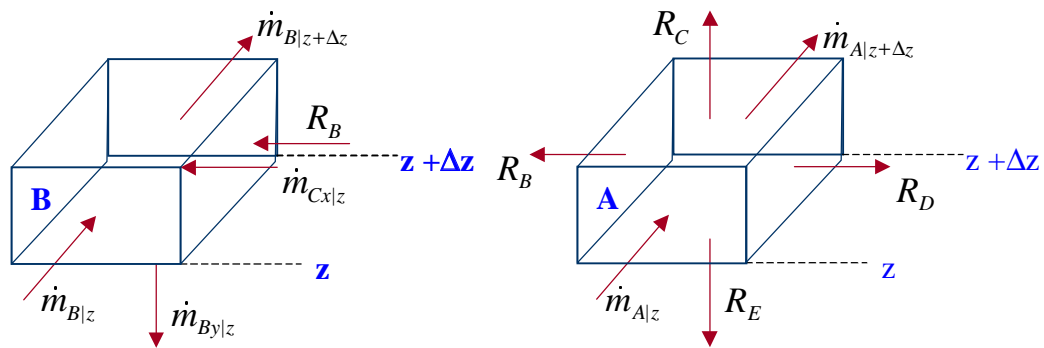


Figure 3.20- Mass balances for regions A and B.

The solid polymer velocity in the direction of the melt films C ( $V_{sy1}$ ) and DE ( $V_{sy2}$ ) can be determined by heat balances over the interfaces A-C and A-DE. The corresponding equations are, respectively:

$$k \frac{\partial T}{\partial y} /_{A-C,melt} - k_s \frac{\partial T}{\partial y} /_{A-C,solid} = \rho_s \lambda V_{sy1} \quad (3.98)$$

$$k_s \frac{\partial T}{\partial y} /_{A-DE,solid} - k \frac{\partial T}{\partial y} /_{A-DE,melt} = \rho_s \lambda V_{sy2} \quad (3.99)$$

## Force balances

The analysis is completed with the equilibrium of forces acting on the solid bed in the  $x$  and  $y$  directions:

$$\frac{\partial P^{(C)}}{\partial x} + \frac{\partial P^{(DE)}}{\partial x} = \frac{2(\tau_{yx/DE} + \tau_{yx/C})}{H_s} \quad (3.100)$$

$$\frac{\partial P^{(C)}}{\partial z} + \frac{\partial P^{(DE)}}{\partial z} = \frac{\partial P}{\partial z} \left( = \frac{\partial P^{(B)}}{\partial z} \right) \quad (3.101)$$

and with a condition of pressure continuity along the solid bed:

$$\frac{\partial P^{(C)}}{\partial x} W_s = + \frac{\partial P^{(DE)}}{\partial x} (W_s + H_s) \quad (3.102)$$

where  $\tau_{yx|DE}$  and  $\tau_{yx|C}$  are the shear stresses acting on the interfaces A-DE and A-C, respectively.

The various system of equations are subjected to the following geometric constraints:

$$\delta_C + H_s + \delta_{DE} = H \quad (3.103)$$

$$W_B + W_s + \delta_{DE} = W \quad (3.104)$$

The discretisation by finite differences is similar to that presented to the other differential equations.

### Power consumption

The mechanical power consumption for the melting zone ( $e_m$ ), results from the contributions of the power dissipated on the melt films C ( $e_{mfC}$ ) and DE ( $e_{mfDE}$ ), on the melt pool ( $e_{mp}$ ), on the flight clearance ( $e_{mcl}$ ) and the power required to build up pressure ( $e_{mbp}$ ):

$$e_m = e_{mfC} + e_{mfDE} + e_{mp} + e_{mcl} + e_{mbp} \quad (3.105)$$

The power required for shearing the melt films and the melt pool results from the relative velocity between the metal surfaces (barrel and screw) and the solid bed:

$$e = \frac{\int_{y=0}^{y_{max}} \left[ \int_{z=0}^{\Delta z} \left( \int_{x=0}^{X'} (V_x(y) \tau_{yx}(y) + V_z(y) \tau_{yz}(y)) dx \right) dz \right] dy}{\int_{y=0}^{y_{max}} dy} \quad (3.106)$$

where  $\tau_{yx}$  and  $\tau_{yz}$  are the shear stresses in the directions  $x$  and  $z$ , respectively.

The integral in direction  $y$  is due to the variation of the velocities in this direction; a weighted average is computed. For melt film C the corresponding expression is:

$$e_{mfC} = \frac{\int_0^{\delta_C} W_s \Delta z (V_{x|C} \tau_{yx|C} + V_{z|C} \tau_{yz|C}) dy}{\int_0^{\delta_C} dy} \quad (3.107)$$

where  $W_s$  is the solid bed width and  $W_A*\Delta z$  is the area were the shear stresses act. For melt film DE is:

$$e_{mfDE} = \frac{\int_0^{\delta_{DE}} (W_s + H_s) \Delta z (V_{x|DE} \tau_{yx|DE} + V_{z|DE} \tau_{yz|DE}) dy}{\int_0^{\delta_{DE}} dy} \quad (3.108)$$

where  $H_s$  is the solid bed height and  $(W_s+H_s)*\Delta z$  is the area were the shear stresses act. Finally, for the melt pool:

$$e_{mp} = \frac{\int_0^H W_B \Delta z (V_{x|B} \tau_{yx|B} + V_{z|B} \tau_{yz|B}) dy}{\int_0^H dy} \quad (3.109)$$

where  $V_{z|B}$  and  $\tau_{yz|B}$  are the average values for each  $y$ , since they vary with  $x$  and  $y$ . The power consumption on the flight clearance and the required to build up pressure are, respectively:

$$e_{mcl} = \frac{V_b^{1+n} k_0 e}{\delta_f^n} \Delta z \quad (3.110)$$

$$e_{mbp} = Q \frac{\partial P}{\partial z} dz \quad (3.111)$$

### 3.6- Melt Conveying

The melt conveying, or pumping zone, develops after melting is completed. It contributes to mixing and to generate the required pressure to force the polymer through the die at a specific output. This, is the most studied functional zone since it determines the mass output of the extruder and its working characteristics can be inferred from a fluid mechanics analysis, without the need of extensive experimental work. Most theoretical analyses published so far considered the following type of simplifications [AME 89, RAU 86]:

- Polymer rheology – purely viscous Newtonian or non-Newtonian fluid.
- Isothermal or non-isothermal conditions.
- One-, two- or three-dimensional flow.
- Down channel convection effects – included or neglected.
- Leakage flow through the screw tips – included or neglected.

- Existing or not existing slip at the walls.

Table 3.1 summarises the assumptions made in the melt conveying models, according to Amellal *et al.* [AME 89]. Fenner *et al.* [FEN 77] compared experimental results with theoretical results obtained using various models. They conclude that, for most practical purposes, a two-dimensional analysis of developing non-isothermal non-Newtonian flow gave the satisfactory predictions.

**Table 3.1- Assumptions of melt conveying models (individual references are given in the review by Amellal *et al.* [AME 89]).**

Models	Assumptions					
	1	2	3	4	5	6
Rowell and Finlayson	Y	Y	2	N	N	N
Carley and Strub	Y	Y	2	N	N	N
Carley, Mallouk and Mckelvey	Y	Y	1	N	N	N
Carley and Mckelvey	Y	Y	1	N	N	N
Mallouk and Mckelvey	Y	Y	1	N	N	N
Mckelvey, Jepson	Y	Y	2	N	N	N
Squires	Y	Y	1	N	N	N
Mori and Matsumoto	N	Y	1	N	N	N
Griffith	N	Y	2	N	N	N
Squires	N	Y	1	N	N	N
Middleman	N	Y	2	N	N	N
Zamodits and Pearson	N	N	2	N	N	N
Dyer, Martin	N	N	2	N	N	N
Kaiser and Smith	N	N	2	Y	N	N
Donovan	N	Y	1	Y	Y	N
Fenner and Williams	N	N	2	Y	N	N
Palit and Fenner	Y	Y	2	N	N	N
Palit and Fenner	N	Y	2	N	N	N
Pittman <i>et al.</i>	Y	Y	2	N	Y	N
Choo, Hami and Pittman	N	Y	2	N	Y	N
Viriyayuthakorn and Kassahun	N	N	3	Y	Y	N
Brucker <i>et al.</i>	N	N	2	Y	Y	N
Meijer and Verbraak	Y	Y	1	N	N	Y

ASSUMPTIONS: 1- Newtonian flow, 2- Isothermal model, 3- Number of dimensions considered, 4- Convection included, 5- Leakage flow taken into account, 6- Slip at wall exists.

More recently, new studies have been reported (see table 3.2). Joo and Kwon [JOO 93] studied the effect of the 3D circulatory flow on the residence time distribution. Kim and Kwon [KIM 95a] suggested a simple approach to determine the screw characteristics for 3D flow, by introducing a Total Shape Factor to correct 2D flow analysis. They also compared the results of a quasi 3D model and of 2D model considering slip and concluded that slip effects are very significant [KIM 95b]. Chiruvella *et al.* [CHI 95b] developed a 2D non-

Newtonian non-isothermal model based on finite differences. Chang and Lin [CHA 95] developed a hybrid finite element finite difference method for simulating the non-Newtonian non-isothermal melt flow on the screw channel. The velocity and pressure fields were obtained using finite elements whereas temperature is computed using finite differences. Lekarou and Brandao [LEK 96] proposed a non-Newtonian non-isothermal model where a finite difference/finite volume method was used to solve the governing equations. More recently, Ghoreishy and Rafizadeh [GHO 96] developed a numerical algorithm based on the finite element method to solve the flow and energy equations under non-Newtonian and non-isothermal conditions. A least squares finite element method is used to solve the flow equations, whereas the energy equation is solved with the Bubnov-Galerkin formulation. Cheng *et al.* [CHE 97] studied the effect of the slip at the screw and barrel using a simple analytical model. Finally, Yu and Hu [YU 98] compared the results obtained with two simple analytical models, one assuming the traditional parallel plates geometry, the other a helical channel. They concluded that the second model reduces to the first when the channel depth-to-screw diameter ratio approaches zero. However, the use of these most sophisticated models needs to take into consideration the high computation times (principally when finite elements are used) that are involved.

**Table 3.2- Assumptions for the melt conveying models.**

Models	References	Assumptions					
		1	2	3	4	5	6
Joo and Kwon	[JOO 93]	N	Y	3	N	N	N
Kim and Kwon	[KIM 95a]	N	Y	3	N	N	N
Kim and Kwon	[KIM 95b]	N	Y	3	N	N	Y
Chiruvella, Jaluria and Abib	[CHI 95b]	N	N	2	Y	N	N
Chang and Lin	[CHA 95]	N	N	2	Y	N	N
Lekarou and Brandao	[LEK 96]	N	N	2	Y	N	N
Ghoreishy and Rafizadeh	[GHO 96]	N	N	2	Y	N	N
Cheng, Xie, Bigio and Briber	[CHE 97]	Y	Y	1	N	N	Y
Yu and Hu	[YU 98]	Y	Y	1	N	N	N

ASSUMPTIONS: 1- Newtonian flow, 2- Isothermal model, 3- Number of dimensions considered, 4- Convection included, 5- Leakage flow taken into account, 6- Slip at wall exists.

The model adopted in this work must be coherent with the previous zones and must be able to predict the most relevant process variables (pressure gradient, power consumption, temperature profile, residence time distribution and degree of mixing). The non-isothermal two-dimensional flow of a non-Newtonian fluid, in the presence of convection must,

therefore, be considered. Figure 3.21 presents the velocity and the temperature profiles for this zone. The following assumptions are made [FEN 77, FEN 79]:

- Gravitational and inertial forces are neglected;
- The molten polymer is a viscous fluid obeying to the power-law;
- The flow is steady;
- Leakage flow and wall slip are neglected;
- The flow is fully developed in the down and cross channel directions (i.e.,  $\partial V_x/\partial x = 0$  and  $\partial V_z/\partial z = 0$ );
- The temperature field is fully developed in the cross channel direction (i.e.,  $\partial T/\partial x = 0$ );
- Heat conduction in the down channel direction can be neglected (i.e.,  $\partial^2 T/\partial z^2 \ll \partial^2 T/\partial y^2$ ).

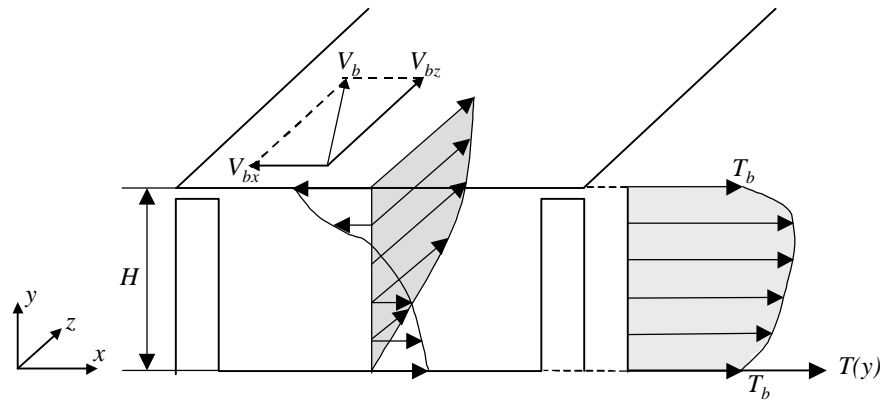


Figure 3.21- Cross-section for melt conveying zone.

Under these conditions, the governing equations are identical to those for the melt pool in the melting zone (equations 3.45, 3.46, 3.78 and 3.79). The relevant boundary conditions are:

$$\begin{cases} V_x(y=0) = 0 \\ V_x(y=H) = -V_{bx} \end{cases} \quad \begin{cases} V_z(x=0) = 0 \\ V_z(x=W) = 0 \\ V_z(y=0) = 0 \\ V_z(y=H) = V_{bz} \end{cases} \quad \begin{cases} T(x=0) = T_s \\ T(x=W) = T_s \\ T(y=0) = T_s \\ T(y=H) = T_b \end{cases} \quad (3.112)$$

### Power consumption

The power consumption ( $e_p$ ) results from the contribution of the power dissipated on the screw channel ( $e_{psc}$ ) on the flight clearance ( $e_{pci}$ ) and from the power required to build up pressure ( $e_{pp}$ ) which are given by equations 3.109 to 3.111, respectively [TAD 70, RAU 86].

## Residence time distribution (RTD) and mixing

The degree of mixing of a particular melt increases with the generation of interfacial area between its individual components and with the average flow residence time inside the extruder. The increase of interfacial area is proportional to the growth of shear strain of the melted polymer. The stress experienced by each polymer particle varies with its position in the screw channel. Particles close to the barrel and to the screw root suffer a greater level of stress than those in the centre. Therefore, the average strain can be used as a relatively simple but satisfying criterion to quantify the degree of mixing in an extruder [PIN 70, BIG 73, BIG 74].

Pinto and Tadmor [PIN 70] computed the Residence Time Distribution (RTD) and the “degree of mixing” (by means of a weighted-average total strain - WATS), assuming the isothermal flow of a Newtonian fluid between parallel plates. Bigg [BIG 73, BIG 74] developed a two-dimensional non-Newtonian isothermal model predicting the residence time and strain distributions. The velocity gradients on the  $x$  and  $z$  directions ( $V_x(y)$  and  $V_z(y)$ ) are computed numerically, assuming constant melt temperature and that  $V_z$  only varies with  $y$ .

The model used in this work follows generally the Bigg’s [BIG 73, BIG 74] analysis, but assumes that the velocity on the  $z$  direction varies with  $x$  and  $y$  and that flow is non-isothermal (equations 3.45, 3.46, 3.78 and 3.79). Since the molten polymer recirculates in the  $x$  direction, it is important to define the position that the same element of fluid occupies in upper ( $y$ ) and lower ( $y_c$ ) portions of the channel (Figure 3.22). These positions can be calculated from:

$$\int_0^{y_c} V_x(y) dy + \int_y^H V_x(y) dy = 0 \quad (1.113)$$

The time fraction that a fluid element spends on the upper portion of the channel is  $t_f$  (consequently, on the lower portion is  $1-t_f$ ).

$$t_f = \frac{1}{1 + \frac{V_x(y)}{V_x(y_c)}} \quad (1.114)$$

Each path-pair has a residence time associated with it -  $t(y)$ :

$$t(y) = \frac{L}{V_L(y)} \quad (1.115)$$

where  $V_L(y)$  is the velocity in the direction of the screw axis, calculated from:

$$V_L(y) = [V_x(y) + \bar{V}_z(y)] \sin \bar{\theta} \cos \bar{\theta} \quad (1.116)$$

and  $\bar{V}_z(y)$  is the average of the  $V_z(x,y)$  velocity in  $x$  direction, i.e.:

$$\bar{V}_z(y) = \sum_{i=0}^N V_z(x_i, y) / (N + 1) \quad (1.117)$$

where  $N$  is the number of increments (see figure 3.9).

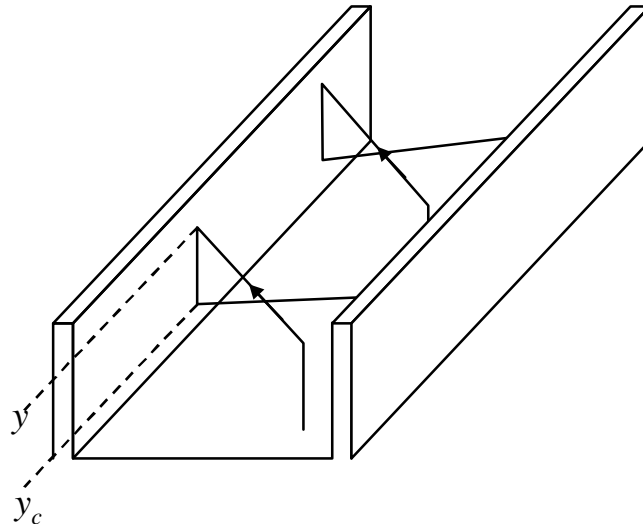


Figure 3.22- Circulation of a melt element along the upper and lower paths.

The weighted average total strain (WATS) can be calculated by integrating the strain experienced by a particle -  $\gamma(y)$  - with respect to the residence time distribution function -  $f(t)$ :

$$\bar{\gamma} = \int_0^{\infty} \gamma(y) f(t) dt \quad (1.118)$$

The residence time distribution function is obtained from:

$$f(t) dt = \frac{d(Q^* + Q_c^*)}{Q^* + Q_c^*} \quad (1.119)$$

where  $f(t)dt$  is the fraction of melt whose residence time lie in the range  $t$  to  $t+dt$ ,  $Q^* + Q_c^*$  is the total volumetric flow rate (i.e.,  $Q$ ),  $dQ^*$  and  $dQ_c^*$  are the differential flow associated with the neighbourhoods of planes  $y$  and  $y_c$ , respectively, so that:

$$d(Q^* + Q_c^*) = [\bar{V}_z(y) + \bar{V}_z(y_c)] dy \bar{W} \quad (1.120)$$

The average velocities are calculated from equation 1.117 for the corresponding  $y$  values.

The strain undergone by a melt element (necessary in equation 1.118) is given the shear rate multiplied by the time of shearing. A particle stays in the extruder a time  $t(y)$ , of which  $t_f$  is spent in the upper path and  $1-t_f$  in the lower path. Consequently,  $\gamma(y)$  is calculated from:

$$\gamma(y) = \dot{\gamma}(y)t(y)t_f + \dot{\gamma}(y_c)t(y)(1-t_f) \quad (1.121)$$

where the total shear rates in the upper and lower paths are determined with the aid of equation 3.80 with the following modification:

$$\frac{\partial V_z}{\partial x} = \frac{\sum_{i=0}^N V_z(x_i, y)}{N+1} \quad (1.122)$$

### 3.7- Computer implementation

This section describes the computer implementation of the individual models described previously. Routines for each one are initially developed. Then, a global model is built up through a coherent linkage between adjacent zones.

As depicted in figure 3.23 and described in greater detail in figure 3.24, the algorithm estimates two initial output values (from the screw geometry in the melt conveying zone and the screw speed) and carries out calculations along the down-channel direction. The down-channel length is divided into small increments. The variables calculated for element  $i$  will be used as input data for element  $i+1$ . The predicted pressure at the die exit is used as a convergence criterion. If this pressure is lower than  $\varepsilon$  (a sufficiently small value) the program stops; otherwise additional computations are carried out with new output values (defined by the Secant Method - figure 3.24). If a maximum number of pre-defined iterations are reached without convergence, this means that the input data (material properties, system geometry and operating conditions) is not adequate.

Simultaneously, another global model of the extrusion process (implemented previously [CUN 94]) will be studied. The model only differs in the theoretical models used for the individual zones, where analytical models are used (except in the calculation of the solid bed temperature profile for the solids conveying zone). Take into account the type of individual models used, the algorithm described and implemented here will be named numerical, whereas the other algorithm will be named analytical. Table 3.3 presents a comparison between the two in terms of the models used for the individual functional zones.

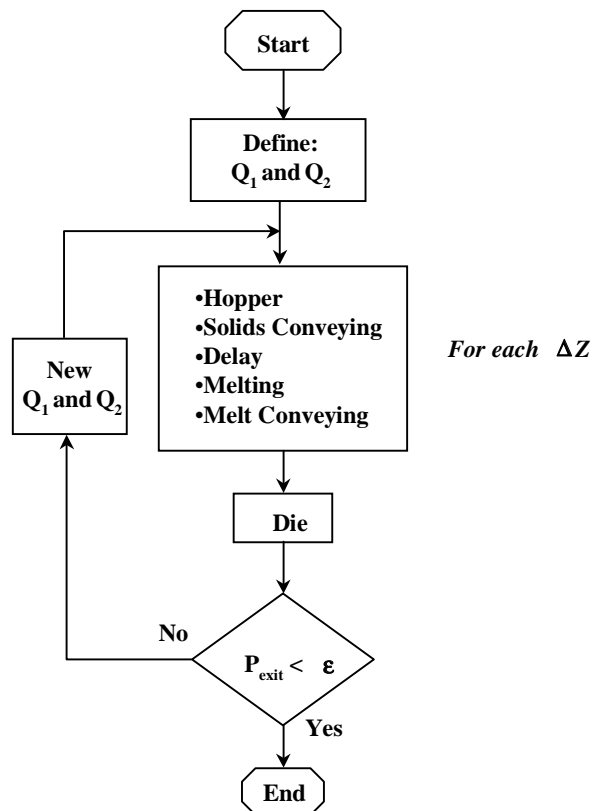


Figure 3.23- Global program structure.

```

Q1
P1 = f(Q1) [using the modelling routine]:
[Hopper, Solids Conveying, Delay Zone I, Delay Zone II
OR Melting, Melt Conveying and Die]
Q2
P2 = f(Q2) [using the modelling routine]:
[Hopper, Solids Conveying, Delay Zone I, Delay Zone II
OR Melting, Melt Conveying and Die]
Iteration = 2
do {
  if (P_iteration - P_iteration-1 > 0) {
    [permute Q_iteration-1 with Q_iteration]
    [permute P_iteration-1 with P_iteration]
  }

  Q_iteration+1 = Q_iteration - (Q_iteration-1 - Q_iteration) * (P_iteration - P_iteration-1) / (1 - P_iteration / P_iteration-1)

  P_iteration+1 = f(Q_iteration+1) [using the modelling routine]:
  [Hopper, Solids Conveying, Delay Zone I, Delay
  Zone II OR Melting, Melt Conveying and Die]
  iteration = iteration + 1
} while ((P_iteration+1 > ε) or (iteration < maximum n° of
iterations))
  
```

Figure 3.24- Global algorithm.

Table 3.3- Comparison between the analytical and the numerical models.

<i>Analytical model</i>	<i>Numerical model</i>
<ul style="list-style-type: none"> <li>• <b>Hopper</b> <ul style="list-style-type: none"> <li>- Walker [WAL 66] analysis (<i>static loading conditions</i>)</li> </ul> </li> <li>• <b>Solids conveying zone</b> <ul style="list-style-type: none"> <li>- Tadmor and Broyer [TAD 72] non-isothermal solid plug</li> </ul> </li> <li>• <b>Delay zone</b> <ul style="list-style-type: none"> <li>- Tadmor and Klein [TAD 70] is used to estimate the zone length</li> <li>- Chung [CHU 75] is used to compute the pressure profile</li> </ul> </li> <li>• <b>Melting zone</b> <ul style="list-style-type: none"> <li>- Tadmor [TAD 70] three-zone melting model, with a power law temperature dependent fluid</li> <li>- Melt temperature was computed assuming viscous dissipation with isothermal barrel and adiabatic screw [AGA 96]</li> </ul> </li> <li>• <b>Melt conveying zone</b> <ul style="list-style-type: none"> <li>- Non-Newtonian model [TAD 70] coupled to the above average melt temperature approach</li> </ul> </li> </ul>	<ul style="list-style-type: none"> <li>• <b>Hopper</b> <ul style="list-style-type: none"> <li>- Walker [WAL 66] <i>analysis (static loading conditions)</i></li> </ul> </li> <li>• <b>Solids conveying zone</b> <ul style="list-style-type: none"> <li>- Non-isothermal solid plug, with heat dissipation at all surfaces</li> </ul> </li> <li>• <b>Delay zone</b> <ul style="list-style-type: none"> <li>- Two sequential steps:               <ol style="list-style-type: none"> <li>1. Solid bed and a melt film near to the inner barrel wall (<i>with heat convection on the radial and longitudinal directions</i>)</li> <li>2. Solid bed surrounded by melt films</li> </ol> </li> </ul> </li> <li>• <b>Melting zone</b> <ul style="list-style-type: none"> <li>- Lindt <i>et al</i> [LIN 85, ELB 84] 5-zone model</li> </ul> </li> <li>• <b>Melt conveying zone</b> <ul style="list-style-type: none"> <li>- 2D non-isothermal flow of a non-Newtonian fluid [FEN 77]</li> </ul> </li> </ul>

## Hopper

The hopper is considered as a sequence of vertical and/or convergent columns containing loose pellets. In figure 3.25  $P_0$  is the boundary condition for section 1,  $P_1$  is the pressure at bottom of section 1 (and boundary condition for section 2), and identically for  $P_2$  and  $P_3$  (which correspond to a boundary condition for the solids conveying zone in the screw). The input data for calculating the vertical pressure profile include the pellets physical properties (density and internal and external friction coefficients), the system geometry and the height of material in the hopper.

## Solids conveying in the screw

The input data comprises the system geometry, the physical and thermal polymer properties and the local operating conditions. Below the hopper aperture the pressure is assumed to be constant and equal to the pressure at the bottom of the hopper. The calculations in this zone are made along small down-channel increments, where the polymer properties are up-dated

for the local pressure and temperature conditions (see figure 3.26). This zone ends when the material adjacent to the barrel surface reaches the polymer melting temperature. At that location the pressure, the solids conveying length, the power consumption, and the transversal temperature profile are known.

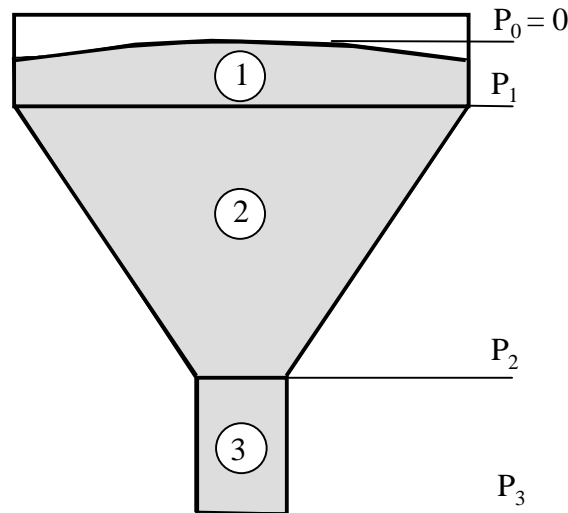


Figure 3.25- Hopper geometry.

### Delay zone

The entry conditions from preceding zone provide the possibility of predicting pressure, film thickness and transversal temperature profiles in the solid bed and in the melt film along the down-channel direction. When the temperature, near to the screw root, reaches the melting point, the zone ends. This zone leads either to a delay zone II or to the melting zone (as stated before, the delay zone II is a particular case of the melting zone). The computation algorithm is presented in figure 3.27. At the end of this zone the zone length, the film thickness, the film and solid bed transversal temperature profiles, the pressure and the mechanical power consumption are computed.

### Melting zone

Calculations for the melting zone require similar data to that of the delay zone. Figures 3.28 and 3.30 show the sequence of calculations for this zone. The results for this zone are pressure, films thickness, solids profile, films and solid bed transversal temperature profiles, melt pool two-dimensional temperature profile and power consumption.

## Melt conveying

The strategy adopted for this zone is illustrated in Figure 3.30. Pressure, two-dimensional temperature profile, power consumption, residence time distribution and weighted average total strain (WATS) constitute the calculations made for this zone.

```

----- Solids Conveying Zone -----
[INPUT DATA]
  • Geometry ( $W, H, \theta, e, \dots$ )
  • Material properties ( $f_s, f_b, \rho_s, \alpha_s, k_s, k_b, T_m$ )
  • Operating conditions ( $N, T_b, T_s, T_{s0}$ )
  • Entrance conditions ( $P_1$ )
 $z \leftarrow HG/\sin(\theta)$ 
 $P \leftarrow P_1$ 
 $T_{s\ mean} \leftarrow T_{s0}$ 
do {
  [Updating material properties for  $P$  and  $T_{s\ mean}$ ]
   $\phi \leftarrow$  equation 3.12
   $P_2 \leftarrow$  equation 3.13
   $T_{s\ i} \leftarrow$  equation 3.28 by finite differences
   $e_w \leftarrow$  equation 3.20
   $T_{s\ mean} \leftarrow$  Average  $T_{s\ i}$ 
   $P \leftarrow P_2$ 
   $z \leftarrow z + \Delta z$ 
} while (  $T_{s\ i}(y = H) < T_m$  )
[RESULTS]
   $Z_s$  (solids conveying length);
   $T_{s\ i}(z = Z_s); P(z = Z_s); e_w(z = Z_s)$ 

```

Figure 3.26- Algorithm for the solids conveying zone.

## Die

The calculations on the die are needed in order to calculate the operational point of the extruder/die combination and to validate experimentally the extrusion theoretical results. Since the objective of this work is to study the extruder (and not the die), the model for this zone should be able to predict pressure gradient values identical to that of the experimental results. Therefore, the pressure gradient in the die is computed using an empirical equation relating pressure and output:

$$\Delta P = C_1 Q^{C_2} \quad (3.123)$$

where  $C_1$  and  $C_2$  are constants determined experimentally.

```

----- Delay Zone I -----
[INPUT DATA]
  • Geometry ( $W, H, \theta, e, \dots$ )
  • Material properties ( $f_s, f_b, \rho_s, \alpha_s, k_s, k_b, k_m, T_m, \eta$ )
  • Operating conditions ( $N, T_b, T_s$ )
  • Entrance conditions ( $Z_s, T_{s_i}(z = Z_s), P(z = Z_s), e_w(z = Z_s)$ )
 $z \leftarrow Z_s$ 
 $P \leftarrow P(z = Z_s)$ 
 $T_{s \text{ mean}} \leftarrow \text{Average } T_{s_i}(z = Z_s)$ 
 $e_w \leftarrow e_w(z = Z_s)$ 
 $\delta_{c0} \leftarrow \delta_f$ 
do {
  [Updating solids properties for  $P$  and  $T_{s \text{ mean}}$ ]
   $P_2 \leftarrow \text{equation 3.70}$ 
  [Calculations on the film]
  do {
     $T_{f_{oi}} \leftarrow (T_{ib} + T_m)/2$ 
     $T_{f \text{ mean}} \leftarrow \text{Average } T_{f_{oi}}$ 
    [Updating melt properties for  $P$  and  $T_{f \text{ mean}}$ ]
     $V_{xi}, V_{zi} \leftarrow \text{Assume linear profile or take profile from previous } z$ 
    do {
       $V_{xoi} \leftarrow V_{xi}; V_{zoi} \leftarrow V_{zi}$ 
       $V_{xi} \leftarrow \text{equation 3.45 by finite differences}$ 
       $V_{zi} \leftarrow \text{equation 3.47 by finite differences}$ 
    } while ( $(V_{xoi} \neq V_{xi})$  and  $(V_{zoi} \neq V_{zi})$ )
     $T_{f_I} \leftarrow \text{equation 3.48 by finite differences}$ 
  } while ( $T_{f_i} \neq T_{f_{oi}}$ )
  [Iterative calculation of  $V_{sy}$ ]
   $T_{s_i} \leftarrow \text{equation 3.58 by finite differences}$ 
   $V_{sy} \leftarrow \text{equation 3.68}$ 
  do {
     $V_{sy0} \leftarrow V_{sy}$ 
     $T_{s_i} \leftarrow \text{equation 3.58 by finite differences}$ 
     $V_{sy} \leftarrow \text{equation 3.68}$ 
  } while ( $V_{sy0} \neq V_{sy}$ )
   $m_{c|z+\Delta z} \leftarrow \text{equation 3.62}$ 
   $m_{A|z+\Delta z} \leftarrow \text{equation 3.65}$ 
  [Iterative calculation of  $H_{sz}$ ]
   $H_{sz} \leftarrow H$ 
  do {
     $H_s \leftarrow H_{sz}$ 
     $\delta_c \leftarrow \text{equation 3.63}$ 
     $H_{sz} \leftarrow H - \delta_c$ 
  } while ( $H_{sz} \neq H_s$ )
   $e_w \leftarrow \text{equation 3.74}$ 
   $T_{s \text{ mean}} \leftarrow \text{Average } T_{s_I}$ 
   $T_{f \text{ mean}} \leftarrow \text{Average } T_{f_I}$ 
   $P \leftarrow P_2$ 
   $z \leftarrow z + \Delta z$ 
} while ( $T_s(y = 0) < T_m$ )
[RESULTS]
 $Z_d$  (length of delay zone I)
 $T_{s_I}(z = Z_d); T_{f_I}(z = Z_d)$ 
 $\delta_c(z = Z_d); P(z = Z_d); e_w(z = Z_d)$ 

```

Figure 3.27- Algorithm for delay zone I.

```

----- Delay Zone II OR Melting Zone -----
[INPUT DATA]
  • Geometry ( $W, H, \theta, e, \dots$ )
  • Material properties ( $f_s, f_b, \rho_s, \alpha_s, k_s, k_b, k_m, \eta$ )
  • Operating conditions ( $N, T_b, T_s$ )
  • Entrance conditions ( $Z_d, \delta_c, T_{s\ i}(z = Z_d), T_{f\ i}(z = Z_d), P(z = Z_d), e_w(z = Z_d)$ )
 $Z \leftarrow Z_s; P \leftarrow P(z = Z_s)$ 
 $T_{s\ mean} \leftarrow \text{Average } T_{s\ i}(z = Z_s)$ 
 $e_w \leftarrow e_w(z = Z_s); \delta_{c0} \leftarrow \delta_c; \delta_{DE0} \leftarrow \delta_f; W_{B0} \leftarrow 2\delta_f$ 
do {
   $P_2 \leftarrow \text{Subroutine DP\_DZ}$ 
  [Iterative calculation of  $V_{sy1}$  and  $V_{sy2}$ ]
     $V_{sy1} \leftarrow \text{equation 3.98}$ 
     $V_{sy2} \leftarrow \text{equation 3.99}$ 
    Do {
       $V_{0sy1} \leftarrow V_{sy1}; V_{0sy2} \leftarrow V_{sy2}$ 
      [Calculation of  $a, T_{s\ iI}$  and  $T_{s\ iII}$ , using the Secant Method -
      until  $T_{s\ iI} = T_{s\ iII}$ , at point  $a$ ]
       $T_{s\ iI} \leftarrow \text{equation 3.83 by finite differences}$ 
       $T_{s\ iII} \leftarrow \text{equation 3.84 by finite differences}$ 
       $V_{sy1} \leftarrow \text{equation 3.98}$ 
       $V_{sy2} \leftarrow \text{equation 3.99}$ 
    } while (( $V_{0sy1} \neq V_{sy1}$ ) and ( $V_{0sy2} \neq V_{sy2}$ ))
   $R_c \leftarrow \text{equation 3.90}; R_{DE} \leftarrow \text{equation 3.93}; m_{C/z} \leftarrow \text{equation 3.87};$ 
   $m_{Cx/z} \leftarrow \text{equation 3.88}; m_{Dex/z} \leftarrow \text{equation 3.89};$ 
   $m_{DE/z} \leftarrow \text{equation 3.92}; m_{C/z+\Delta z} \leftarrow \text{equation 3.86};$ 
   $m_{DE/z+\Delta z} \leftarrow \text{equation 3.91}; m_{A/z+\Delta z} \leftarrow \text{equation 3.94};$ 
   $m_{B/z+\Delta z} \leftarrow \text{equation 3.96}; m_{By} \leftarrow \text{equation 3.97}$ 
  [Iterative calculation of  $H_{sz}$  and  $W_{sz}$ ]
     $H_{sz} \leftarrow H; W_{sz} \leftarrow W_{B0}$ 
    do {
       $H_s \leftarrow H_{sz}; W_s \leftarrow W_{sz}$ 
       $\delta_c \leftarrow \text{equation 3.87}$ 
       $\delta_{DE} \leftarrow \text{equation 3.92}$ 
       $H_{sz} \leftarrow H - \delta_c - \delta_{DE}$ 
       $W_{sz} \leftarrow \text{equation 3.95}$ 
    } while (( $H_{sz} \neq H_s$ ) and ( $W_{sz} \neq W_s$ ))
   $e_w \leftarrow \text{equation 3.105}$ 
   $X/W \leftarrow W_{sz}/W$  [Solids Profile]
   $T_{s\ mean} \leftarrow \text{Average } T_{s\ iI} \text{ and } T_{s\ iII}$ 
   $T_{f\ mean}$  (zone B, C or DE)  $\leftarrow \text{Average } T_{f\ i}$  (zone B, C or DE)
   $P \leftarrow P_2$ 
   $z \leftarrow z + \Delta z$ 
} while ( $X/W > 1\%$ )
[RESULTS]
 $Z_m$  (length of melting zone)
 $T_{B\ i}(z = Z_m)$ 
 $P(z = Z_m)$ 
 $E_w(z = Z_m)$ 

```

Figure 3.28- Algorithm for delay zone II and melting zone.

```

----- Subroutine DP_DZ -----
dp/dz0 ← dp/dz from previous increment
dp/dzD ← dp/dzD from previous increment
do {
  dp/dzD0 ← dp/dzD
  [Zone C]
  do {
    TC mean ← Average TC 0I
    [Updating melt properties for P and TC mean]
    Vxi and Vzi ← Assume linear profile or take profile from previous z
    do {
      Vxoi ← Vxi; Vzoi ← Vzi
      Vxi ← equation 3.45; Vzi ← equation 3.47 by finite differences
    } while ((Vx0I ≠ Vzi) and (Vxoi ≠ Vzi))
    TC i ← equation 3.48 by finite differences
  } while (TC i ≠ TC 0i)
  [Zone DE]
  do {
    TDE 0i ← (Ts + Tm)/2; TDE mean ← Average TDE 0I
    [Updating melt properties for P and TDE mean]
    Vxi and Vzi ← Assume linear profile or take profile from previous z
    do {
      Vxoi ← Vxi; Vzoi ← Vzi
      Vxi ← equation 3.45; Vzi ← equation 3.47 by finite differences
    } while ((Vx0I ≠ Vxi) and (Vzoi ≠ Vzi))
    TB i ← equation 3.48 by finite differences
  } while (TDE i ≠ TDE 0i)
  dp/dzD ← equations 3.100 and 3.102
} while (|dp/dzD0 - dp/dzD| < error)
if (wB<H)
  then [Zone B - unidimensional]
  do {
    TB 0i ← (Ts + Tm)/2; TB mean ← Average TB 0i
    [Updating melt properties for P and TB mean]
    Vxi and Vzi ← Assume linear profile or take profile from previous z
    do {
      Vxoi ← Vxi; Vzoi ← Vzi
      Vxi ← equation 3.45; Vzi ← equation 3.47 by finite differences
    } while ((Vx0I ≠ Vxi) and (Vzoi ≠ Vzi))
    TB i ← equation 3.48 by finite differences
  } while (TB i ≠ TB 0i)
  else [Zone B - two-dimensional]
  do {
    TB 0ij ← (Ts + Tm)/2; TB mean ← Average TB 0ij
    [Updating melt properties for P and TB mean]
    Vxi, Vzij ← Assume linear profile or take profile from previous z
    do {
      Vxoi ← Vxi; Vzoi ← Vzij
      Vxi ← equation 3.45 by finite differences
      Vzij ← equation 3.78 by finite differences
    } while ((Vx0I ≠ Vxi) and (Vz0ij ≠ Vzij))
    TB ij ← equation 3.79 by finite differences
  } while (TB ij ≠ TB 0ij)
dp/dz ← equation 3.101
[RESULTS]
dp/dz
TC I
TDE I
TB ij

```

Figure 3.29- Melting zone: algorithm for the calculation of  $dp/dz$ .

```

----- Melt Conveying -----
[INPUT DATA]
• Geometry ( $W, H, \theta, e, \dots$ )
• Material properties ( $f_s, f_b, \rho_s, \alpha_s, k_s, k_b, k_m, \eta$ )
• Operating conditions ( $N, T_b, T_s$ )
• Entrance conditions ( $Z_m, T_{B\ ij}(z = Z_m), P(z = Z_m), e_w(z = Z_m)$ )
 $z \leftarrow Z_m$ 
 $P \leftarrow P(z = Z_m)$ 
 $T_{mean} \leftarrow$  Average  $T_{B\ ij}(z = Z_m)$ 
 $e_w \leftarrow e_w(z = Z_m)$ 
  do {
     $T_{mean} \leftarrow$  Average  $T_{0ij}$ 
    [Updating melt properties for  $P$  and  $T_{mean}$ ]
     $V_{xi}$  and  $V_{zij} \leftarrow$  Assume linear profile or take profile from previous zone
    do {
       $V_{xoi} \leftarrow V_{xi}$ 
       $V_{z0ij} \leftarrow V_{zij}$ 
       $V_{xi} \leftarrow$  equation 3.45 by finite differences
       $V_{zij} \leftarrow$  equation 3.78 by finite differences
    } while ( $(V_{x0i} \neq V_{xi})$  and  $(V_{z0ij} \neq V_{zij})$ )
     $T_{ij} \leftarrow$  equation 3.79 by finite differences
  } while ( $T_{ij} \neq T_{0ij}$ )
   $RTP \leftarrow$  equation 3.120
   $WATS \leftarrow$  equation 3.119
[RESULTS]
 $P$ 
 $T_{ij}$ 
 $RTP$ 
 $WATS$ 

```

Figure 3.30- Algorithm for the melt conveying zone.

## 4- EXPERIMENTAL WORK

### 4.1- Polymer properties

A High Density Polyethylene blown film extrusion grade (NCPE 0928, from BOREALIS) was used in the experimental part of the work. Some of the properties presented in Table 4.1 were determined experimentally (viscosity, melt density, specific heat, heat of fusion and melting temperature). As to the remaining properties, due to the impossibility to make their experimental determination, it was decided to opt by values existent in the literature for similar grades of the same polymer.

Viscosity curves were determined at typical extrusion shear rates (between 6 and 300 s<sup>-1</sup>) and temperatures (160, 190 and 220 °C) using a twin-bore capillary rheometer (ROSAND RH-7-2, see Figure 4.1). The experiment is computer controlled, the user only defining the set of descent speed of the pistons. The tests were made at constant speed, the shear rate being proportional to this velocity and the shear stress being calculated from the pressure read by a transducer at bottom of the barrels. The Bagley and Rabinowitsch corrections are performed automatically in order to obtain the real value of the viscosity. The flow curves (appendix B) for the three temperatures considered allow the calculation of the power law constants (Table 4.1).

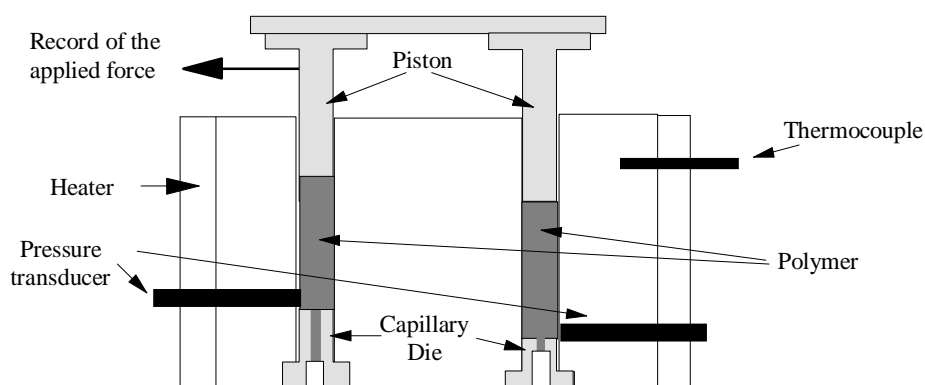


Figure 4.1- Capillary rheometer scheme.

The melt density has been determined using the same capillary rheometer, but adjusted to construct the diagram pressure/volume/temperature (PVT). The PVT test relates the volume filled by a fixed quantity of material with pressure and temperature. In this test only one barrel of the rheometer is used, Figure 4.2. The experimental procedure involves the compression (at

constant speed and fixed temperature) of a known quantity of material while the pressure and the volume are recorded. The test was made at three typical extrusion temperatures (160, 190 and 220 °C). Relating melt density with temperature and pressure it is possible to obtain the constants of the corresponding equation (Table 4.1). The PVT curves were presented in appendix B.

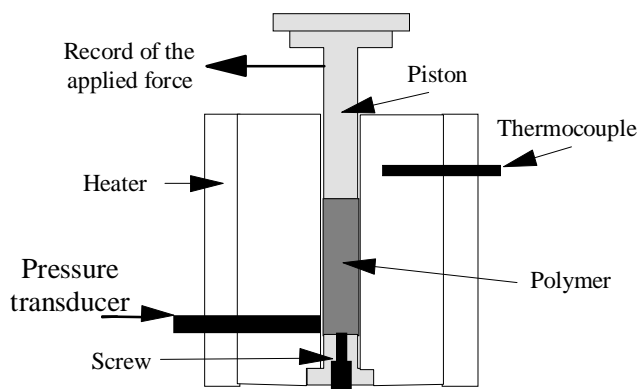


Figure 4.2- Capillary rheometer scheme, adjusted to PVT tests.

The specific heat, heat of fusion and the melting temperature were determined experimentally with a PERKIN ELMER Differential Scanning Calorimeter (DSC 7). This device is constituted by two ovens, where it is possible to vary the temperature of both the sample and the reference, and by two temperature sensors, as shown in Figure 4.3. This device is based in the Flux Compensation Principle: the signal detected is a measure of the difference between the heat fluxes that cross the ovens of the sample and the reference. These heat fluxes were received independently by each one of the ovens, so that the sample oven temperature is equal to the reference oven temperature (with differences less than 0.01 °C). The results obtained are presented in Appendix B and summarised in Table 4.1.

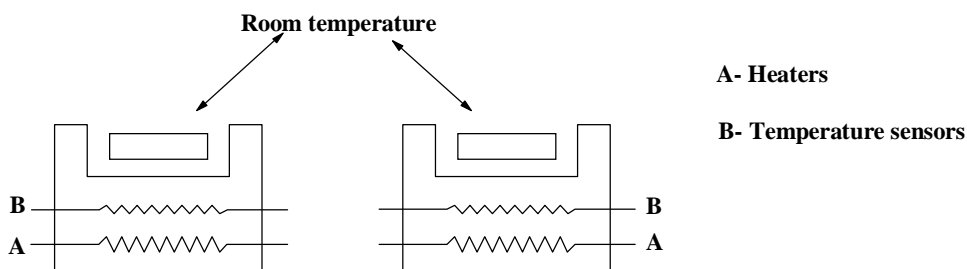


Figure 4.3- DSC scheme.



Although the extruder is able to control 6 independent zones, as shown in Figure 4.4, the heater bands were grouped into three zones plus the die (for direct comparison with the computations, as will be discussed later).

The extruder was instrumented with flush-mounted pressure and temperature dynisco-type transducers, as shown in figure 4.5. A computer equipped with a data acquisition board was used to read the pressure, whereas the temperature was read with temperature indicators. The power consumption was obtained from the motor amperage indicated by the machine control system. The extruder was equipped with a pneumatic screw extraction device, specially developed for this work, thus making it possible to determine the length of screw required for melting.

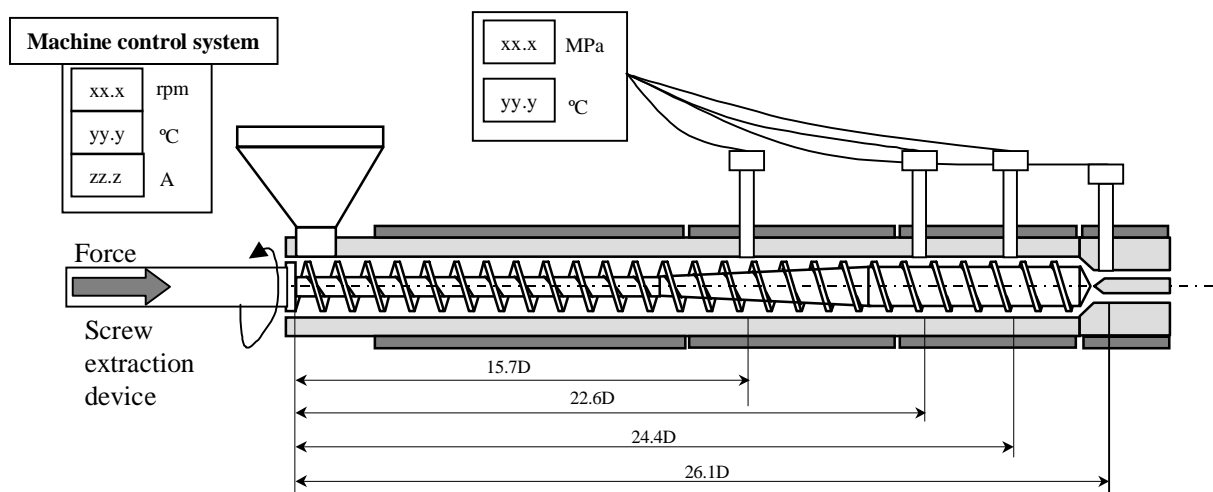


Figure 4.2- Layout of the pressure/temperature transducers and screw extraction device.

The experimental procedure for the extruder experiments is the following:

- i) Connect the extruder using the pre-defined operating conditions;
- ii) Wait until the process stabilises (circa 30 minutes);
- iii) Read and record the motor amperage indicated by the machine control system;
- iv) Read and record the temperature and pressure values using the data acquisition system;
- v) Extract the screw:
  - a) Stop the machine;
  - b) Disconnect the temperature resistances;
  - c) Take off the die;
  - d) Connect the screw extraction device and collect the screw outside the extruder;
  - e) Take the polymer from the screw channel marking the number of the spires;

#### 4.3- Statistical design of experiments

Considering the time consuming and cost intensive characteristics of the experimental work involved in the trial-and-error optimisation of the extrusion operating conditions for specific polymer/equipment combinations, its relevance in determining the influence of and the interactions between the various input variables [MON 91], a full factorial design of experiments was adopted.

As seen in Chapter 1, this type of analysis consists in the study of the process response observed when the input variables are changed, as well as in the possibility to relate these changes with the input variables. The independent variables susceptible of influencing the experimental results (dependent or output variables) are classified in several levels of intensity. The effect of a factor is defined as the change in response that results from a change in the factor level. The interaction between factors corresponds to the different responses observed when the level of one factor is changed, and the differences in response between the levels of this factor are not identical at all levels of the other factors [MON 91].

Table 4.2 presents the four independent factors chosen to be studied in this work (screw speed,  $N$  and three-barrel temperatures,  $T_1$ ,  $T_2$  and  $T_3$ ). Since each factor is varied at three levels,  $3^4$  experiments should be carried out. Table 4.3 lists the experiments, which are to be performed in random order. In order to identify the possible interactions between variables it was necessary to replicate the experiments; in the present study, each experiment was replicated three times, thus increasing the total amount of work to 243 experiments. In order to minimise the required effort only mass output, melt temperature (at die entrance) and mechanical power consumption were monitored for each experiment.

Table 4.2- Definition of factors and levels for the experiments.

FACTORS (4)			LEVELS (3)		
Rotation speed (rpm)		<b>N</b>	10	30	50
Barrel Temperatures (°C)	Zone 1	$T_1$	150	170	190
	Zone 2	$T_2$	160	180	200
	Zone 3	$T_3$	170	190	210

Two types of analysis were performed with this experiments, namely an Analysis of Variance (ANOVA) and a Multivariate Analysis of Variance (MANOVA) [CHA 96]. In the former, the analysis is performed on each of the dependent variables. In the MANOVA analysis the four

variables are considered simultaneously in order to detect a potential degree of correlation between them.

**Table 4.3- List of experiments.**

Experiment No.	$T_1$ (°C)	$T_2$ (°C)	$T_3$ (°C)	$N$ (rpm)
A1, A2, A3	150	160	170	10, 30, 50
A4, A5, A6	150	160	190	10, 30, 50
A7, A8, A9	150	160	210	10, 30, 50
A10, A11, A12	150	180	170	10, 30, 50
A13, A14, A15	150	180	190	10, 30, 50
A16, A17, A18	150	180	210	10, 30, 50
A19, A20, A21	150	200	170	10, 30, 50
A22, A23, A24	150	200	190	10, 30, 50
A25, A26, A27	150	200	210	10, 30, 50
A28, A29, A30	170	160	170	10, 30, 50
A31, A32, A33	170	160	190	10, 30, 50
A34, A35, A36	170	160	210	10, 30, 50
A37, A38, A39	170	180	170	10, 30, 50
A40, A41, A42	170	180	190	10, 30, 50
A43, A44, A45	170	180	210	10, 30, 50
A46, A47, A48	170	200	170	10, 30, 50
A49, A50, A51	170	200	190	10, 30, 50
A52, A53, A54	170	200	210	10, 30, 50
<b>A55, A56, A57</b>	190	160	170	10, 30, 50
A58, A59, A60	190	160	190	10, 30, 50
A61, A62, A63	190	160	210	10, 30, 50
A64, A65, A66	190	180	170	10, 30, 50
A67, A68, A69	190	180	190	10, 30, 50
A70, A71, A72	190	180	210	10, 30, 50
A73, A74, A75	190	200	170	10, 30, 50
A76, A77, A78	190	200	190	10, 30, 50
A79, A80, A81	190	200	210	10, 30, 50

#### 4.4- Experiments related to the assessment of GAs

As seen in section 2.3, extrusion optimisation with GAs starts with a population of points well distributed along the search space and proceeds until virtually all population elements have identical values. In the process, as new generations are created, the average performance of the population improves progressively. As discussed later, it was decided to carry out experiments using the operating conditions predicted for specific generations and to monitor the value and the evolution of the objective function. The list of experiments and

corresponding generation number is presented in Table 4.4 (see also Figure 5.22). The output, melt temperature at extruder exit, pressure along the barrel, power consumption and solids bed profile were monitored.

**Table 4.4- List of experiments to assess the optimisation results.**

<b>Experiment Number</b>	<b>Processing Conditions</b>				<b>Generation</b>
	<i>N</i> (rpm)	$T_1$ (°C)	$T_2$ (°C)	$T_3$ (°C)	
<b>Exp1</b>	29	165	180	190	0
<b>Exp2</b>	46	163	172	188	5
<b>Exp3</b>	48	160	168	185	10
<b>Exp4</b>	49	156	164	193	15
<b>Exp5</b>	50	153	161	189	20
<b>Exp6</b>	50	151	161	175	30
<b>Exp7</b>	50	150	160	170	40
<b>Exp8*</b>	44	165	176	188	0

## 5- RESULTS AND DISCUSSION

### 5.1- Introduction

In this chapter the most important numerical modelling and Genetic Algorithm parameters will be defined. The predictions of the modelling package will be discussed and compared with experimental data. Two case studies involving the optimisation of the operating conditions and screw design will be studied in detail. Comparison with experimental trial-and-error optimisation results will be used to assess the methodology.

### 5.2- Case studies

The extrusion case studies presented in this section will be used as reference for the optimisation of the operating conditions and for the screw design. These examples will be followed by both, the computational and the extrusion experiments.

#### a) **Optimisation of the operating conditions**

This example will deal with the optimisation of the operating conditions, i.e., the aim is to set the screw speed ( $N$ ) and the barrel temperature profile in three zones ( $T_1$ ,  $T_2$  and  $T_3$ ) of the Leistritz extruder available. Table 5.1 shows their range of variation.

**Table 5.1- Range of variation of the processing conditions.**

<b>Processing conditions</b>	<b>Minimum</b>	<b>Maximum</b>
Screw speed (rpm)	10	50
Barrel Temperature – Zone 1 (°C)	150	190
Barrel Temperature – Zone 2 (°C)	160	200
Barrel Temperature – Zone 3 (°C)	170	210

Therefore, each chromosome will be formed by 4 parts (one for each variable) each having 6 genes, with a total length  $l = 24$  (Figure 5.1).

<b>N</b> <b>(6)</b>	<b><math>T_1</math></b> <b>(6)</b>	<b><math>T_2</math></b> <b>(6)</b>	<b><math>T_3</math></b> <b>(6)</b>
------------------------	---------------------------------------	---------------------------------------	---------------------------------------

Figure 5.1- Chromosome structure.

Table 5.2 defines the criteria to optimise, their corresponding objective (maximisation or minimisation) and the allowable limits ( $X_{i \min}$  and  $X_{i \max}$ ). The relative importance is established by a set of weights ( $w_i$ ) - Table 5.3. Five case studies were considered.

Table 5.2- Criteria definition.

Criteria	Objective	$X_{i \min}$	$X_{i \max}$
Output (Kg/hr)	Maximise	1	9
Length of screw required for melting (mm)	Minimise	200	821
Melt temperature ( $^{\circ}\text{C}$ )	Minimise	150	210
Power consumption (W)	Minimise	0	3000

Table 5.3- Weights of the individual criteria.

Case Studies	Weights			
	$W_1$	$W_2$	$W_3$	$W_4$
OF1	0.5	0.2	0.2	0.1
OF2	0.2	0.5	0.2	0.1
OF3	0.2	0.2	0.5	0.1
OF4	0.1	0.2	0.2	0.5
OF5	0.25	0.25	0.25	0.25

### b) Screw design

The methodology adopted for screw design will be illustrated with an example. The aim is to design a three-zone screw, i.e., to optimise the geometrical parameters shown in Figure 5.2 that satisfy the criteria contained in Table 5.4.

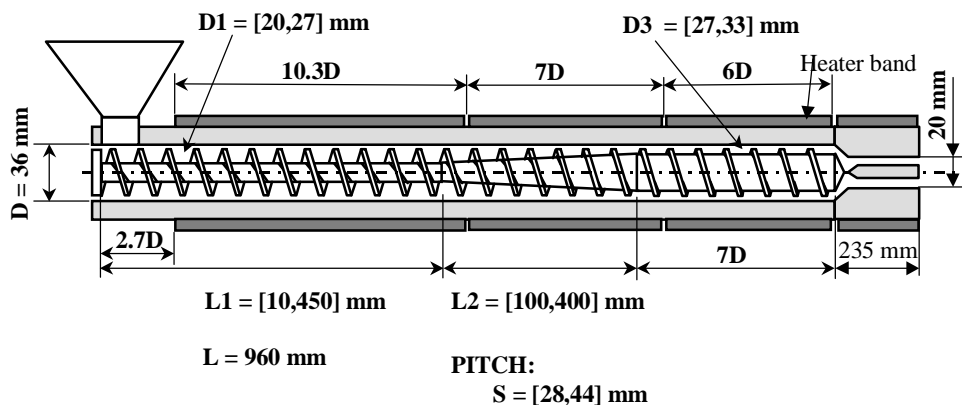


Figure 5.2- Designing a screw: parameters to optimise.

As shown in Table 5.5, various situations will be studied successively. Different individual objectives, multiple objectives but with different criteria weights, variations in the processing conditions, or the use of various polymers, will be considered. The use of various polymers in the same extruder will be simulated by considering the extrusion of HDPE, LDPE and PVC,

each under its typical processing conditions. The optimisations will be made using GAs with objective function and using the analytical model. Some additional runs, where the multiobjective optimisation GA and the numerical model are used, will also be made. The LDPE and PVC properties were presented in Appendix B.

**Table 5.4- Criteria to satisfy.**

Criteria	Objective	$X_{i \min}$	$X_{i \max}$
Output (Kg/hr)	Maximise	0	15
Length of screw required for melting (mm)	Minimise	200	936
Melt temperature (°C)	Minimise	160	230
Power consumption (W)	Minimise	0	10000
Mixing quality (WATS)	Maximise	0	1300

**Table 5.5- Runs for screw design (objective function GA).**

Run	Aim of the Optimisation	Optimisation Criteria (Weights)					Processing conditions				Polymer		
		Q	T	L	P	W	N	T1	T2	T3			
1	Individual Criteria	1	0	0	0	0	50	150	160	170	HDPE		
2		0	1	0	0	0	50	150	160	170	HDPE		
3		0	0	1	0	0	50	150	160	170	HDPE		
4		0	0	0	1	0	50	150	160	170	HDPE		
5		0	0	0	0	1	50	150	160	170	HDPE		
6	Multiple Criteria	Different Relative Weights	0.5	0.1	0.2	0.1	0.1	50	150	160	170	HDPE	
7			0.2	0.2	0.2	0.2	0.2	50	150	160	170	HDPE	
8			0.2	0.3	0.2	0.1	0.2	50	150	160	170	HDPE	
9			0.1	0.1	0.2	0.5	0.1	50	150	160	170	HDPE	
6		Reproducibility	0.5	0.1	0.2	0.1	0.1	50	150	160	170	HDPE	
10			0.5	0.1	0.2	0.1	0.1	50	150	160	170	HDPE	
11			0.5	0.1	0.2	0.1	0.1	50	150	160	170	HDPE	
12		Processing Conditions	0.5	0.1	0.2	0.1	0.1	10	150	160	170	HDPE	
13			0.5	0.1	0.2	0.1	0.1	30	150	160	170	HDPE	
6			0.5	0.1	0.2	0.1	0.1	50	150	160	170	HDPE	
14		Screw Pitch	0.5	0.1	0.2	0.1	0.1	50	150	160	170	HDPE	Constant
15			0.5	0.1	0.2	0.1	0.1	50	150	160	170	HDPE	Variable
6		Different Materials	0.5	0.1	0.2	0.1	0.1	50	150	160	170	HDPE	
16			0.5	0.1	0.2	0.1	0.1	50	150	160	170	LDPE	
17			0.5	0.1	0.2	0.1	0.1	50	170	180	200	PVC	
18		Viscosity	0.5	0.1	0.2	0.1	0.1	50	150	160	170	HDPE*	Lower
19			0.5	0.1	0.2	0.1	0.1	50	150	160	170	HDPE*	Higher

### 5.3- Modelling results

#### 5.3.1- **Setting the numerical modelling parameters**

The results of the numerical modelling of the plasticating polymer extrusion process depend on the initial input values of some parameters. Some of these are associated with the numerical algorithm (e.g., the grid size in the transversal plane -  $xy$ , length of the increment in the down-channel direction), while others concern to process variables (initial thickness of the films surrounding the solid bed, initial melt pool width, criterion to estimate the length of delay zone II, screw temperature along the solids conveying zone).

##### a) **Grid size in the transversal plane - $xy$**

The use of a small grid to model a process using finite differences leads, almost invariably, to more accurate results. However, since this is also obtained at the expense of a greater computation time, a careful balance needs to be made, particularly if the modelling package is to be used in connection with an optimisation algorithm. In order to establish this, various runs were made using a different number of grid points, as indicated in Table 5.6 and studying the variation of the responses of the parameters listed in Figure 5.3.

**Table 5.6- Number of grid points.**

Run number	Number of grid points	
	X	Y
1	5	5
2	8	8
3	10	10
4	12	12
5	13	13
6	14	14
7	15	15
8	20	20
9	25	25
10	30	30

Figures 5.4 to 5.8 show the evolution of single valued responses *versus* the number of grid points (line with full symbols), and their relative difference to the preceding value (line with open symbols). Results obtained with less than 8 grid points are very poor; results obtained with 10 to 15 points are reasonable (relative differences lower than 5%). Above 15 grid points

the relative differences are lower than 2%. The oscillations of the relative differences for some responses do not represent any additional error of the numerical model.

- Single values:
  - output,
  - maximum pressure,
  - power consumption,
  - melt temperature at the extruder exit,
  - length of screw required for melting,
- Profiles along down-channel direction ( $Z$ ):
  - solid bed,
  - pressure,
  - melt temperature,
  - power consumption,
  - thickness of the film close to the barrel surface,
- Cross-temperature and velocity profiles in the down-channel direction.

Figure 5.3- Response parameters to study.

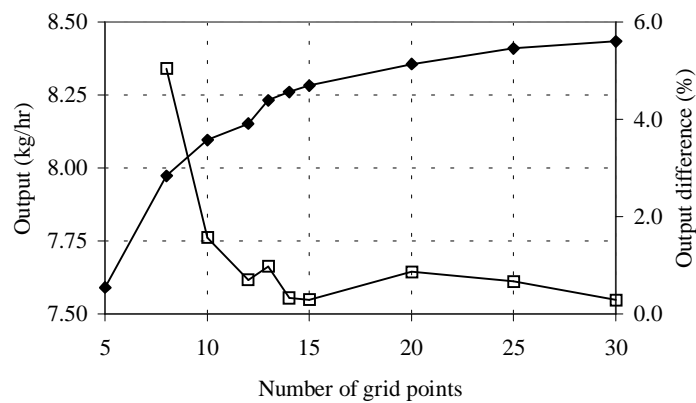


Figure 5.4- Output and relative difference vs. number of grid points.

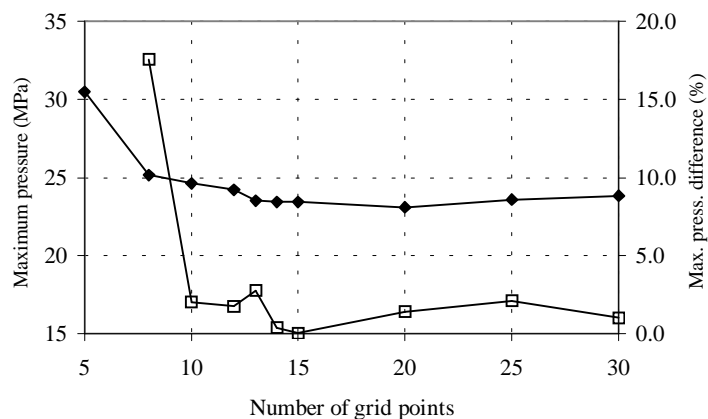


Figure 5.5- Maximum pressure and relative difference vs. number of grid points.

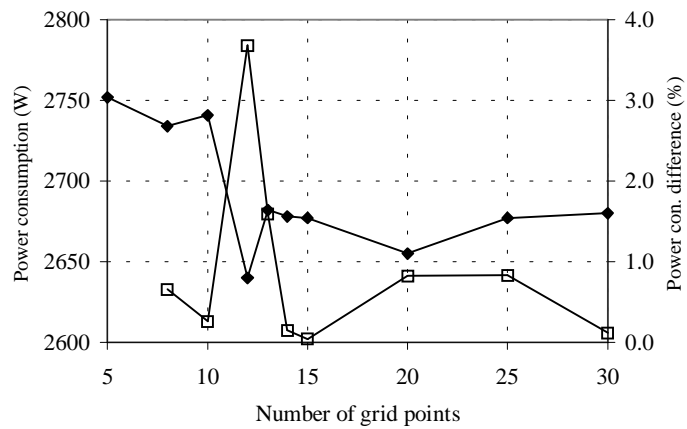


Figure 5.6- Power consumption and relative difference vs. number of grid points.

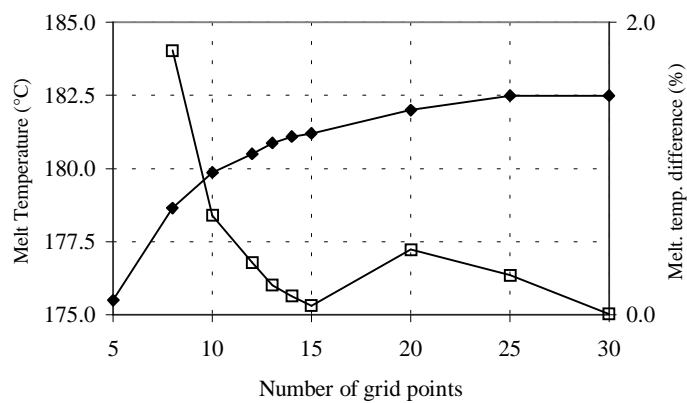


Figure 5.7- Melt temperature and relative difference vs. number of grid points.

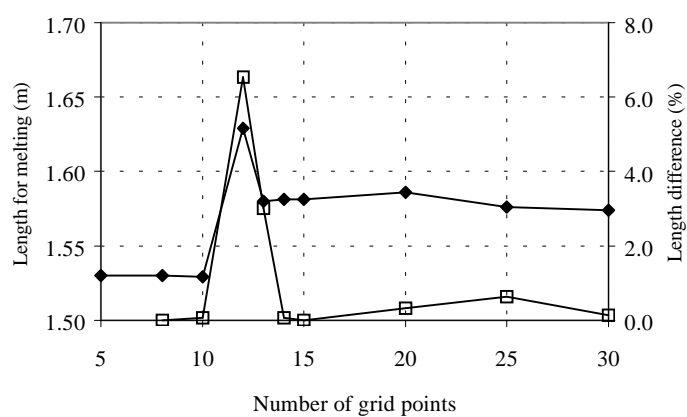


Figure 5.8- Length required for melting and relative difference vs. number of grid points.

Figures 5.9 and 5.10 represent the effect of the grid size for the pressure and melt temperature profiles, where a bigger grid influence was detected. Above 5 grid points the profiles become virtually identical.

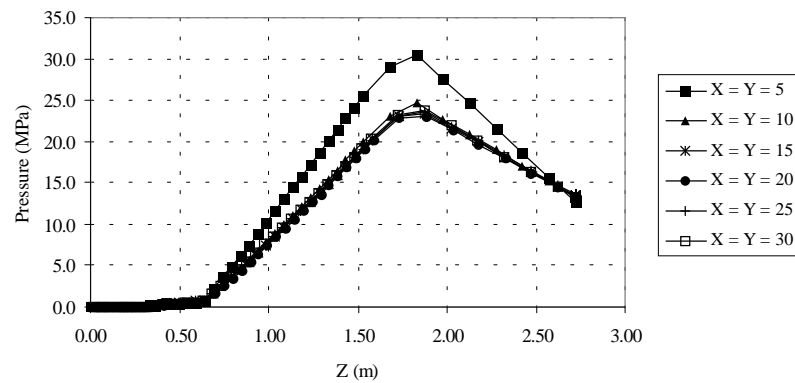


Figure 5.9- Pressure profile vs. number of grid points.

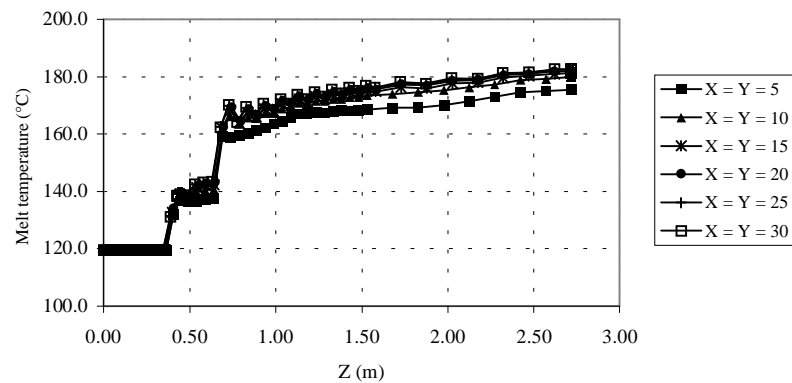


Figure 5.10- Melt temperature profile vs. number of grid points.

Figure 5.11 presents transversal temperature and velocity profiles for 5 and 20 grid points. Cross-sections in the solids conveying, delay, melting and melt conveying zones were considered. The profiles on the left have the same shape and order of magnitude than those on the right.

The computation time required for the various runs is identified in Figure 5.12. As expected, computationally time growth exponentially upon a linear increase of the number of grid points.

Considering the results presented, it seems that the most adequate grid size to use depends on the application. If the modelling package is to be used in association with an optimisation algorithm, where it needs to be used many times, a grid size of 10 seems preferable. If the objective is to study a specific processing situation, where a few runs are needed, a grid size of at least 15 points will be more advisable.

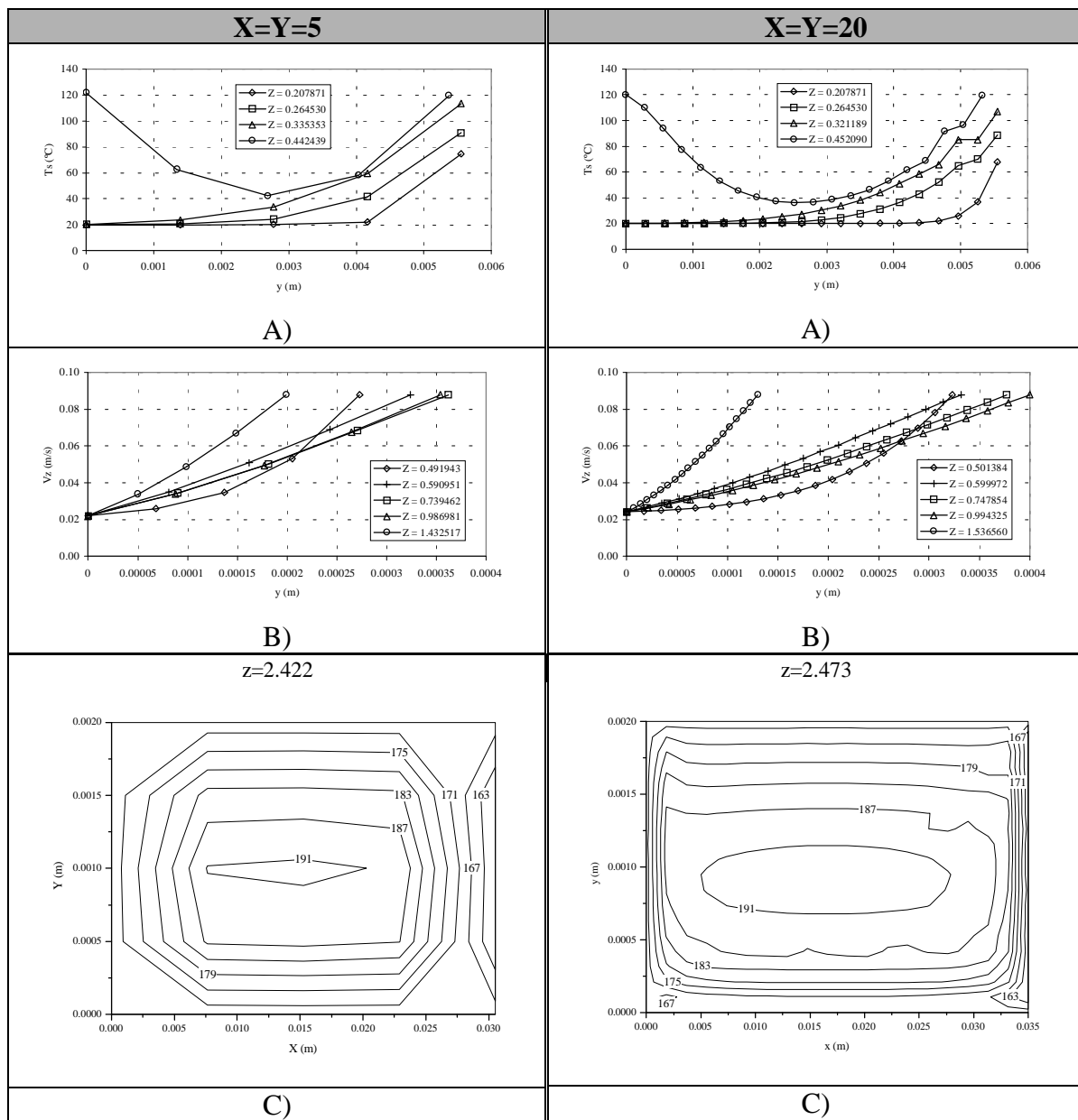


Figure 5.11- Transversal profiles: A) solid bed temperature profile for the solid and delay zones; B)  $V_z$  velocity profile in zone C for the melting zone; C) two-dimensional temperature profile in the pumping zone.

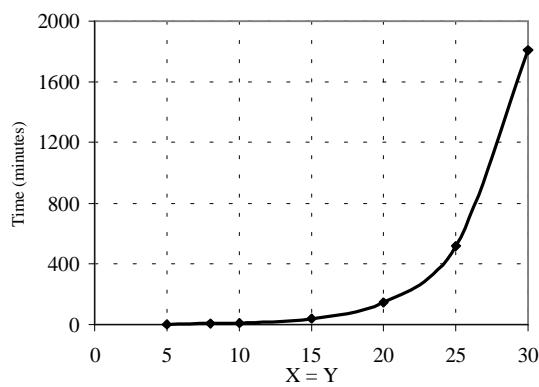


Figure 5.12- Computation time versus number of grid points.

### b) Increment along the down-channel direction - $z$

The effect of the size of the increment used in the down-channel direction on the stability of the results was identified after carrying out the runs shown in Table 5.7.

**Table 5.7- Number of increments in  $z$  direction.**

Run number	Number of increments in $z$ direction (ZB)
1	80
2	90
3	100
4	110
5	120
6	130

Again, changes in output, maximum pressure, power consumption, melt temperature, length of screw required for melting, with different increments along the down-channel direction were studied. Above 100 elements the maximum pressure is stable (variability lower than 3%, as shown in Figure 5.13), and the screw length required for melting varies less than 9% (Figure 5.14). The variability of the output, power consumption and melt temperature is inferior, respectively, to 2%, 5% and 0.2% (see appendix C). Obviously the use of a larger number of increment points requires greater computation times but, as shown in Figure 5.15 this increase is not relevant, principally when compared with their growth when the grid size increases, as settled before. The profiles of process variables along the down-channel direction become unstable for 80 or less increments (particularly in the case of pressure, solid bed and film thickness profiles).

Therefore, it can be inferred from the above that it should use at least 100 increments.

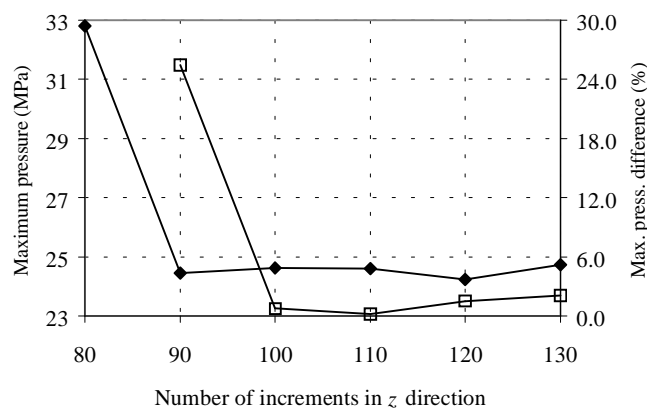


Figure 5.13- Maximum pressure and relative difference vs. number of increments in  $z$  direction.

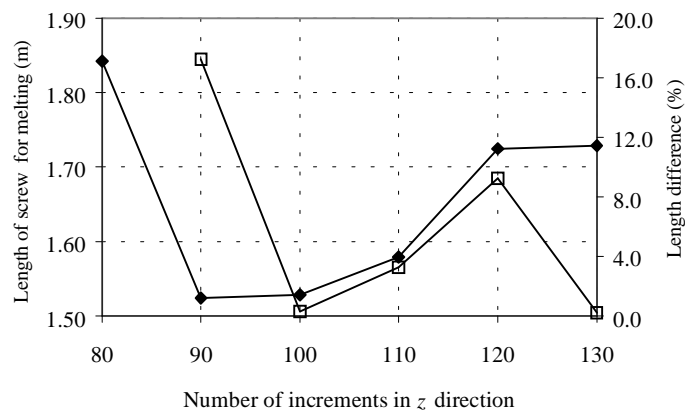


Figure 5.14- Length required for melting and relative difference *vs.* number of increments in  $z$  direction.

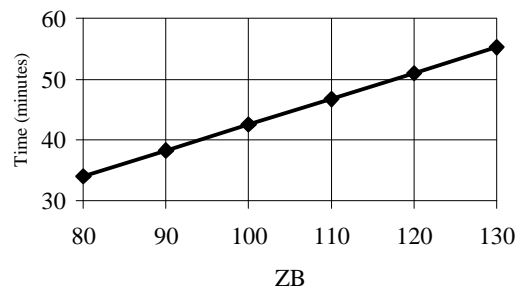


Figure 5.15- Computation time *versus* the number of increments in  $z$  direction.

### 5.3.2- Parameters definition

#### a) Initial thickness of the film close to the barrel surface

Three runs were made in order to study the influence of the initial thickness of the film close to barrel surface (zone C, Figure 3.13) on the results. An initial value of this film is needed at the beginning of delay zone I. The results are shown in Table 5.8, where the flight clearance ( $\delta_p$ ) is equal to 0.1 mm. No significant differences are perceived. A similar behaviour would be obtained upon considering profiles along the down-channel direction, particularly the film thickness profile (Figure 5.16).

#### b) Initial thickness of the film close to the screw root and passive flank

Three runs were also used to study the influence of the initial thickness of the film close to the screw root (zone E) and to the screw passive flank (zone D) surfaces (Figure 3.16). These

variables must be assumed at the beginning of delay zone II, where they are considered to be equal. Table 5.9 and Figure 5.17 shows that differences between runs can attain 6.5% in the case of maximum pressure and for screw length required for melting. Then, any of these values can be used for this parameter.

Table 5.8- Effect of the initial thickness of the film close to barrel surface.

Run	$\delta_{C0}$	Output (kg/hr)	Maximum Pressure (MPa)	Power Consumption (W)	Melt Temperature (°C)	Length for Melting (m)
1	$\delta_f$	8.097	24.63	2741	179.86	1.529
2	$2\delta_f$	8.097	24.63	2735	179.86	1.529
3	$4\delta_f$	8.104	24.58	2727	179.85	1.529
<b>Maximum difference (%)</b>		0.09	0.20	0.51	0.006	0.0

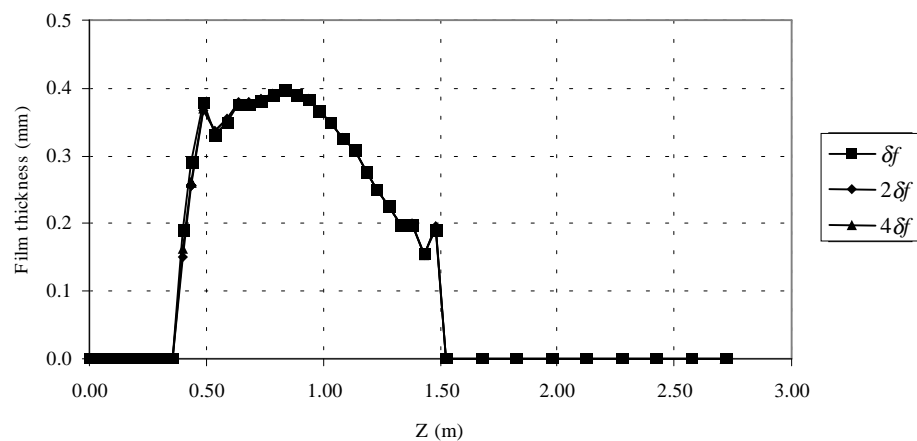


Figure 5.16- Film thickness profile vs. initial thickness value.

Table 5.9- Effect of the initial thickness of film close to screw and passive flank surfaces.

Run	$\delta_{D0}$	Output (kg/hr)	Maximum Pressure (MPa)	Power Consumption (W)	Melt Temperature (°C)	Length for Melting (m)
1	$\delta_f$	8.097	24.63	2741	179.86	1.529
2	$2\delta_f$	8.054	25.14	2641	179.44	1.628
3	$4\delta_f$	8.160	25.68	2735	179.76	1.529
<b>Maximum difference (%)</b>		1.3	6.5	3.8	0.23	6.5

### c) Initial melt pool width (or thickness of the film close to the passive flank)

The effect of this parameter (zone B, Figure 3.15) was studied through the 6 runs identified in Table 5.10. At the beginning of delay zone II, it starts as a thin film, whose width increases as melting proceeds. Power consumption and length required for melting are the most sensitive

parameters (7.5% and 12.9%, respectively). However, if runs 1 and 6 are ignored, the differences are, almost, null. Figure 5.18 illustrates the effect of this initial value on the solid bed profile. Only for  $W_{B0}$  equal to  $30\delta_f$  some differences are perceived. Consequently, any value in the interval  $[2\delta_f, 15\delta_f]$  can be used for this parameter.

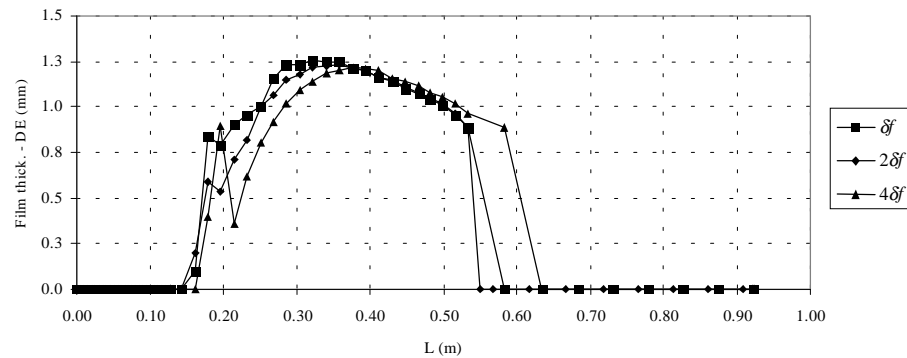


Figure 5.17- Film thickness profiles for zone DE vs. initial thickness of this film.

Table 5.10- Effect of the initial width of the melt pool.

Run	$W_{B0}$	Output (kg/hr)	Maximum Pressure (MPa)	Power Consumption (W)	Melt Temperature ( $^{\circ}\text{C}$ )	Length for Melting (m)
1	$\delta_f$	8.086	24.25	2694	179.79	1.727
2	$2\delta_f$	8.097	24.63	2741	179.86	1.529
3	$4\delta_f$	8.098	24.66	2740	179.86	1.529
4	$8\delta_f$	8.096	24.69	2740	179.88	1.529
5	$15\delta_f$	8.089	24.77	2739	179.88	1.529
6	$30\delta_f$	8.113	25.61	2550	179.76	1.529
<b>Maximum difference (%)</b>		0.33	5.6	7.5	0.067	12.9

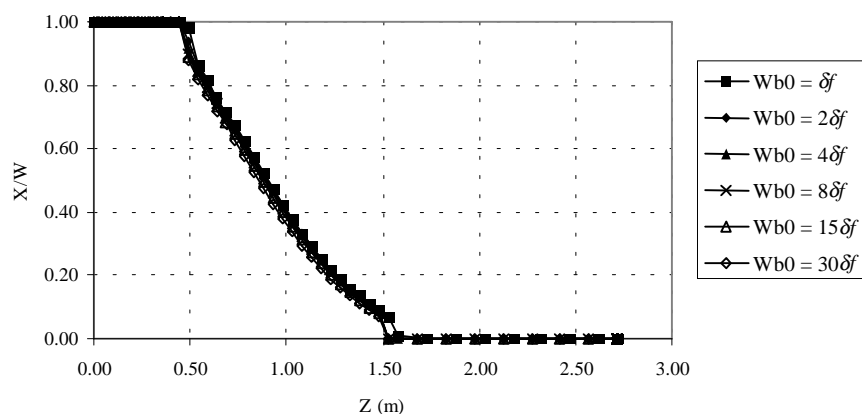


Figure 5.18- Effect of the initial width of the melt pool on the solid bed profile.

#### d) Screw temperature upon solids conveying

Generally, the screw temperature is not known, except when the screw is refrigerated and the temperature is controlled. Therefore, it was assumed that the screw temperature in the delay and melting zones is given by equation 3.61 and that in the pumping zone it equals the barrel temperature. The screw temperature in the solids conveying zone needs to be set. The runs listed in Table 5.11 were made for that purpose. Three situations are considered: a) temperature equal to the inlet polymer temperature, b) average of local barrel temperature and c) adiabatic screw. The relative differences only are significant in the case of the length of screw required for melting for the second situation. However, it is necessary to note that the value of the friction coefficient between the solid polymer and the screw surface used in the calculations is small (equal to 0.25). This means that the influence of the method to compute the heat exchanged and/or generated in the screw surface will be attenuated. Since it is desirable that this coefficient will be the smallest possible, in order to improve the solids conveying capacity, it will not be considered in this study. Therefore, in the remaining calculations the screw will be considered adiabatic. This is what is more realistic in the major part of the practical extrusion situations [AGA 96].

Table 5.11- Effect of the screw temperature value on solids conveying zone.

Run	$T_{screw}$	Output (kg/hr)	Maximum Pressure (MPa)	Power Consumption (W)	Melt Temperature (°C)	Length for Melting (m)
1	$T_{s0}$	8.097	24.63	2741	179.86	1.529
2	$(T_b+T_{s0})/2$	8.115	24.06	2693	179.80	1.726
3	Adiabatic	8.129	23.89	2686	179.80	1.579
<b>Maximum difference (%)</b>		0.40	3.10	2.05	0.03	12.9

### 5.3.3- Assessing the modelling results

The computational results were assessed by direct comparison with responses measured experimentally. As shown in Table 4.2, four independent variables (screw speed and 3 barrel temperatures) were varied within a practical operating window. A statistical design of experiments defined 81 runs, involving replication (Table 4.3).

## Extrusion experiments

Table 5.12 presents the results obtained with the extrusion experiments. The table lists the significant terms (5% level) for the multivariate (MANOVA) and univariate (ANOVA) analyses. According to the results of the multivariate analysis all main effects and the majority of the two-way interactions are statistically significant. However, when the effect of melt temperature is considered individually, one can conclude that barrel temperatures  $T_1$  and  $T_2$ , and corresponding two-way interactions do not appear to be important.

Table 5.12- Factorial analysis – responses of the extrusion experiments  
(\* statistically significant, -- statistically non-significant).

EFFECT	Multivariate analysis	Univariate analysis		
		Output	Temperature	Power
Intercept	*	*	*	*
<b>N</b>	*	*	*	*
$T_1$	*	*	--	*
$T_2$	*	*	--	*
$T_3$	*	*	*	*
$N*T_1$	*	*	--	*
$N*T_2$	*	*	--	*
$N*T_3$	*	*	*	*
$T_1*T_2$	*	*	--	--
$T_1*T_3$	--	*	--	--
$T_2*T_3$	--	--	--	--
$N*T_1*T_2$	--	*	--	--

Figures 5.19 and 5.20 show graphically some of the responses observed. Mass output, melt temperature and power consumption are plotted against screw speed, at various levels of  $T_1$ ,  $T_2$  and  $T_3$ . The values of all the variables increase with screw speed. The output increases due to the corresponding increase of the drag capacity, but at the expense of an increase in power consumption. The small increase in melt temperature is mainly due to viscous dissipation in the melt conveying zone, since the time available for heat conduction from the barrel diminishes.

The output does not change when barrel temperatures  $T_1$  and  $T_2$  vary, for a screw speed of 10 rpm, and exhibits low sensitivity to  $T_3$ . The insensitivity to  $T_1$  and  $T_2$  was expected, since the operating point for a given extruder/die system is mainly dictated by the pumping zone and by

the die, i.e., the influence of these barrel temperatures on the final melt temperature should be small, specially for small screw speeds.

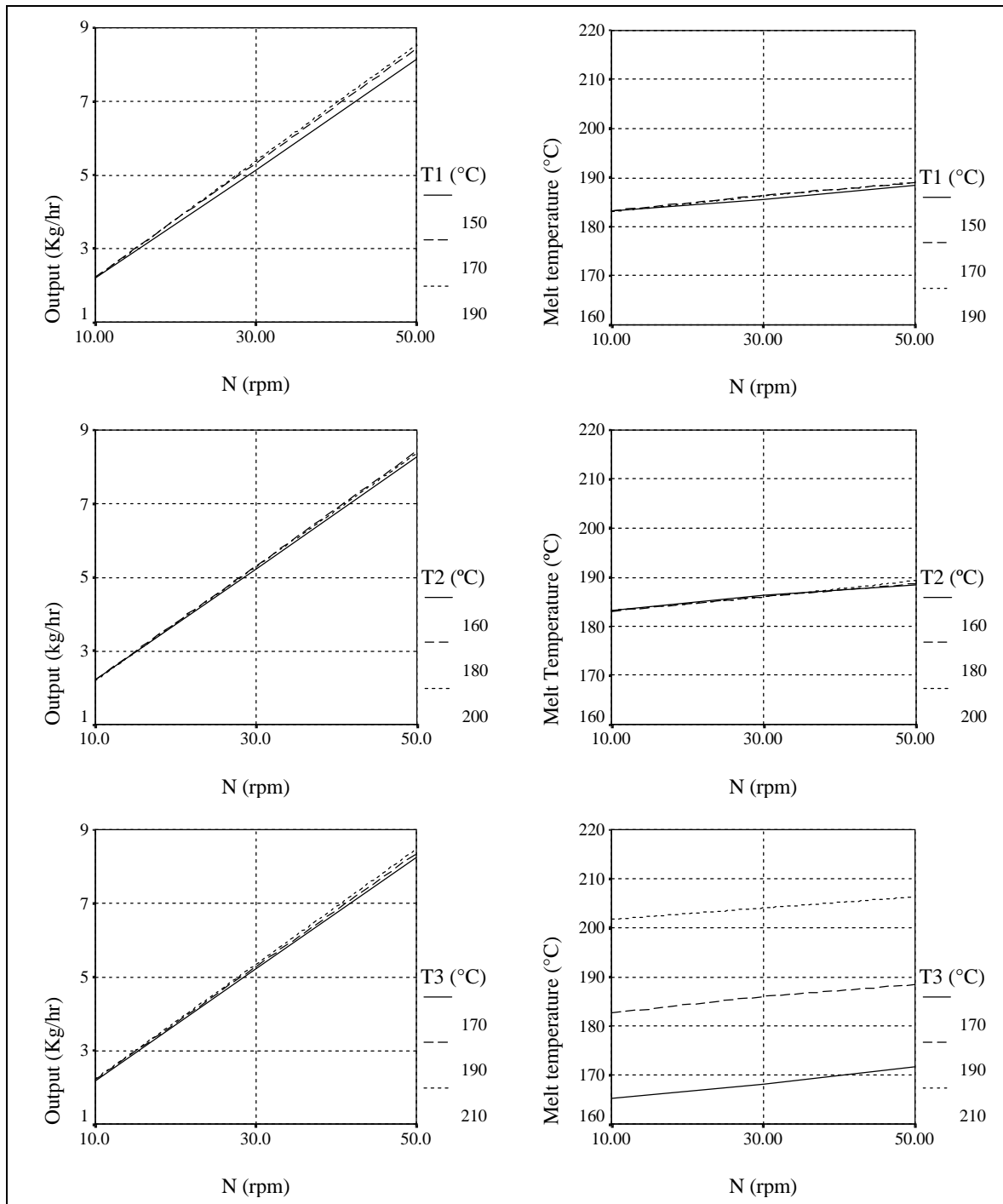


Figure 5.19- Output and melt temperature vs. screw speed – extrusion experiments.

Melt temperature is only dependent on  $T_3$ , which is certainly due to the fact that melt temperature is measured at the end of zone 3. Again the process seems to be controlled by heat conduction. These results would be probably different with another polymer exhibiting high viscosity levels and lower temperature dependence (e.g. HDPE with fillers).

Finally, power consumption, for small screw speeds (10 rpm), exhibits the same behaviour as output, but for higher screw speeds the variation is in the opposite sense, i.e., it diminishes with increasing barrel temperature.

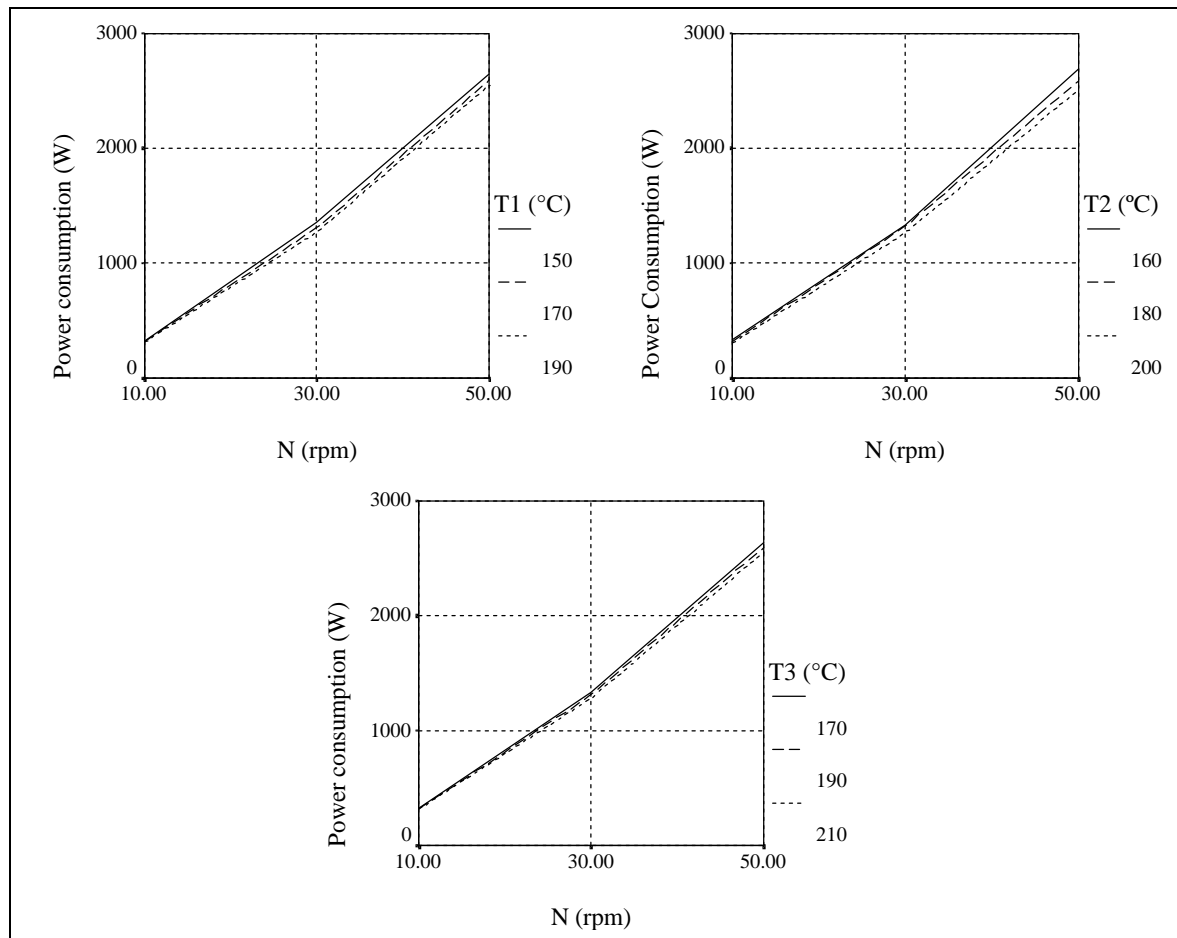


Figure 5.20- Power consumption and length of screw required for melting vs. screw speed – extrusion experiments.

### Analytical model

Table 5.13 lists data equivalent to that of Table 5.12, but now for the responses of the analytical modelling package. All the main effects are significant, either when the individual (ANOVA) or the global (MANOVA) behaviour are considered. The model is insensitive to the effect of two-way interactions of barrel temperatures  $T_1$  and  $T_2$  on the output, but is sensitive to their main effects.

The symbols between brackets identify the differences in relation to the experimental data. A univariate analysis identifies many differences in the behaviour of output and melt temperature. Differently of the experimental responses, the analytical ones are not able to consider the effect of the most two-way interactions on the output. In practice,  $T_1$  and  $T_2$  do not seem to affect the melt temperature, since the process is controlled by heat conduction,

whereas the analytical model is not able to take this into consideration. The differences for the multivariate analysis only occur for the effect of 3 two-way interactions ( $N*T_1$ ,  $T_1*T_2$  and  $T_2*T_3$ )

Table 5.13- Factorial analysis – responses of the analytical model  
(\* statistically significant, -- statistically non-significant).

EFFECT	Multivariate analysis	Univariate analysis			
		Output	Temperature	Power	Length
Intercept	*	*	*	*	*
<b>N</b>	*	*	*	*	*
$T_1$	*	*	(*)	*	*
$T_2$	*	*	(*)	*	*
$T_3$	*	*	*	*	*
$N*T_1$	(--)	(--)	--	(--)	*
$N*T_2$	*	(--)	(*)	*	--
$N*T_3$	*	*	(--)	*	*
$T_1*T_2$	(--)	(--)	--	--	--
$T_1*T_3$	--	(--)	--	--	--
$T_2*T_3$	(*)	(*)	(*)	(*)	--

Some of the results obtained for this case are shown in Figures 5.21 and 5.22, but now the length of screw required for melting is also included. The effect of screw speed on the length of screw required for melting seems to be mainly determined by heat conduction in the melting zone, since when  $T_1$  increases the length required for melting diminishes. Concerning to the other parameters is possible to verify that globally the behaviour is similar to that observed for the experimental results, although some differences are identified:

- In practice all barrel temperatures (especially for high screw speeds) influence output, whereas the analytical model is not able to take this effect into consideration. This probably happens because the model is not able to consider the influence of the melt temperature on the output, i.e., the effect of the increase in melt temperature due to the increase in barrel temperatures  $T_1$  and  $T_2$  does not affect the output.
- The model predictions for the output are significantly smaller than that of the practice (the differences remain between 0.5 and 0.9 kg/hr).

- The analytical model responses predict the effect of barrel temperatures  $T_1$  and  $T_2$  on the melt temperature, whereas the experimental results do not.

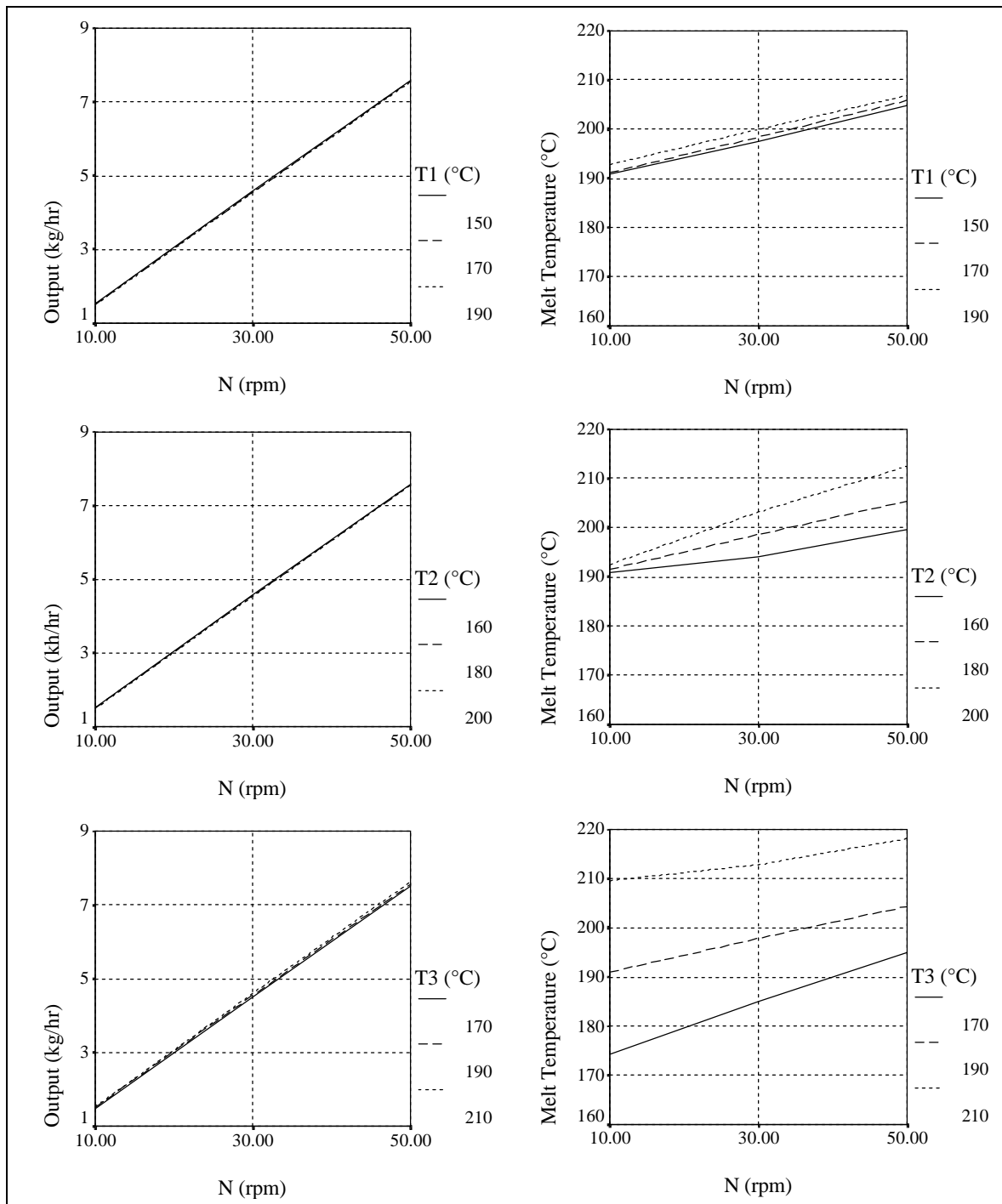


Figure 5.21- Output and melt temperature vs. screw speed – analytical model.

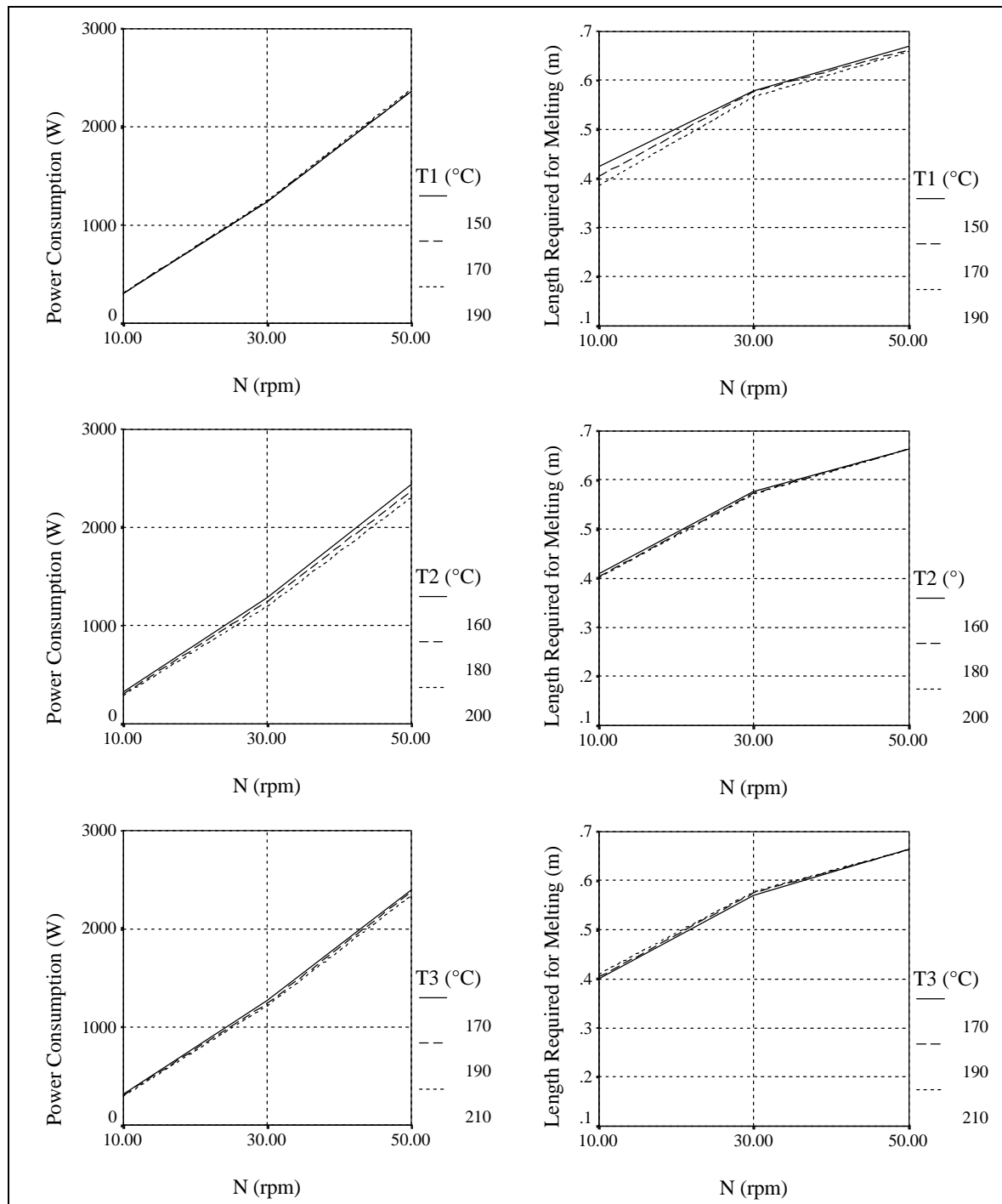


Figure 5.22- Power consumption and length of screw required for melting vs. screw speed – analytical model.

#### Numerical model

Table 5.14 and Figures 5.23 and 5.24 depict the numerical modelling data. All the main effects are significant except for  $T_2$  on the output, which does not exist here. The symbols between square brackets indicate differences in relation to the analytical results, whereas the symbols between circular brackets indicate disagreement with experimental data. In terms of the responses observed (Figures 5.23 and 5.24) the behaviour is identical to that of the

previous approaches (experimental and analytical model), the differences will be discussed next.

**Table 5.14- Factorial analysis – responses of the numerical model**  
 (\* statistically significant, -- statistically non-significant).

EFFECT	Multivariate analysis	Univariate analysis			
		Output	Temperature	Power	Length
Intercept	*	*	*	*	*
<b>N</b>	*	*	*	*	*
$T_1$	*	*	(*)	*	*
$T_2$	*	[(--)]	(*)	*	*
$T_3$	*	*	*	*	*
$N*T_1$	[*]	[*]	[(*)]	[*]	*
$N*T_2$	*	[--]	(*)	[(--)]	[*]
$N*T_3$	*	[(--)]	[*]	*	*
$T_1*T_2$	(--)	--	[(*)]	[(--)]	[*]
$T_1*T_3$	--	--	--	--	--
$T_2*T_3$	[--]	[--]	[--]	[--]	--

The comparison of the numerical results (Table 5.13) with the experimental ones (Table 5.14) reveals fewer differences. In this case, the multivariate analysis only differs in  $T_1*T_2$  term. The univariate analysis is also improved, except for the effect on melt temperature, where 5 differences exist. The differences observed between the experimental and the numerical model responses are the following:

- The numerical model does not take into account the effect of  $T_2$  on the output;
- Barrel temperatures  $T_1$  and  $T_2$  have some influence on melt temperature predicted by the numerical model;
- The power consumption calculated by the numerical model increases with  $T_1$ .

Finally, the comparison between the analytical and the numerical models reveals some differences, principally when the univariate analysis of the output, melt temperature and power consumption are considered. However, the numerical results are closer to the experimental ones than those of the analytical model are.

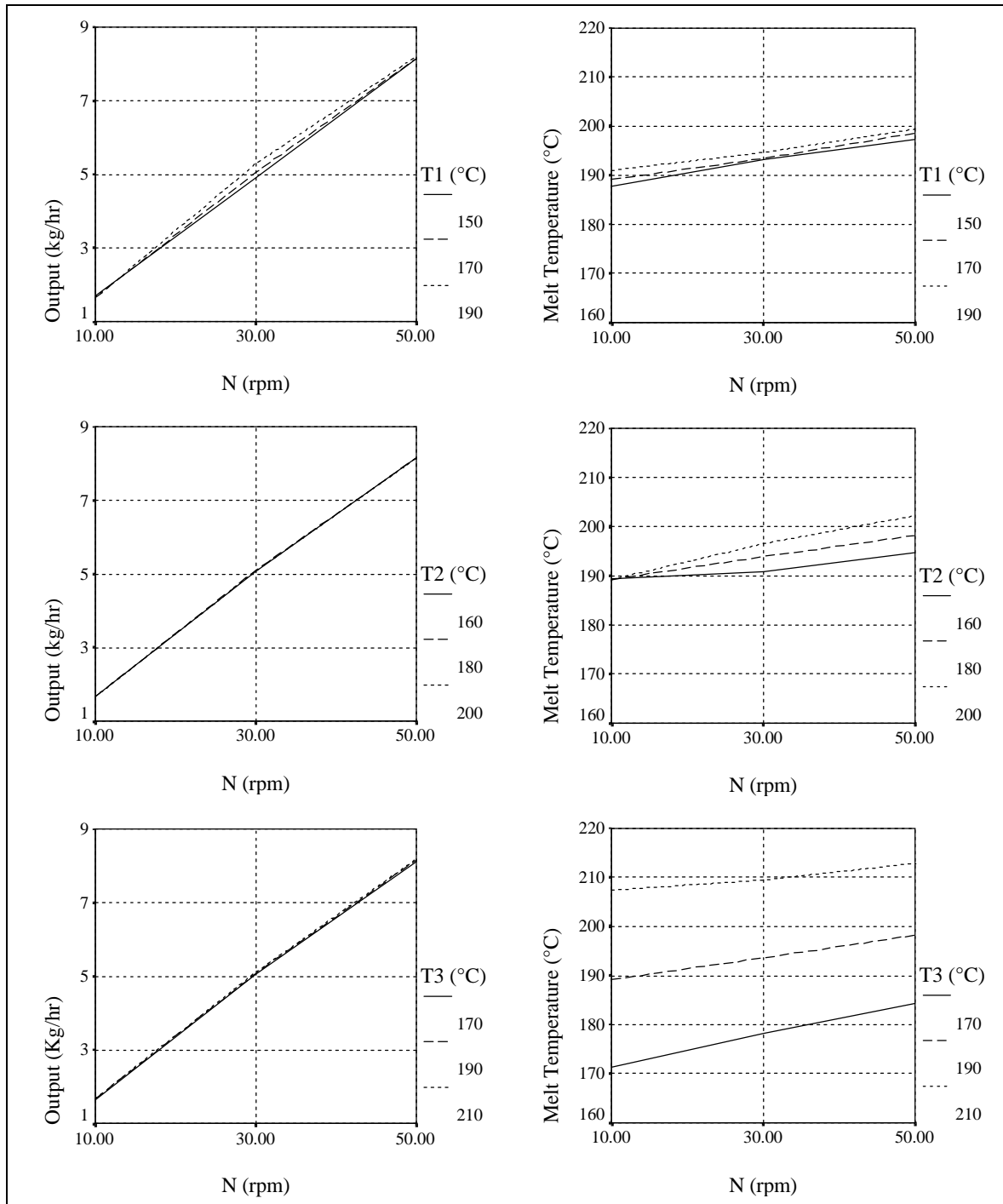


Figure 5.23- Output and melt temperature vs. screw speed – numerical model.

The global behaviour of the numerical model is identical to that observed for the analytical.

The disagreements are:

- The importance of  $T_2$  for output is null in the numerical model;
- The output prediction made by the numerical model are higher than that of the analytical and closer to the experimental ones;

- The length of screw required for melting, calculated with the numerical model, is circa 0.15 meters lower than those obtained with the analytical model. The reason for that is due to the increase of solid bed temperature provided by friction dissipation in all surfaces of the screw channel (barrel and screw root), whereas in the analytical model only the dissipation on the barrel surface is considered.

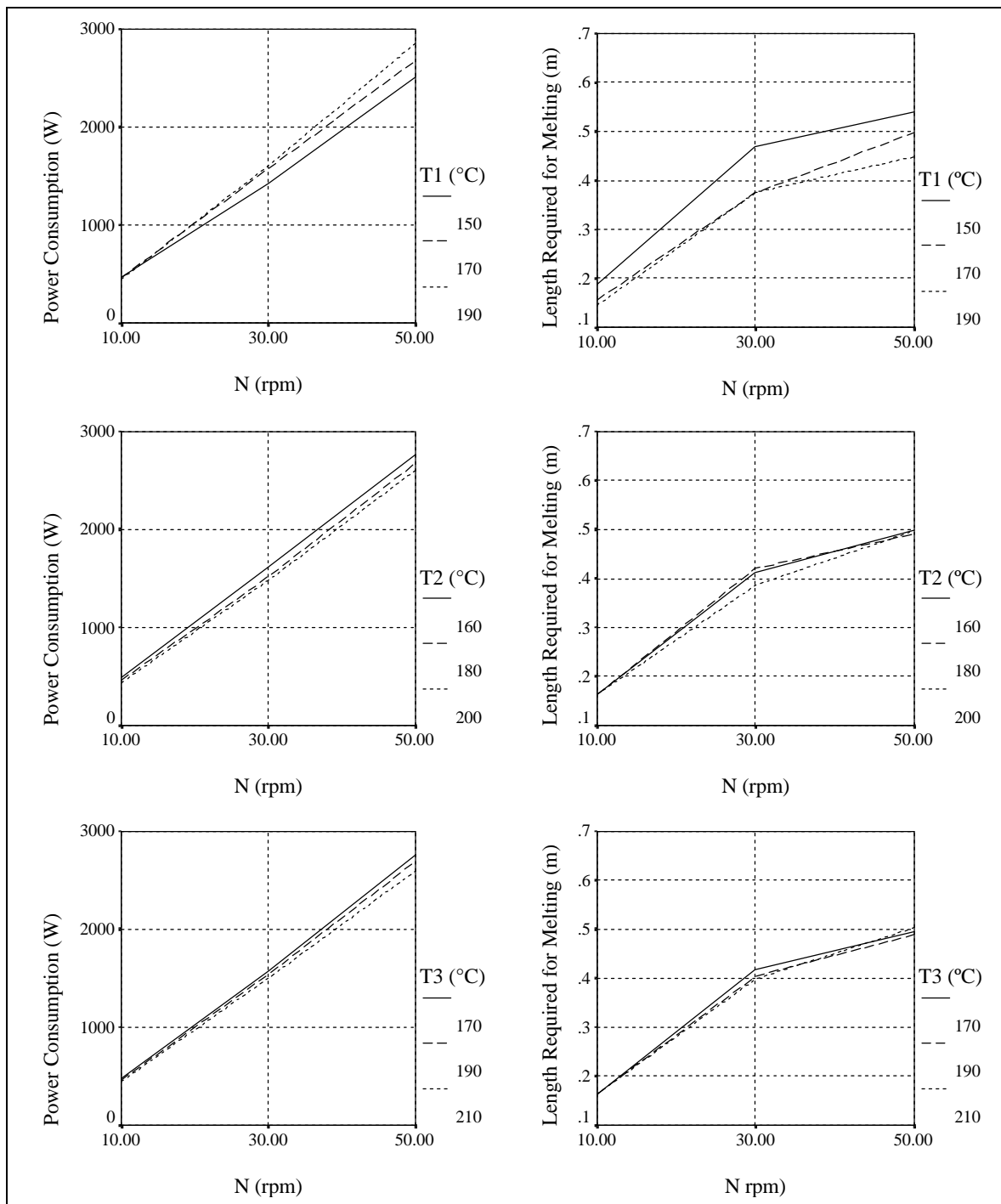


Figure 5.24- Power consumption and length of screw required for melting vs. screw speed – numerical model.

At this point, it will be important to verify whether the differences in the responses of the two mathematical models adopted will affect the results of the optimisation algorithm. Table 5.15 report the results obtained for the case studies presented in Tables 5.2 and 5.3. The criterion length of screw required for melting will not be considered (thus rendering OF2 meaningless), since no experimental data is available.

**Table 5.15- Best operating window.**

Type of results	Parameter	Case studies			
		OF1	OF3	OF4	OF5
Extrusion experiments	<b>N (rpm)</b>	50	10-30	10	10
	<b>T1 (°C)</b>	190	190	150-190	170-190
	<b>T2 (°C)</b>	180-200	200	200	200
	<b>T3 (°C)</b>	170	170	170	170
“Analytical” model	<b>N (rpm)</b>	50	10	10	10
	<b>T1 (°C)</b>	150	150	150	150
	<b>T2 (°C)</b>	160	160	160	160
	<b>T3 (°C)</b>	170	170	170	170
Numerical Model	<b>N (rpm)</b>	50	10	10	10
	<b>T1 (°C)</b>	190	150	150	150
	<b>T2 (°C)</b>	160	200	200	200
	<b>T3 (°C)</b>	170	170	170	170

The results are very similar, especially for screw speed  $N$  and barrel temperature  $T_3$ . As far as barrel temperatures  $T_1$  and  $T_2$  are concerned, the numerical results are slightly closer to the real ones than those produced with the analytical approach.

Figure 5.25 shows the evolution of the optimisation of example OF1 (see Table 5.3) of the above case study when the analytical model is adopted (Table 5.15) in terms of the practical operating window instead of the criteria. The line in bold represents the average of 30% of the best elements of the population and the thin line represents the average of 75% of the best elements of the population. As explained in section 4.5, it was considered as relevant not only to assess the final results of the optimisations (as done above in Table 5.15), but also to monitor the evolution along the various generations. For that purpose, the experimental and predicted solutions of the generations identified in Table 4.4 were directly compared.

This is done in Table 5.16, where output, melt temperature, power consumption and length of screw required for melting, are listed for the experimental (E), analytical (A) and numerical (N) approaches. As expected, numerical results are closer to the experimental data. As the search proceeds the output increases from 5.33 to 7.93 kg/hr, since for this case study the

greater weight is given for the maximisation of the output. This grow is obtained at expenses on the increase of the power consumption. The simultaneous observation of Figure 5.25 and Table 5.16 allows one to conclude that: the first criteria that stabilise are output and power consumption (after the 20<sup>th</sup> generation), which depend directly of the screw speed (the first parameter that stabilises); then, stabilises melt temperature (after the 30<sup>th</sup> generation), which depends mainly of the barrel temperature T3; finally stabilises the screw length for melting (after the 40<sup>th</sup> generation) that depends from the barrel temperatures T1 and T2 (where the melting occurs).

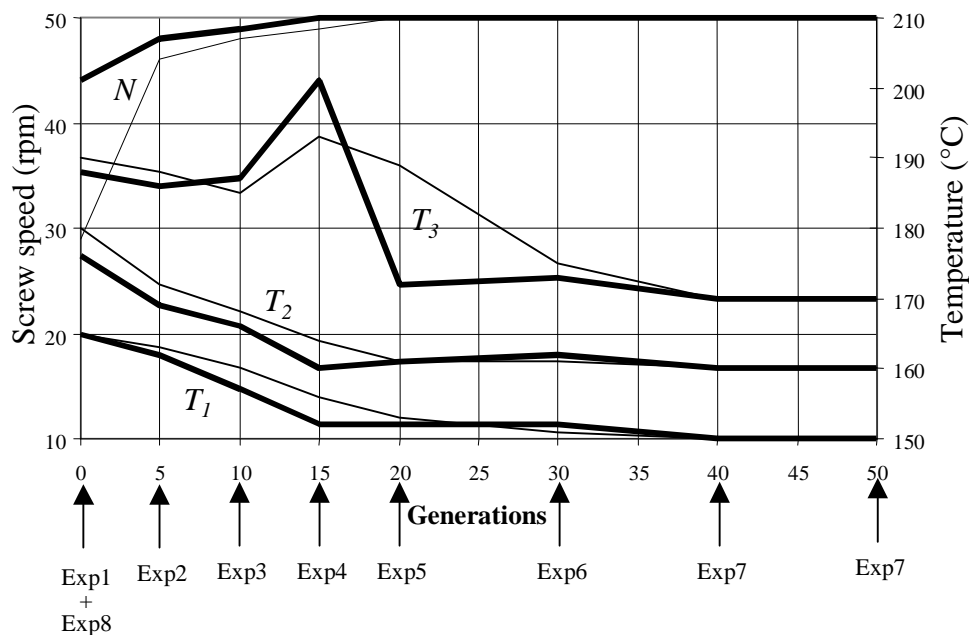


Figure 5.25- Operating window.

Table 5.16- Comparison between experimental and computational data (E- experimental, A- analytical computations, N- numerical computations).

Exp. N°	Output (kg/hr)			Melt temperature (°C)			Power consumption (W)			Length (m)		
	E	A	N	E	A	N	E	A	N	E	A	N
Exp1	5.33	4.45	4.79	184	196	194	1256	1238	1344	0.905	1.563	1.526
Exp2	7.54	7.05	7.52	184	196	194	2307	2245	2398	0.937	1.787	1.577
Exp3	7.46	7.36	7.84	184	193	192	2408	2386	2502	0.856	1.818	1.646
Exp4	7.93	7.51	7.98	191	196	197	2514	2440	2488	0.997	1.825	1.720
Exp5	7.96	7.68	8.15	186	193	194	2622	2541	2539	1.138	1.823	1.784
Exp6	7.91	7.65	8.08	174	186	184	2793	2549	2595	0.953	1.831	1.760
Exp7	7.93	7.66	8.11	175	188	187	2736	2538	2515	0.856	1.831	1.828
Exp8	7.50	6.75	7.22	183	197	195	2207	2102	2269	0.953	1.787	1.565

Table 5.17 shows the global objective function for the three approaches (using the weights defined in Table 5.3 for example OF1). The global objective function value increases as the

search proceeds for all approaches (experiments 1 to 7), and follows the corresponding output values (Table 5.16).

It is possible to conclude that both the analytical and the numerical methods conduct the optimisation to the same result that is similar to the experimental. In this example (OF1) barrel temperatures  $T_1$  and  $T_2$  have less relative importance than the other two ( $N$  and  $T_3$ ) do.

**Table 5.17- Global objective function for experimental and computational data.**

Exp. No.	Generation	Global Objective Function		
		E	A	N
<b>Exp1</b>	0	0.2788	0.2272	0.2445
<b>Exp2</b>	5	0.3738	0.3385	0.3649
<b>Exp3</b>	10	0.3697	0.3525	0.3789
<b>Exp4</b>	15	0.3857	0.3579	0.3824
<b>Exp5</b>	20	0.3860	0.3662	0.3902
<b>Exp6</b>	30	0.3903	0.3672	0.3906
<b>Exp7</b>	40	0.3921	0.3692	0.3909
<b>Exp8</b>	0	0.3734	0.3251	0.3515

#### 5.4- Optimisation results

##### 5.4.1- **Setting the GAs parameters**

The objectives of this section are:

- define the value for the most important Genetic Algorithm general parameters using an objective function;
- verify if the new method of multiobjective optimisation with GAs, developed in this work, is able to attain the Pareto frontier;
- define the multiobjective GA parameters to use in the optimisation of the extrusion process.

The definition of the GA general parameters will be made using the extrusion optimisation example depicted in section 5.1 (example OF1 – Table 5.3). Three benchmark problems [SRI 95] will be used to verify the functionality of the Reduced Pareto Set Genetic Algorithm (RPSGA) method, developed here, when compared with the Niche Pareto Genetic Algorithm (NPGA) method [HOR 93, HOR 94]. At the same time some multiobjective optimisation GA parameters will be defined for both methods. Finally, these methods will be used to define the same parameters, but now using the extrusion optimisation problem - OF1.

## GENERAL PARAMETERS

As discussed before, despite the existing theories [GOL 89a, GOL 89b, BÄC 91, GOL 92] on the definition of the best optimisation parameters, such as population length, selection and crossover methods, crossover and mutation rates, practice as shown that the decision must be made based on empirical information. Therefore, using as a starting point the order of magnitude of values that were used in the literature [GOL 89a], experiments were carried out using a Pentium 166MHz personal computer. In order to simplify this study, due to the greater number of parameters, each one will be considered independently of the others, ignoring the effect of possible interactions between them.

### a) Population length

Three runs of the optimisation algorithm are made using three different population lengths (100, 200 and 300 individuals). Figure 5.26 shows the global objective function *versus* calculation time, using the population length as a parameter.

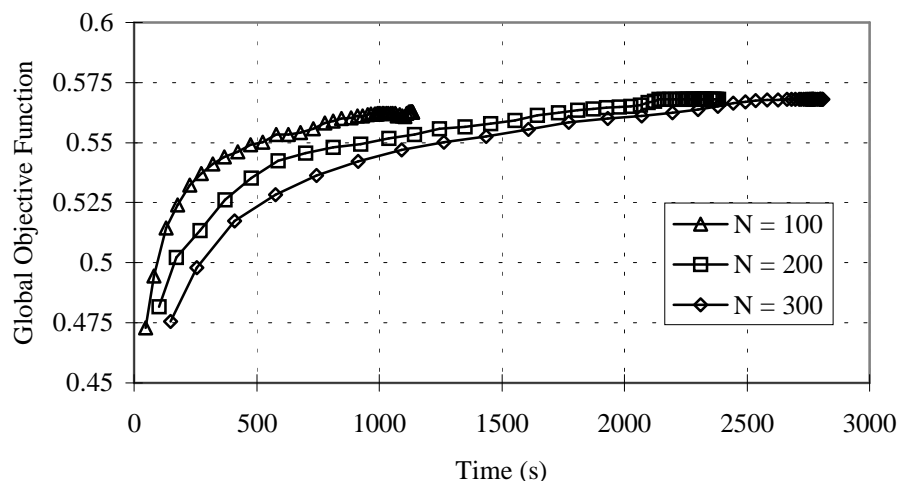


Figure 5.26- Influence of the population length ( $p_c=70\%$ ,  $p_m=0.2\%$ ).

If the population length is excessively low ( $N=100$ ), it might not be possible to process sufficient schemes in order to obtain the optimum [GOL 89b, GOL 92]. In this case, the ideal length is  $N=200$ , since the maximum value of the objective function is reached. The use of a larger population length ( $N=300$ ) does not improve the algorithm performance and increases the computation time.

### b) Crossover rate

The importance of the crossover rate on GAs is associated with the number of schemata that will be possible to process. Figure 5.27 illustrates this fact by representing the global objective function *versus* calculation time for three different crossover rates. Only crossover rates above 50% guarantee that the global objective function is at its maximum. A crossover rate of 70% seems to be adequate.

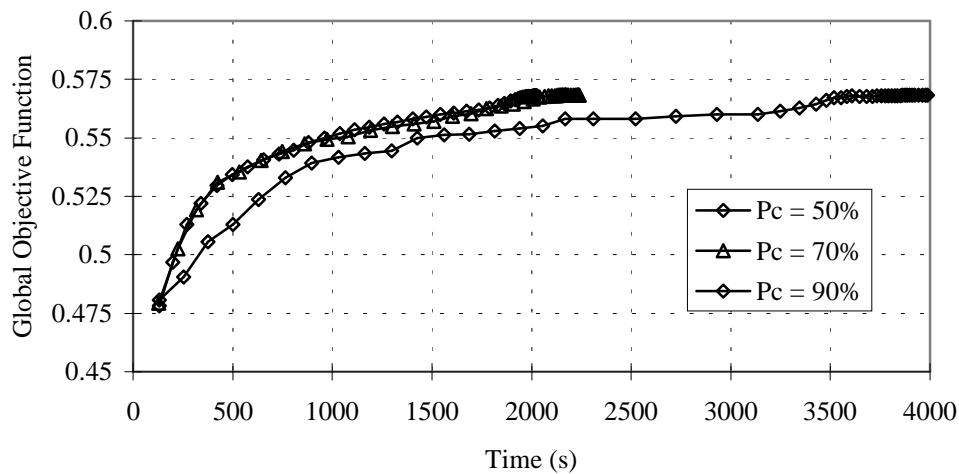


Figure 5.27- Influence of the crossover rate ( $N=200$ ,  $p_m=0.2\%$ ).

### c) Mutation rate

As in nature, mutation rate must be small. Figure 5.28 shows that for values between 0.2% and 1.0%, the final results exhibit small differences.

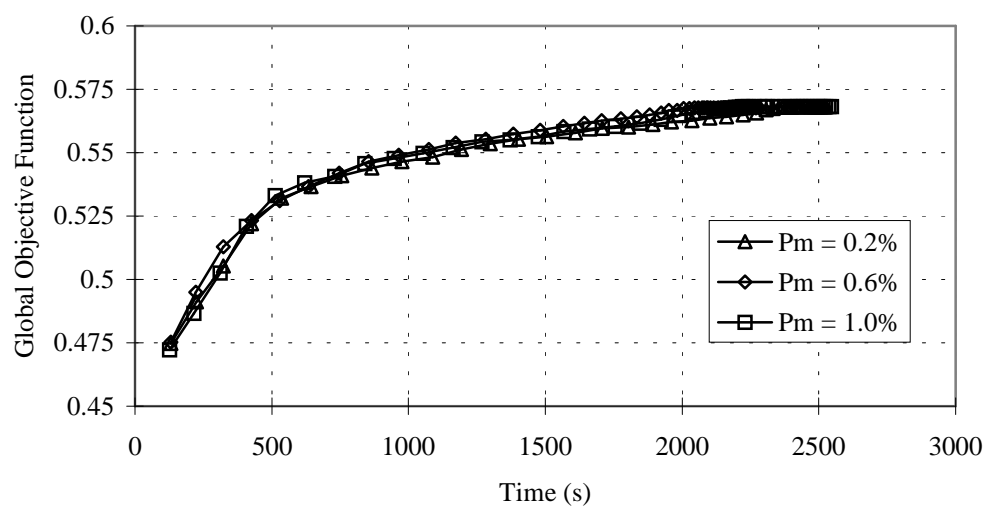


Figure 5.28- Influence of the mutation rate ( $N=200$ ,  $p_c=70\%$ ).

### d) Selection operator

Figure 5.29 compares the performance of the proportional, linear ranking and exponential ranking methods used during first stage of selection (attribution of a value to the objective function). The differences observed are due to the relative selection pressure inherent to the different ranking methods and to their capacity for exploring new search space areas (balance between “*exploitation*” and “*exploration*”). In this case, the use of an exponential ranking scheme seems more appropriate.

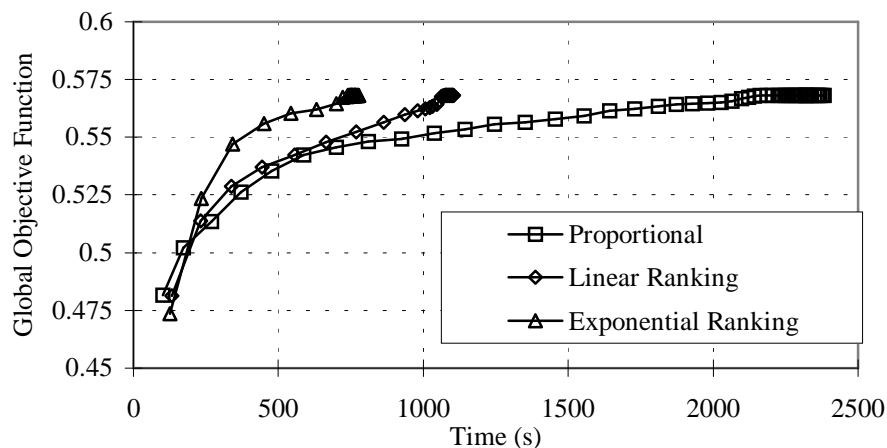


Figure 5.29- Importance of the method used in the 1<sup>st</sup> step of the selection.

However, ranking also depends on specific parameters. The exponential ranking method depends on the  $c$  parameter (equation 2.9) that controls the selection pressure. Theoretically this parameter can vary between 0 and 1, but in practice only values near 1 (exclusive) produces good results. Figure 5.30 shows that although different values produce similar results  $c = 0.99$  allows attaining the maximum value of the objective function.

The parameter  $SP$  (equation 2.8) controls the selection pressure for the linear ranking scheme. Figure 5.31 shows the results obtained with 3 values for this parameter, its range of variation is  $1 < SP \leq 2$ . The optimisation performance decreases when the value of this parameter is lower. This is easily explained by the fact that for greater values of  $SP$  the selection pressure is larger.

#### e) Crossover operator

It is not possible to define theoretically which is the better crossover technique to apply in each particular situation. The choice of the better technique only is possible through the experimental verification of their performance. Figure 5.32 shows the results obtained with

crossover in two points and uniform crossover. Moreover, the better performance of the optimisation with uniform crossover the differences are not significant.

Thus, it is possible to conclude that the best GA parameters to use are  $N=200$ ,  $p_c=70\%$  and  $p_m$  between 0.2 and 1%. As selection operator can be used, by order of preference, exponential ranking scheme with  $c=0.99$ , linear ranking scheme with  $SP=2$  or proportional value. Concerning to the crossover operator, both of the two types studied (two-points or uniform) show similar performance.

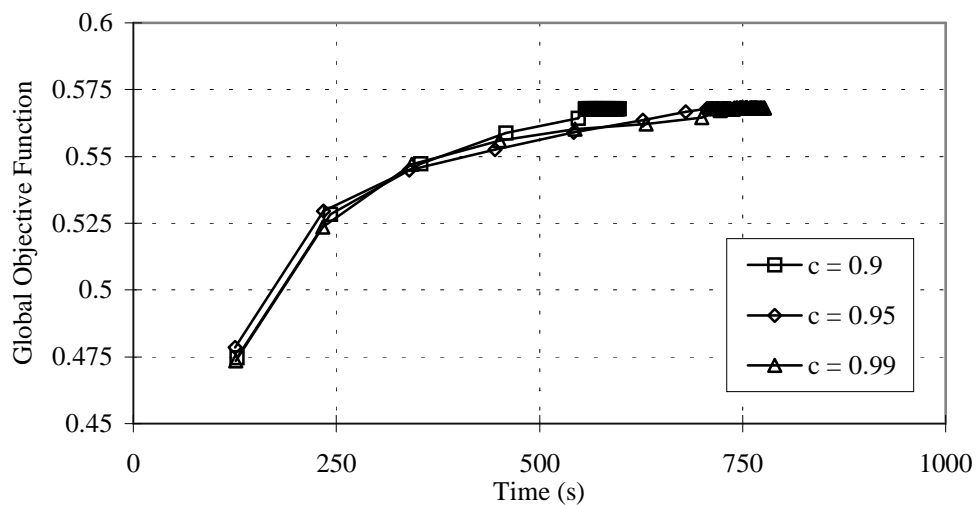


Figure 5.30- Importance of the  $c$  parameter – exponential ranking.

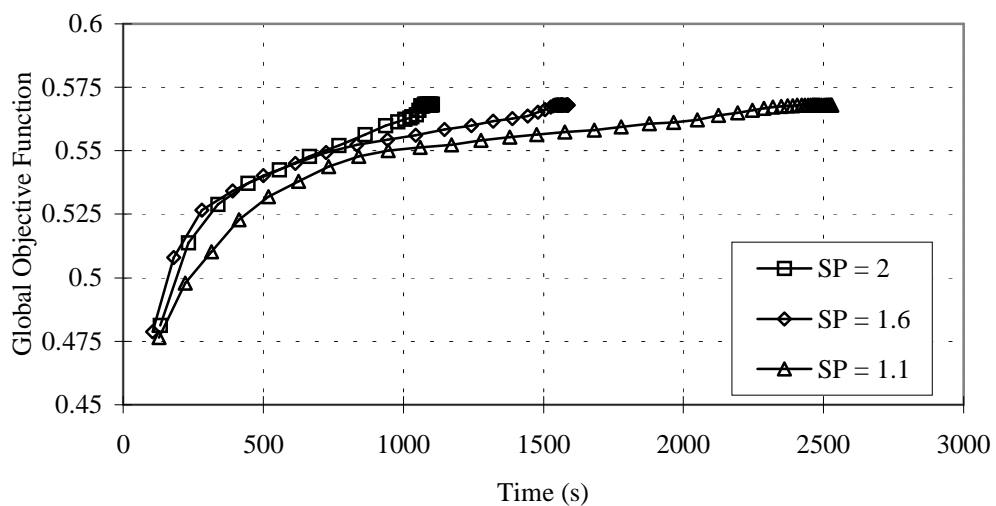


Figure 5.31- Importance of  $SP$  parameter – linear ranking.

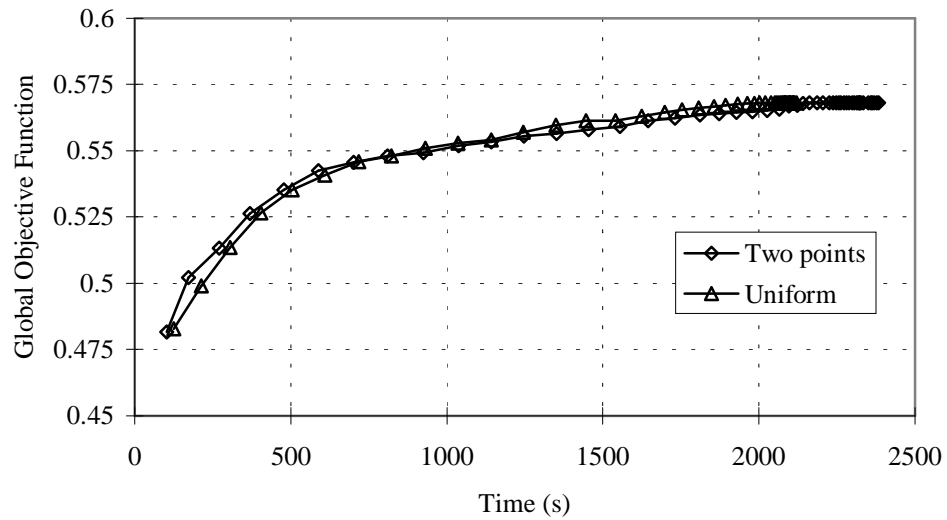


Figure 5.32- Importance of the crossover type.

### MULTIOBJECTIVE OPTIMISATION PARAMETERS

In order to verify the functionality of the multiobjective optimisation algorithm developed here (RPSGA), three benchmark problems [SRI 95] will be studied here before tackling the extrusion process. The methods based on tournament selection (NPGA) and of reduced Pareto set (RPSGA) will be compared for each case.

#### a) Benchmark problems

##### Problem F1:

$$\text{Minimise } f_{11} = x^2 \quad (5.1)$$

$$\text{Minimise } f_{12} = (x - 2)^2$$

Figure 5.33 represents the Pareto frontier for the two functions,  $f_{11}$  and  $f_{12}$ . The nondominated points are located for  $0 < x < 20$  and for  $f_{11}$  and  $f_{12}$  between 0 and 4.

##### Problem F2:

$$\begin{aligned} \text{Minimise } f_{21} &= -x && \text{if } x \leq 1 \\ &= -2 + x && \text{if } 1 < x < 3 \\ &= 4 - x && \text{if } 3 < x \leq 4 \\ &= -4 + x && \text{if } x > 4 \end{aligned} \quad (5.2)$$

$$\text{Minimise } f_{22} = (x - 5)^2$$

The Pareto frontier is represented in Figure 5.34.

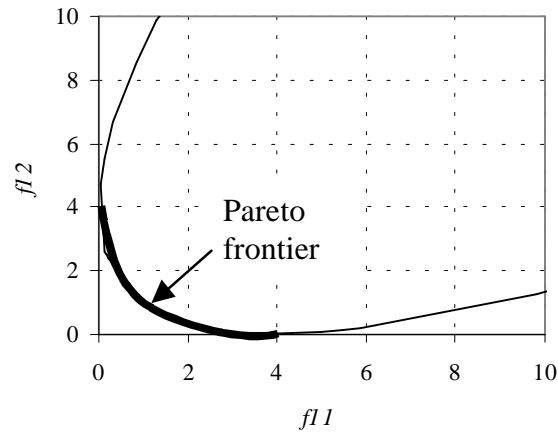


Figure 5.33- Pareto frontier for problem F1.

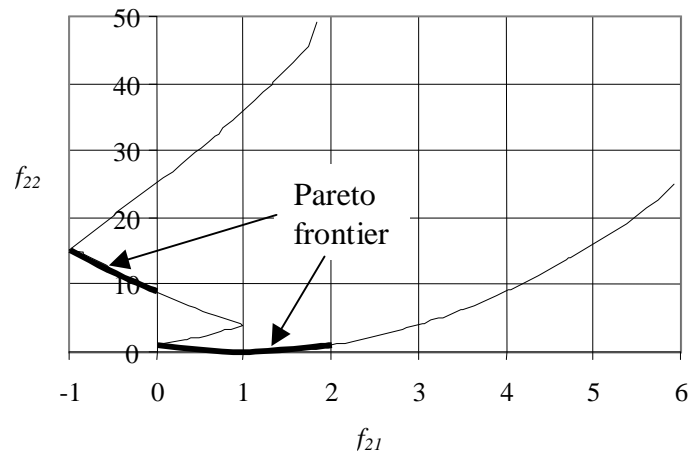


Figure 5.34- Pareto frontier for problem F2.

**Problem F3:**

$$\text{Minimise } f_{31} = (x_1 - 2)^2 + (x_2 - 1)^2 + 2$$

$$\text{Minimise } f_{32} = 9x_1 - (x_2 - 1)^2 \quad (5.3)$$

Subject to :

$$x_1^2 + x_2^2 - 225 \leq 0$$

$$x_1 - 3x_2 + 10 \leq 0$$

The Pareto region for this problem is confined to a line given by:  $x_1 = -2.5$  and  $2.5 \leq x_2 \leq 14.79$ .

The performance of a multiobjective optimisation algorithm can be assessed by evaluating how uniform the distribution of the population along the entire Pareto frontier is and whether

it is maintained throughout successive generations. The measurement of this distribution can be made with the chi-square deviation form [SRI 95]:

$$t = \sqrt{\sum_{i=1}^{q+1} \left( \frac{n_i - \bar{n}_i}{\sigma_i} \right)^2} \quad (5.4)$$

where  $q$  is the number of desired optimal points and the  $(q+1)^{\text{th}}$  subregion is the dominated region,  $n_i$  is the number of individuals present in the  $i^{\text{th}}$  subregion of the nondominated region,  $\bar{n}_i$  is the expected number of individuals in the  $i^{\text{th}}$  subregion of the nondominated region, and  $\sigma_i^2$  is the variance of individuals in the  $i^{\text{th}}$  subregion of the nondominated region, given by:

$$\sigma_i^2 = \bar{n}_i \left( 1 - \frac{\bar{n}_i}{N} \right) \quad i = 1, 2, \dots, q \quad (5.5)$$

When the population is successfully distributed along the Pareto border, the value of the performance measure is the lowest possible.

## PROBLEM F1

The computations listed in Tables 5.18 (tournament selection method) and 5.19 (reduced Pareto set method) were made. Three GA parameters will be considered: the radius of a circumference that is the maximum distance between chromosomes ( $\sigma_{\text{share}}$ ), the size of the comparison set ( $t_{\text{dom}}$ ) and the indifference limits above which the performance of the solutions is considered as similar (*limits*). The values used here are of the order of magnitude of values that were used in the literature. Table 5.20 presents the values assumed for the other relevant optimisation parameters.

**Table 5.18- Runs for problem F1 – tournament selection.**

Run	$\sigma_{\text{share}}$	$t_{\text{dom}}$ (% of $N$ )
1	0.1	30
2	0.1	20
3	0.1	13
4	0.1	10
5	0.001	30
6	0.001	20
7	0.001	13
8	0.001	10
9*	0.001	13

**Table 5.19- Runs for problem F1 –reduced Pareto set.**

Run	$\sigma_{\text{share}}$	limits
10	0.1	0.1
11	“	0.01
12	“	0.001
13	0.01	0.01
14	0.001	“
15	0.001	0.001
16*	0.001	0.01
17*	“	0.001

**Table 5.20- Algorithm parameters.**

Number of generations (NG)	200
Population length ( $N$ )	100
Chromosome length ( $l$ )	14
Crossover rate ( $CR$ )	0.7
Mutation rate ( $MR$ )	0.004
$x$ range	[-10, 10]
Precision	0.001

The performance measure for the first 4 runs is presented in Figure 5.35. As can be observed, their value deteriorates during the search. Since it is not easy to distinguish between the individual curves, a moving average of the performance values will be used in the following. This is represented in Figure 5.36, where:

$$MA_i = \frac{\sum_{j=1}^i t_j}{i} \quad i = 1, 2, \dots, NG \quad (5.6)$$

In this equation  $t_j$  is the performance measure for generation  $j$  and  $NG$  is the total number of generations.

The improvement obtained in Figure 5.37 with the values of  $\sigma_{\text{share}}$  and  $t_{\text{dom}}$  for runs 5 to 8 is evident. The value of the moving average decreases rapidly (i.e., the performance increases) from 10 to 5 in the first 50 generations, afterwards it is maintained at the same level during the 200 generations. A careful observation of the corresponding Pareto curves would show that the best distribution along the Pareto frontier is obtained with run 7, covering the entire frontier and attaining values for  $f_{11}$  close to 0.

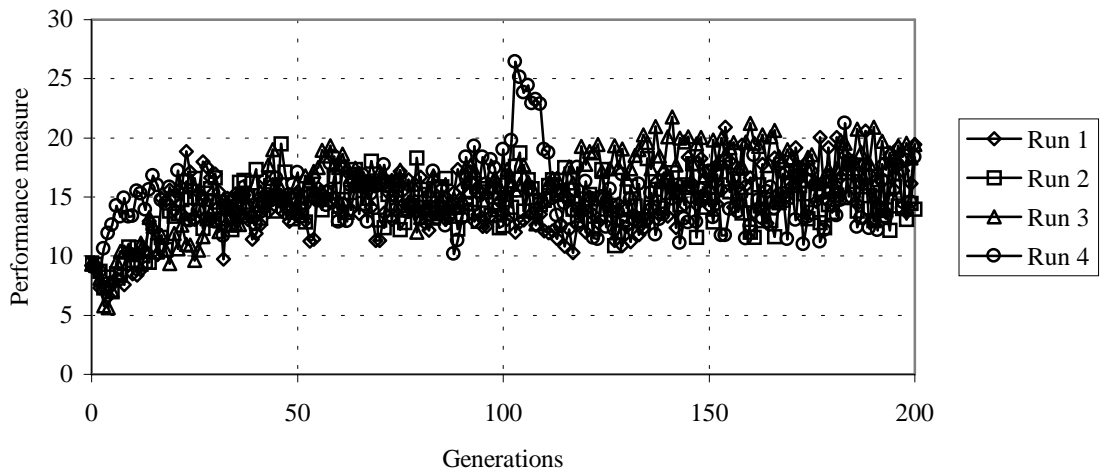


Figure 5.35- Problem F1: performance measure for runs 1 to 4.

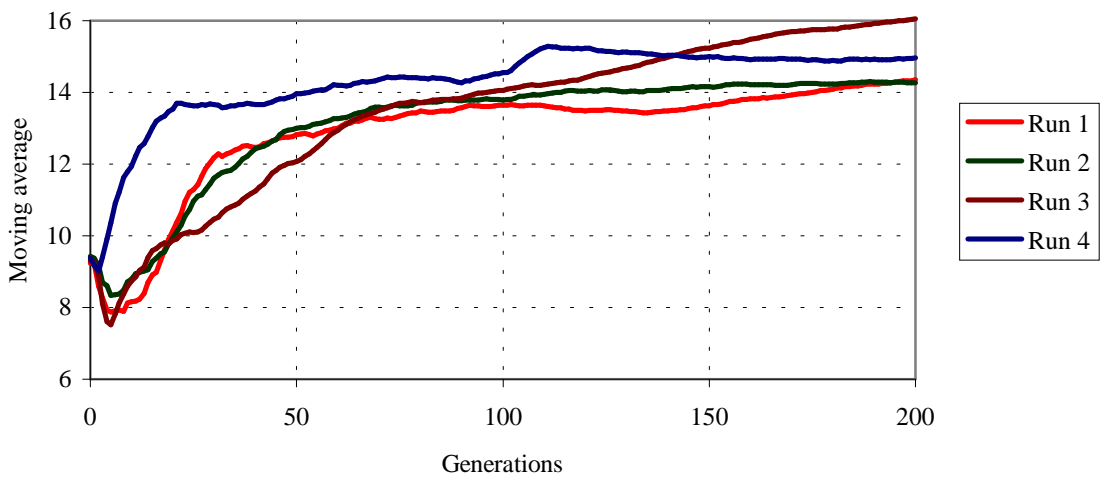


Figure 5.36- Problem F1: moving average for runs 1 to 4.

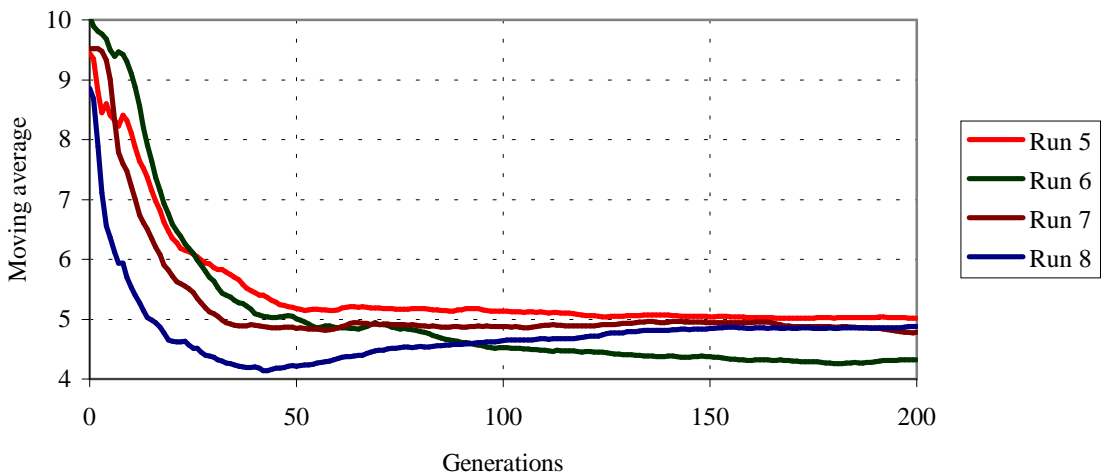


Figure 5.37- Problem F1: moving average for runs 5 to 8.

At this point, the reasons explaining the considerable oscillation on the performance measure reported above are not clear. Consequently, an additional run (run 9) without mutation, but with the other parameters equal to those used in run 7 was made. Since the same type of oscillation was obtained, mutation is not to blame. Instead, crossover between certain nondominated individuals that produce dominated offspring could cause this behaviour.

Figure 5.38 represents the moving average along the several generations for runs 10 to 12, where the reduced Pareto set method was applied with different *limit* values (0.1, 0.01 and 0.001, respectively). It is not possible to make a clear distinction between them. However, their performance is inferior to that obtained with run 7, where tournament selection was applied.

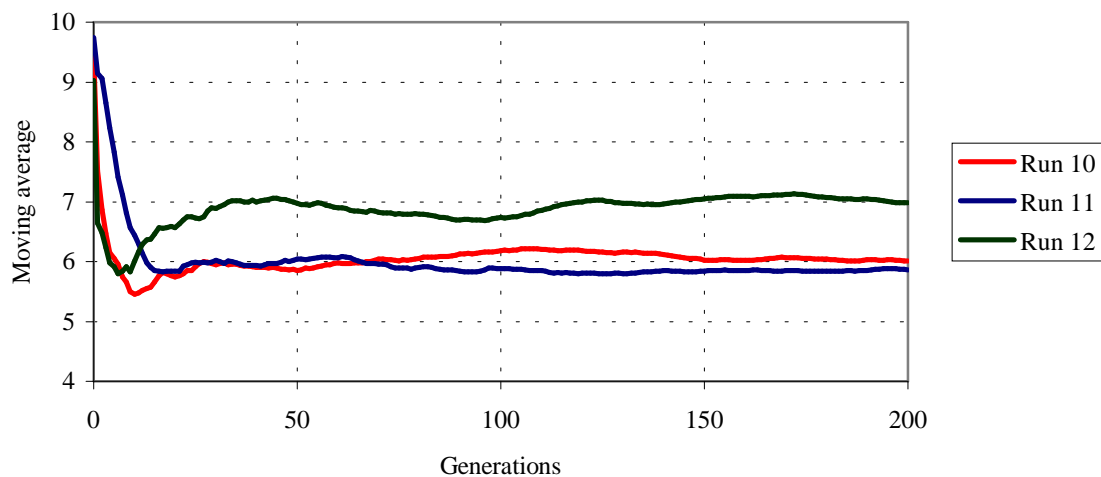


Figure 5.38- Problem F1: moving average for runs 10, 11 and 12.

The influence of  $\sigma_{share}$  can be identified by carrying out runs 11, 13 and 14 (Table 5.19). The shape of the curves would be similar to those of Figure 5.38. Whereas the performance value of run 11 oscillates around 6, that of runs 13 and 14 decreases to 4.

Figure 5.39 shows the moving average of runs 14 to 17, thus illustrates the influence of the *limit* values and the absence of mutation (see Table 5.19). Run 16 ( $\sigma_{share}=0.001$ , *limits* = 0.01 and without mutation) seems to be the best choice. The direct analysis of the Pareto frontiers would provide the same conclusions.

Finally, a direct comparison between Niched Pareto Genetic Algorithm (NPGA) and Reduced Pareto Set Genetic Algorithm (RPSGA) will be made. Figure 5.40 shows the moving average

and the Pareto frontiers for runs 7 (NPGA) and 16 (RPSGA). The reduced Pareto set method seems to exhibit the best results.

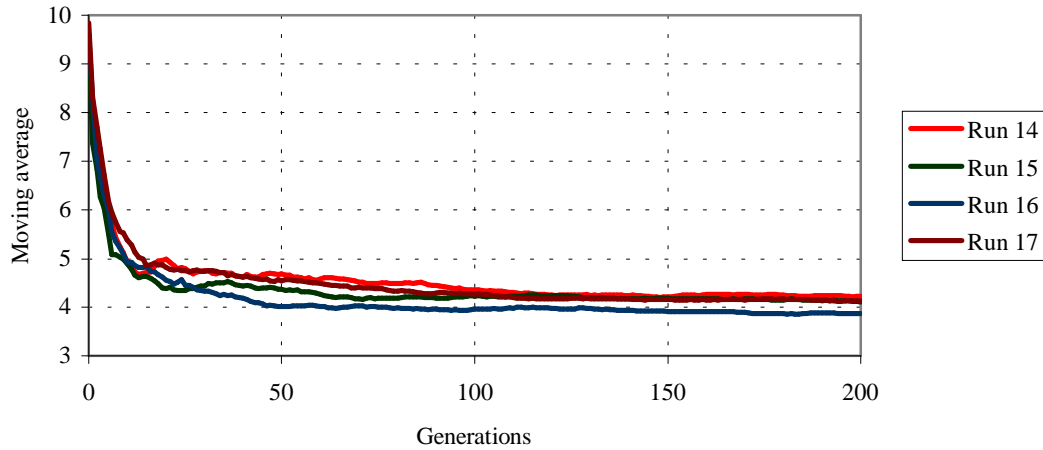


Figure 5.39- Problem F1: moving average for runs 14 to 17.

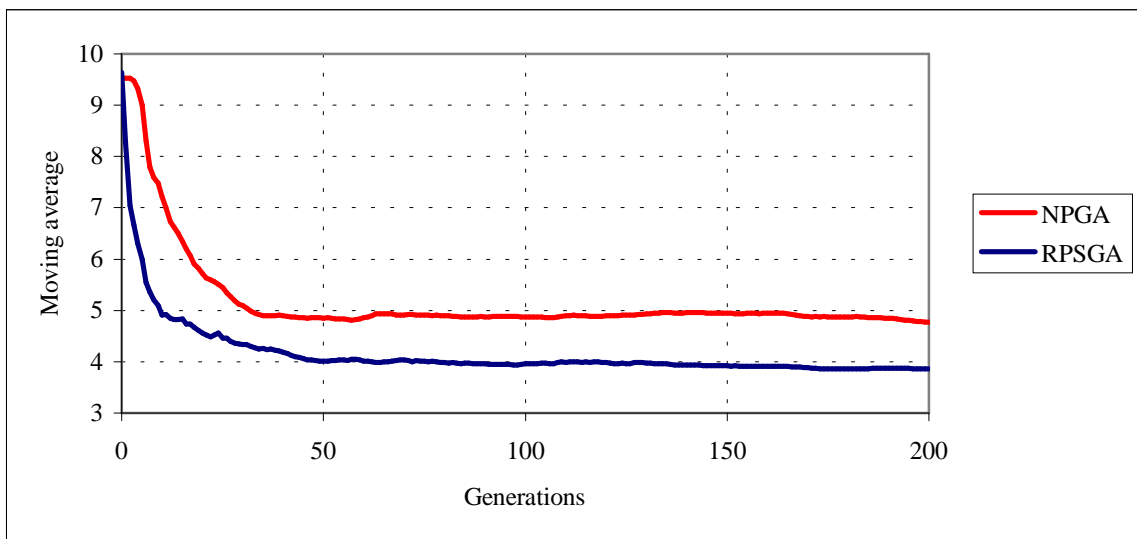


Figure 5.40- Problem F1: moving average for NPGA and RPSGA methods.

## PROBLEM F2

In this case, the best results obtained are shown in Figure 5.41 using the parameters given in Table 5.21. The two methods have similar performance. Nevertheless, for values of  $f_{21}$  near 0 and 2, the reduced Pareto set method appears to get a better distribution of points.

**Table 5.21- Algorithm parameters for problem F2.**

<i>Number of generations</i>	200
Population length	100
Chromosome length	14
Crossover rate	0.7
Mutation rate	0.004
$x$ range	[-2, 10]
Precision	0.001
$\sigma_{share}$	0.01
<i>Limits</i>	0.01

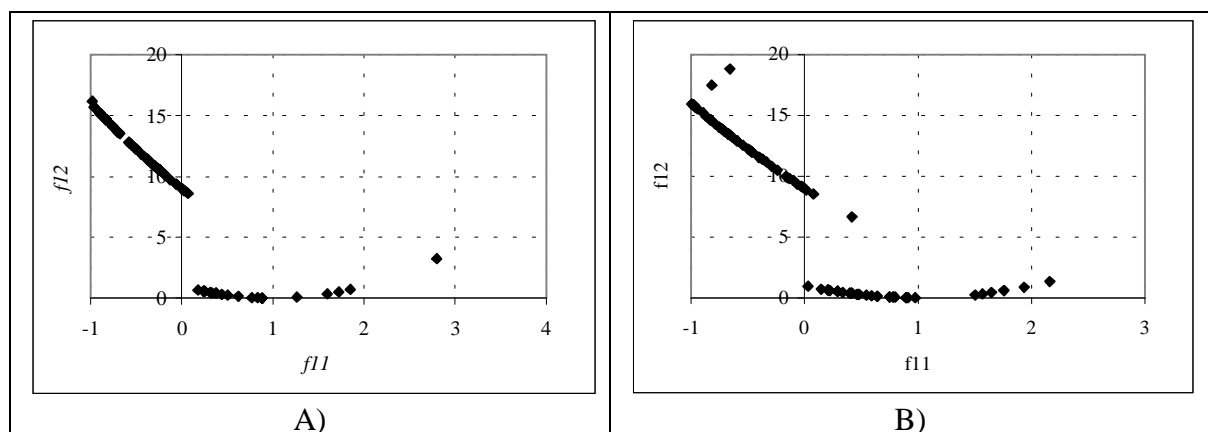


Figure 5.41- Pareto frontier for problem F2: A) NPGA; B) RPSGA.

### PROBLEM F3

Since this problem has two variables to optimise and its domain of actuation is restricted by two inequalities, it requires the use of robust optimisation schemes. The Pareto region is confined to a line given by  $x_1 = -2.5$  and  $2.5 \leq x_2 \leq 14.79$ . Several runs were made, where the values of  $\sigma_{share}$  and *limits* were tested. The parameters used are again given in Table 5.21, except for the  $x_1$  and  $x_2$  range of variation ( $-20 \leq x_1, x_2 \leq 20$ ) and the value of  $\sigma_{share}$  (0.001 for NPGA). The best results produced by the two methods are shown in Figure 5.42. While the points corresponding to the NPGA method are dispersed around  $x_1 \in [-2.6, -2.1]$  and  $4.66 \leq x_2 \leq 14.58$ , the values of the RPSGA method converge to  $x_1 = -2.3$ , and  $4.7 \leq x_2 \leq 14.82$ . Clearly, the optimal Pareto frontier was not reached. Probably, this would only be possible by transforming this problem into an unconstrained optimisation one, for example using an exterior penalty function [SRI 95].

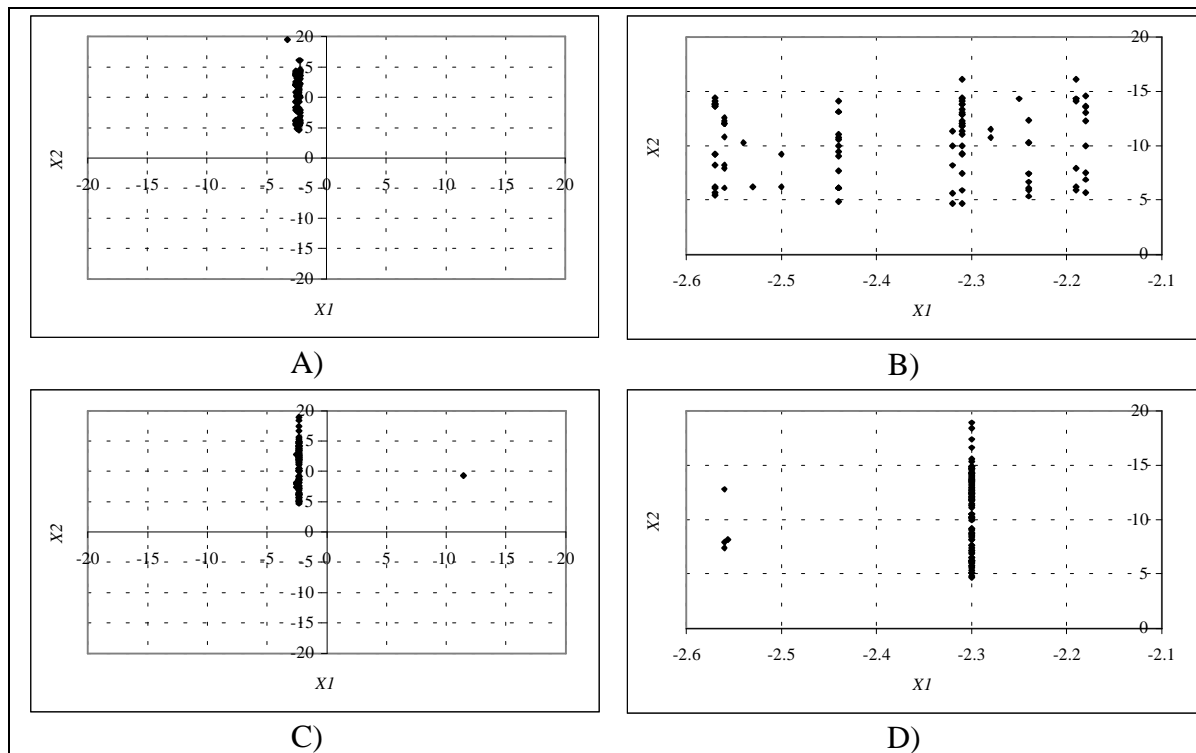


Figure 5.42- Pareto frontiers (variables domain): A) NPGA; B) ditto enlarged; C) RPSGA; D) ditto enlarged.

### b) Extrusion process

In order to test the same optimisation approaches in the optimisation of an extrusion problem, the example defined in Table 5.1 (case study OF1 in section 5.1), in order to satisfy the criteria set in Table 5.2 will be adopted, but now using the multiobjective optimisation GA, instead of an objective function. For that purpose, the multiobjective optimisations (**mo**) listed in Table 5.22 were carried out (using the following optimisation parameters:  $N=500$ ,  $CR=0.7$ ,  $MR=0.004$ ,  $NG=50$  and  $l=24$ ).

Table 5.22- Multiobjective optimisation computations.

Run	Opt. method	$\sigma_{share}$	Limits	Observations
mo1	Tournament selection	0.01	--	Repeated 5 times
mo2	“	0.001	--	
mo3	<b>Reduced Pareto set</b>	0.01	0.1	
mo4	“	“	0.01	
mo5	“	“	0.001	Repeated 5 times
mo6	“	0.1	0.01	
mo7	“	0.01	“	Equal to mo4
mo8	“	0.001	“	

The use of “full” Pareto curves to compare these results is not an easy assignment, due to their similarity and the large number of individuals on both populations (see Figure 5.43, where the

Pareto Curve for two criteria – screw length required for melting an output – were depicted, as an example).

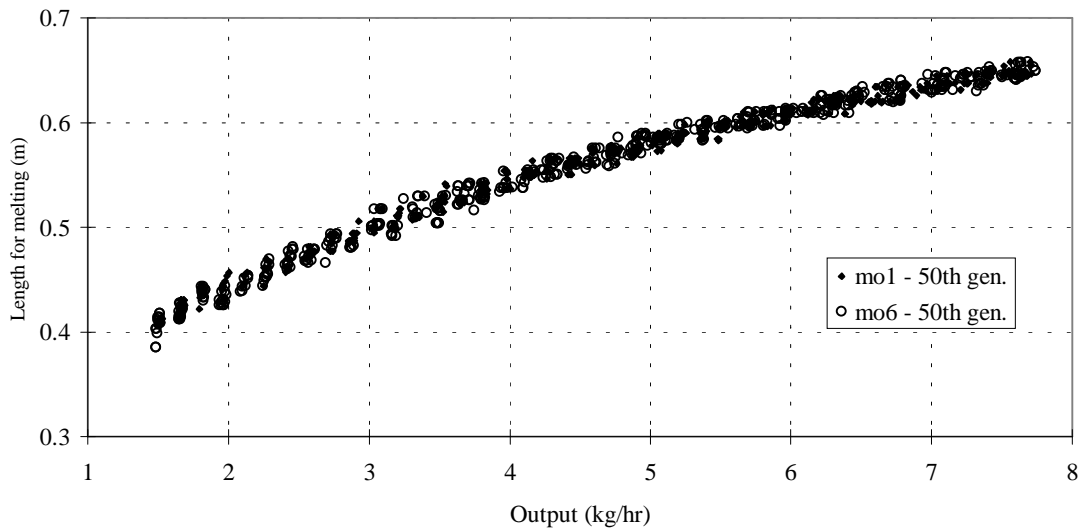


Figure 5.43- Pareto frontier for runs **mo1** and **mo6**.

As proposed earlier, these limitations can be overtaken if the populations are simplified by means of the reduced Pareto set algorithm. Figure 5.44 presents the corresponding Pareto frontiers, in the criteria domains, for runs **mo1** and **mo6**, where the output (only criterion to maximise) is plotted against length of screw required for melting, melt temperature and power consumption. If the frontiers are analysed individually, it is possible to conclude that run **mo6** is better. However, the best points in one Pareto frontier, e.g., output *versus* length for melting, can be the poorest points on another partial frontier, e.g., output *versus* melt temperature.

Consequently, an alternative method will be used to compare the results. The best results will be compared upon affecting the weights of Table 5.3 to final population (generation 50), using the objective function defined by equation 2.22.

Figure 5.45 shows the values of the global objective function for runs **mo1** and **mo2** (Table 5.22). Clearly, the **mo1** run is superior in all the cases studied.

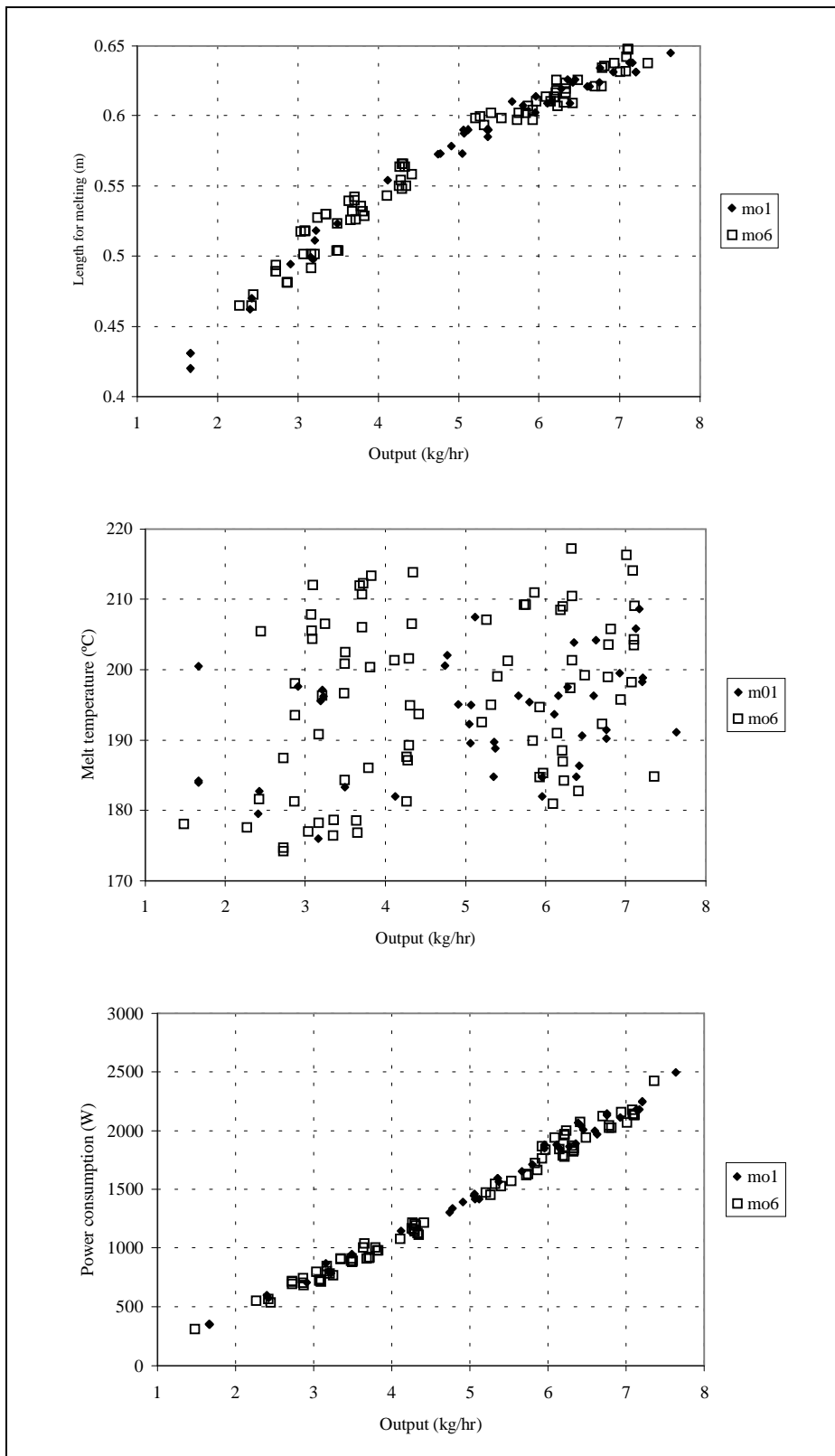


Figure 5.44- Reduced Pareto frontiers in the criteria domains.

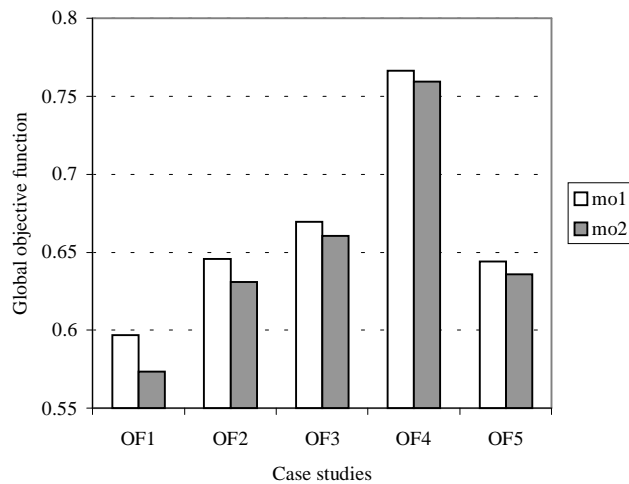


Figure 5.45- Global objective function for runs **mo1** and **mo2**.

Figure 5.46 shows the results obtained when *limits* are varied (runs **mo3** to **mo5**, Table 5.22), the best run seems to be **mo4** when *limits* is equal to 0.01. The influence of  $\sigma_{share}$  is presented in Figure 5.47 (runs **mo6** to **mo8**). The best performance is obtained when  $\sigma_{share}$  is equal to 0.1 (run **mo6**).

Another important matter to take into consideration is the reproducibility of the results. In order to estimate this, runs **mo1** (NPGA) and **mo5** (RPSGA) were repeated 5 times each. Given the results obtained (Figures 5.51 and 5.52), NPGA method seems to be stable than the RPSGA method. However, if the 3 best results provided by each one are compared (Figure 5.50), the differences are not impressive, but runs **mo5c** and **mo5e**, corresponding to RPSGA method are the best.

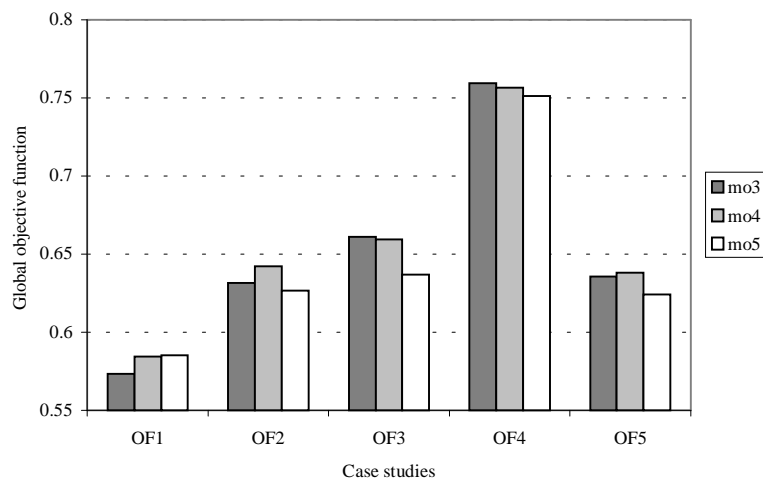


Figure 5.46- Global objective function for runs **mo3** to **mo5**.

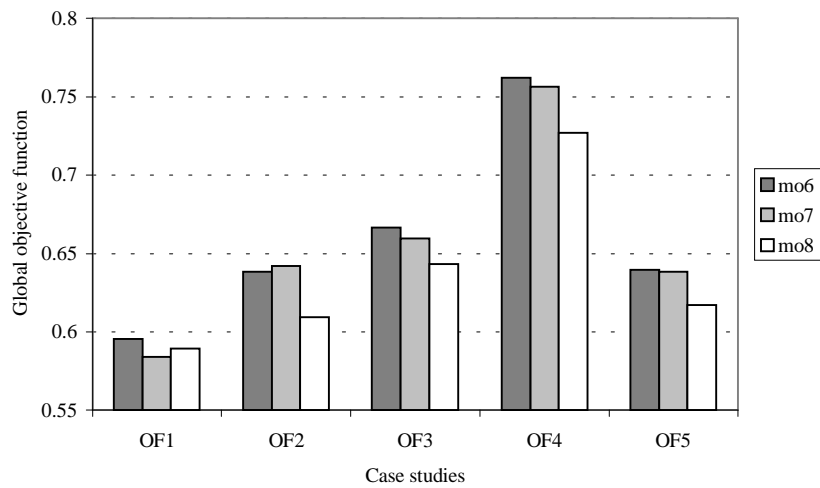


Figure 5.47- Global objective function for runs **mo6** to **mo8**.

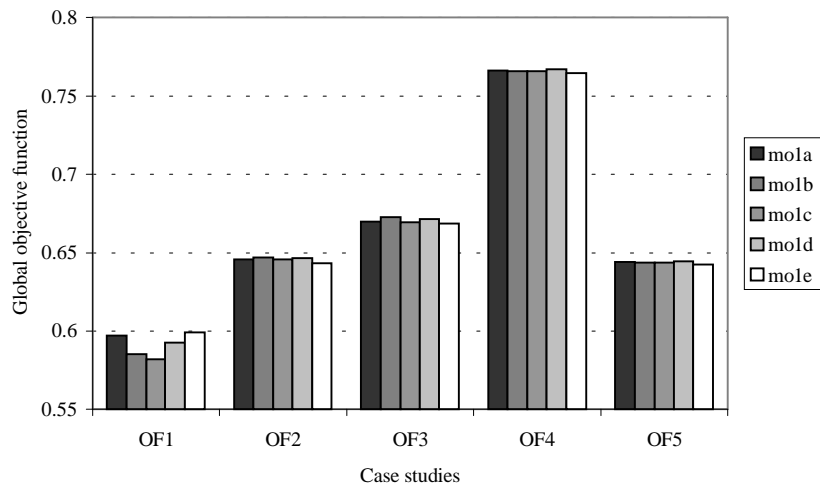


Figure 5.48- Global objective function for runs **mo1 (a, b, c, d, e)**.

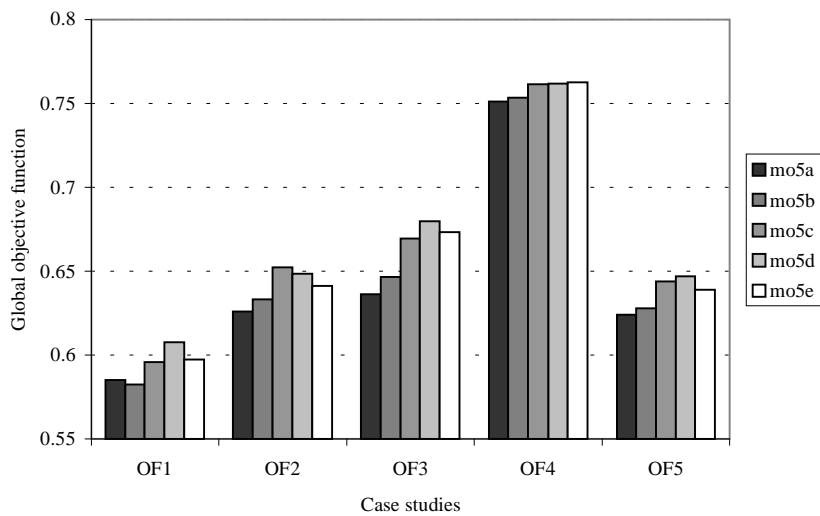


Figure 5.49- Global objective function for runs **mo5 (a, b, c, d, e)**.

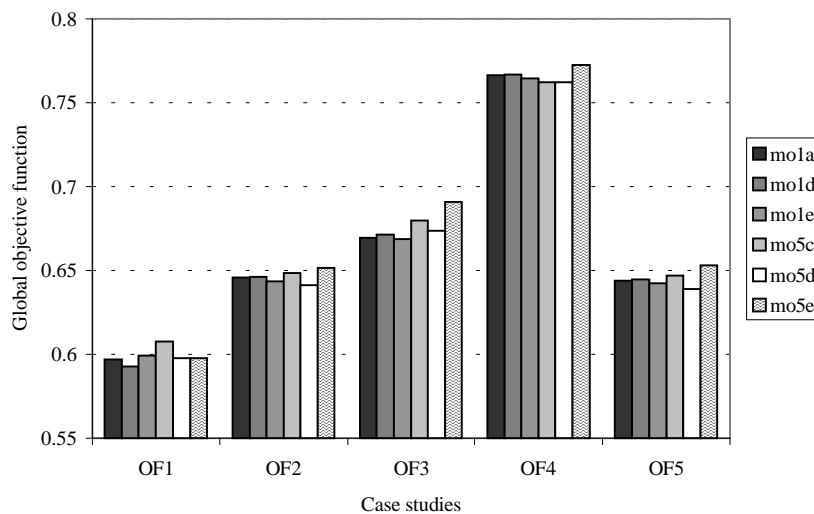


Figure 5.50- Comparison between NPGA and RPSGA methods.

#### 5.4.2- Optimisation of the operating conditions

As settled before, one of the main objectives of this work is to optimise automatically the operating conditions for a given extruder/polymer combination. This means, for example, to define the screw speed and barrel temperatures profile that produce the better extruder performance, i.e., that maximise the output and the degree of mixing, minimise the screw length required for melting, the melt temperature, the power consumption and the residence time of an extrusion process. Not only some of these individual objectives are contradictory, but also they can have different importance to the process. The use of an objective function, as represented by equation 2.22, easily permits the change of the relative importance of the several criteria, and by this way to determine the corresponding optimal conditions. However, when it is necessary to make this change a new run of the optimisation algorithm needs to be performed. This difficulty can be undertaken using a multiobjective optimisation methodology as those presented before, namely the Niched Pareto Genetic Algorithm (NPGA) and the Reduced Pareto Set Genetic Algorithm (RPSGA) methods. In this case the result is a Pareto frontier where all the optimal conditions were represented. The decision-maker only needs to take into consideration the trade-off between the relevant criteria in order to choose the corresponding optimal solution.

To optimise the operating conditions will be used an example where the objective is to set the screw speed and the barrel temperature profile in three zones in order to maximise the output and to minimise the screw length required for melting, the melt temperature and the power consumption. For that the values of Tables 5.1 (range of variation of operating conditions), 5.2 (criteria definition) and 5.3 (weights of the individual criteria) will be used. This example will be studied for all cases of Table 5.3 using both the Genetic Algorithm with objective function (equation 2.22) and the Reduced Pareto Set Genetic Algorithm (RPSGA), and for each one the analytical and the numerical models. Finally, these results will be compared with experimental results obtained in a Leistritz extruder (Table 4.3). Table 5.23 presents the numerical and the GA parameters used for the optimisation types studied.

**Table 5.23- Numerical and GA parameters used in the optimisations.**

Parameter	Optimisation type			
	Objective function		Reduced Pareto Set	
	Analytical	Numerical	Analytical	Numerical
Number of increments in Z direction	100	100	100	100
Number of grid points in transversal plane	--	10	--	10
Initial thickness of the film close to the barrel	--	$\delta_f$	--	$\delta_f$
Initial thickness of the film close to the screw root and passive flank	--	$\delta_f$	--	$\delta_f$
Initial melt pool width	--	$2\delta_f$	--	$2\delta_f$
Screw temperature upon solids conveying	--		--	
Population length	200	200	500	500
Crossover rate	70	70	70	70
Mutation rate	2	2	2	2
Selection operator	exp. ranking + roulette wheel			
Crossover operator	two points	two points	two points	two points
Number of generations	50	50	50	50
Chromosome length	24	24	24	24
$\sigma_{share}$	--	--	0.1	0.1
<i>limits</i>	--	--	0.01	0.01

**NOTE:**  $\delta_f$  - flight clearance.

Figure 5.51 shows the evolution of the global and the individual objective functions as the search proceeds for case study OF1. The optimisation process seems to converge after 20 generations. During the search the growth of the global objective function follows the evolution of the output individual criterion, given their higher relative importance. Simultaneously the other criteria deteriorate during this process. Obviously, the output growth is achieved at expenses of power consumption. Likewise, a higher output implies short residences times and consequently an increase on the screw length required to melting the

polymer. Furthermore, the viscous dissipation increases with the output, which has a consequence the increases of the melt temperature.

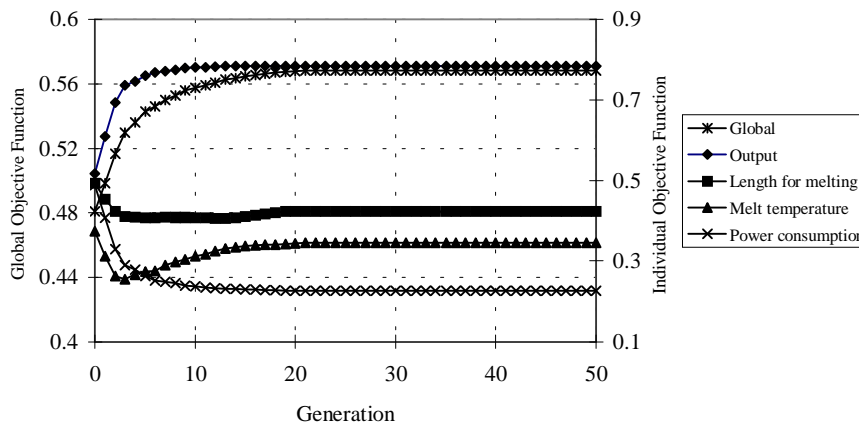


Figure 5.51- Genetic Algorithm optimisation of global and individual objective functions (case study OF1, Table 5.3).

The convergence of the genetic search is achieved when a reasonable number of population individuals have the same value. Figure 5.52 shows the evolution of the global objective function considering the best individual and the average of best 30, 50, 75 and 100% of the population. The best individual of each generation converges rapidly and maintains its value. Likewise, the average of 30, 50 and 75 % of the population converge to the same value and maintain it. This does not happens for the average of 100% of the population, because in all the generations mutation has a (small) probability to occurs, which due to its characteristics can produces considerable modifications on some individuals. Thus, the use of an average of 75% of the population as a convergence criterion seems to be adequate.

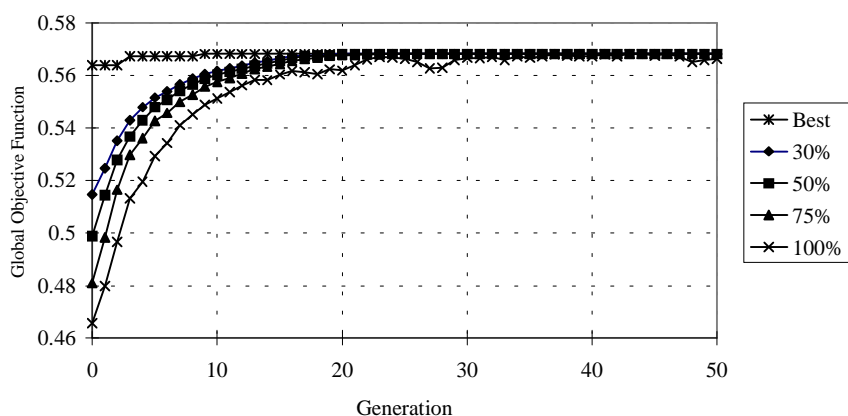


Figure 5.52- Evolution of global objective function for the average of the best and the average of best 30, 50, 75 and 100% of the population.

The evolution of the genetic algorithm optimisation can also be followed using the parameters to optimise, screw speed and barrel temperatures in three zones. Figure 5.53 presents the

evolution of the mean value of the best 75 and 30% population individuals of each generation (bold and thin contour lines, respectively), forming the practical operating window. The initial variation range is also represented. The best algorithm performance relatively to Figure 5.25 is due to the use here of improved GA parameters.

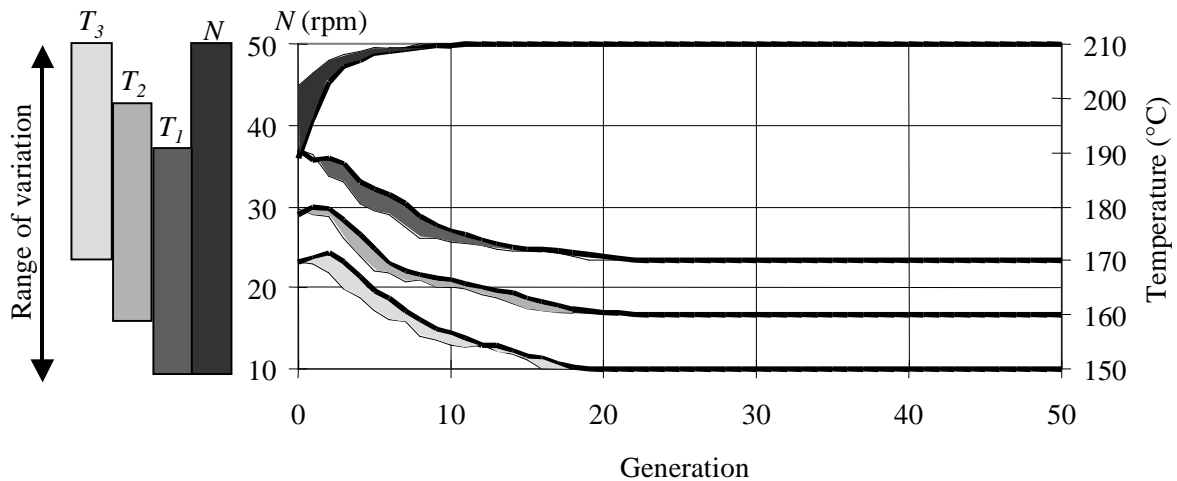


Figure 5.53- Practical operating window. Bold contours: mean value of the best 75% chromosomes; thin contours: mean values of the best 30% chromosomes.

Figure 5.54, where the evolution of the global and individual objective functions for case studies OF2 to OF5 (Table 5.3) are represented, demonstrates that the results are sensitive to the relative importance of the process variables. This point is clearly confirmed by observation of the results obtained for case studies OF1 and OF4, where the weights affecting the output and the power consumption are interchanged. The behaviour of the global objective function is similar to that of the most important individual criterion. These two criteria are not only conflicting in the objective function (usually the aim is to maximise the output and minimise the power consumption), but also in their interaction (as increasing the output requires more power).

The use of a multiobjective optimisation methodology as the one developed in this work, Reduced Pareto Set Genetic Algorithm (RPSGA), easily permits with one run to obtain, not only the 5 solutions represented by each one of the cases studied, but the entire Pareto frontier. Figure 5.55 shows the Pareto frontiers obtained in the optimisation of the operating conditions using both the RPSGA and the numerical model (Table 5.23). These curves are graphed as a function of mass output assuming these as the most important criterion; however, they can be represented as a function of any other criteria. The decision-maker can choose a desirable value for the output (if this is the most important criterion, as in the case

study OF1) see the value of the other criteria (Figure 5.55-A) and relate this point with the corresponding operating conditions (Figure 5.55-B). However, since this is a multidimensional problem is possible that optimal points for given two criteria could not be optimal for any other two criteria.

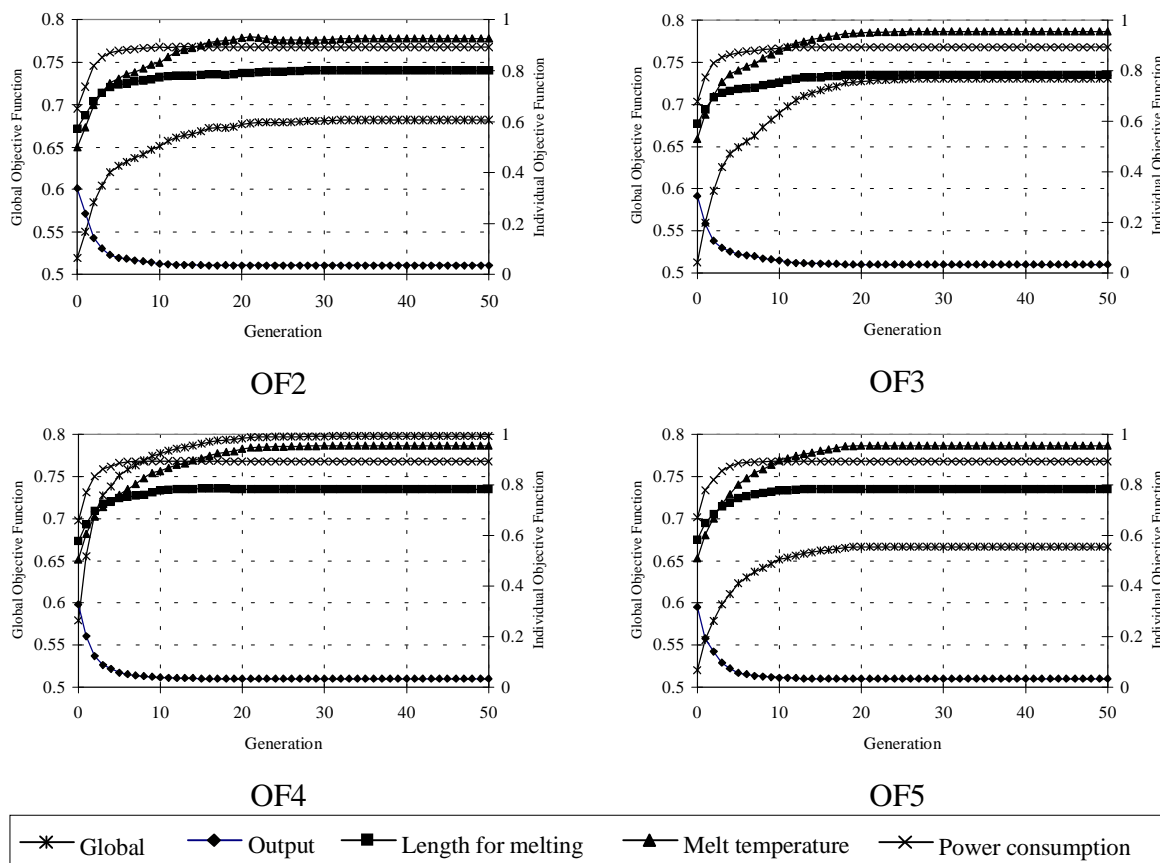


Figure 5.54- Evolution of the global and individual objective functions for case studies OF2 to OF5.

Table 5.24 shows the results corresponding to the maximisation of equation 2.22 and using the analytical model. The data indicates that:

- When the most important criterion is output maximisation, screw speed converges to its maximum value – OF1;
- When the weight attributed to the minimisation of the length of screw required for melting is higher, barrel temperature for zone 1 is also higher, since melting occurs predominantly here – OF2;
- Minimisation of length of the screw required for melting, melt temperature or power consumption is always achieved when the screw speed is at its lowest possible value (10 rpm) – OF2 to OF4;

- Melt temperature at the extruder exit is at its minimum, using the lowest barrel temperature profile – OF3.

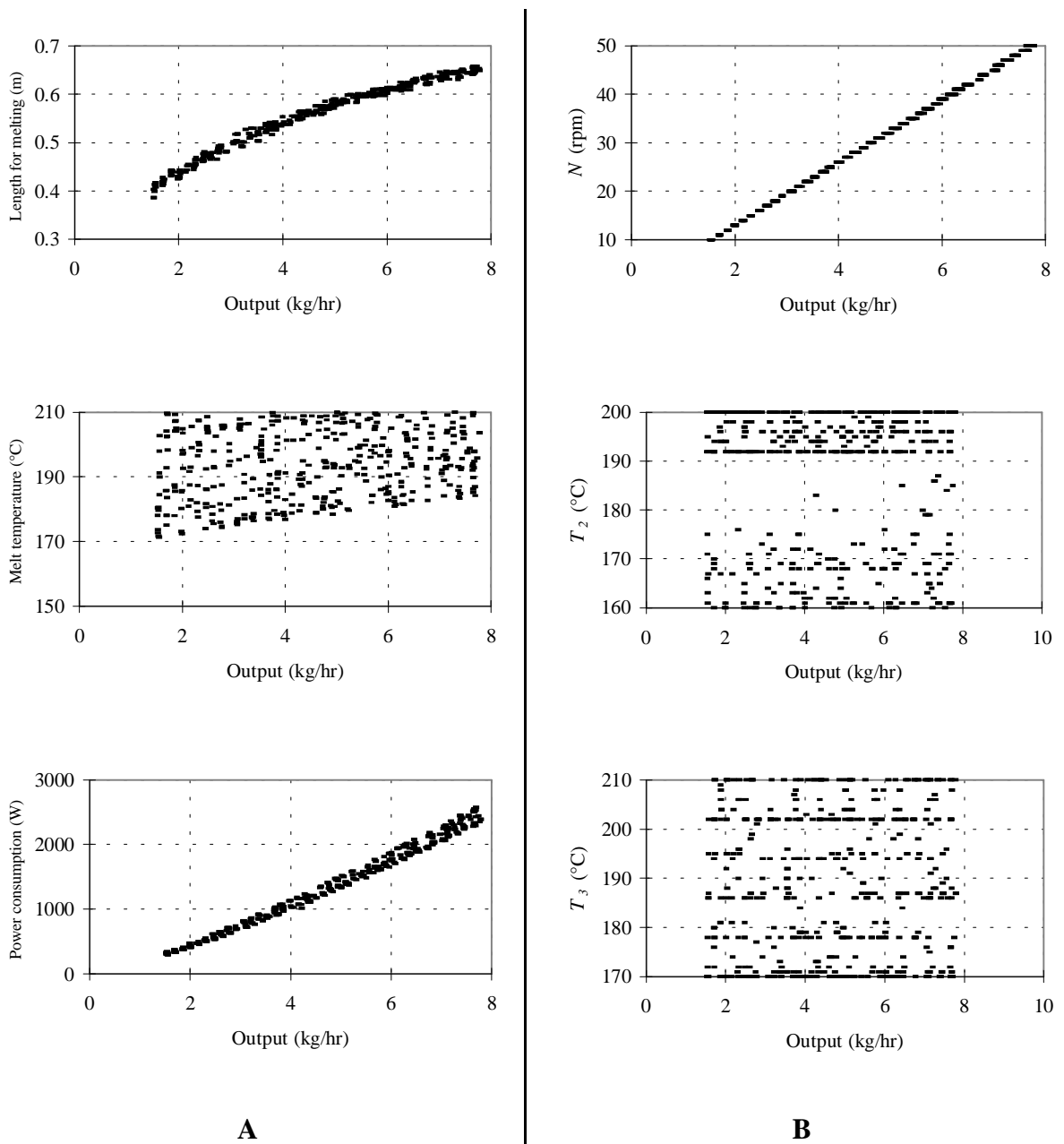


Figure 5.55- Pareto optimal set: A) criteria efficient frontiers; B) operating conditions efficient frontiers.

If the same problem is solved using a multiobjective optimisation methodology, the final result is a Pareto frontier where, in principle, all the set of weights are represented. For that reason, the use of a specific combination of weights, is only possible through an indirect approach. In this case, the objective function was applied to the same final generation, using successively the various weights, and the best individual of each set of weights is chosen. Table 5.25 presents the corresponding operating values.

**Table 5.24- Operating conditions for OF optimisation – analytical model.**

	<b>OF1</b>	<b>OF2</b>	<b>OF3</b>	<b>OF4</b>	<b>OF5</b>
<b>N (rpm)</b>	50	10	10	10	10
<b>T1 (°C)</b>	150	167	152	152	151
<b>T2 (°C)</b>	160	170	161	170	160
<b>T3 (°C)</b>	170	170	170	170	170

**Table 5.25- Operating conditions for RPS – analytical model.**

	<b>Cases under study</b>				
	<b>OF1</b>	<b>OF2</b>	<b>OF3</b>	<b>OF4</b>	<b>OF5</b>
<b>N (rpm)</b>	50	10	10	10	10
<b>T1 (°C)</b>	154	174	154	154	154
<b>T2 (°C)</b>	161	166	161	161	161
<b>T3 (°C)</b>	170	170	170	170	170

The values in Tables 5.24 and 5.25 are similar. Differences exist for  $T_2$  in *Case* OF4 (9°C), but they have little importance as suggested by the experimental data (Table 5.13).

As discussed previously, the biggest advantage of a multiobjective optimisation is the possibility of testing “all” the combinations of weights only with one run. Therefore, the decision-maker, upon obtaining the Pareto frontier from a multiobjective optimisation scheme, possesses the necessary information to made decisions about the process.

If the objective function is now optimised using the numerical model, the data presented in Table 5.26 is obtained. A comparison with the results obtained with the analytical model (Table 5.24) shows that case studies OF1 and OF4 have different  $T_1$  and  $T_2$ , respectively and that case study OF3 has a distinct screw speed. In the case of multiobjective optimisation using the numerical model (Table 5.27) the differences are more important.

**Table 5.26- Operating conditions for OF optimisation – numerical model.**

	<b>Cases under study</b>				
	<b>OF1</b>	<b>OF2</b>	<b>OF3</b>	<b>OF4</b>	<b>OF5</b>
<b>N (rpm)</b>	50	13	17	10	12
<b>T1 (°C)</b>	184	165	151	155	155
<b>T2 (°C)</b>	165	177	162	196	172
<b>T3 (°C)</b>	170	170	170	170	170

**Table 5.27- Operating conditions for RPS – numerical model.**

	Cases under study				
	OF1	OF2	OF3	OF4	OF5
<b>N (rpm)</b>	50	27	10	10	10
<b>T1 (°C)</b>	188	184	177	177	177
<b>T2 (°C)</b>	164	180	193	193	193
<b>T3 (°C)</b>	173	170	170	170	170

In order to compare and discuss the optimisation results obtained either by extrusion experiments or by computations, three approaches were considered namely factorial design of experiments, GAs with an objective function and multiobjective optimisation with GAs. In the first case, it is possible to define the operating conditions through extrusion experiments, analytical results, or numerical results. In the remaining approaches, analytical or numerical modelling were considered.

In this study the intent is to optimise the operating conditions (screw speed, and barrel temperature profile – Table 5.1) in order to maximise the output and to minimise the melt temperature and the power consumption (Table 5.2). In order to be possible the comparison between the approach that uses experimental results and the others, the minimisation of the screw length required for melting will not be considered. Thus, Table 5.3 is transformed into Table 5.28.

**Table 5.28- Weights of the individual criteria.**

Case Studies	Weights			
	$W_1$	$W_2$	$W_3$	$W_4$
OF1'	0.6	0	0.3	0.1
OF2'	--	--	--	--
OF3'	0.2	0	0.6	0.2
OF4'	0.1	0	0.3	0.6
OF5'	0.(3)	0	0.(3)	0.(3)

Tables 5.29 to 5.32 summarise the results obtained on the optimisation of the operating conditions for the case studies OF1' (Table 5.29), OF3' (Table 5.30), OF4' (Table 5.31) and OF5' (Table 5.32).

When more importance is given to output (case study OF1' - Table 5.28), screw speed converges to its maximum possible value in all the approaches. The differences between them occur for  $T_1$  and  $T_2$ . While the values of  $T_1$  obtained with the approaches that use the numerical model are closer to the corresponding experimental values, the values of  $T_2$  for both models are different. This is due to the fact that, for the analytical model, the output does not

seem to vary with barrel temperatures but melt temperature does (Figure 5.21); consequently the melt temperature criterion assumes some importance. For the numerical model  $T_2$  does not affect the output, whereas has some influence on melt temperature (Figure 5.23)

**Table 5.29- Results of the various approaches for OF1'.**

<b>Optimisation type</b>	<b>Model</b>	<b><math>N</math> (rpm)</b>	<b><math>T_1</math> (°C)</b>	<b><math>T_2</math> (°C)</b>	<b><math>T_3</math> (°C)</b>
Factorial design	Experimental	50	190	180-200	170
Factorial design	Analytical	50	150	160	170
Factorial design	Numerical	50	190	160	170
Objective function GA	Analytical	50	150	160	170
Objective function GA	Numerical	50	182	166	170
Reduced Pareto Set GA	Analytical	50	154	161	170
Reduced Pareto Set GA	Numerical	50	180	165	173

Table 5.30 presents the results when the main criterion is the minimisation of melt temperature at the exit of the extruder. As the experimental data suggests, the last barrel temperature determines melt temperature (Table 5.12) and then the values of  $T_1$  and  $T_2$  converge to their maximum possible value. Screw speed does not seem to be determinant since it converges to values between 10 and 30 rpm. This happens due to the small weight attributed to the output criterion. Analytical computational results indicate that this objective is achieved with the lowest barrel temperature profile and the lowest screw speed. This is explained by the fact that, when this mathematical model is used, barrel temperatures  $T_1$  and  $T_2$  have some importance (Table 5.13) and the variation of melt temperature with the screw speed is non negligible (Figure 5.21). For the approaches that use the numerical model, when the screw speed is small (factorial design and RPSGA) the value of  $T_2$  is the greatest possible. This is justified by the fact that for screw speed equal to 10 rpm melt temperature does not vary with  $T_2$  (Figure 5.23).

The minimisation of the power consumption (case study OF4' – Table 5.31) is accomplished with the lowest screw speed. The results of all approaches are very similar, the greater differences occur on  $T_2$  for the analytical results. Being the power consumption behaviour, as a function of screw speed and  $T_2$ , similar in all the approaches, the differences observed are probably due to the sensitivity to melt temperature (Figures 5.19 to 5.24).

When is given equal importance to the criteria (case study OF5' – Table 5.32) the results are similar to those of the previous two case studies as well as the reasons for this behaviour.

**Table 5.30- Results of the several approaches for OF3´.**

<b>Optimisation type</b>	<b>Model</b>	<b>N (rpm)</b>	<b>T<sub>1</sub> (°C)</b>	<b>T<sub>2</sub> (°C)</b>	<b>T<sub>3</sub> (°C)</b>
Factorial design	Experimental	10-30	190	200	170
Factorial design	Analytical	10	150	160	170
Factorial design	Numerical	10	150	200	170
Objective function GA	Analytical	10	152	161	170
Objective function GA	Numerical	17	151	162	170
Reduced Pareto Set GA	Analytical	10	154	161	170
Reduced Pareto Set GA	Numerical	11	157	200	171

**Table 5.31- Results of the several approaches for OF4´.**

<b>Optimisation type</b>	<b>Model</b>	<b>N (rpm)</b>	<b>T<sub>1</sub> (°C)</b>	<b>T<sub>2</sub> (°C)</b>	<b>T<sub>3</sub> (°C)</b>
Factorial design	Experimental	10	150-190	200	170
Factorial design	Analytical	10	150	160	170
Factorial design	Numerical	10	150	200	170
Objective function GA	Analytical	10	152	170	170
Objective function GA	Numerical	10	155	196	170
Reduced Pareto Set GA	Analytical	10	154	161	170
Reduced Pareto Set GA	Numerical	11	157	200	171

**Table 5.32- Results of the several approaches for OF5´.**

<b>Optimisation type</b>	<b>Model</b>	<b>N (rpm)</b>	<b>T<sub>1</sub> (°C)</b>	<b>T<sub>2</sub> (°C)</b>	<b>T<sub>3</sub> (°C)</b>
Factorial design	Experimental	10	170-190	200	170
Factorial design	Analytical	10	150	160	170
Factorial design	Numerical	10	150	200	170
Objective function GA	Analytical	10	151	160	170
Objective function GA	Numerical	12	155	172	170
Reduced Pareto Set GA	Analytical	10	154	161	170
Reduced Pareto Set GA	Numerical	11	157	200	171

### 5.4.3- Screw design

Screw design, i.e., the optimisation of the screw geometry parameters, is a very challenging task. First of all, the number of parameters to optimise can vary widely. This means that the use of GAs requires the manipulation of a chromosome of variable length, that needs to “accommodate” the eventual existence of mixing sections, barrier compression zone, grooves on the barrel, etc. Another important aspect is the multi-modality of the search space, which constitutes an additional problem for the algorithm. Moreover, the practical definition of the screw geometry must involve complex situations, such as processing a single polymer under a relatively wide operating window, a single polymer but with varying properties (various

grades) or even several polymers. This means that not only the optimisation of a number of objectives are pursued, but the sensitivity of those objectives to changes in the process variables must also be considered.

Such an analysis is complete only if the operating conditions and the mechanical behaviour of the screws are examined. The design of a screw with optimal process performance needs to take into account the mechanical strength to support the stresses required by the conveying process. Variables such as the torsional strength of the screw root, strength of the screw flight and lateral deflection of the screw are fundamental and need to be carefully thought about.

In this section, a preliminary study on the optimisation of the screw geometrical parameters, using Genetic Algorithms with objective function (Figure 5.2), in order to satisfy the criteria of Table 5.4 will be made (Table 5.5). Taken into account the multi-modality of this optimisation problem (as will be seen next), the use of a multiobjective algorithm that produces a set of solutions (Pareto frontier) can be useful in order to obtain various similar answers with one run. Therefore, four runs of the optimisation procedure using the Reduced Pareto Set Genetic Algorithm, for case studies 6 to 9 with multiple criteria and different relative weights (Table 5.5) will also be made. Finally, an example where the aim is to design a conventional screw (Figure 5.2), to use with 3 different materials (HDPE, LDPE and PVC), in order to satisfy the criteria of Table 5.4 and to obtain the most equilibrated performance will be studied. The processing conditions were maintained constant, case studies (or runs) 6, 16 and 17 (Table 5.5).

#### a) GA with objective function

Figure 5.56 shows the results obtained when the aim of the optimisation considers only the individual criteria. An identical screw is obtained when the objectives are to maximise the output ( $Q$  – run 1) and minimise the power consumption ( $P$  – run 4). In this case the channel depth in the metering zone is the largest possible ( $D_3 = 27$  mm) and the compression ratio is small ( $CR = 1.73$ ), since such a screw offers small resistance to the flux. When the objectives are to minimise the length of screw required for melting ( $L$  – run 3) and to maximise the degree of mixing ( $W$  – run 5) the channel depth converge for a small value ( $D_3 = 32.8$ ) and the compression ratio is greater ( $CR = 5$ ). Furthermore, this screw has the largest metering zone length ( $20.3D$ ). Here the objective is to melt the polymer earlier in order to have, not only a small melting zone, but also a bigger degree of mixing. Since the melting occurs essentially in

the melt conveying zone of the process. The minimisation of the melt temperature ( $T$  – run 2) is achieved with a screw with a compression ratio equal to 4 and with the greatest possible value for the internal screw diameter (equivalent to small channel depth). This reveals that the increase on the melt temperature is not due to viscous dissipation but is controlled by heat conduction (as concluded before – section 5.4).

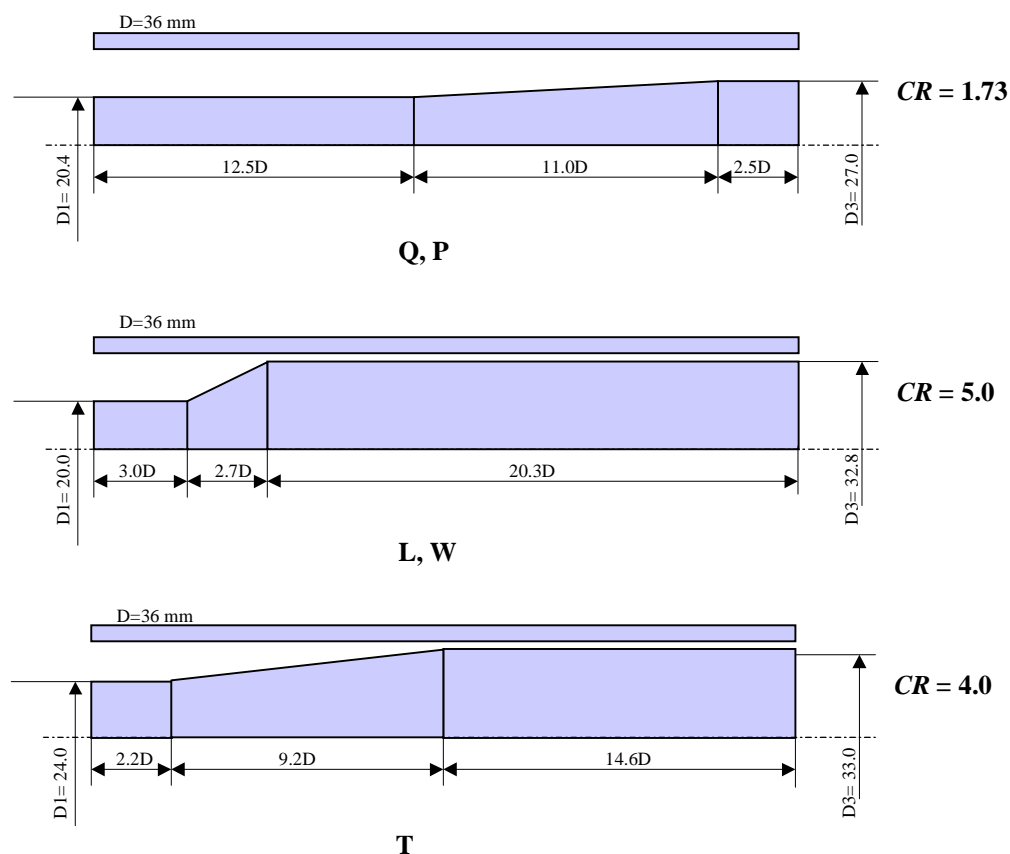


Figure 5.56- Influence of the individual criteria.

The results for different relative weights are presented in Figure 5.57. As can be seen, when greater weight is given to the maximisation of the output (run 6), the screw is similar to that obtained when the maximisation of the output and the minimisation of power consumption are considered alone (runs 1 and 4). The screws differ in the length of the compression zone, since here some importance is given to the minimisation of the screw length required for melting and the maximisation of the mixing degree. The screw obtained in this case reflects a compromise between higher outputs (run 1) and these two criteria. In the remaining cases the screw obtained is the same and is identical to that obtained when the screw length required for melting and the degree of mixing are considered alone (run 3 and 5). Again a compromise

between objectives is obtained, but now the screw reflects the small importance of the output by decreasing the internal screw diameter from 32.8 to 31.9 mm.

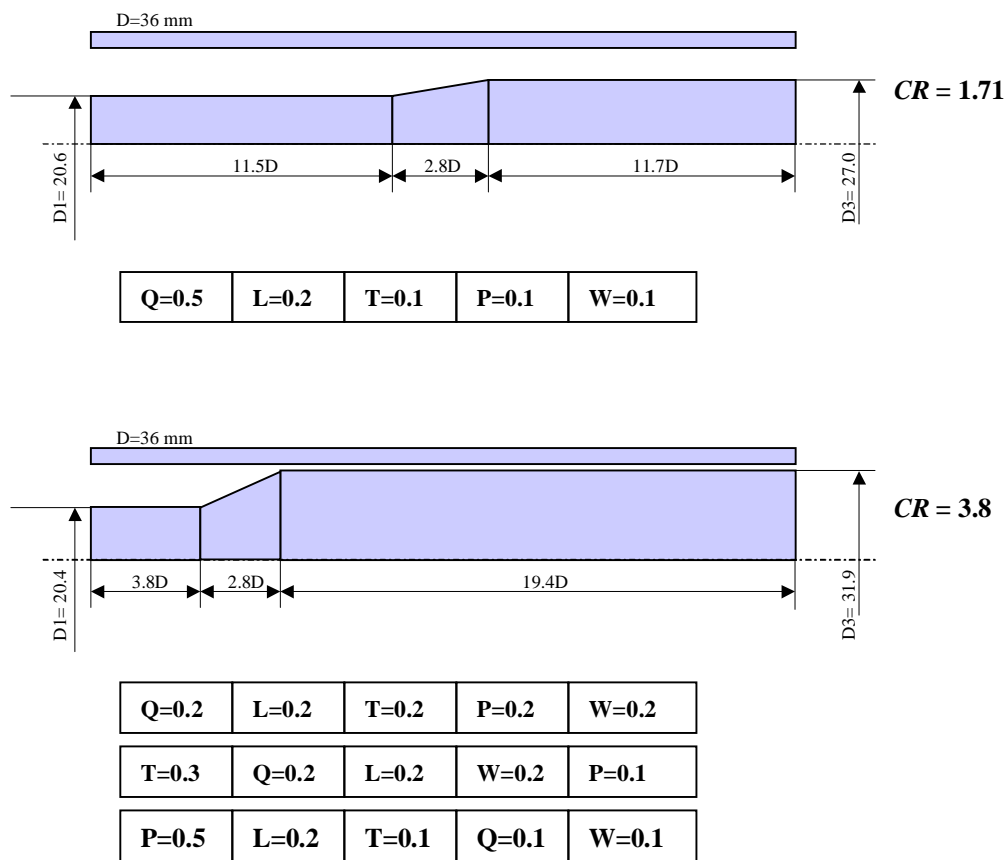


Figure 5.57- Influence of the different relative weights.

At this point it will be important the study of the reproducibility of the results and to verify if this optimisation problem is multi-modal. Figure 5.58 shows the results obtained when 3 runs of the same optimisation problem are made using the same criteria and operating conditions (runs 6, 10 and 11). The algorithm converges for two different solutions; this probably means that the problem is multimodal [GOL 87]. In order to confirm this task the global objective function is plotted against two of the parameters to optimise ( $L_1$  and  $L_2$ ) - see Figure 5.59. As can be seen, there are various maxima distributed at random along the search space.

Figure 5.60 shows the influence of screw speed on the design of a screw. As the screw speed increases the compression ratio decreases and the compression zone is transferred from the beginning to the middle of the screw. The screw obtained with 10 rpm (run 12) has a channel depth the smallest possible. In this case it was necessary to have a small channel depth in order to increase the polymer compression capacity of the screw. When the screw speed increases the melting of the polymer occurs later on the screw (runs 13 and 6), since the residence time of the polymer inside the extruder decreases. Consequently the compression

zone follows this behaviour because during the melting phase it was necessary to compress the polymer in order to increase the melting capacity.

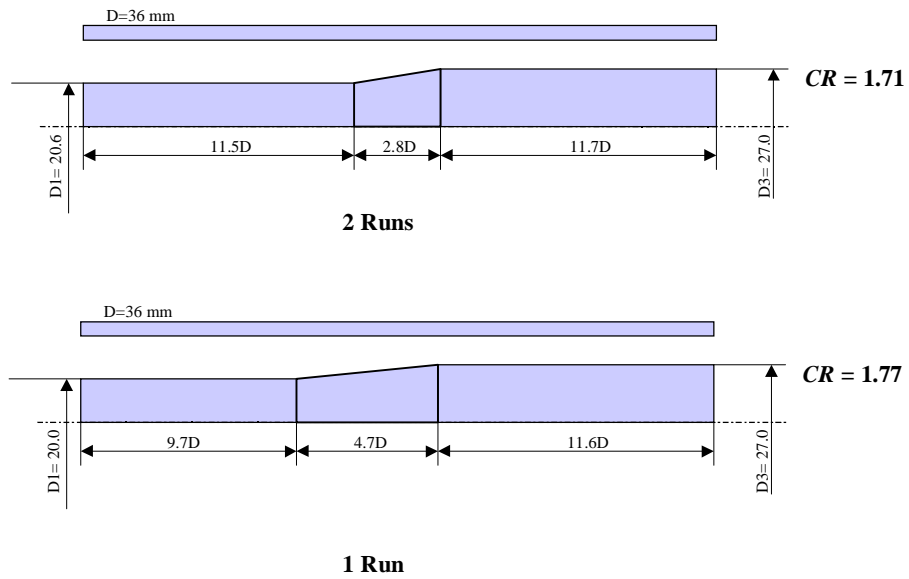


Figure 5.58- Study of the reproducibility.

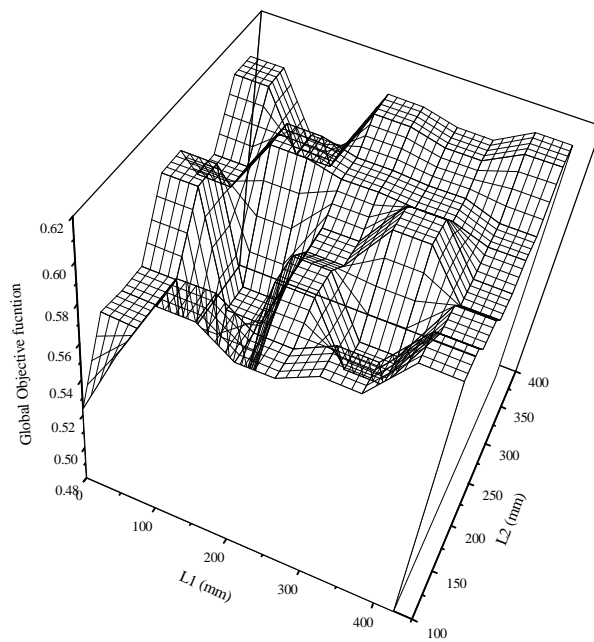


Figure 5.59- Global objective function versus  $L_1$  and  $L_2$ .

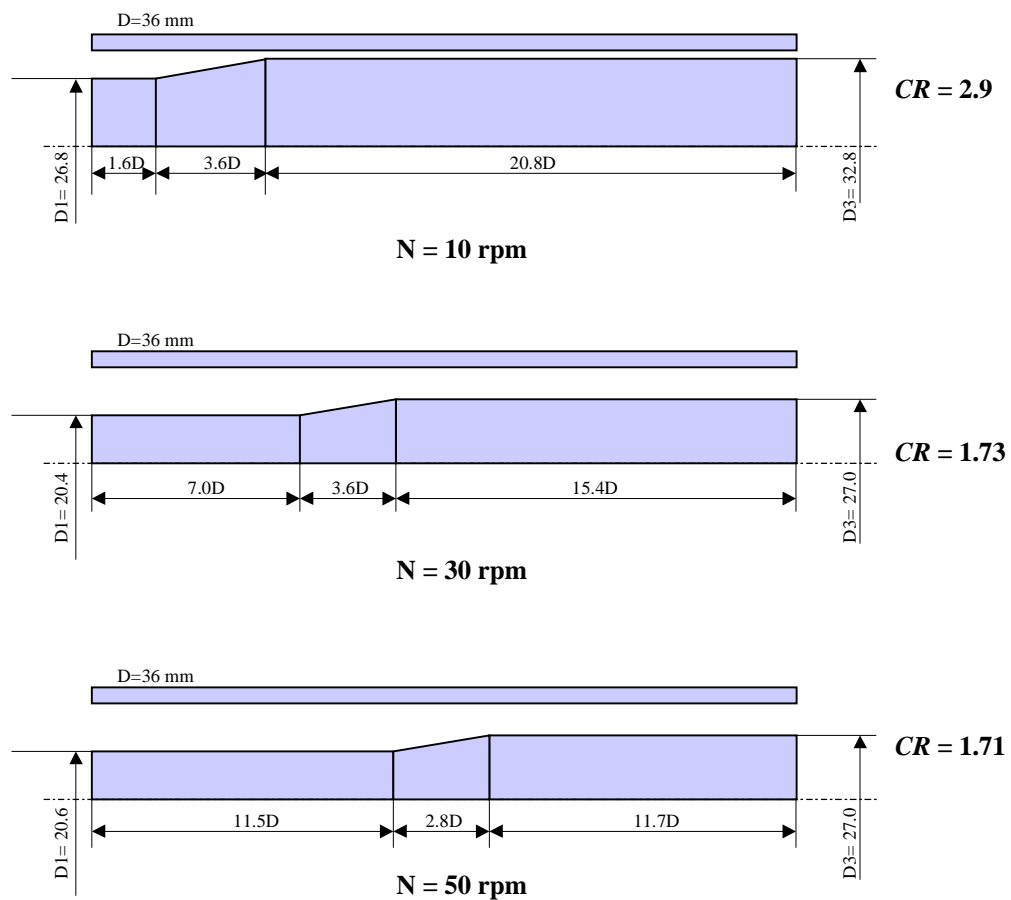


Figure 5.60- Influence of the processing conditions (screw speed).

The influence of barrel temperature profile on the screw design optimisation will be studied with an example where the 3 screws obtained with 3 different screw speeds (Figure 5.60, runs 12, 13 and 6) were subjected to 3 different barrel temperature profiles (Table 5.33).

**Table 5.33- Barrel temperature profiles.**

	$T1$ (°C)	$T2$ (°C)	$T3$ (°C)
<b>Profile 1</b>	150	170	190
<b>Profile 2</b>	160	180	200
<b>Profile 3</b>	170	190	210

Figure 5.61 shows their behaviour in terms of the global objective function determined using the 5 criteria and the weights correspondent to run 6 (Table 5.5). The variation of the global objective function with screw speed and barrel temperature profiles is linear. The best screw for 10 rpm is that obtained with  $N=10$  rpm and Profile 1. The screw obtained with  $N=50$  rpm and Profile 1 shows the best performance for screw speeds of 30 and 50 rpm. This is probably due to the similitude of the two last screws in terms of the channel depth.

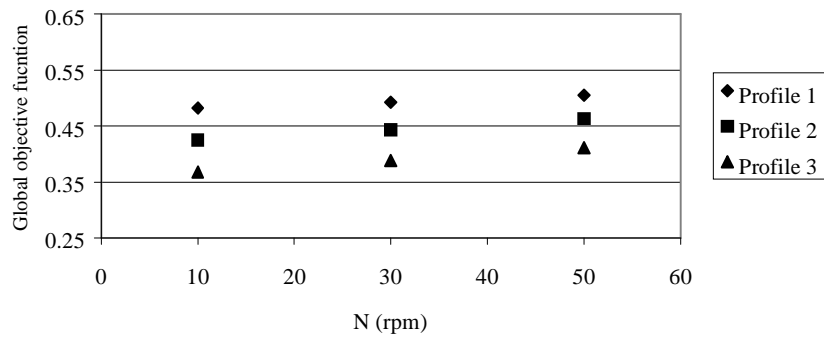
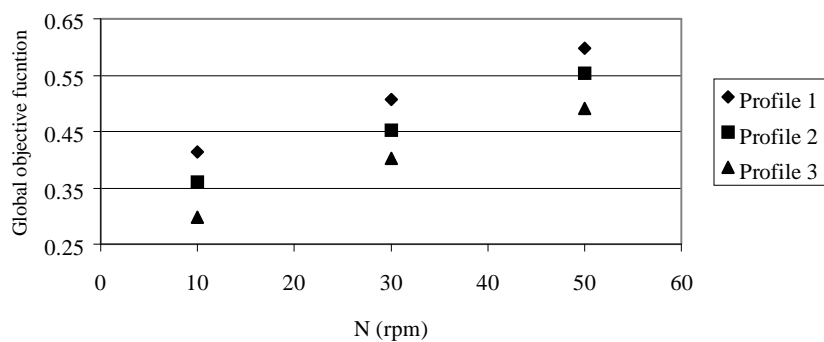
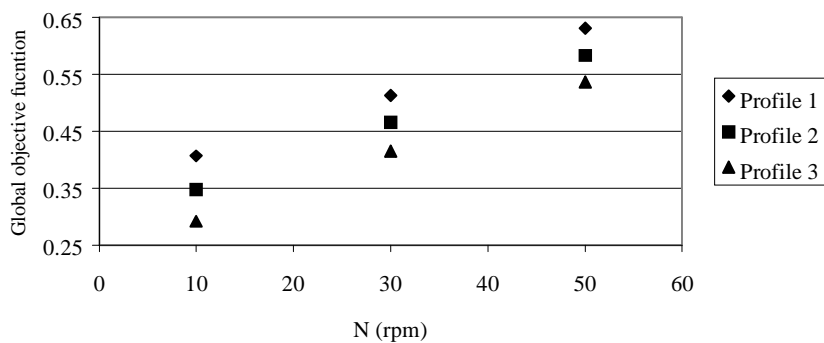
**A****B****C**

Figure 5.61- Influence of the barrel temperature profile: A) screw for N=10rpm; B) screw for N=30rpm; C) screw for N=50rpm.

Figure 5.62 presents the results obtained in the screw design optimisation, but now including additionally the screw pitch as a parameter to optimise. Two situations are studied: constant screw pitch along the screw (run 14) and different screw pitch for each geometrical zone (run 15). For both cases the screw obtained has a screw pitch that corresponds to a helix angle of  $21^\circ$ . Generally this value is equal to  $17.7^\circ$ , correspondent to a square screw where the pitch is equal to the screw external diameter.

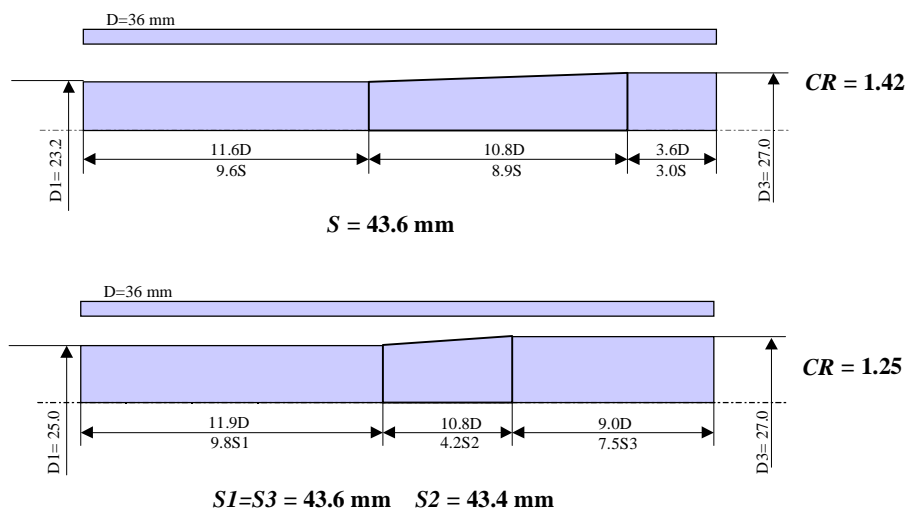


Figure 5.62- Influence of the pitch.

The influence of different materials on the screw design is presented in Figure 5.63 (runs 6, 16 and 16). The screws obtained for the two polyolefines (runs 6 and 16, respectively for HDPE and LDPE) are identical, since they have similar properties. However, the localisation of the compression zone of the screw optimised for LDPE (run 16) is closer of the feed zone, probably due to its lower thermal conductivity (Appendix B). The larger compression zone of the screw optimised for PVC (run 17) is probably due to its higher viscosity (Appendix B).

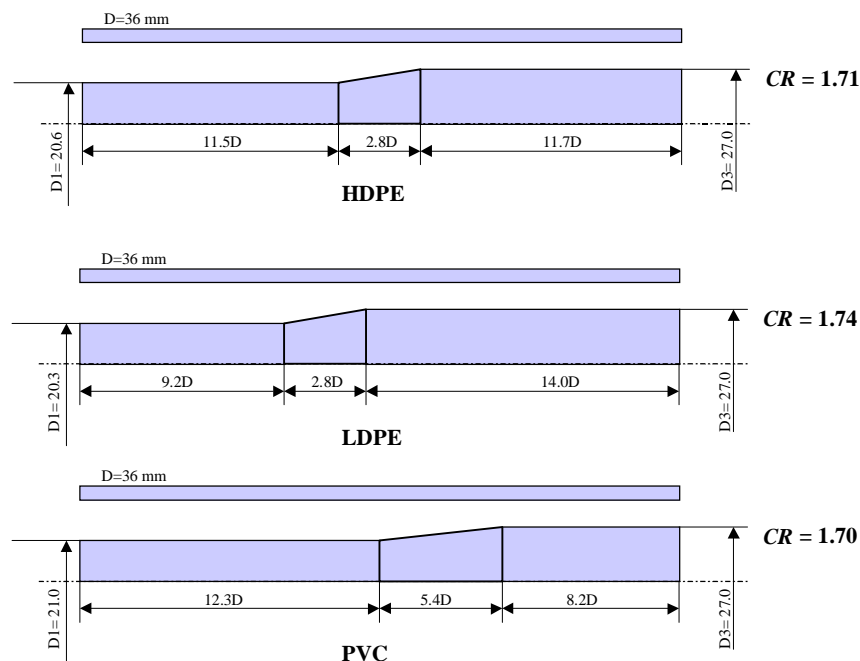


Figure 5.63- Influence of different materials.

Finally, if some changes in the viscosity level of an HDPE (runs 18, 6 and 19) and the corresponding optimisations are performed, three different screws are obtained (Figure 5.64).

The optimal screws for low (run 18) and high (run 19) viscosity levels have a smaller compression ratio and a higher length of the compression zone than that obtained when a medium viscosity level (run 6) is considered.

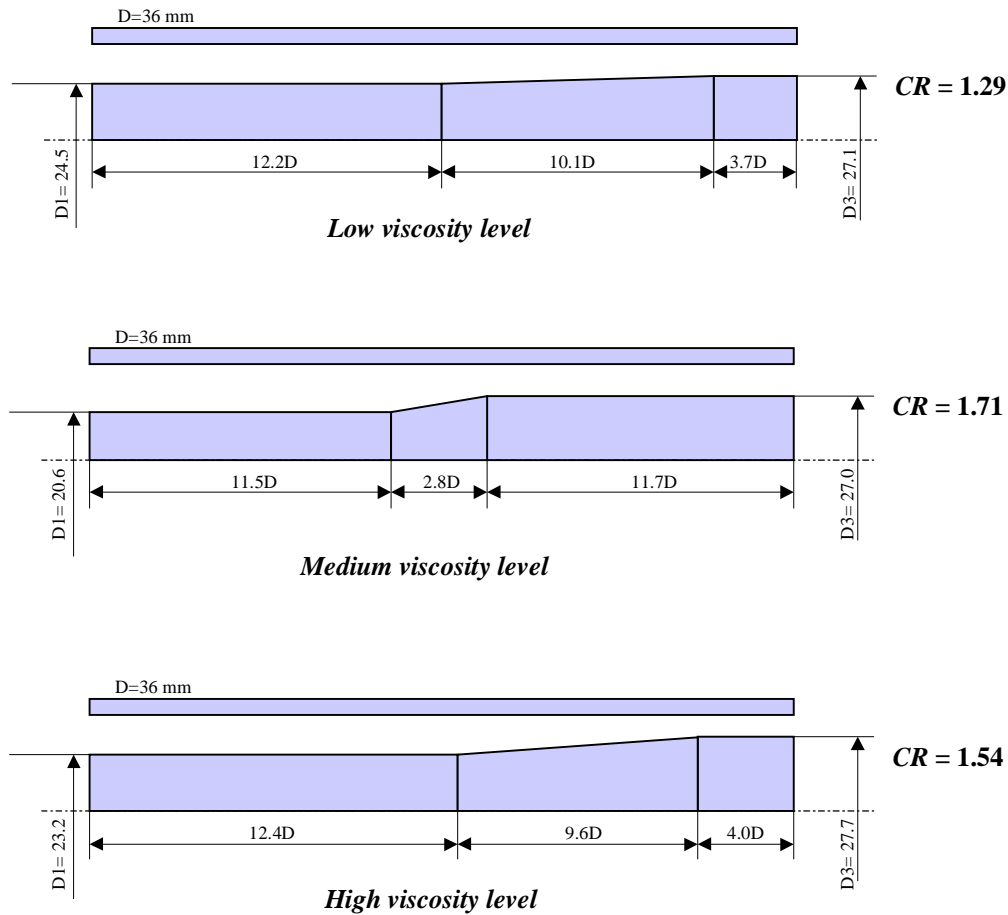


Figure 5.64- Influence of the viscosity level.

## b) Multiobjective optimisation with RPSGA method

Table 5.34 shows the 6 best results obtained on the screw design optimisation of the cases corresponding to runs 6 to 9 (Table 5.5). In this case, the optimisation was performed using the Reduced Pareto Set Genetic Algorithm (RPSGA) using the parameters presented in Table 5.23 (analytical model). The last generation (50) was ordered in function of a global objective function (equation 2.22) computed using the weights corresponding to runs 6 to 9. Then, the 6 best individuals are chosen. The 6 screws of each run are similar to those obtained before (Figure 5.57) and between themselves. The advantage of this method (RPSGA) is that the decision-maker has now multiple optimal alternatives, which in principle take into account the multi-modality of the problem.

**Table 5.34- Screws geometry and corresponding criteria values obtained using RPSGA.**

	$L_1$ (xD)	$L_2$ (xD)	$D_1$ (mm)	$D_3$ (mm)	$Q$ (kg/hr)	$L_T$ (m)	T (°C)	$e_w$ (W)	WATS	CR
Run 6	12.4	6.4	20.0	27.2	11.90	0.8203	165.1	2256	66.37	1.82
	12.2	9.6	20.0	27.8	11.83	0.8553	164.6	2134	49.25	1.95
	12.4	3.3	21.6	27.2	11.69	0.7845	166.7	2403	88.00	1.64
	12.1	5.6	20.4	27.6	11.59	0.7884	166.5	2343	88.51	1.86
	12.4	6.9	20.0	28.0	11.56	0.8113	166.1	2283	78.01	2.00
	12.4	5.0	21.6	28.0	11.47	0.7857	167.6	2419	93.44	1.80
Run 7	3.5	2.8	22.8	31.8	4.526	0.322	191.8	2481	847.2	3.14
	3.8	2.9	20	31.6	4.334	0.319	191.9	2389	834.4	3.64
	3.3	3.2	20.4	31.8	4.432	0.326	191.9	2434	844.6	3.71
	3.3	3.2	21.2	31.8	4.448	0.328	191.6	2437	841.4	3.52
	4.4	2.9	20.6	31.6	4.908	0.346	190.2	2374	765.5	3.50
	3.2	2.8	20.4	31.2	3.807	0.302	193.8	2291	845.1	3.25
Run 8	3.5	2.8	22.8	31.8	4.526	0.322	191.8	2481	847.2	3.14
	3.3	3.2	21.2	31.8	4.448	0.328	191.6	2437	841.4	3.52
	3.3	3.2	20.4	31.8	4.432	0.326	191.9	2434	844.6	3.71
	4.3	2.8	21.6	31.8	4.844	0.34	190.7	2522	801.1	3.43
	3.8	2.9	20	31.6	4.334	0.319	191.9	2389	834.4	3.64
	3.8	2.8	20	31.6	6.165	0.357	189.1	2773	683.2	3.64
Run 9	3.2	2.8	20.4	31.2	3.807	0.302	193.8	2291	845.1	3.25
	3.2	2.8	20.4	31.2	3.807	0.302	193.8	2291	845.1	3.25
	3.8	2.9	20	31.6	4.334	0.319	191.9	2389	834.4	3.64
	2.5	3.5	20.5	31.3	4.201	0.312	193.1	2375	818.6	3.30
	3.3	2.9	20	31.2	4.255	0.313	192.9	2367	800.6	3.33
	4.4	2.9	20.6	31.6	4.908	0.346	190.2	2374	765.5	3.50

*c) Optimal screw to use with 3 different polymers*

As described at the beginning of this section, the objective here is to design a screw that can be used with 3 different polymers, with the most overall performance. In order to achieve that the optimisation strategy is the following:

- 1- Make 3 different optimisations, one for each material (as those made before - Figure 5.63).
- 2- Make a single optimisation, where the “global” objective function is the average of the global objective function for each material.
- 3- Make a single optimisation, where the “global” objective function is the sum of the minimum individual functions (Max-Min) for all materials, affected by the respective weight, calculated as follows:

$$FO_i = \sum_{j=1}^q w_j \text{Min} (F_{j,k}) \quad (5.7)$$

where,  $q$  is the number of criteria,  $w_j$  is the weight attributed to each and  $F_{j,k}$  is the individual objective function for criterion  $j$  and material  $k$ .

- 4- Chose a screw, based on an analysis of gains and losses of optimisations 2 and 3 relatively to the individual optimisations 1.

In order to do this, each of these 5 optimisations was repeated 10 times (to overcome the multi-modality problem). Therefore, 5 different screws are obtained corresponding to the best of each set of 10 runs. The best screw obtained for each material will be compared with the screws obtained using the average and the Min-Max global objective functions. This comparison will be made in terms of: output (Figure 5.65), power consumption (Figure 5.66), specific energy - power/output ratio - (Figure 5.67), screw length required for melting (Figure 5.68), WATS (Figure 5.69), melt temperature (Figure 5.70) and melt/barrel temperatures ratio (Figure 5.71).

Given the higher weight attributed to output maximisation, the screws have higher output, power consumption and screw length required for melting as well as lower WATS. The screws obtained for each polymer have higher output (Figure 5.65) and lower specific energy (Figure 5.67). The screw obtained with the Min-Max objective function is better than the one obtained with the average objective function. If the screw obtained with the Min-Max objective function is chosen the losses in terms of the output are circa 3 kg/hr for HDPE, less than 1 kg/hr for LDPE and circa 2 kg/hr for PVC. The losses in terms of specific energy are circa 0.03 J/kg for HDPE and less than 0.001 J/kg for LDPE and PVC. Concerning screw length required for melting and WATS criteria the best screw is obtained with the average objective function, but the performance of the screw obtained with the Min-Max objective function is almost as good. Finally, for all the polymers studied, the performance in terms of the melt temperature and melt/barrel temperature ratio criteria is identical. It is possible to conclude that the screw obtained with the Min-Max objective function has better performance than the obtained with the average objective function.

At this point, to choose a screw the decision-maker needs to make a balance between two costs. The costs in terms of output if the screw obtained with the Min-Max objective function is chosen and the costs associated to the manufacture of three screws and to the time needed to change them on the extruder if the three screws obtained alone are chosen.

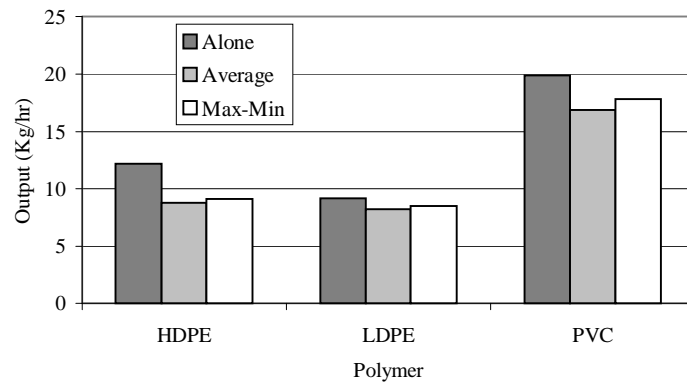


Figure 5.65- Output versus polymer and optimisation strategy.

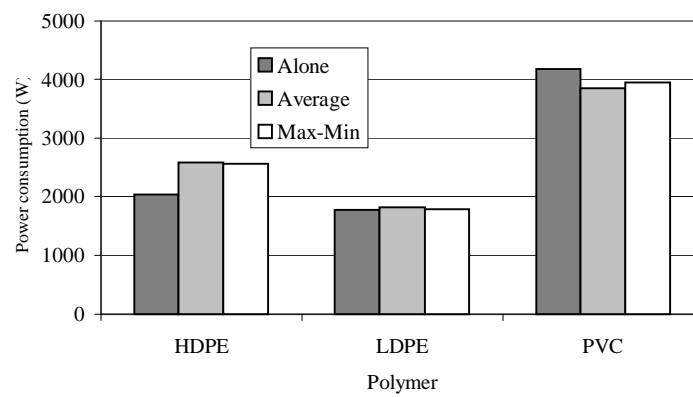


Figure 5.66- Power consumption versus polymer and optimisation strategy.

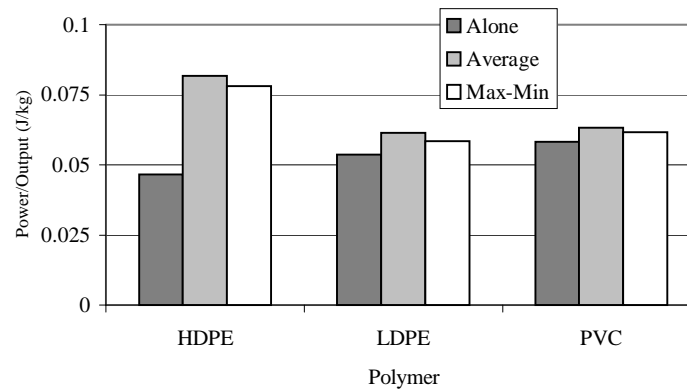


Figure 5.67- Specific energy versus polymer and optimisation strategy.

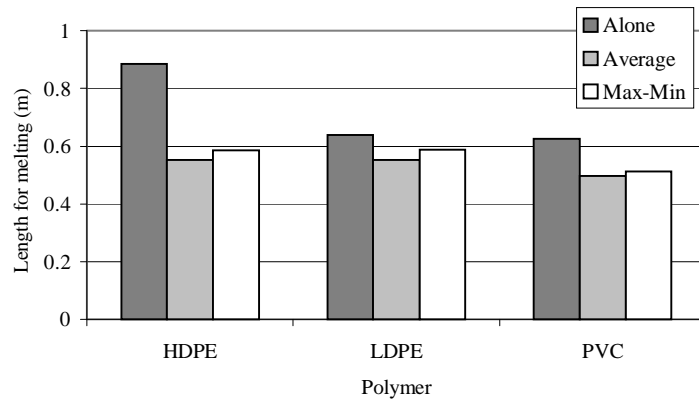


Figure 5.68- Length for melting versus polymer and optimisation strategy.

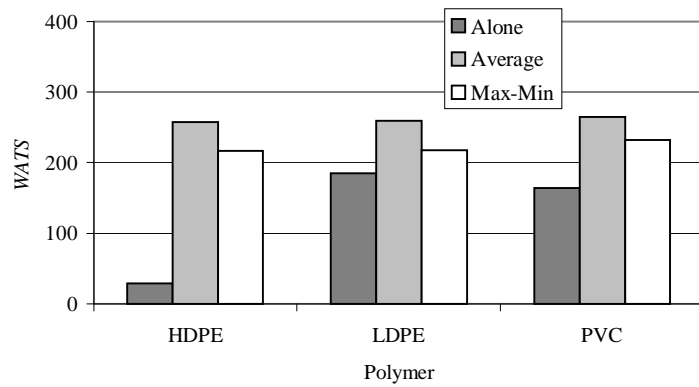


Figure 5.69- Mixing quality versus polymer and optimisation strategy.

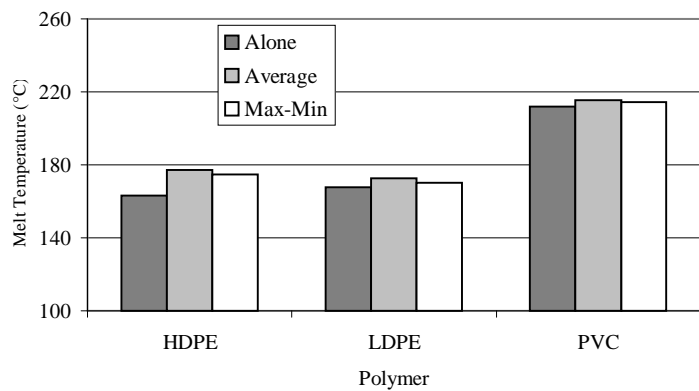


Figure 5.70- Melt temperature versus polymer and optimisation strategy.

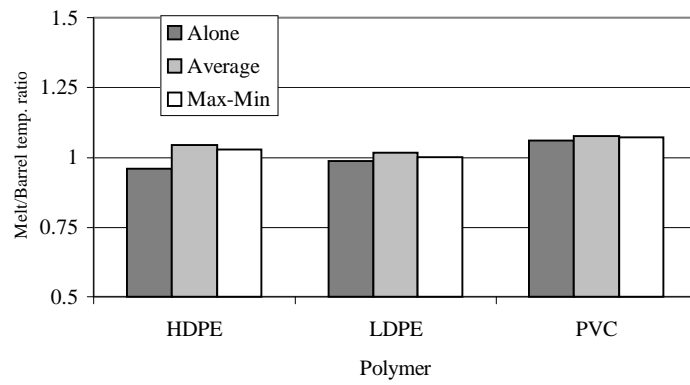


Figure 5.71- Melt/barrel temperature ratio versus polymer and optimisation strategy.

## 6- CONCLUSIONS

An optimisation approach to solve “automatically” single screw extrusion inverse problems was proposed and implemented in this work. The scheme developed was applied to the setting of the optimal operating conditions of an existing extruder and to the design of new extrusion screws.

Genetic Algorithms are of easy application, show the capacity to deal with complex search spaces, do not require any sort of additional information and the results are sensitive to the process parameters with physical meaning. Furthermore, GAs can be changed to take into account the existence of several criteria to be satisfied simultaneously, which is a characteristic of most real world optimisation problems. The approach based on the weighting of several individual criteria requires the *a priori* definition of the weights, the results having been shown to be sensitive to changes in these weights. However, if the decision-maker needs to change the relative importance of the criteria, the program needs to be run again. Conversely, the approach based on the concept of Pareto’s optimality allows the definition of Pareto frontiers between all the criteria only with one run. In this case if the user wants to define the criteria values to be satisfied in order to choose either the operating point or the screw geometry, a trade-off between the different criteria and parameters to optimise will be established.

The comparison between experimental and computational results produced by two different models clarifies the importance of the modelling package. It is clear that, when the numerical modelling routine is used, the optimisation results are closer to the experimental ones, regardless of the application of factorial design or genetic algorithm optimisation methods. One drawback of such methods is that the computation time grows exponentially. However, this question is becoming progressively less relevant given the exponential increase of computational power and the fact that a trial-and-error approach is avoided.

The Reduced Pareto Set Genetic Algorithm (RPSGA) multiobjective optimisation method developed in this work showed a good performance when applied to both benchmark and extrusion problems. The comparison with the Niche Pareto Genetic Algorithm (NPGA) shows that there is not a clear winner, the main advantage of the RPSGA method lying in the reduction of the Pareto set, especially in problems that require large populations.

In this work it was clearly demonstrated that a fundamental step of optimisation strategies using GAs is the definition (or setting) of its parameters (crossover and mutation rates,

population length, etc). The appropriate choice of these parameters increases the performance of the optimisation algorithm in terms of both the best results and the least time needed by the computations. This type of analysis is always required if changes on the optimisation conditions are to be made (number of variables to optimise, type of these variables, etc). The parameter values obtained in this work can be used as a starting point for new studies.

The running of the numerical modelling package implemented in this work depends on some parameters that were defined *a priori*. The parameter most susceptible of influencing the results is the grid size in the transversal plane -  $xy$ , which is related with the used numerical algorithm (finite differences, in this case). As expected, if the number of grid points increase (i.e., the grid size decreases) the model predictions improves but at the expense of computation time. It was determined that the best grid size, when the numerical modelling package is to be used by the optimisation algorithm (were it needs to be run several times), is 10 grid points. With this grid size it is possible to obtain good optimisation results with reasonable computation time. Conversely, if the objective is to study a specific processing situation, where only a few runs are needed a grid size of at least 15 points is recommended.

The setting of the increment length in the down-channel direction does not offer any difficulty, since in this case the increase in computation time is not important. Other parameters concerned to process variables (initial thickness of the films surrounding the solid bed, initial melt pool width, criterion to estimate the length of delay zone II, screw temperature along the solids conveying zone) were also defined. In this case the choice of the corresponding values is trivial and does not offer special attention, except in the case of the screw temperature where the best option is to consider the screw to be adiabatic

The assessment of the optimisation results of the computational operating conditions obtained by the three approaches (factorial design, genetic algorithms with an objective function and reduced Pareto set genetic algorithm) and using the two theoretical models of the extrusion process (analytical and numerical) allows one to conclude that the approaches where the numerical model is used yield better result. Differences only occur for barrel temperatures  $T_1$  and  $T_2$ .

The results obtained for screw design show that the optimisation algorithm is sensitive to the importance of the different criteria, to changes in the operating conditions and to changes in the polymer properties. The study of the reproducibility of the optimisation algorithm and the graphical representation of the global objective function as a function of two parameters to

optimise shows that this is a multimodal problem. Finally, a methodology to verify the possibility of using just one screw for three different polymers (LDPE, HDPE and PVC) was studied. In this, in order to choose a screw(s) the decision-maker needs to strike a balance between the cost related with the losses in output (if the decision is to use just one screw for the three polymers) and the costs related to the manufacture of three screws and time needed to change them on the extruder.

## 7- SUGGESTIONS FOR FURTHER WORK

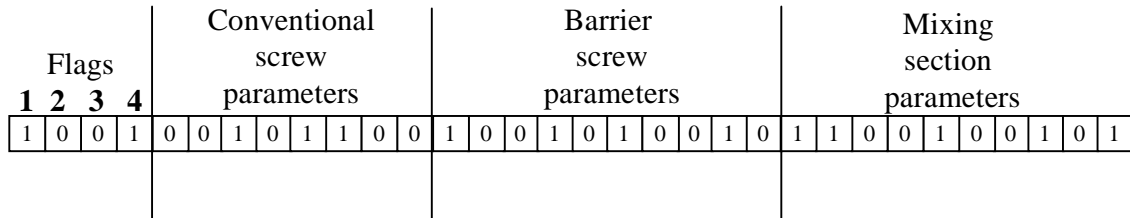
Several interesting and challenging studies can be carried out to extend the present work, some possibilities being:

- i) To further develop the optimisation methodology for screw design with GAs by extending the numerical analysis used in this work to the modelling of barrier screws and mixing sections.
- ii) To extend this methodology to the modelling of the plasticating phase of injection moulding (reciprocating-screw) that can be included in an optimisation methodology (as the one used in this work) for the setting of the operating conditions and for screw and non-return valve design.
- iii) To apply the methodology developed in this work to the optimisation of the operating conditions and for screw design of co-rotating twin-screw extruders.
- iv) Given the computational time consumed by the modelling package, improvements in the discretisation with finite differences should be pursued. For example, the Crank-Nicolson scheme may be replaced by the A.D.I. (Alternating-Direction Implicit) scheme, particularly in the case of two-dimensional analysis.

In the optimisation methodology with GAs for screw design, the choice between the screw configuration, i.e., the definition of whether the screw is conventional or barrier-type and if it has mixing sections or not, will be made automatically. The simple chromosome described in chapter 2 will be modified in order to include the geometrical parameters (of the conventional and barrier screws and of the mixing sections), two flags that indicate if the screw is conventional, barrier-type and/or has mixing sections and two flags that will define the type of the barrier screw and mixing sections. Figure 7.1 illustrates this purpose. The GA evaluates each chromosome thus defined and the final result includes a screw that can be conventional or barrier-type and can include or not mixing sections depending on the flag values.

The application of this optimisation methodology to twin-screw extrusion will be accomplished using the “LUDOVIC” commercial modelling package, which was developed at CEMEF (Centre de Mise en Forme de Matières Plastiques), Sophia-Antipolis, France. This programme is able to compute melt temperature profile, residence time distribution, pressure profile, mixing degree, power consumption and shear rates for a given twin-screw extruder geometry, operating conditions and polymer properties. Therefore, it will be possible to

optimise the operating conditions such as screw speed, barrel temperature profile and feed rate, as well as screw design. In the latter case the parameters to consider are the number, type, localisation and geometry of the various screw sections.



Flag 1: = 0 - conventional screw  
= 1 - barrier screw

Flag 2: = 0 - without mixing sections  
= 1 - with mixing sections

Flag 3: = 0 - barrier screw type 1  
= 1 - barrier screw type 2

Flag 4: = 0 - mixing section type 1  
= 1 - mixing section type 2

Flags 3 and 4 can have more than 1 gene in order to accommodate more barrier screw and mixing section types.

Figure 7.1- Chromosome definition for global screw design.

## 8- REFERENCES

- [AGA 96] J.F. Agassant, P. Avenas, J. Sergent, *La Mise en Forme des Matières Plastiques*, Lavoisier, 3<sup>rd</sup> edition, Paris (1996).
- [AME 89] K. Amellal, P.G. Lafleur, B. Arpin, *Computer Aided Design of Single-Screw Extruders*, pp. 277-317, in A.A. Collyer, L.A. Utracki (eds), *Polymer Rheology and Processing*, Elsevier (1989).
- [ATT 80] G. Attalla, P. Podio-Guidugli, *On Modelling the Solids Conveying Zone of a Plasticating Extruder*, Polym. Eng. Sci., **20**, pp. 709-715 (1980).
- [BÄC 91] T. Bäck, *Optimal Mutation Rates In Genetic Search*, Proc. Forth Int. Conf. on Genetic Algorithms, pp. 2-8 (1991).
- [BAK 85] J.E. Baker, *Adaptive Selection Methods for Genetic Algorithms*, Proc. First Int. Conf. on Genetic Algorithms, pp. 101-111 (1985).
- [BAK 87] J.E. Baker, *Reducing Bias and Inefficiency in The Selection Algorithms*, Proc. Second Int. Conf. on Genetic Algorithms, pp. 14-21 (1987).
- [BEA 93a] D. Beasley, D.R. Bull, R.R. Martin, *An Overview of Genetic Algorithms: Part 1, Fundamentals*, University Computing, **15**, pp. 58-69 (1993).
- [BEA 93b] D. Beasley, D.R. Bull, R.R. Martin, *An Overview of Genetic Algorithms: Part 2, Research Topics*, University Computing, **15**, pp. 170-181 (1993).
- [BEA 93c] D. Beasley, D.R. Bull, R.R. Martin, *A Sequential Niche Technique for Multimodal Function Optimisation*, Evolutionary Computation, **1**, pp. 101-125 (1993).
- [BIG 73] D.M. Bigg, *Mixing in a Single Screw Extruder*, Ph. D. Thesis, University of Massachusetts (1973).
- [BIG 74] D.M. Bigg, S. Middleman, *Mixing in a Screw Extruder. A Model for Residence Time Distribution and Strain*, Ind. Eng. Chem. Fundam., **13**, pp. 66-71 (1974).
- [BIG 77] D.M. Bigg, *Principles of Laminar Mixing with Application to the Polymer Extrusion Process*, Sci. Tech. Polymer Process. – Int. Conference, pp. 945-983 (1977).
- [BLI 95] T. Blicke, L. Thiele, *A Comparison of Selection Schemes Used in Genetic Algorithms*, TIK – Report n° 11, Computer Eng. and Communications Network Lab (TIK), Zurich, Switzerland (1995).
- [BOE 90] D. Boes, A. Krämer, V. Lohrbäcker, A. Scheneiders, *30 Years of the Grooved Bush Extruder*, Kunststoffe Germ. Plast., **80**, pp. 659-664 (1990).
- [BRO 72] E. Broyer, Z. Tadmor, *Solids Conveying in Screw Extruders – Part I: A modified Isothermal Model*, Polym. Eng. Sci., **12**, pp. 12-24 (1972).
- [BRO 86] D.C. Brown, B. Chandrasekaran, *Knowledge and Control for a Mechanical Design Expert System*, Computer, **19**, pp. 92-100 (1986).
- [BRO 97] J. Broszeit, *Finite-Element Simulation of Circulating Steady Flow for Fluids of the Memory-Integral Type: Flow in a Single-Screw Extruder*, J. Non-Newt. Fluid Mech., **70**, pp. 35-58 (1997).

- 
- [CAM 95] G. A. Campbell, N. Dontula, *Solids Transport in Extruders*, Int. Polym. Process., **10**, pp. 30-35 (1995).
- [CHA 95] R.Y. Chang, K.J. Lin, *The Hybrid FEM/FD Computer Model for Analysis of the Metering Section of a Single-Screw Extruder*, Polym. Eng. Sci., **35**, pp. 1748-1757 (1995).
- [CHA 96] C. Chatfield, A.J. Collins, *Introduction to Multivariate Analysis*, Chapman & Hall (1996).
- [CHE 97] B. Cheng, Y. Xie, D.I. Bigio, R.M. Briber, *Extrusion Flow in Partially Filled Screw Channel Subject to Wall Slip*, SPE-ANTEC Tech. Papers, (electronic version) (1997)
- [CHI 95a] A.J. Chipperfield, P.J. Fleming, *Parallel Genetic Algorithms*, In: *Handbook of Parallel and Distributed Computing*, A.Y. Zomaya (Ed), McGraw Hill, New York, pp. 1034-1059 (1995).
- [CHI 95b] R.V. Chiruvella, Y. Jaluria, A.H. Abib, *Numerical Simulation of Fluid Flow and Heat Transfer in a Single-Screw Extruder with Different Dies*, Polym. Eng. Sci., **35**, pp. 261- 273 (1995).
- [CHU 71] C.I. Chung, *Plasticating Single-Screw Extrusion Theory*, Polym. Eng. Sci., **11**, pp. 93-98 (1971).
- [CHU 75] C.I. Chung, *Maximum Pressure Developed by Solid Conveying Force in Screw Extruders*, Polym. Eng. Sci., **15**, pp. 29-34 (1975).
- [COV 95] J.A. Covas, *The Inverse Problem in Polymer Processing*, pp. 385-406, in J.A. Covas et al. (eds), *Rheological Fundamentals of Polymer Processing*, Kluwer Academic Publishers, Dordrecht (1995).
- [COV 99] J.A. Covas, A.G. Cunha, P. Oliveira, *An Optimisation Approach to Practical Problems in Plasticating Single Screw Extrusion*, Polym. Eng. Sci., **39**, pp. 443-456 (1999).
- [COX 80] A.P.D. Cox, R.T. Fenner, *Melting Performance in the Single Screw Extrusion of Thermoplastics*, Polym. Eng. Sci, **20**, pp. 561-571 (1980).
- [CUN 94] A.G. Cunha, *Simulação do Processo de Extrusão*, Master Thesis, Univ. do Minho, Braga (1994).
- [DAR 56] W.H. Darnell, E.A.J. Mol, *Solids Conveying in Extruders*, SPE J., **12**, pp. 20-29 (1956).
- [DAV 91] L. Davis, *Handbook of Genetic Algorithms*, Van Nostrand Reinhold (1991).
- [DEB 89] K. Deb, D.E. Goldberg, *An Investigation of Niche and Species Formation in Genetic Function Optimization*, Proc. Third Int. Conf. on Genetic Algorithms. Morgan Kauffman, pp. 41-49 (1989).
- [DeJ 90] K. De Jong, W.M. Spears, *An Analysis of the Interactions Roles of Population Size and Crossover in Genetic Algorithms*, In H.-P. Schwefel and R. Männer, editors, *Parallel Problem Solving from Nature*, pp. 38-47, Spring-Verlag (1990).

- 
- [DIR 93] R.W. Dirado, A. Garcia-Rejon, *Modelling of Membrane Inflation in Blow Moulding: Neural Network Prediction of Initial Dimensions from Final Part Specifications*, Adv. Polym. Technol., **12**, pp. 3-24 (1993).
- [DIR 95] R.W. Dirado, M. Lato, A. Garcia-Rejon, *Neural Network Boolean Prediction of Melt Fracture*, Plast. Rubber Composites and Appl, **23**, pp. 127-130 (1995).
- [ELB 84] B. Elbirli, J.T. Lindt, S.R. Gottgetreu, S.M. Baba, *Mathematical Modelling of Melting of Polymers in a Single-Screw Extruder*, Polym. Eng. Sci., **24**, pp. 988-999 (1984).
- [FAN 91] S. Fang, L. Chen, F. Zhu, *Studies on the Theory of Single Screw Plasticating Extrusion. Part II: Non-Plug Flow Solid Conveying*, Polym. Eng. Sci., **31**, pp. 1117-1122 (1991).
- [FAS 94] F. Fassihi-Tash, N. Sherkat, *In-exact Decision Support for the Design of Plasticating Extruder Screws*, Polymat'94, UK, pp. 434-438 (1994).
- [FEN 77] R.T. Fenner, *Developments in the Analysis of Steady Screw Extrusion of Polymers*, Polymer, **18**, pp. 617-635 (1977).
- [FEN 79] R.T. Fenner, *Principles of Polymer Processing*, McMillan, London (1979).
- [FOG 66] L.J. Fogel, A.J. Owens, M.J. Walsh, *Artificial Intelligence Through Simulated Evolution*, Wiley Publishing, New York (1966).
- [FON 93] C.M. Fonseca, P.J. Fleming, *Genetic Algorithms for Multiobjective Optimization: Formulation, Discussion and Generalization*, Proc. Fifth Int. Conf. on Genetic Algorithms, Morgan Kaufman, pp. 416-423 (1993).
- [GHO 96] M.H.R. Ghoreishy, M. Rafizadeh, *Numerical Simulation of Thermoplastic Melt Flow in Single Screw Extruder Using Finite Element Method*, Plastics, Rubber and Comp. Process. and Appl., **25**, pp. 120-125 (1996).
- [GOL 71] E. Goldacker, *Untersuchungen zur Inneren Reibung von Pulvern, Insbesondere in Hinblick auf Die Förderung in Extrudern*, Diss. RWTH Aachen, 1971.
- [GOL 85] D.E. Goldberg, *Alleles, Loci, and the TSP*, Proc. First Int. Conf. on Genetic Algorithms, pp. 154-159 (1985).
- [GOL 87] D.E. Goldberg, J. Richardson, *Genetic Algorithms with Sharing for Multimodal Function Optimization*, Proc. Second Int. Conf. on Genetic Algorithms, pp. 41-49 (1987).
- [GOL 89a] D.E. Goldberg, *Genetic Algorithms in Search, Optimisation and Machine Learning*, Addison-Wesley (1989).
- [GOL 89b] D.E. Goldberg, *Sizing Populations for Serial and Parallel Genetic Algorithms*, Proc. Third Int. Conf. on Genetic Algorithms, pp. 70-79 (1989).
- [GOL 92] D.E. Goldberg, K. Deb, J.H. Clark, *Genetic Algorithms, Noise, and the Sizing of Populations*, Complex Systems, **6**, pp. 333-362 (1992).
- [GOR 91] M. Gorges-Schleuter, *Explicit Parallelism of Genetic Algorithms through Population Structures*, In H.-P. Schwefel and R. Männer, editors, Parallel Problem Solving from Nature, pp. 150-159, Springer-Verlag (1991).

- 
- [GRI 62] R.M. Griffith, *Fully Developed Flow in Screw Extruders*, Ind. Eng. Chem. Fundam., **1**, pp. 180-187 (1962).
- [GRÜ 84] E. Grünschloss, *Calculation of the Mean Coefficient of Barrel Friction in Grooved Feed Sections*, Kunststoffe Germ. Plast., **74**, pp. 405-409 (1984).
- [HAN 96] C.D. Han, K.Y. Lee, N.C. Wheeler, *Plasticating Single-Screw Extrusion of Amorphous Polymers: Development of a Mathematical Model and Comparison with Experiment*, Polym. Eng. Sci., **36**, pp. 1360-1376 (1996).
- [HOL 75] J.H. Holland, *Adaptation in Natural and Artificial Systems*, University of Michigan Press (1975).
- [HOR 93] J. Horn, N. Nafpliotis, *Multiobjective Optimisation Using the Niche Pareto Genetic Algorithm*, IlliGAL Report No. 93005, Illinois Genetic Algorithms Laboratory, University of Illinois at Urbana-Champaign (1993).
- [HOR 94] J. Horn, N. Nafpliotis, D.E. Goldberg, *A Niche Pareto Genetic Algorithm for Multiobjective Optimization*, Proc. First IEEE Conf. on Evolutionary Computation, pp. 82-87 (1994).
- [HUA 93] H.X. Huang, Y.C. Peng, *Theoretical Modelling of Dispersive Melting Mechanism of Polymers in an Extruder*, Adv. Polym. Techn., **12**, pp. 343-352 (1993).
- [HYU 90] K.S. Hyun, M.A. Spalding, *Bulk Density of Solid Polymer Resins as a Function of temperature and Pressure*, Polym. Eng. Sci., **30**, pp. 571- 576 (1990).
- [HYU 96] K.S. Hyun, M.A. Spalding, C.E. Hinton, *Theoretical and Experimental Analysis of Solids Conveying in Single-Screw Extruders*, SPE-ANTEC Tech. Papers, pp. 199-207 (1996).
- [HYU 97] K.S. Hyun, M.A. Spalding, *A New Model for Solids Conveying in Single-Screw Plasticating Extruders*, SPE-ANTEC Tech. Papers, (electronic version) (1997).
- [JOO 93] J.W. Joo, T.H. Kwon, *Analysis of Residence Time Distribution in the Extrusion Process Including the Effect of 3-D Circulatory Flow*, Polym. Eng. Sci., **33**, pp. 959-970 (1993).
- [KAC 72] L. Kacir, Z. Tadmor, *Solids Conveying in Screw Extruders – Part III: The Delay Zone*, Polym. Eng. Sci., **12**, pp. 387-395 (1972).
- [KIM 95a] S.J. Kim, T.H. Kwon, *A Simple Approach to Determining Three-Dimensional Screw Characteristics in the Metering Zone of Extrusion Processes Using a Total Shape Factor*, Polym. Eng. Sci., **35**, pp. 274-283 (1995).
- [KIM 95b] S.J. Kim, T.H. Kwon, *Development of Numerical Simulation Methods and Analysis of Extrusion Processes of Particle-Filled Plastic Materials Subject to Slip at the Wall*, Powder Tech., **85**, pp. 227-239 (1995).
- [KOZ 91] J.R. Koza, *Evolving a Computer Program to Generate Random Numbers Using the Genetic Programming Paradigm*, Proc. of the Fourth Int. Conf. on Genetic Algorithms, Morgan Kauffman, pp. 37-44 (1991).
- [LEE 90] K.Y. Lee, C.D. Han, *Analysis of the Performance of Plasticating Single-Screw Extruders with a New Concept of Solid-Bed Deformation*, Polym. Eng. Sci., **30**, pp. 665-676 (1990).

- 
- [LEK 96] C. Lekakou, J. Brandao, *Extrusion of Polypropylene. Part II: Process Analysis of the Metering Zone*, **36**, pp. 56-64 (1996).
- [LIN 85a] J.T. Lindt, B. Elbirli, *Effect of the Cross-Channel Flow on the Melting Performance of a Single-Screw Extruder*, *Polym. Eng. Sci.*, **25**, pp. 412-418 (1985).
- [LIN 85b] J.T. Lindt, *Mathematical Modelling of Melting of Polymers in a Single-Screw Extruder – A Critical Review*, *Polym. Eng. Sci.*, **25**, pp. 585-588 (1985).
- [LOV 73] J.G.A. Lovegrove, J.G. Williams, *Solids Conveying in a Single Screw Extruder; The Role of Gravity Forces*, *J. Mech. Eng. Sci.*, **15**, pp. 114-122 (1973).
- [MAD 59] B.H. Maddock, *A Visual Analysis of Flow and Mixing in Extruder*, *Soc. Plast. Eng. J.*, **15**, pp. 383-394 (1959).
- [MAH 92] S.W. Mahfoud, *Crowding and Pre-selection Revisited*, *Parallel Problem Solving From Nature*, **2**, pp. 27-36 (1992).
- [MAH 94] S.W. Mahfoud, *Crossover Interactions Among Niches*, *Proc. First IEEE Conf. on Evolutionary Computation*, pp. 188-193 (1994).
- [MAH 95] S.W. Mahfoud, *A Comparison of Parallel and Sequential Niching Methods*, *Proc. Sixth Int. Conf. on Genetic Algorithms*, pp. 136-143 (1995).
- [MEN 92] W. Mendenhall, T. Sincich, *Statistics for Engineering and Sciences*, 3<sup>rd</sup> ed., Maxwell MacMillan Int. Editions (1992).
- [MIT 97] A.R. Mitchell, D.F. Griffiths, *The Finite Difference Method in Partial Differential Equations*, John Wiley & Sons, Chichester (1980).
- [MON 91] D.C. Montgomery, *Design and Analysis of Experiments*, 3<sup>rd</sup> ed., John Wiley and Sons, New York (1991).
- [O'BR 92] K. O'Brian, *Computer Modelling for Extrusion and Other Continuous Polymer Processes*, Carl Hanser Verlag, Munich (1992).
- [PAL 72a] K. Palit, R.T. Fenner, *Finite Element Analysis of Slow Non-Newtonian Channel Flow*, *AIChE J.*, **18**, pp. 628-633, (1972).
- [PAL 72b] K. Palit, R.T. Fenner, *Finite Element Analysis of Two-Dimensional Slow Non-Newtonian Channel Flows*, *AIChE J.*, **18**, pp. 1163-1170, (1972).
- [PAS 92] PASS, *Polymer Analysis & Simulation Software*, Polymer Processing Institute (1992).
- [PIN 70] G. Pinto, Z. Tadmor, *Mixing and Residence Time Distribution in Melt Screw Extruders*, *Polym. Eng. Sci.*, **10**, pp. 279-288 (1970).
- [POT 85] H. Potente, *Methods of Calculating Grooved Extruder Feed Sections*, *Kunststoffe Germ. Plast.*, **75**, pp. 439-441 (1985).
- [POT 88] H. Potente, *The Forced Feed Extruder Must be Reconsidered*, *Kunststoffe Germ. Plast.*, **78**, pp. 355-363 (1988).
- [POT 89] H. Potente, M. Koch, *New Aspects in the Design of Extruders with a Forced Feeding Section*, *Int. Polym. Process.*, **4**, pp. 208-218 (1989).

- 
- [POT 93] H. Potente, B. Klarholz, *Systematic Optimisation of Single-Screw Plasticating Units*, PPS IX Annual Meeting, pp. 353-354 (1993).
- [POT 94] H. Potente, B. Klarholz, *A Computer Aided Engineering Concept for the Design and Optimisation of a Single-Screw Plasticating Units*, PPS X Annual Meeting, pp. 35-36 (1994).
- [POT 96] H. Potente, M. Zelleröhr, *Quality-Functions for the Optimisation of Single-Screw Plasticating Units*, PPS XII Annual Meeting, Sorrento, Italy, pp. 345-346 (1996).
- [POT 97] H. Potente, M. Zelleröhr, *Optimisation of Single-Screw Extruders with Statistical Methods*, PPS XIII Annual Meeting, Secausus N.J., USA, pp. (1997).
- [POW 89] D.J. Powell, S.S. Tong, M.M. Skolnick, *EnGENEous Domain Independent, Machine Learning for Design Optimization*, Proc. Third Int. Conf. on Genetic Algorithms. Morgan Kaufman, pp. 151-159 (1989).
- [RAU 82a] R. Rautenbach, H. Peiffer, *Model Calculation for the Design of the Grooved, Feed Section of Single-Screw Extruders*, Kunststoffe Germ. Plast., **72**, pp. 137-143 (1982).
- [RAU 82b] R. Rautenbach, H. Peiffer, *Throughput and Torque Characteristics of Grooved Feed Sections in Single-Screw Extruders*, Kunststoffe Germ. Plast., **72**, pp. 262-266 (1982).
- [RAU 86] C. Rauwendaal, *Polymer Extrusion*, Hanser Publishers, Munich (1986)
- [RAU 98] C. Rauwendaal, T.A. Osswald, G. Tellez, P.J. Gramann, *Flow Analysis in Screw Extruders-Effect of Kinematic Conditions*, Inter. Polym. Process., **13**, pp. 327-333 (1998).
- [REC 73] I. Rechenberg, *Evolutionsstrategie: Optimierung Technischer Systeme nach Prinzipien der Biologischen Evolution*, Frommann-Holzboog, Stuttgart (1973).
- [ROS 85] M.A. Roseman, J.S. Gero, *Reducing the Pareto Optimal Set in Multicriteria Optimization*, Eng. Optim., **8**, pp. 189-206 (1985).
- [RUM 86] D.E. Rumelhart, G.E. Hinton, R.J. Williams, *Learning Internal Representations by Error Propagation*, in D.E. Rumelhart and J.L. McClelland (eds), MIT Press, pp. 318-362 (1986).
- [RUT 89] R.A. Rutenbar, *Simulated Annealing Algorithms: An Overview*, IEEE Circuits and Devices Magazine, **1**, pp. 19-26 (1989).
- [SMI 94] D.E. Smith, D.A. Tortorelli, C.L. Tucker III, *Sensitivity Analysis and Optimization of Polymer Sheet Extrusion Dies*, IME'94 – ASME Winter Annual Meeting, Chicago (1994).
- [SPA 92] M.A. Spalding, K.S. Hyun, *Coefficients of Dynamic Friction as a Function of Temperature, Pressure, and Velocity for Several Polyethylene Resins*, SPE-ANTEC Tech. Papers, pp. 2542-2545 (1992).
- [SPA 93] M.A. Spalding, D.E. Kirkpatrick, K.S. Hyun, *Coefficients of Dynamic Friction for Low Density Polyethylene*, Polym. Eng. Sci., **33**, pp. 423-430 (1993).

- 
- [SPA 95a] M.A. Spalding, K.S. Hyun, *Coefficients of Dynamic Friction as a Function of Temperature, Pressure, and Velocity for Several Polyethylene Resins*, Polym. Eng. Sci., **35**, pp. 557-563 (1995).
- [SPA 95b] M.A. Spalding, K.S. Hyun, S.R. Jenkins, D.E. Kirkpatrick, *Coefficients of Dynamic Friction and the Mechanical Melting Mechanism for Vinylidene Chloride Copolymers*, Polym. Eng. Sci., **35**, pp. 1907-1916 (1995).
- [SPE 91] W.M. Spears, K.A. De Jong, *An Analysis of Multi-Point Crossover*, Foundations of Genetic Algorithms, pp. 301-315 (1991).
- [SPE 93a] W.M. Spears, K.A. De Jong, T. Bäck, D.B. Fogel, H. Garis, *An Overview of Evolutionary Computation*, European Conf. On Machine Learning, pp. 442-459 (1993).
- [SPE 93b] W.M. Spears, *Crossover or Mutation?*, Foundations of Genetic Algorithms, **2**, pp. 221-237 (1993).
- [SRI 95] N. Srinivas, K. Deb, *Multiobjective Optimization Using Nondominated Sorting in Genetic Algorithms*, Evolutionary Computation, **2**, pp. 221-248 (1995).
- [STE 95] M.J. Stevens, J.A. Covas, *Extruder Principles and Operation*, 2<sup>nd</sup> ed., Chapman & Hall, London (1995).
- [STR 61] L.F. Street, Int. Plast. Eng., **1**, pp. 289 (1961).
- [STR 92] S.R. Strand, M.A. Spalding, K.S. Hyun, *Modelling of the Solids-Conveying Section of a Starve-Fed Single-Screw Plasticating Extruder*, SPE-ANTEC Tech. Papers, pp. 2537-2541 (1992).
- [SYS 89] G. Syswerda, *Uniform Crossover in Genetic Algorithms*, Proc. Third Int. Conf. on Genetic Algorithms, pp. 2-9 (1989).
- [SYS 91] G. Syswerda, *Schedule Optimization Using Genetic Algorithms*, in L. Davis, editor, Handbook of Genetic Algorithms, chapter 21, pp. 332-349, Van Nostrand Reinhold (1991).
- [TAD 67] Z. Tadmor, I.J. Duvdevani, I. Klein, *Melting in Plasticating Extruders - Theory and Experiments*, Polym. Eng. Sci., **7**, pp.198- 217 (1967).
- [TAD 70] Z. Tadmor, I. Klein, *Engineering Principles of Plasticating Extrusion*, Van Nostrand Reinhold, New York (1970).
- [TAD 72] Z. Tadmor, E. Broyer, *Solids Conveying in Screw Extruders – Part II: Non Isothermal Model*, Polym. Eng. Sci., **12**, pp. 378-386 (1972).
- [THO 89] J.R. Thomas, A.G. Cohn, *An Expert System for Hollow Extrusion Die Design*, Research Report 150, Dept. of Computer Science, Univ. of Warwick, UK (1996).
- [THO 95] F.W. Thomson, *Particulate Polymer Handling and Storage Engineering*, pp. 71-112, in M. Narkis, N. Rosenzweig (eds.), *Polymer Powder Technology*, Wiley, Chichester, UK (1995)
- [TOL 75] H. Tolle, *Optimisation Methods*, Springer-Verlag, New York (1975).
- [VIR 84] M. Viriyayuthakorn, B. Kassahun, *A Three Dimensional Model for Plasticating Extrusion Screw Design*, SPE-ANTEC Tech. Papers, pp. 81-84 (1985).

- 
- [WAL 66] D.M. Walker, *An Approximate Theory for Pressures and Arching in Hoppers*, Chem. Eng. Sci., **21**, pp. 975-997 (1966).
- [WAL 73] J.K. Walters, *A Theoretical Analysis of Stresses in Axially-Symmetric Hoppers and Bunkers*, Chem. Eng. Sci., **28**, pp. 779-789 (1973).
- [WAS 89] P.D. Wassesman, *Neural Computing Theory and Practice*, Van Nostrand Reinhold (1989).
- [WOR 94] J. Wortberg, B. Klarholz, S. Meyer-Katona, *Expert-Knowledge-Based Analysis of Extrusion Process*, Kunststoffe Plast Europe, **84**, pp. 26-30 (1994).
- [YAM 98] J.A. Yamamuro, D. Penumadu, G.A. Campbell, *Modelling Solids Conveying in Polymers Extruders*, Int. Polym. Process., **13**, pp. 3-8 (1998).
- [YU 98] Q. Yu, G. Hu, *Development of a Helical Coordinate System and Its Applications to Analysis of Polymer Flow in Screw Extruders. Part II: A Helical Channel Model for Single Screw Extruders*, Polym. Eng. Sci., **38**, pp. 819-830 (1998).
- [ZHU 91] F. Zhu, L. Chen, *Studies on the Theory of Single Screw Plasticating Extrusion. Part I: A new Experimental Method for Extrusion*, Polym. Eng. Sci., **31**, pp. 1113-1116 (1991).
- [ZIE 83] O.C. Zienkiewicz, K. Morgan, *Finite Elements and Approximation*, John Wiley & Sons, New York (1983).